



**LUMINESCENCE CHRONOLOGY OF RAISED  
MARINE TERRACES, SOUTH-WEST NORTH  
ISLAND, NEW ZEALAND**

**BY**

**Geoffrey Alastair Thomas Duller**

**A thesis submitted in fulfilment of the award of the degree of Doctor of  
Philosophy at the University of Wales**

**Institute of Earth Studies, University of Wales, Aberystwyth**

**December 1992**

# ABSTRACT

This thesis aims to test the validity of standard (multiple aliquot additive dose and regeneration) methods of luminescence dating using potassium feldspars as the dosimeter. In addition, methods are developed to allow more rapid, and more precise, measurements of the equivalent dose of a sample by making all luminescence measurements on a single aliquot.

Dune sands, varying in age from modern to approximately 350 ka, collected from the southwestern part of North Island, New Zealand, have been dated using thermoluminescence (TL) and infrared stimulated luminescence (IRSL) methods. Comparison with independent age estimates shows that reliable luminescence ages can be obtained over the period from the present day to 130 ka using standard methods on grains greater than 100 $\mu$ m diameter. The use of IRSL measurements reduces the uncertainty in the determination of a residual luminescence level, and thus makes it possible to date younger sediments than when using TL.

Several methods of equivalent dose determination based upon using a single aliquot of a sample are described. An additive dose method is found to be most suitable for the samples studied. The loss of signal due to preheating is best corrected using a dose correction method. The method is found to give results similar to those determined using standard methods of equivalent dose determination for the suite of samples from New Zealand.

Experiments into the nature of the IRSL signal from potassium feldspars show that increasing the temperature of the sample increases the size of the trapped charge population that is probed. Other experiments suggest that the trapped charge populations that give rise to the IRSL and TL signals are different.

# STATEMENT

The work presented in this thesis has not already been accepted in substance for any degree and is not being concurrently submitted in candidature for any degree. The work is the result of my own investigations unless otherwise stated.

Geoffrey Duller

Ann G. Wintle (supervisor)

# Contents

<b>Abstract</b>	i
<b>Statement</b>	ii
<b>Contents</b>	iii
<b>Acknowledgements</b>	vii
<b>Chapter 1: Introduction</b>	
1.1 Luminescence dating methods	1
1.2 The physics of luminescence	1
1.2.1 The advantages of measuring luminescence from potassium feldspars	2
1.2.2 Thermoluminescence (TL)	3
1.2.3 Infrared stimulated luminescence (IRSL)	3
1.3 The application of luminescence methods to the dating of Quaternary sediments	4
1.4 Aims of the thesis	6
<b>Chapter 2: Dune sands in the Wanganui, Horowhenua and Manawatu regions, New Zealand</b>	
2.1 Geological setting	7
2.1.1 Sediment types and sources	9
2.1.2 Tephra stratigraphy and chronology	9
2.1.3 Age of the Mt.Curl Tephra and Rangitawa Pumice	10
2.2 Dune phases identified in the Horowhenua and Manawatu regions	12
<b>Chapter 3: Sample collection and preparation</b>	
3.1 Precautions in sample collection	14
3.2 Sample preparation	14
3.2.1 Potassium feldspar separation	15
3.2.2 Use of hydrofluoric acid for etching the surface of potassium feldspar grains	16
3.3 Mounting of samples	17
<b>Chapter 4: Equipment and measurement</b>	
4.1 The Risø automated TL reader	18
4.1.1 The TL set	18
4.1.2 The IRSL add-on unit	18
4.1.3 The GLSL add-on unit	19
4.1.4 Software development	19

4.2	The Daybreak IRSL set	19
4.3	Filters	20
	4.3.1 Infrared rejection	20
	4.3.2 Emission and absorption characteristics for feldspars	21
	4.3.3 Filter characteristics	22
4.4	Bleaching	23
4.5	Irradiation	23
4.6	Sample normalization	23
	4.6.1 Weight normalization	24
	4.6.2 Natural normalization	24
	4.6.3 Second glow normalization	29
4.7	Preheating	31
	4.7.1 Preheating at 100°C	32
	4.7.2 Preheating at 140°C	33
	4.7.3 Preheating for single aliquots	33
	4.7.4 Implications of preheating experiments for our understanding of the relationship between IRSL and TL	35
4.8	Laser ablation inductively coupled plasma mass spectrometry	35

## **Chapter 5: The application of standard methods of equivalent dose determination to samples of known age**

5.1	Previous attempts to compare luminescence dating methods based upon potassium feldspar with known age samples	38
5.2	Description of samples analyzed	40
5.3	Dosimetry	44
	5.3.1 Emission counting	44
	5.3.2 Element concentrations	46
	5.3.3 Comparison of dosimetric methods	46
	5.3.4 Internal dose rate determination	49
5.4	Equivalent dose determination	53
	5.4.1 Additive dose method	55
	5.4.2 Regeneration method	56
	5.4.3 Temperature shifting of TL data	56
	5.4.4 Fading tests	57
	5.4.5 Comparison of EDs determined using various methods	59
	5.4.6 Comparison between equivalent dose values and normalization factors	61
5.5	Comparison of luminescence and geological age estimates	61
5.6	Conclusions	65

## **Chapter 6: Regeneration using a single aliquot**

6.1	Advantages of using a single aliquot	67
6.2	Advantages of using regeneration	68
6.3	Description of the method	68
6.4	Application to GDNZ 5	69
	6.4.1 Reproducibility of results	69
	6.4.2 Comparison with standard methods of ED determination	69

6.4.3	Effect of progressive changes in sensitivity	70
6.5	Effect of elevated temperatures on IRSL	71
6.5.1	Effect of temperature upon the IRSL signal	71
6.5.2	Effect of IR exposure at different temperatures upon the IRSL residual	73
6.5.3	Effect of IR exposure at different temperatures upon TL	75
6.5.4	The relationship between IRSL, temperature and TL	75
6.6	The relationship between TL, IRSL and GLSL signals from potassium feldspars	77
6.6.1	The effect of preheating at different temperatures	77
6.6.2	The effect of IR exposure upon TL, IRSL and GLSL	78
6.6.3	The effect of green light exposure upon TL, IRSL and GLSL	78
6.6.4	Comparison of trapped charge distributions measured using IRSL and TL	79
6.6.5	Implications for the relationship between the TL, IRSL and GLSL signals from potassium feldspar	81
6.7	Effect of using a solar simulator to produce a residual signal	82
6.8	Use of regeneration for source inter-calibration	85
6.8.1	Determination of the most appropriate method	85
6.8.2	Advantages of this method of calibration	88
6.9	Conclusions	89

## **Chapter 7: Additive dose using a single aliquot**

7.1	Advantages of using the additive dose method	90
7.2	The effect of preheating	90
7.3	Luminescence correction methods	93
7.3.1	Luminescence correction method A	93
7.3.2	Luminescence correction method B	95
7.3.3	Testing luminescence correction method B	98
7.3.4	Comparison of equivalent doses determined using standard methods and single aliquot results corrected using luminescence correction method B	99
7.3.5	Problems when applying luminescence correction method B to non-linear growth curves	101
7.4	Dose correction method	103
7.4.1	Description of the method	104
7.4.2	Testing the method on samples with linear growth	106
7.4.3	Testing the method on samples with non-linear growth	107
7.4.4	Comparison of equivalent doses determined using standard methods and single aliquot results corrected using the dose correction method	107
7.4.5	Conclusions	108

## **Chapter 8: Application of the additive dose single aliquot method to dating of Koputaroa phase dunes**

8.1	Koputaroa phase dunes	110
8.2	Description of samples analyzed	110
8.3	Results from single aliquot analysis	111
8.4	Implications for the age and duration of the Koputaroa dune phase	114
8.5	Conclusions	115

## **Chapter 9: Conclusions**

9.1	Luminescence dating using potassium feldspars	116
9.1.1	Comparison of luminescence age estimates with those derived from other methods	116
9.1.2	Dating Koputaroa phase dunes	117
9.2	The use of single aliquot methods for equivalent dose determination	118
9.3	Characteristics of the infrared stimulated luminescence signal from potassium feldspars	119
9.4	Directions for further study	121

## **Appendix I: Sites from which samples were collected for luminescence dating**

AI.1	McLeavy road	123
AI.2	Paiaka road	124
AI.3	Manawatu River section	124
AI.4	Penny road	124
AI.5	Mt.Curl Tephra type site	124
AI.6	Koputaroa road	125
AI.7	Te Waka road	125
AI.8	Hokio Beach	126
AI.9	Heatherlea	126
AI.10	Papaiaatonga Lake road	126
AI.11	Whenuakura River	126
AI.12	Rangitatau East road (Bushy Park Section)	127

## **Appendix II: Source calibrations**

AII.1	Calibration against the Risø gamma source	128
AII.2	Intercalibration of Daybreak and Risø $\beta$ -sources	130

## **Appendix III: Single aliquot results for samples from The Netherlands and the United States of America**

AIII.1	Single aliquot EDs corrected using luminescence correction method B	133
AIII.2	Single aliquot EDs corrected using the dose correction method	135

<b>References</b>	<b>137</b>
-------------------	------------

## Acknowledgements

I am very happy to be able to thank everyone in the Luminescence laboratory in Aberystwyth for their help and support in the undertaking of this work; Dr Ann Wintle, Fiona Musson, Sheng-Hua Li, Kate Richardson and Michèle Clarke. Their ruthless proof reading of manuscripts and constructive discussions about avenues of research have made the laboratory a stimulating and productive environment in which to work. Invaluable technical support in Aberystwyth has been provided by Dave Kelly and Jeff Rooke, frequently saving the day when equipment has gone horribly wrong.

It has been my great fortune during the writing of this thesis to have had three visits to the Risø national laboratory in Denmark at the kind invitation of Dr Lars Bøtter-Jensen. He and Henrik Christiansen have helped me understand the intricacies of the Risø automated TL/OSL reader on which the majority of the work presented here was carried out. These visits have also been stimulating occasions with long discussions about luminescence with Dr Bøtter-Jensen and Dr Vagn Mejdahl.

Much of my background information on the Quaternary geology of south-west North Island New Zealand was gained while I was working in the department of Geography at Massey University, New Zealand. I was made very welcome there by Chris Muckersie, Dr Mike Shepherd and Dr John McArthur, all of whom also helped in sample collection. Additional samples were collected with the help of Dr Alan Palmer (Department of Soil Science, Massey University) and Dr Brad Pillans (Department of Geology, Victoria University, Wellington).

My thanks must also go to Jane and my family for not thinking me too strange even though I did decide, of my own free will, to work in a darkened room for three years of my life, and for their support during that time. All the postgraduates on G-floor have made life very entertaining during my stay in Aberystwyth and I thank the owners of the Half-Way Inn for stocking such exceedingly good cider.

This research has been supported by NERC studentship GT4/88/GS/103.

# CHAPTER 1: Introduction

## 1.1 Luminescence dating methods

A number of luminescence dating methods have been applied to Quaternary sediments over the past decade and a half, all based on the same principle. Measurement of the luminescence signal from detrital minerals from a sedimentary unit allows an estimate of the ionizing radiation dose to which the sediment has been exposed since deposition of the unit (the sample's 'equivalent dose' or ED). Together with the ED, measurements of the radiation dose rate enable an age to be derived for the sample using the equation,

$$\text{Age (yr)} = \frac{\text{Equivalent Dose (Gy)}}{\text{Dose Rate (Gy/yr)}}$$

where the S.I. unit for absorbed radiation dose is the gray (Gy). Various luminescence measurements may be made to estimate the ED and, in order to understand the advantages, disadvantages and limitations of such measurements, it is necessary to briefly outline the physical basis of luminescence.

## 1.2 The physics of luminescence

Luminescence is the stimulated emission of light, from an insulator or a semi-conductor, following the previous absorption by the sample of energy from radiation. McKeever (1985) distinguishes three classes of luminescence behaviour depending upon the period of time between absorption of the radiation and the emission of light. For fluorescence and short-term phosphorescence this period of time is  $\leq 10^{-4}$ s. The type of luminescence behaviour that is of interest in this study is classed as 'long-term phosphorescence' by McKeever (1985) where the period of time between exposure to radiation and emission of light is  $\geq 10^{-4}$ s.

Only semi-conductors or insulators exhibit luminescence phenomena because a prerequisite for such behaviour is the existence of an energy band structure where the valence band is separated from the conduction band by a 'forbidden energy gap' which electrons may not occupy (figure 1.2). Luminescence can be explained as the result of the release of energy, in the form of photons, due to the transfer of charge between the

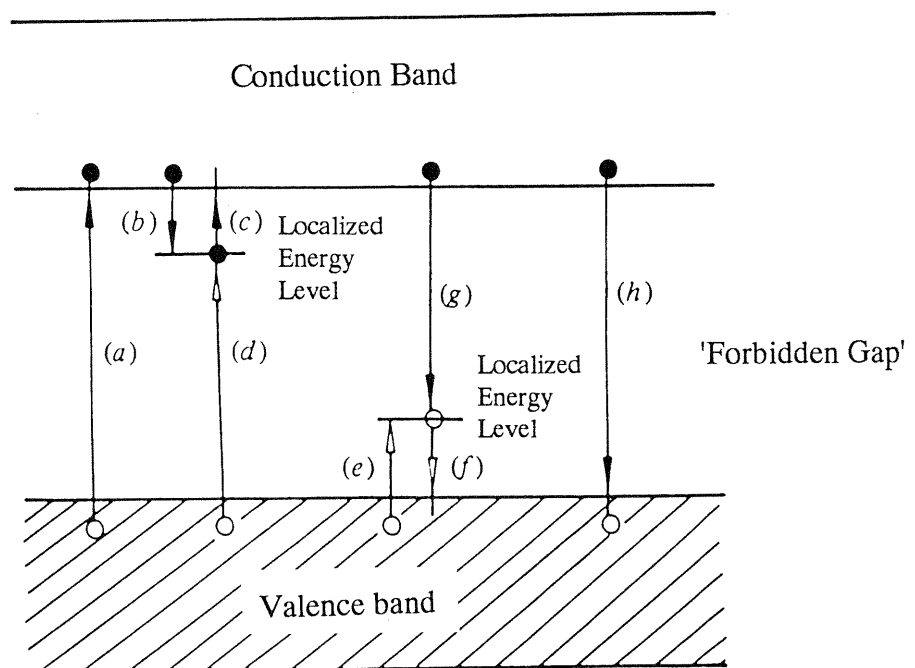


Figure 1.2: Energy band diagram showing common electronic transitions in crystalline semiconductors (from McKeever 1985). Electrons; solid circles; electron transitions, solid arrows; holes, open circles; hole transitions, open arrows.

conduction and valence bands. Exposure to radiation causes ionization which involves charge being excited from the valence band to the conduction band (transition (a) in figure 1.2). The free hole and electron, produced as a result of this ionization, are able to wander within the valence and conduction bands respectively. The energy added to the lattice by the source of radiation will be released by de-excitation of the electron back to the valence band (e.g. transition (h) in figure 1.2) and this energy may be in the form of phonons or photons. Where these two transitions occur within less than  $10^{-4}$ s the process is termed fluorescence or short-term phosphorescence.

In all natural materials the crystal structure is distorted (e.g. by the substitution of one ion by another with a different ionic radius) and this introduces localized energy levels, within the 'forbidden gap' between the valence and conduction bands, where charge may now occur. In materials with these localized energy levels, charge excited to the conduction band may now undergo transition (b) (in figure 1.2) and become 'trapped' in this localized energy level. Equally, free holes within the valence band may undergo transition (e) and become trapped there. Subsequently, seconds or years after ionization, this 'trapped charge' may be released into the conduction or the valence bands by the addition of thermal or optical energy. From there the charge may be de-excited via transitions ((a),(h),(d) or (g) in figure 1.2) to give luminescence. This 'long-term phosphorescence' is the process that is used for dating Quaternary sediments. In this study three types of luminescence are studied. The first is thermoluminescence (TL) where transitions (c) or (f) (from figure 1.2) are initiated by heating the sample, and the other two are types of optically stimulated luminescence (OSL) where optical stimulation causes the transitions. Two wavelength bands are used for optical stimulation in this thesis, infrared (880-80nm), giving rise to infrared stimulated luminescence (IRSL), and a green waveband (515-560nm), giving rise to green light stimulated luminescence (GLSL).

### 1.2.1 The advantages of measuring luminescence from potassium feldspars

Although stimulated luminescence can be obtained from several common minerals, quartz and potassium feldspar are the most frequently used for dating Quaternary sediments. This is primarily because of their natural abundance in sedimentary materials. Potassium rich feldspars are used as the dosimeter in all the work presented in this thesis. Relatively little luminescence work has previously been undertaken using this mineral fraction, quartz being a more ubiquitous and popular choice. However, potassium feldspars have three major advantages over quartz for luminescence dating.

- A) Their luminescence signal continues to grow at far higher doses than does that from quartz. This means that, in theory, one should be able to date older samples using potassium feldspars.
- B) A major uncertainty in the determination of the annual dose rate is caused by the dependence of the external dose rate upon the presence of interstitial water between the grains. When using quartz, almost 100% of the dose rate is derived from outside of the grain and so any uncertainty in the water content has a large effect. However, a significant proportion of the annual radiation dose that grains of feldspar receive originates from within the grains themselves. This is primarily due to the large potassium content (approximately 10% by weight). The effect of uncertainties in interstitial water content are therefore less important.
- C) An optically stimulated luminescence signal can be measured from potassium feldspars using stimulation in the near infrared (800-1000nm, Hütt *et al.* (1988)). Infrared emitting diodes provide a cheap and convenient method of stimulation (Bailiff and Poolton, 1989) compared with the large, and expensive, laser installation (e.g. an argon-ion laser emitting at 514.5nm) used to obtain an OSL signal from quartz (though recently a cheaper alternative using a stimulating waveband from 420-560nm filtered from the output of a halogen bulb has been developed (Bøtter-Jensen and Duller, 1992)). An IRSL unit has been specifically designed to fit on the Risø automated TL/OSL reader (Bøtter-Jensen *et al.*, 1991), and this has enabled complex sequences of heating, irradiation, and TL and IRSL measurements to be made under computer control.

### 1.2.2 Thermoluminescence (TL)

The most common method of stimulating luminescence is by heating samples to 450°C or 500°C at a rate of 1 to 10°C/s. As samples are heated, charge from progressively deeper traps is emptied into the conduction and valence bands, from where it is able to recombine and generate luminescence. A plot of thermoluminescence (TL) versus sample temperature can then be made. Figure 1.2.2 shows such a plot for a sample of potassium feldspar from GDNZ 1.

### 1.2.3 Infrared Stimulated Luminescence (IRSL)

A major advantage of using feldspars is that they produce a large optically stimulated luminescence (OSL) signal when exposed to infrared photons. This type of optically

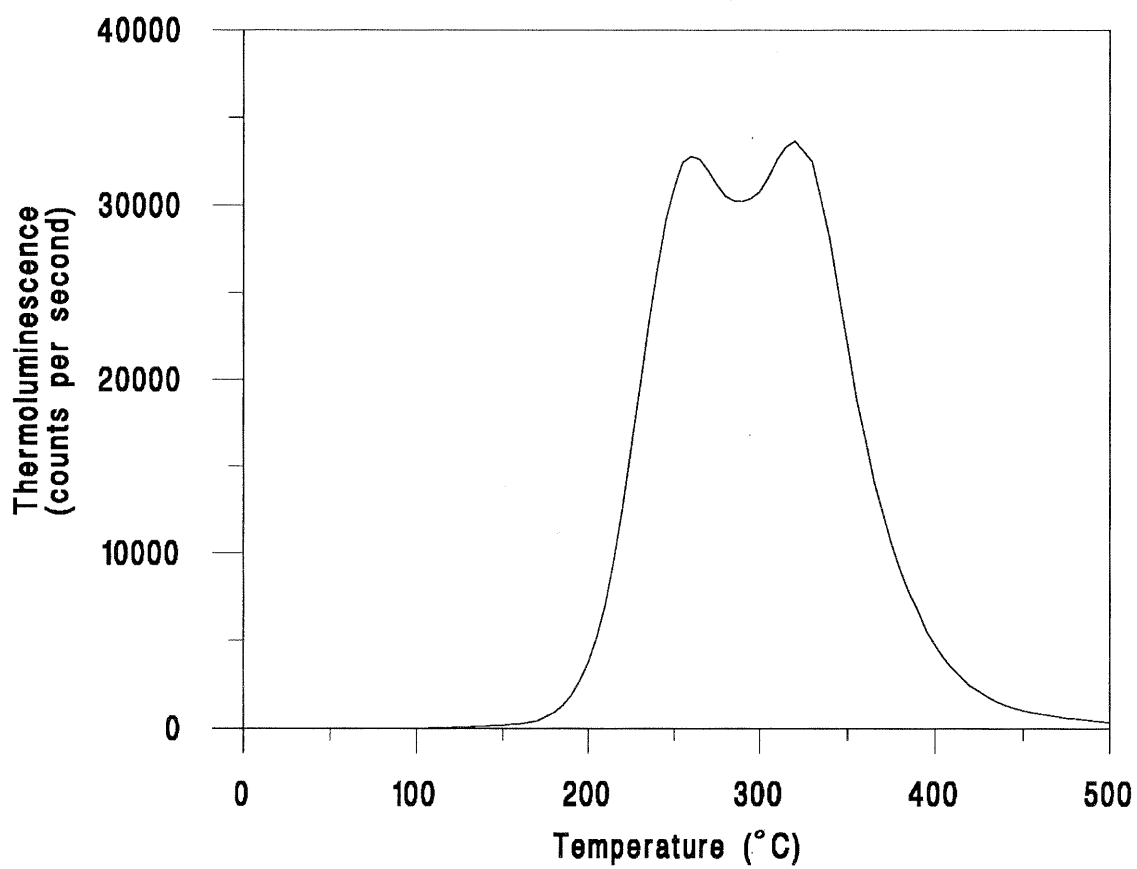


Figure 1.2.2: Thermoluminescence glow curve for potassium feldspar separated from sample GDNZ 1. The sample was heated at a rate of 3°C/s and the luminescence detected through a 5-58 and BG-39 filter combination.

stimulated luminescence is called infrared stimulated luminescence (IRSL).

Hütt *et al.* (1988) and Hütt and Jaek (1989) proposed that IRSL from feldspars is a thermo-optical process. They envisaged a two-step process for the eviction of electrons from traps that are of interest in dating (figure 1.2.3(a)). An infrared photon (880nm or 1.37eV) has insufficient energy to raise an electron from the deep trap to the conduction band (this deep trap has a thermal activation energy of 1.55eV, and an optical activation energy of 2.25eV, in the Hütt and Jaek (1989) model). Instead the electron is trapped in a shallow trap following exposure to IR, and from there it may fall back to the deep trap, or it may be raised to the conduction band by the addition of ambient thermal energy (~0.2eV) from the crystal lattice at room temperature. Some of the characteristics of the IRSL signal, as described by various authors (Hütt *et al.* 1988, Duller and Wintle 1991, Duller and Bøtter-Jensen 1992, and Bailiff 1992), can be explained by a model such as that described above. No other model has yet been suggested.

A major advantage of using photons rather than heat to evict trapped charge, is that only the most light-sensitive traps are being probed. It has been shown that the IRSL signal is reduced far more rapidly upon exposure to light than the TL signal (Godfrey-Smith *et al.* 1988 and table 5.4).

Exposure of potassium feldspar samples to continuous IR radiation releases a luminescence signal that decays with exposure time. If the sample is exposed for a number of seconds a plot of the IRSL signal per second versus exposure time can be made (figure 1.2.3(b)). As the length of the exposure increases the IRSL signal falls as the trapped charge population that it is measuring becomes depleted. Short exposures to IR (e.g. 0.1 seconds) are all that are necessary to measure the IRSL signal and such measurements are effectively non-destructive. This contrasts with TL measurements where the heating of the sample erases the signal and may cause changes in the luminescence signal generated per unit radiation dose.

### 1.3 The application of luminescence methods to the dating of Quaternary sediments

For luminescence to be useful as a dating method the signal must be reset by some physical process in the natural environment. Heating the sediment to high temperatures (>300-500°C) empties charge from all the traps and the luminescence signal is set to zero. Luminescence dating of ceramic materials, and sediments heated by volcanic activity,

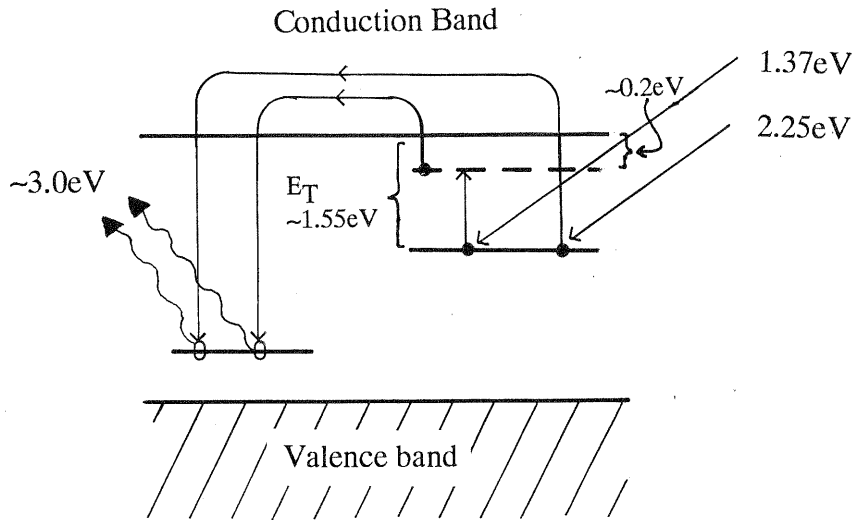


Figure 1.2.3(a): Energy diagram of optically stimulated luminescence processes in potassium feldspar modified from the Hütt and Jaek (1989) model.

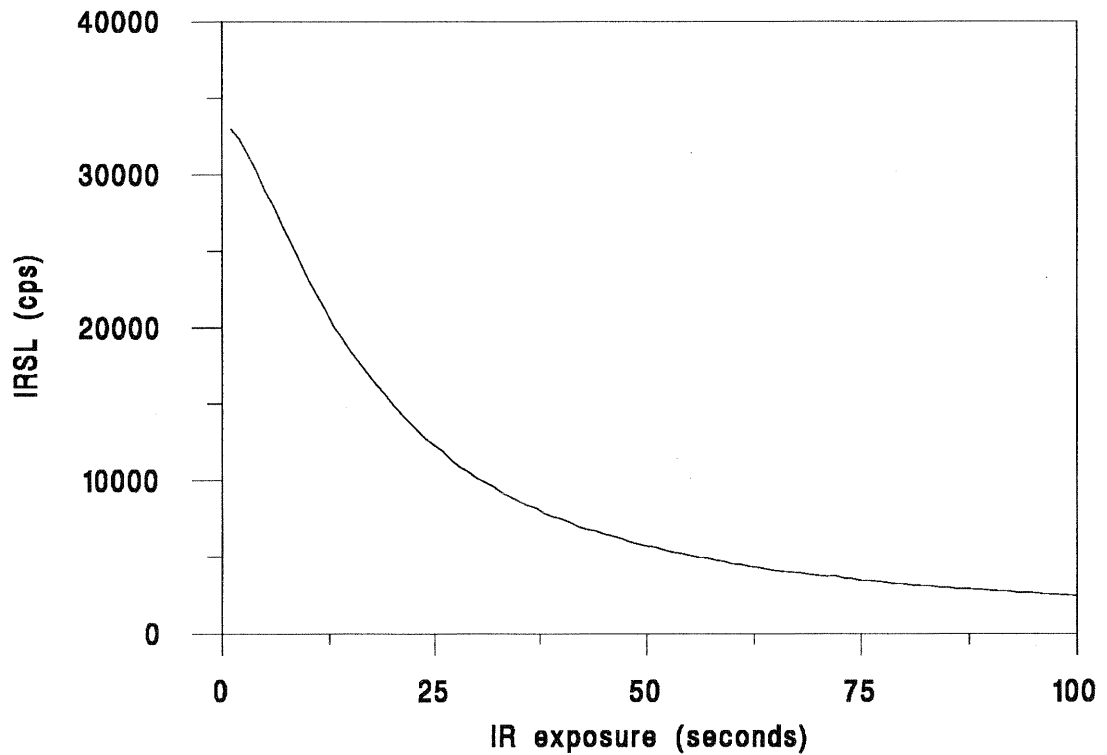


Figure 1.2.3(b): The decay of the IRSL signal during measurement, for potassium feldspar separated from sample GDNZ 1.

assume this type of zeroing of the luminescence signal. Sedimentary environments do not reach a sufficiently high temperature for this mechanism to be effective. However, trapped charge may be released by photons as well as by heat. Exposure of sediments to light during transport or deposition reduces the trapped charge population, and this is the event dated when applying luminescence methods to sediments. Exposure to sunlight does not empty all the trapped charge in the crystal and a residual luminescence signal still remains at the time of deposition. This level may be estimated by experiments within the laboratory. For any given exposure to sunlight this residual level is lower when measured using OSL rather than TL.

Following resetting of the luminescence signal at the time of deposition and burial, exposure to natural ionizing radiation leads to an initially linear growth in luminescence with dose. As the cumulative radiation dose to which the sample has been exposed increases, the number of traps remaining empty decreases. At large doses very few of the electrons and holes liberated by the ionizing radiation are able to find vacant traps. Thus as the cumulative radiation dose increases, the trapping of charge becomes less and less efficient, and when further exposure to radiation causes no increase in the luminescence signal, the latter is said to be 'saturated'. This limits the radiation dose (and hence the age) that can be measured using this type of technique.

As discussed in section 1.1 luminescence dating requires the determination of two parameters. The first is the radiation dose that the sample has been exposed to since the time of deposition. This is known as the 'Equivalent Dose' (ED) and is measured in grays (Gy). The second parameter is the annual radiation dose that mineral grains in the sample would have received when buried. Ionizing radiation within the environment comes principally from radioactive decay of isotopes of potassium, rubidium, uranium and thorium. For potassium feldspars the total radiation flux can be divided into three components. Firstly, the presence of any of these isotopes within the feldspar grains themselves gives the internal dose. Secondly, the presence of any of these isotopes in the material surrounding the feldspar grains gives the external dose. Finally, an additional source is cosmic radiation originating from outside the Earth's atmosphere to give the cosmic dose. The sum of all these components gives the dose rate measured in grays per year (Gy/yr). The age of the sample can then be determined using the equation given in section 1.1.

## 1.4 Aims of the thesis

This thesis has three broad aims:-

- A) To test various luminescence dating methods using potassium feldspar as the dosimeter. Previous attempts (e.g. Balescu *et al.* 1991) have been hindered by the lack of samples with good independent age control. A sequence of raised marine terraces near Wanganui, New Zealand, together with several tephra horizons found in the area, offer an opportunity to test these methods.
  
- B) To apply luminescence dating methods to dunes with poor age control. In the Manawatu and Horowhenua regions, 100 km to the south-east of Wanganui, are relict dunes collectively known as the Koputaroa dune phase. The dunes are unusual in that they are known to have been active immediately prior to the time of the last glacial maximum (e.g. Hesp and Shepherd, 1978), though there is very little control on when dune activity started and finished. Given the topography of this part of New Zealand, and assuming a eustatic drop in sea level at 20ka of at least 100m, the coastline would have been in excess of 30km distant (see chapter 2). Hence luminescence dating will be used to provide ages for a number of sections that have been classified as belonging to the Koputaroa dune phase, and thus to gain some insight into the time period over which they were active.
  
- C) To develop and investigate methods of ED determination using potassium feldspar that allow faster, and/or more precise, age determinations than existing methods. Using existing methods, dating is a slow and labour-intensive process. This is a major hindrance since it prevents the processing of a large number of samples from a section or area. Luminescence measurements using IR are non-destructive and this has enabled the development of methods of ED determination based upon a single aliquot of a sample. A consequence of these developments has been a need for investigation of the fundamental behaviour of the IRSL signal from potassium rich feldspars.

# **CHAPTER 2: Dune sands in the Wanganui, Horowhenua and Manawatu regions, New Zealand**

The samples analyzed in this thesis have been collected from the Wanganui, Horowhenua and Manawatu regions in the southern part of the North Island of New Zealand. This area contains a diverse array of Quaternary sediment types spanning a broad time range. This chapter describes the geological framework of the area from which these samples were taken.

## 2.1 Geological Setting

The two principal islands making up New Zealand lie astride the boundary of the Pacific and Indo-Australian tectonic plates (figure 2.1(a)). The nature of the plate boundary changes significantly as it passes through the country. South of the South Island, the Pacific Plate is overriding the Indo-Australian Plate, but as the boundary passes onto the South Island the relative motion between the plates becomes predominantly transform and this gives rise to the Alpine Fault. Further north the precise nature of the boundary is unknown through Cook Strait, but off the east coast of the North Island the Pacific Plate is being subducted beneath the Indo-Australian Plate. A large accretionary prism has formed and part of this can be seen in the structure of the east coast of the North Island. Compression, due to collision of the two plates, has caused the uplift of greywacke ranges that run parallel to the east coast of the North Island, inland from the accretionary prism. Further west from the line of subduction, the Taupo Graben is dominated by arc volcanics (the Taupo Volcanic Zone, TVZ), with three volcanic cones active at present. Subduction to the north of New Zealand is expressed in the Tonga-Kermadec Island-Arc System.

The area studied in this thesis is the coastal strip of the North Island running from Hawera in the north-west to Otaki in the south (figure 2.1(b)). The entire area lies within the southern Wanganui depositional basin. This has been a depositional centre for most of the Plio-Pleistocene with up to 4000m of sediment accumulating in that time (Anderton 1981). The basin is a broad half-graben orientated NNE-SSW, bounded to the west by basement highs (D'Urville and Patea highs) and to the east by several major faults (Turakina and Rangitikei faults), separating it from the greywacke axial ranges running NNE-SSW through the North Island. The basin has evolved through time with the depositional centre moving from a

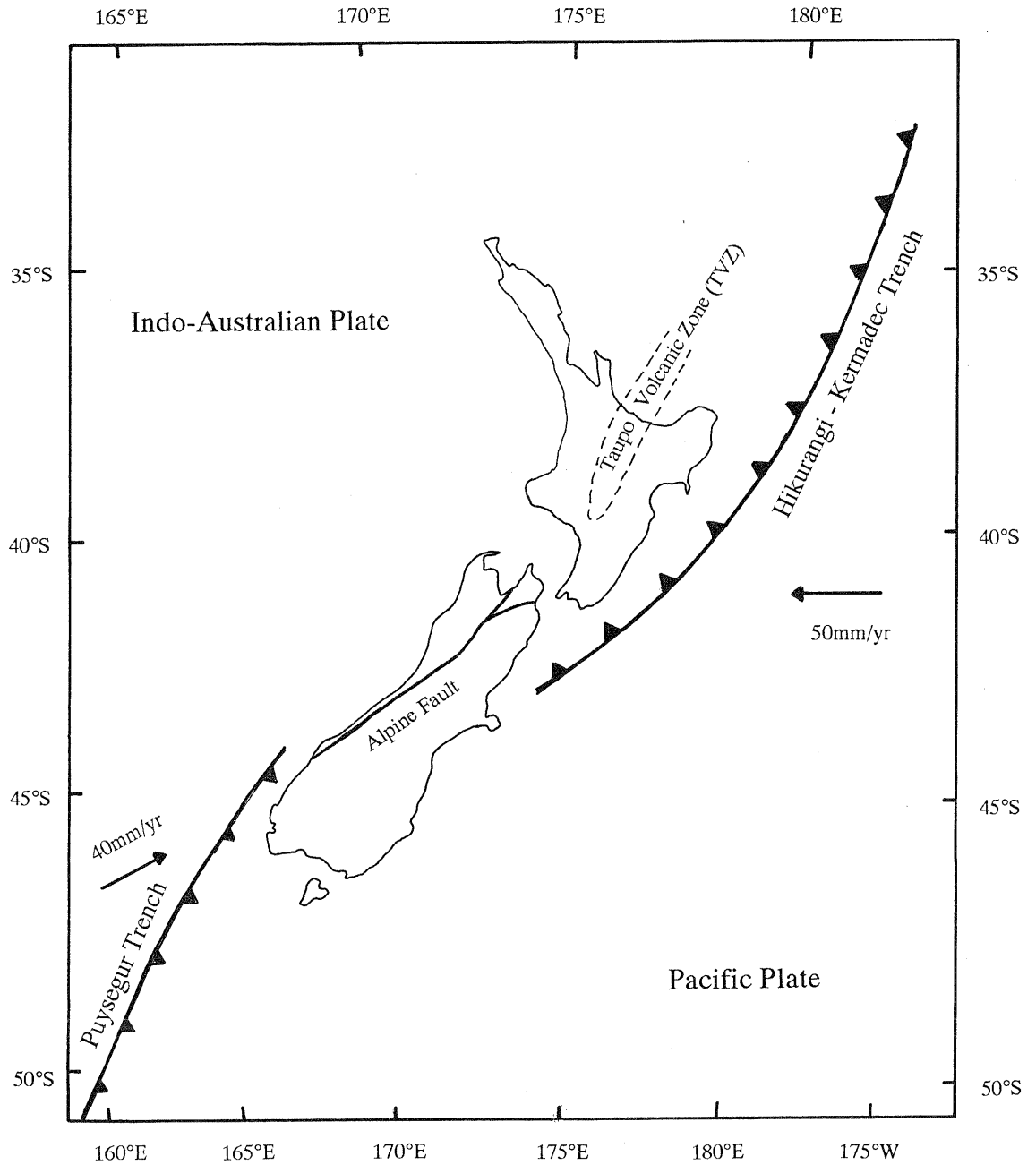


Figure 2.1(a) Map showing the position and relative motions of the major tectonic plates in the vicinity of New Zealand (after Berryman *et al.* 1992).

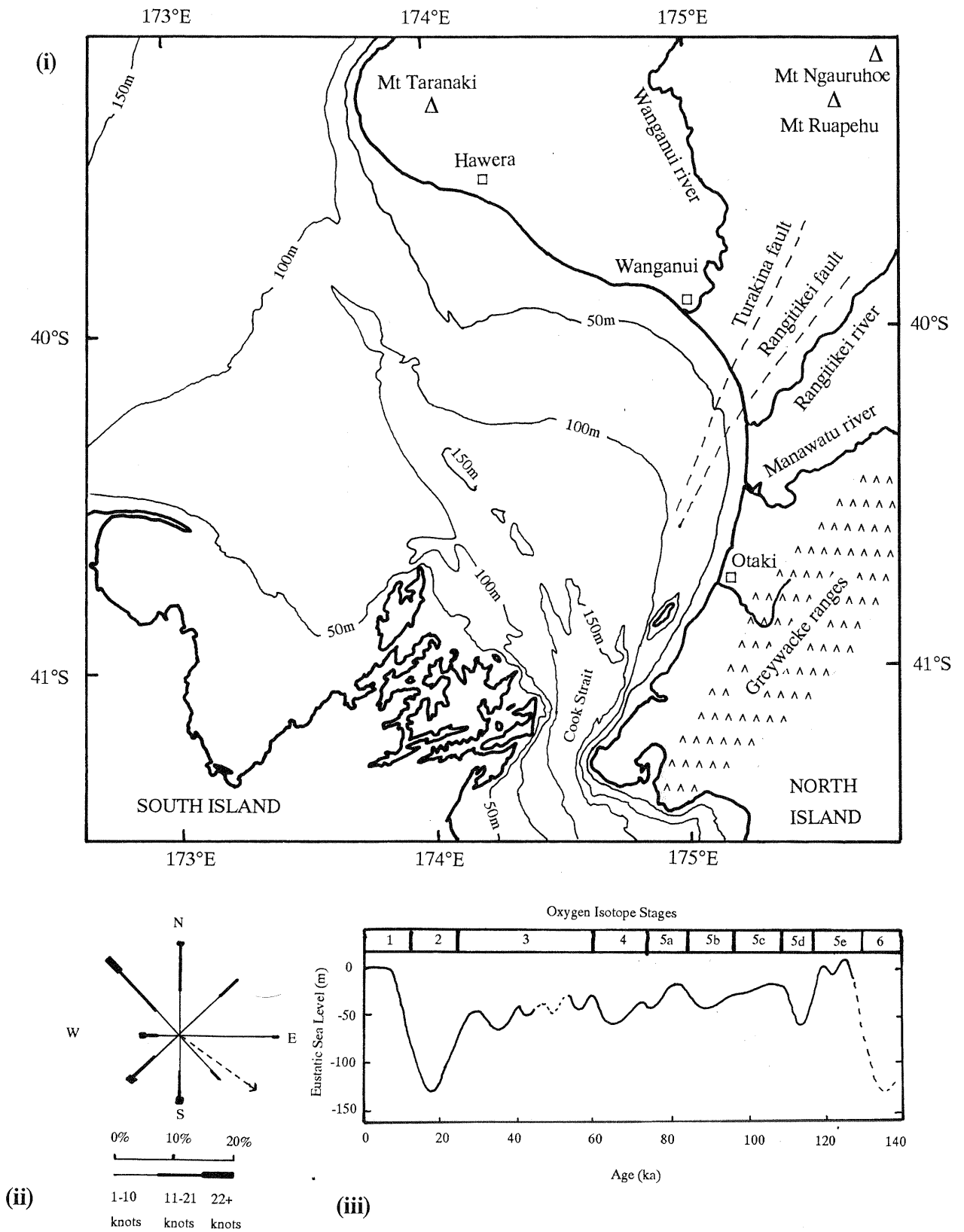


Figure 2.1(b): (i) South-Western part of the North Island of New Zealand and the northern part of the South Island. Bathymetry data is taken from Lewis (1979). (ii) Wind rose for Te Horo compiled for the period 1972-1976 (Muckersie pers. comm.). The Freyberger sand drift potential is shown as the dashed arrow. (iii) Sea level change for the last 140 kyr derived from dating of coral terraces on the Huon peninsula (from Chappell and Shackleton (1986)).

position centred on Hawera in the late Pliocene, to Wanganui in the early Pleistocene, and finally to a position approximately 50km south of Wanganui today. Thus although much of the area has been subsiding, there has been an element of tilting (shore-normal at Wanganui) that has led to the uplift and exposure of a Plio-Pleistocene sequence north of Wanganui. Anderton (1981) interprets the basin as being an extension of the Taupo Graben, although the relationship between the two areas is obscured by the volcanic activity in the Taupo Volcanic Zone. The movement of the depositional centre results from the southward migration of the subduction zone beneath northern New Zealand.

Deposition within the Wanganui basin has closely matched the rate of subsidence and most of the sediments laid down during the Plio-Pleistocene are shallow marine. Today none of the continental shelf within the Taranaki bight is deeper than 150m, and the majority of the area is much shallower than this (Lewis 1979, figure 2.1(b)). Sea level has fallen during the Quaternary by as much as 120m on many occasions and has exposed much of the continental shelf in this area.

Along the coastline, from Hawera to Wanganui, the combination of uplift and changes in sea level has created a series of marine cut terraces extending up to 20km inland and to heights of 300m above present sea level (Pillans 1983, figure 2.1(c)). These typically consist of a wave cut surface rising slightly in altitude to a fossil sea cliff at the landward margin. Marine sands commonly overlie the wave cut surface, and these are covered in turn by terrestrial deposits (loess, tephra, lahar deposits, fluvial sediments and dune sands). South-east of Wanganui the combination of faulting, associated with the Turakina and Rangitikei faults, and lateral erosion by the Rangitikei river, have combined to prevent the preservation of an extensive series of marine terraces. The only terrace that can be identified over some parts of this area is a heavily dissected surface known as the Tokomaru marine terrace, which is believed to date from the last interglacial (Hesp and Shepherd, 1978).

Luminescence dating of the dune sands on these raised marine terraces is the subject of one part of this thesis. Many of the surfaces on which the dunes are found have had ages assigned to them on the basis of amino-acid racemization results from wood fragments found in marine cover beds overlying the terrace treads (Pillans 1983). The amino-acid racemization results have been calibrated using fission track dates for the Rangitawa pumice (see section 2.1.3). Additional information is available in some sections through the cover beds on the terraces where tephras, that act as stratigraphic, and in some cases chronostratigraphic,

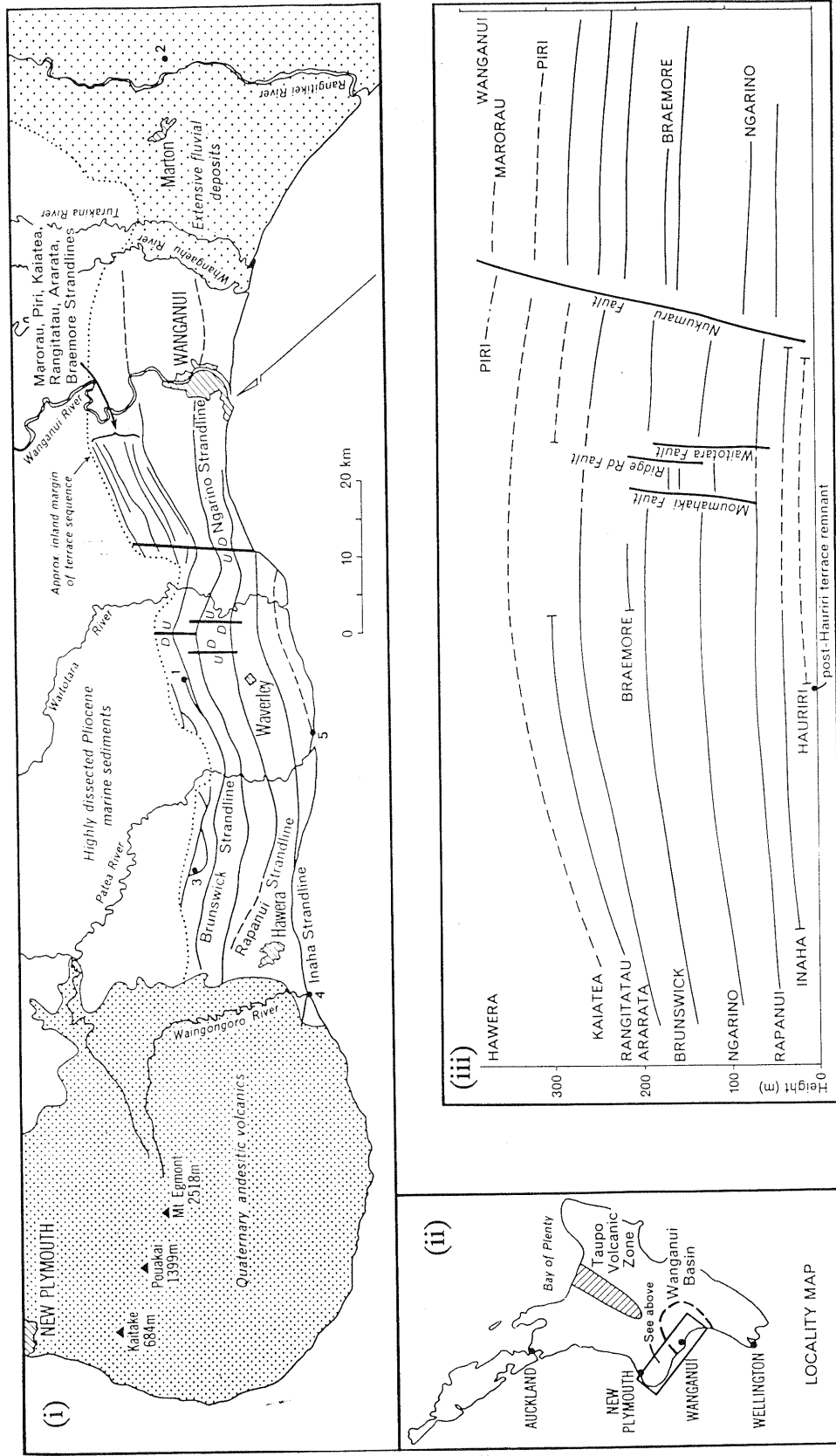


Figure 2.1(c): (i) Map showing the locations of terrace strandlines in the area between Hawera and Wanganui. (ii) Map showing the area illustrated in map (i) relative to the rest of North Island New Zealand and the Taupo Volcanic Zone. (iii) Shore-parallel deformation pattern, indicated by variation in strandline heights, between Hawera and Wanganui. All figures taken from Pillans (1983).

markers can be found. Dune sands from these terraces constitute the samples of 'known' geological age on which luminescence dating methods are to be tested.

### 2.1.1 Sediment types and sources

Sediment is transported into the Wanganui basin from three major sources. Firstly, sediments derived from the greywacke axial ranges are transported down the Rangitikei river, Manawatu river and many smaller streams in the east and south of the basin. Cowie (1964a) has suggested that during episodes of cold climate these rivers became braided, with broad stream channels from which fine grained material could be deflated by aeolian activity giving rise to the extensive loess deposits found in the region.

The two other possible sources of sediment are the volcanic centres of Taranaki and Taupo. Volcanic ash is found over all of the area studied here (see section 2.1.2). Closer to the two volcanic centres lahar deposits and ignimbrites are common. Today, much of the marine sand along the coastline from Taranaki to Wellington is mafic, volcanically derived sand.

### 2.1.2 Tephra stratigraphy and chronology

Andesitic and rhyolitic volcanoes in the Taupo Volcanic Zone, and the area around Taranaki further to the west, have produced a series of airfall tephtras that can be traced over the area studied in this thesis. A number of these have been traced into the South Pacific (Kyle and Seward 1984 and Froggatt *et al.* 1986), but many more can be traced within North Island, New Zealand forming invaluable stratigraphic markers. Correlation of tephtra layers from one site to another is based upon major element geochemistry. Many tephtra are also used as chronostratigraphic markers based upon radiocarbon or fission track ages. Froggatt and Lowe (1990) have reviewed the geochemistry, nomenclature, distribution and age of major silicic tephtras from the North Island over the past 50,000 yrs, but a far longer record is known to exist back to at least 2.8Ma (Seward 1979).

Within the area studied, four tephtra horizons are of major geological importance. In order of increasing age these are, Taupo Pumice, Kawakawa tephtra, Mt.Curl tephtra and Rangitawa pumice.

Taupo Pumice originates from an eruption in the Taupo volcanic centre about 6,000 yrs BP. The total eruptive volume is estimated at 133km<sup>3</sup> (Froggatt and Lowe, 1990) and the pumice forms a major marker horizon in Holocene deposits. However it is not relevant to any of the samples collected in this study.

Kawakawa tephra was first identified in the Manawatu area as a distal ash unit, and named the Aokautere Ash (Cowie 1964b). Subsequently it has been linked with major ignimbrite units near the Taupo eruptive centre, and the whole unit is now called the Kawakawa tephra. Many radiocarbon dates have been determined for this unit (Froggatt and Lowe, 1990) but the most reliable estimate is that by Wilson *et al.* (1988) working on charcoal fragments found within the ignimbrite member. These gave a mean age of 22,590±230<sup>14</sup>C yrs BP. Using the <sup>14</sup>C calibration derived from U/Th dating of corals (Bard *et al.* 1990) this would place eruption of the Kawakawa tephra at approximately 24 ka. The distal ash has been traced to deep-sea sediments as far as 4000km south-east of New Zealand (Kyle and Seward 1984). However, within the area of this study the ash is between 1-15cm in thickness and thus easily recognizable. The Mt.Curl Tephra and the Rangitawa Pumice are discussed below.

### 2.1.3 Age of the Mt.Curl Tephra and Rangitawa Pumice

Pillans (1983) proposed a chronology for the flight of marine terraces running from Hawera to Wanganui based upon amino-acid racemization values determined for wood found in many of the cover units on the terraces. The results of these amino-acid measurements were calibrated using a fission track age for the Rangitawa Pumice. This date was the linch-pin for the whole terrace chronology.

Rangitawa Pumice was first mentioned by Te Punga (1952) and subsequently dated using fission track methods on glass and zircons (table 2.1.3). Within the Wanganui basin another rhyolitic tephra that was commonly used as a stratigraphic marker was Mt.Curl Tephra (Milne 1973). This too has been fission track dated several times (table 2.1.3). The stratigraphic position of these tephras upon the marine terrace surfaces, and within the loess appeared perfectly consistent with the fission track ages determined prior to 1992 (Pillans, 1988).

Table 2.1.3

Fission track ages determined for the Mt. Curl Tephra and the Rangitawa Pumice by various authors.

<b>Mt. Curl Tephra</b>			<b>Rangitawa Pumice</b>		
<u>Study</u>	<u>Material</u>	<u>Age (ka)</u>	<u>Study</u>	<u>Material</u>	<u>Age (ka)</u>
Kohn (pers.comm. in Milne, 1973)	glass	230±40	Seward (1976)	glass	380±40
Seward (1979)	zircon	230±60	Boellstorff and Te Punga (1977)	glass	390±100
Pillans and Kohn (1981)	glass	230±50	Pillans and Kohn (1981)	glass	370±70
Pillans and Kohn (1981)	zircon	240±50	Pillans and Kohn (1981)	zircon	370±50
Kohn <u>et al.</u> (1992)	zircon	340±30	Kohn <u>et al.</u> (1992)	zircon	400±90
Kohn <u>et al.</u> (1992)		Combined weighted mean for the two tephra: 350±40 ka			

However, Froggatt et al. (1986) working on tephra recovered from deep sea cores and from sections on land, showed that the two tephra were indistinguishable on the basis of major element geochemistry. They suggested that they were correlative and proposed an age of 254±2 ka based upon spectral analysis of the oxygen isotope record from the deep sea core (DSDP 594) in which the tephra was recovered. This view was reinforced by the similarity in the appearance of the two tephra in the field, and by the inability to find both tephra in a single section.

When samples were collected for this study (1988) it was considered that the two tephra were distinct (e.g. Pillans 1988), and that the fission track dates were reliable. However, the record from deep sea core DSDP 594 has been reanalyzed by Nelson (1988) who revised the position of the Brunhes-Matuyama boundary and certain microfossil datums in the core. The new chronology provided for the core by this analysis dates the tephra identified by Froggatt et al. (1986) at 335±10 ka.

Recently Kohn et al. (1992) have produced a series of new fission track ages for the Rangitawa and Mt.Curl tephra using zircons (table 2.1.3). At their respective type sites, they yielded ages of 400±90 ka and 340±30 ka respectively. On the basis of these dates, the

similarity of the geochemical signatures of the tephtras, and the inability to find the two tephtras in a single section, they considered the two tephtras to be correlative. Along with dates for samples of the tephtras from other sites Kohn *et al.* (1992) calculated a weighted mean age for the tephtra of  $350\pm 40$  ka ( $1\sigma$ ). Previous dates obtained for the Mt. Curl Tephtra are believed to have been underestimated because of under-etching in the laboratory preparation of the samples during fission track analysis (Pillans pers.comm.). The new age of  $350\pm 40$  ka, produced on the basis of the fission track dating, is used in this thesis.

## 2.2 Dunes phases identified in the Horowhenua and Manawatu regions

The majority of dunes found within the cover beds of the Wanganui terrace sequence do not show any characteristic topographic form because they are overlain by younger deposits. However, along the coastline south-east from Wanganui extensive areas are covered either by active dunes, or relict dunes with a distinct morphology. These were first studied by Cowie (1963) who distinguished four phases of activity based upon the degree of soil development on the dune surface. These were called (from youngest to oldest), Waitarere, Motuiti, Foxton and Koputaroa, and were tentatively assigned ages of 0-100yrs BP, 500-1,000yrs BP, 2,000-4,000yrs BP and 10,000-15,000yrs BP. Shepherd and Lees (1987) used  $^{14}\text{C}$  dating of peat found within dunes of Foxton age to suggest that this phase of dune activity was initiated as early as 5,500-6,000 yrs BP, but that it was still active as late as 1,600 yrs BP.

The age of the Koputaroa dunes suggested by Cowie (1963) was largely based upon the presence of Kawakawa tephtra within certain dune sections. Additionally the existence of dunes of this phase lying upon parts of an alluvial fan (Ohakea surface, Palmer *et al.* 1988), at Otaki, show that at that location they must have begun to form after deposition of the Ohakea surface. Subsequently, the cessation of aggradation of the Ohakea surface has been dated at between 10-12 ka (Palmer *et al.*, 1988) and the Kawakawa tephtra at  $22,590\pm 230^{14}\text{C}$  yrs BP (mean of four radiocarbon ages, Wilson *et al.*, 1988). The majority of the dunes of the Koputaroa phase lie upon the Tokomaru marine terrace. This is thought to be last interglacial in age (Hesp and Shepherd, 1978), and this is the maximum limit to the age of the dune phase.

The origin of the Koputaroa dunes is as uncertain as their age. On the basis of their altitude (approximately 30m a.s.l.) and the eustatic lowering of sea level that occurred during the last glaciation, Cowie (1963) suggested that the dunes could not be related to the coast, and thought it more likely that they originated from braided rivers. On the basis of heavy mineral content, and grain roundness, Shepherd (1985) thought that at least some of the Koputaroa phase dunes were derived from a marine source. However given the low relative sea level at 24 ka, this required that the dunes migrated about 30km inland. The determination of the period during which dunes of the Koputaroa phase were active is the second main aim of this thesis and is pursued in chapter 8.

Chapters 3 and 4 describe sample collection and preparation, and the basic equipment and techniques used for luminescence dating in this thesis. In chapter 5 these techniques are applied to samples of dune sand, collected from the Wanganui, Horowhenua and Manawatu regions, for which independent age estimates are available.

## **CHAPTER 3: Sample Collection and Preparation**

### 3.1 Precautions in sample collection

The nature of luminescence dating methods means that the primary precaution to be observed when sampling is not to expose the sample to light. With the use of IRSL and other optically stimulated luminescence methods, in addition to TL, this requirement has become even more stringent (e.g. table 5.4 which shows how rapidly the IRSL signal may be bleached). All samples used in this thesis were collected in one of two ways. The first method was to use metal tins, about 10cm in diameter and 15cm in depth. These were pushed into the section. In the laboratory the outer surface of the sediment within the tins was removed. Unfortunately this could only be carried out where the sample was sufficiently soft to allow the tin to be pushed in.

Where this was not possible a second method was employed; the sample was collected whilst the section was shielded from light by a large ( $>3\text{m}^2$ ) sheet of black plastic. From underneath this sheet the section was cleaned back to ensure that reworked material was not included. The sample was then put into a black plastic bag.

When selecting sample sites, three criteria were considered. Firstly, quartzo-feldspathic sands were chosen in preference to very mafic samples. This was to ensure that a sufficient quantity of potassium feldspar could be separated. Secondly, samples were taken from homogeneous units to simplify the dosimetry. This was especially important since a gamma spectrometer was not available when collecting the samples. Finally, only dune sands were sampled. These were preferred over beach sands due to the greater extent of bleaching that occurred at deposition.

### 3.2 Sample Preparation

All laboratory preparation was undertaken in subdued orange light to prevent loss of the luminescence signal during sample processing and measurement. Spooner(1987) measured the transmission characteristics of various filters manufactured by 'Chris James' (figure 3.2(a)). In the Aberystwyth laboratory eight layers of Deep Orange (158) have been used to filter light from standard neon strip lights, and light levels are kept as low as possible.

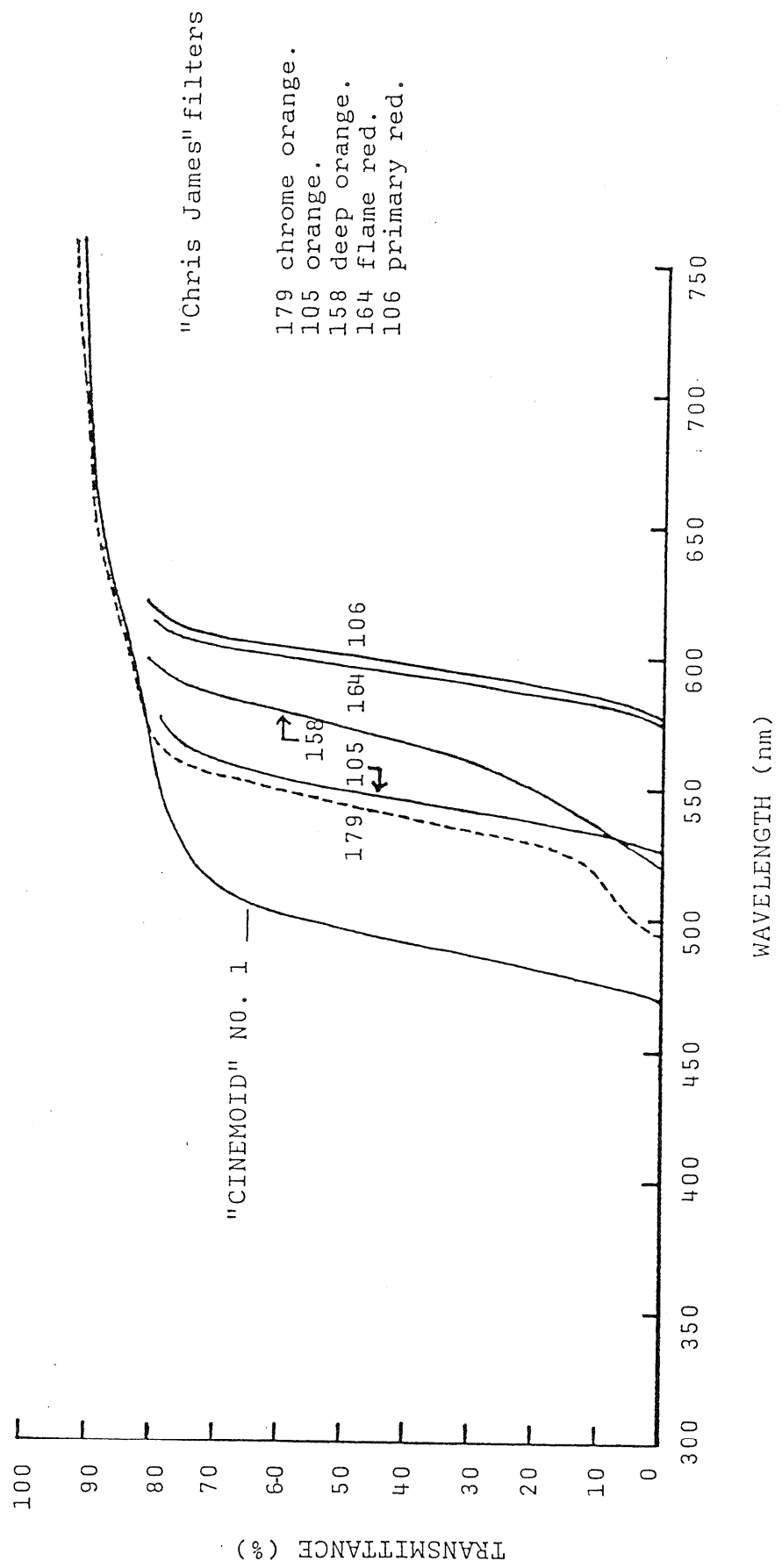


Figure 3.2(a): Transmission characteristics of a selection of "Chris James" colour filters (from Spooner, 1987).

Sample preparation followed the standard method as used by Mejdahl(1985) and Kolstrup *et al.* (1990). Samples first had their carbonates removed using HCl (10%) and their organics using H<sub>2</sub>O<sub>2</sub> (30%). Many of the samples from this part of New Zealand were found to have significant amounts of fine material (<50µm). Dry sieving was not effective at removing this material from the larger grain sizes. Thus samples were dispersed in 0.05M Sodium Oxalate and then wet sieved through a 50µm nylon mesh. This procedure was repeated 3-4 times until the water washed through the sieve was clear.

The material remaining in the 50µm mesh was then dried and sieved through a stack of 4 inch diameter stainless steel sieves. Sieves of 90, 125, 150, 180, 212, 250, 300 and 355µm aperture were used. In this way a narrow size range could be obtained. It is important to separate a narrow grain size range since calculations of both the internal and external dose rates are dependent upon the grain diameter. For a hypothetical sample with an internal potassium content of 10% and external dose rates typical of the samples studied here (1.2Gy/ka infinite matrix β-dose and 0.8Gy/ka γ dose), figure 3.2(b) shows the effect for various mean grain sizes of altering the size range used for equivalent dose determination upon the error in the dose rate calculated. For simplicity no errors were assigned to any variable other than the grain size, and no alpha doses were included. It is clear that the choice of a narrow grain size is highly advantageous. For this study the grain size from 180-211µm was used wherever possible to keep this error to less than 2%.

Figure 3.2(c) shows the grain size distributions for a number of the samples, determined using the range of sieves available. The data are not complete since the material finer than 50µm was removed prior to sieving. However, the histograms do show that the majority of samples showed a peak in their grain size distribution at about 150-250µm.

### 3.2.1 Potassium feldspar separation

The normal method for the extraction of a potassium feldspar rich fraction is based upon density separation. In spite of attempts in the field to sample only quartzo-feldspathic rich units, some of the samples were very dark in colour. Performing density separation upon these samples was time consuming since up to 50% of the sample by weight consisted of material with a specific gravity greater than 2.70. To speed up the procedure, prior to density separation samples were repeatedly run through a Cook Magnetic Separator (forward slope 30°, side slope 10°) at currents increasing from 0 to 1.9A. This removed a large proportion of the mafic minerals, which tend to have higher magnetic susceptibilities than quartz and feldspars.

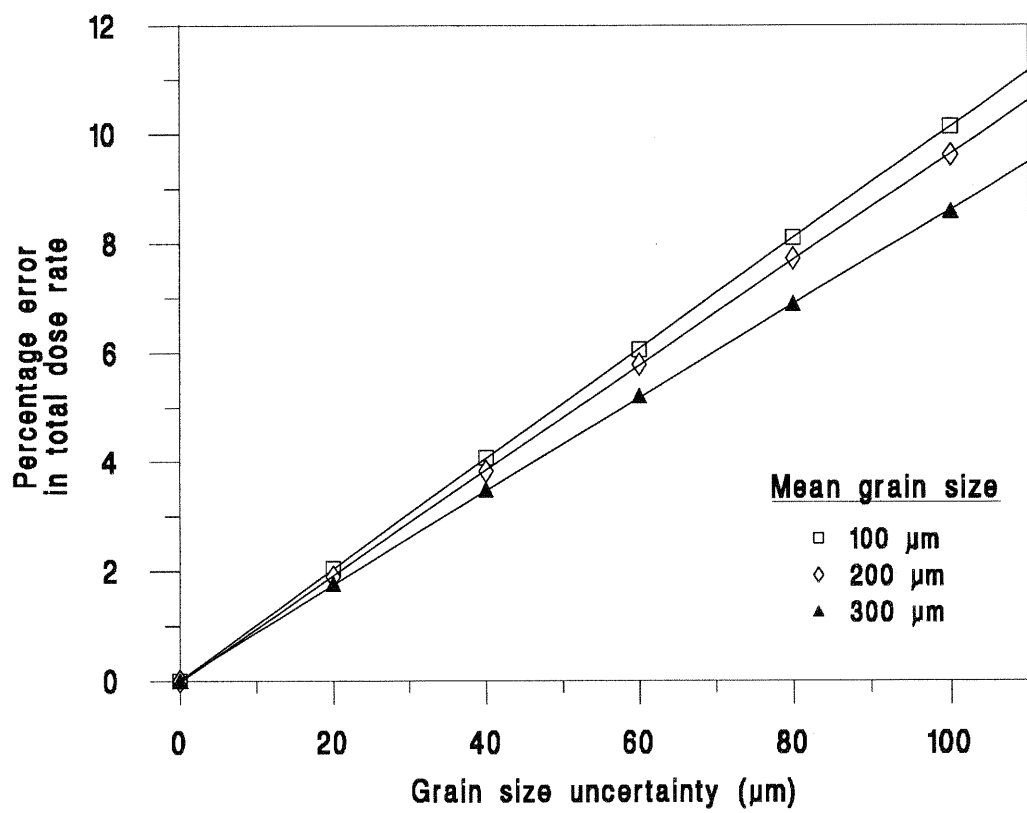


Figure 3.2(b): The effect of uncertainties in the grain size selected for ED determination upon the calculated total dose rate for a variety of different mean grain sizes. See text for details of the assumptions used.

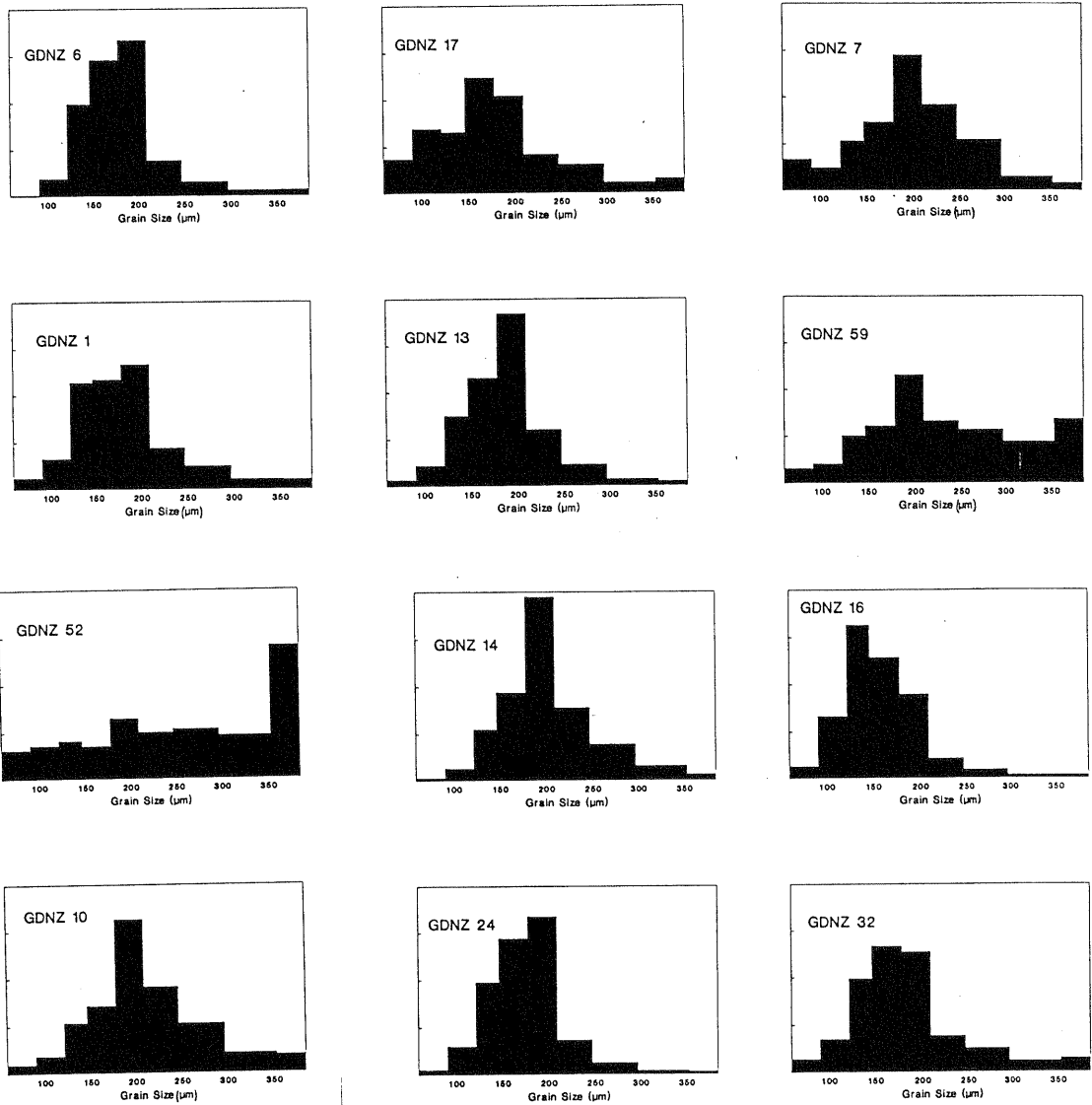


Figure 3.2(c): Grain size histograms for a number of the samples analyzed.

Samples were then separated according to density using solutions of sodium polytungstate with a specific gravity of 2.62, 2.58 and 2.53. An initial separation divided material with densities greater than and less than  $2.62 \text{ g cm}^{-3}$ , and was used to separate the feldspars from the quartz and heavy minerals. The material with a specific gravity less than 2.62 was then separated using solutions with specific gravities of 2.58, and additionally 2.53 sometimes, to give a potassium rich feldspar portion with specific gravity less than 2.58 and greater than 2.53. The final separation of material using a solution at a specific gravity of 2.53 was initially used, but it was found that virtually no material had a specific gravity less than 2.53 and so it was not used for samples prepared later.

### 3.2.2 Use of hydrofluoric acid for etching the surface of potassium feldspar grains

Initially potassium-rich feldspar fractions separated from samples used in this study were etched in 10% hydrofluoric (HF) acid for 40 minutes. This was carried out using light-tight Nalgene bottles that could have HF added and poured off via black Nalgene tubes, under normal lighting conditions, without exposing the sample to light. This procedure was considered much safer than using an HF fume cupboard in a dark room.

HF etching is designed to remove the alpha irradiated outer layer of the grain to simplify the dosimetry. However, from a consideration of the crystal structure of feldspars it seems highly unlikely that HF etching of a grain will remove a uniform 'shell' around the grain as assumed. It would seem far more likely that etching will preferentially occur along crystal planes, so causing the grains to split and disintegrate. Some evidence for this is the cloudy nature of the HF acid when poured off after etching, and the large loss of mass sometimes seen (up to 30% by weight). Scanning Electron Microscopy (SEM) of etched and unetched grains of GDNZ 17 (figure 3.2.2) shows that prior to etching the grain surfaces are generally smooth and the grains are rounded as expected given the aeolian origin of the sediment. After etching many of the grains show deep etch pits and accentuation of cleavage planes and other lines of weakness.

Etching with HF has been promoted on the basis of its long use in archaeological dating procedures. Etching with 48% HF acid has been used to remove the outer 'shell' of quartz inclusions used in the dating of pottery for three reasons (Aitken 1985, p.256). Firstly, uranium and thorium may have diffused into the outer layers of the grains from the surrounding matrix during firing. Secondly, it was feared that diffusion of iron and other impurities during firing would complicate the glow curve shape because of the introduction of TL traps and luminescence centres. Finally, it was used to remove the

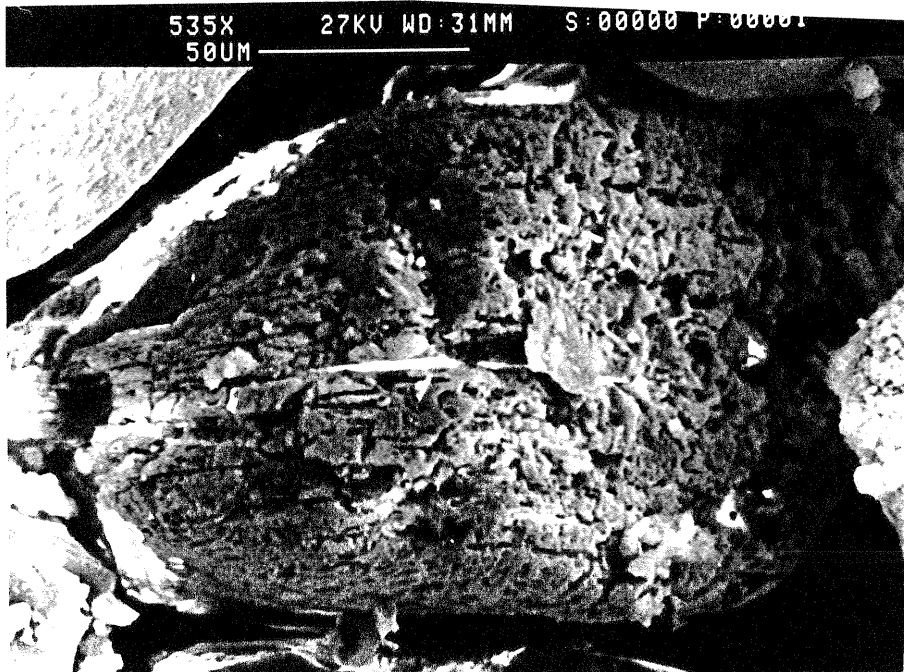
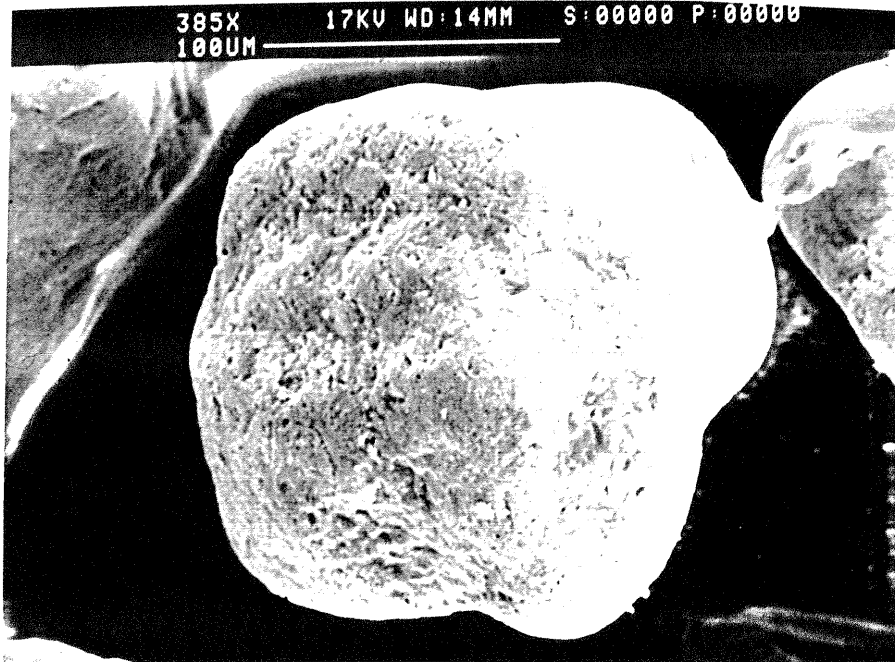


Figure 3.2.2: Scanning electron microscope image of potassium-rich feldspar grains (specific gravity less than 2.58) before (above) and after (bottom) etching with 10% hydrofluoric acid for 40 minutes.

outer, alpha dosed, layer of the quartz to simplify the dosimetry. This contribution can be fairly significant if the annual dose rate is low, but it is highly dependent upon the water content of the sediment.

Etching has been automatically adopted when dating potassium feldspar, firstly in pottery and then in sediments. However, when one considers the reasons for its use, as listed above, none are relevant for potassium feldspars extracted from sediments. In particular, the uncertainty in the alpha dose rate, due mainly to uncertainties in the water content, is relatively small since the internal beta dose rate due to the high potassium content, and the external beta and gamma dose rates, are so large. Thus samples prepared later during this study have not been etched and their total dose rates have been calculated accordingly (see table 5.3.3.).

### 3.3 Mounting of samples

For ease of handling, normalization, bleaching and dosing, samples were mounted on 9.7mm diameter aluminium discs following the method described by Spooner (1987). Discs were sprayed with 'Silkospray' silicone oil while being held in a frame, the cover of which was designed to prevent silicone oil from landing on the outer 1mm rim of the disc. This was to prevent grains from sticking to the edge of the disc where they could easily be dislodged. Sample weights varied from about 4-10mg per disc. Weights larger than this were avoided where possible since a monolayer was desired. Heating of the sample on disc did cause the grains of some samples to become relatively loose, and great care was needed if the discs were handled following TL measurement (see section 4.6).

## CHAPTER 4: Equipment and Measurement

### 4.1 The Risø automated TL reader

The majority of luminescence measurements in this study were made using a Risø TL-DA-10 automated thermoluminescence reader with an IRSL add-on unit (Bøtter-Jensen *et al.*, 1991). The system comprises a carousel capable of holding 24 samples, a hotplate, an array of infrared diodes and a beta source. Luminescence is measured using an EMI 9635QB photomultiplier tube, with a dark count of approximately 200cps. All of these features run under computer control allowing excellent reproducibility.

#### 4.1.1 The TL set

The Risø hotplate can be heated up to 700°C, though the reader in Aberystwyth is set to an upper limit of 500°C to prevent melting of aluminium sample discs. It is driven by a 12-bit D-to-A converter giving 4096 temperature increments (a resolution of 0.12°C), with feedback provided by a Ni/Cr thermocouple. The accuracy with which the sample is heated is dependent upon the thermal inertia of the hotplate and sample, and the heating rate used. In order to minimise any temperature differences between the sample and the hotplate, a heating rate of 3°C/s was normally used, with approximately 2 litres per minute of argon used as an inert gas to fill the chamber. Figure 4.1.1 shows a schematic diagram of the Risø automated TL reader.

#### 4.1.2 The IRSL add-on unit

Thirty-one infrared emitting diodes were used in measurements of infrared stimulated luminescence (IRSL). The diodes used were TEMT 484 (880Δ80nm) as described by Spooner and Franks (1990). Infrared power was kept constant using feedback from the output of a single diode, transmitted through a light guide to a photodiode maintained at a constant temperature. Initially the unit was run with a diode current of 70mA and some instability in power output was seen. However all measurements reported here were made with a diode current of 40mA. This is under the 50mA limit for stable operation described by Spooner and Franks (1990). Diode power was measured using a photodiode calibrated at Risø, and gave a value of approximately 32mW/cm<sup>2</sup>. No shutter was used in the system since no instability has been reported for diodes run at these currents. Also, the switch on time of the diodes is far superior to that of any shutter (<<1ms, Christiansan pers. comm.). Figure 4.1.2 shows a schematic diagram of the IRSL add-on unit for the Risø reader.

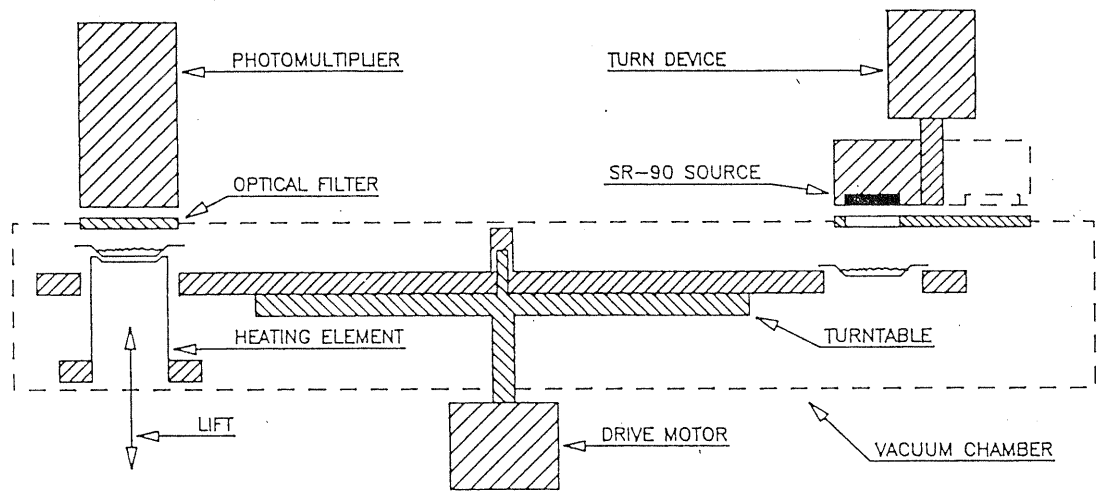


Figure 4.1.1: Schematic diagram showing the main elements of the Risø automated TL reader (from Bøtter-Jensen 1988).

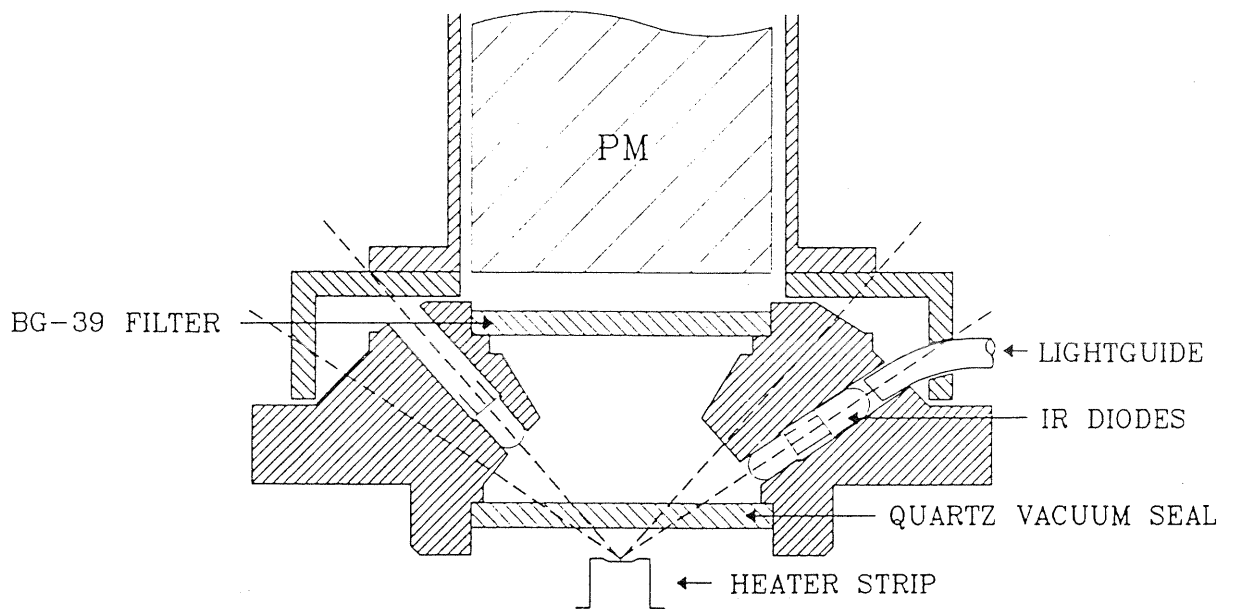


Figure 4.1.2: Schematic diagram of the IRSL add-on unit for the Risø automated reader (from Bøtter-Jensen *et al.*, 1991).

### 4.1.3 The GLSL add-on unit

A limited number of measurements were made using a Green Light Stimulated Luminescence (GLSL) system developed to fit onto the Risø automated reader (figure 4.1.3(a)). GLSL was accomplished by exposure of the sample to a green wavelength band filtered from a 75W halogen bulb. The system was designed for the stimulation and detection of luminescence from quartz (Bøtter-Jensen and Duller, 1992), but was easily changed to optimize it for GLSL measurements on potassium feldspars. Luminescence was measured through a filter combination (12mm of Corning 7-59 and 5mm of Schott BG-39) designed to give maximum sensitivity at 400nm, a major emission peak of potassium feldspar (Huntley *et al.* 1991). Wavelengths from 515-560nm were filtered from the halogen bulb using 6mm of OG-515 and a short-wave-pass interference filter giving a power of  $6.5\text{mW cm}^{-2}$  at the sample. Within the GLSL unit a ring of 13 IR diodes (Telefunken TSHA 6203, peak emission  $875\Delta 80\text{nm}$ , current 40mA, power at the sample  $42\text{mW cm}^{-2}$ ) were used to stimulate IRSL. Figure 4.1.3(b) shows the combined filter transmittance for the detection windows used for GLSL (and IRSL in section 6.6) measurement (A), the combined filter transmittance for filtering the light from the halogen bulb (B), and the emission spectrum for TSHA 6203 IR diodes.

### 4.1.4 Software Development

Software initially available from Risø to run the IRSL add-on unit was limited in that the shortest measurement time possible was one second, and there was no way of controlling the hotplate at the same time. Thus there was no way of ensuring at what temperature IRSL measurements were made. Four pieces of software were written to enable full control of the IRSL add-on. SCAN enabled IRSL measurement for any combination of the 24 positions for periods down to 0.001s. TOL enabled rapid IRSL and TL measurements to be made as a sample was heated from room temperature up to a maximum of 500°C (section 6.5.1). TOB allowed continuous IRSL measurement at elevated temperatures (up to 200°C), and SINGLE enabled a complex sequence of IRSL measurements, radiation doses, IR exposure, and preheating to be performed fully automatically (see chapters 6 and 7).

## 4.2 The Daybreak IRSL set

IRSL measurements for ED determinations on the known age samples were made using a unit built in Aberystwyth, based upon the design by Spooner *et al.* (1990). This used 12

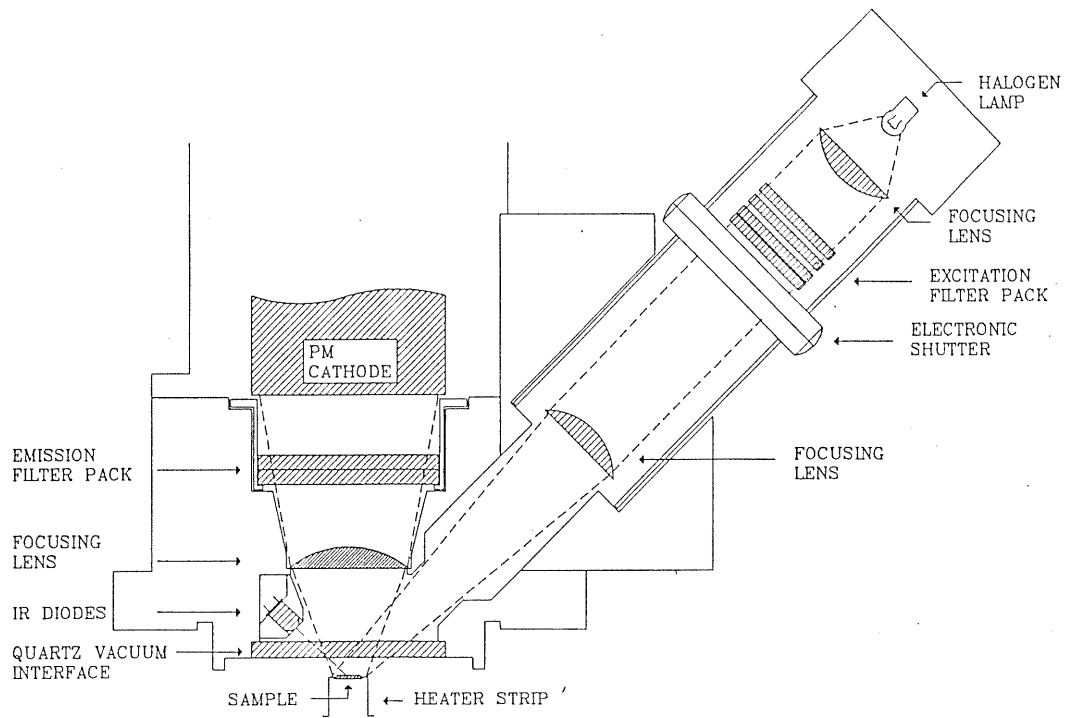


Figure 4.1.3(a): Schematic diagram of the GLSL add-on unit for the Risø automated reader (from Bøtter-Jensen and Duller, 1992).

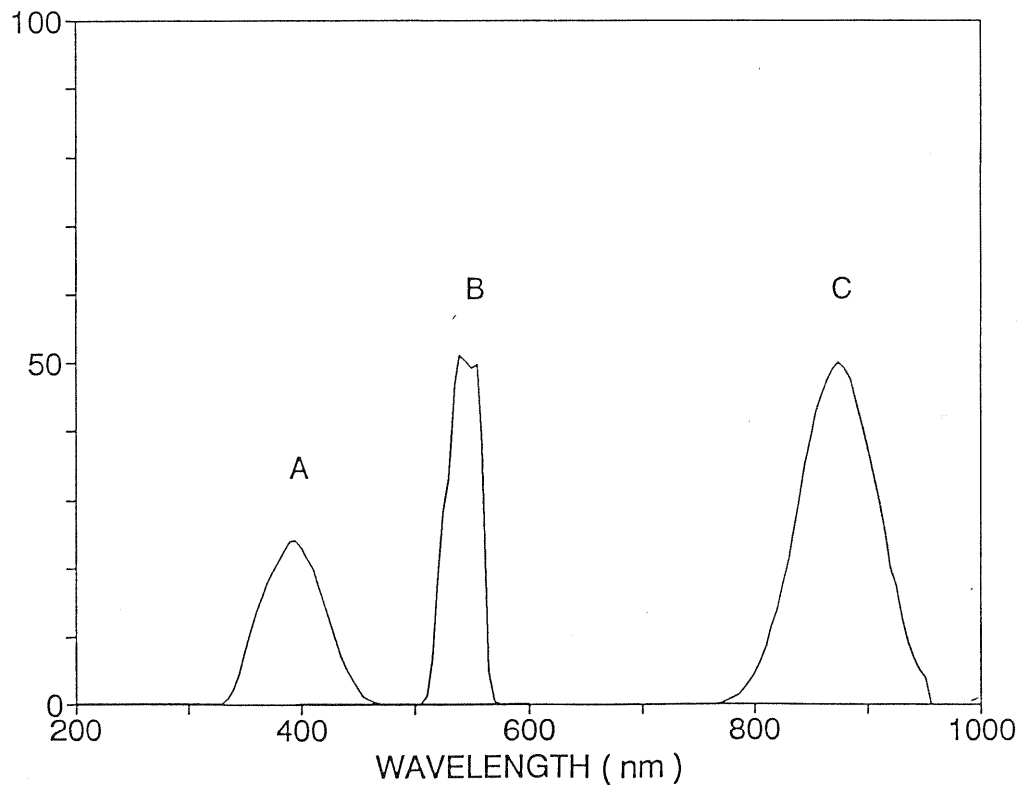


Figure 4.1.3(b): Stimulation and detection windows used with the GLSL add-on unit (from Duller and Bøtter-Jensen, 1992). Luminescence is detected through 12mm of Corning 7-59 and 5mm of Schott BG-39 (A). GLSL is stimulated using a waveband from 515-560nm (B), and IRSL using diodes emitting at 875 $\pm$ 80nm (C).

TEMT 484 diodes, run at approximately 20mA. Feedback was based upon the IRSL reflected from within the measurement chamber as described by Spooner *et al.* (1990). The IR power at the sample was  $7\text{mW}/\text{cm}^2$  as measured using a photodiode calibrated at Risø. The unit was designed to fit on top of a standard Daybreak TL oven, but no attempt was made to control the temperature of the sample. IRSL measurements could be made for as little as 0.01s with data collected on an EG&G Ortec Ace MCS card. In general, measurements were made for 0.1s. The reproducibility of these measurements was determined by making 100 repeat 0.1s measurements on a single disc of GDNZ 1. A linear regression line was then fitted (figure 4.2(a)), and the residuals from this line plotted as a histogram (figure 4.2(b)). An approximately normal distribution can be seen with a standard deviation equivalent to 2.5% of the signal. Given the other uncertainties in luminescence dating (i.e. normalization, calibration of radioactive sources, bleaching etc.) this precision was considered acceptable.

### 4.3 Filters

The past few years have seen a vast increase in the amount of data available concerning the emission and stimulation spectra of various minerals (see section 4.3.2). This allows a more informed choice of emission filter to be made although Andersson *et al.* (1990) have suggested that it is not possible to separate the emission from quartz or feldspar on the basis of wavelength. Filters are placed in front of the photomultiplier tube (PMT) not only to select emission at a specific wavelength, but also in order to reject signals at other, unwanted, wavelengths. The response of the PMT must also be considered when calculating the sensitivity of the system to specific signals.

#### 4.3.1 Infrared rejection

When measuring either TL or IRSL, it is important to reject unwanted radiation in the near infrared. For IRSL this is scattered IR from the stimulating diodes emitting at  $880\pm 80\text{nm}$ . In the case of TL it is black body radiation, whose wavelength is dependent upon the temperature to which the sample is taken. In this study the Chance-Pilkington HA-3 was used as a heat absorbing filter when making TL measurements. This filter was chosen for its broad transmission in the visible and UV parts of the spectrum (figure 4.3.1).

Using infrared as a stimulation source it is essential to use an effective IR rejecting filter. The Schott BG-39 has proved most suitable for this (figure 4.3.1). It has higher rejection at about 880nm than the HA-3, and it has higher transmission in the visible part of the spectrum, but it does not transmit well in the UV and effectively cuts at 320nm.

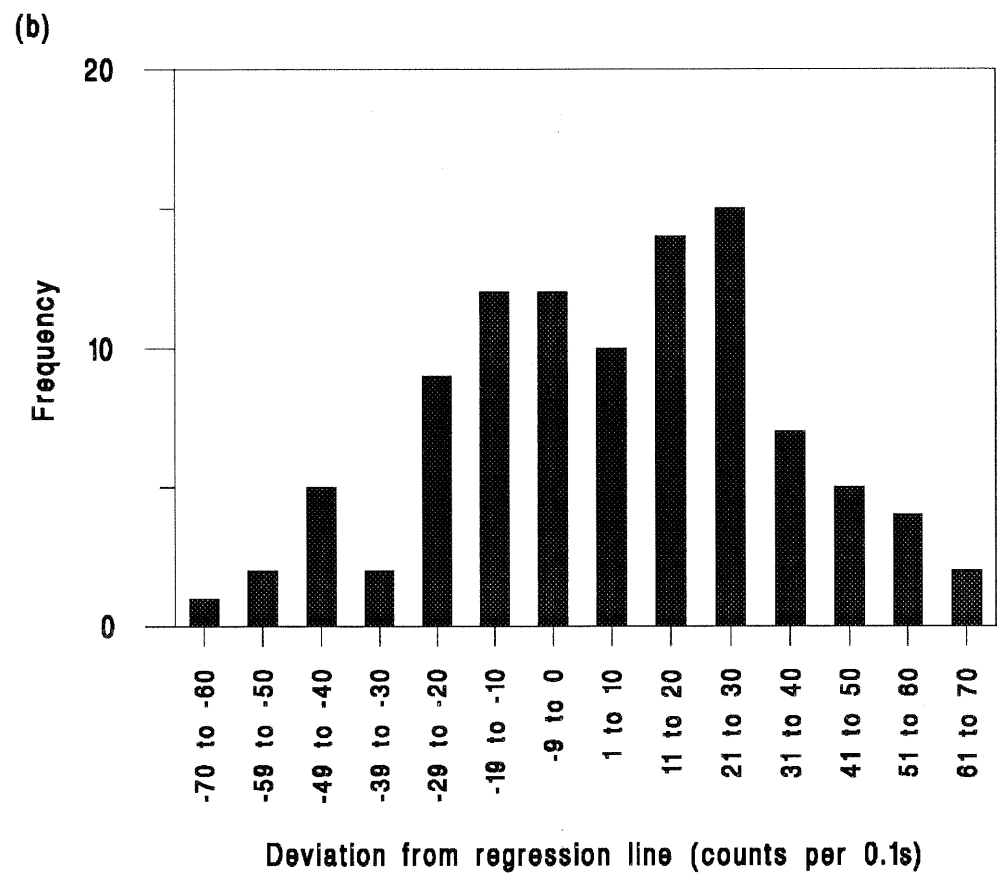
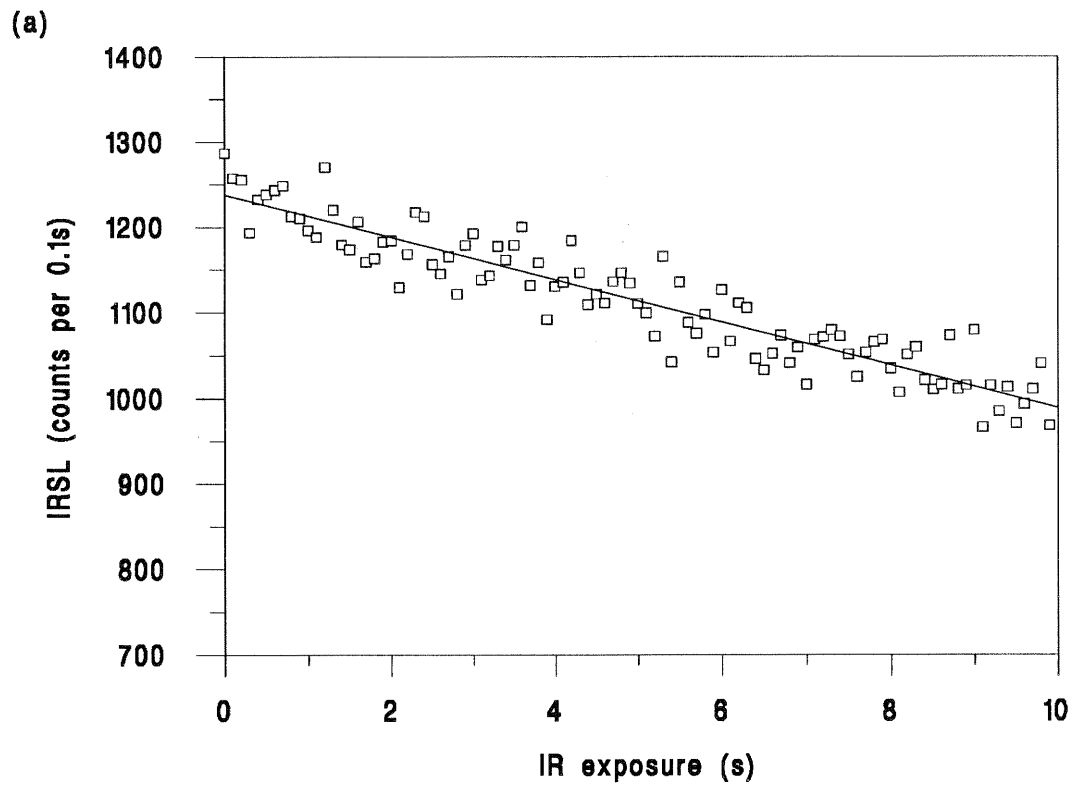


Figure 4.2: (a) Repeated 'short shine' measurements on an aliquot of sample GDNZ 1 with a best-fit linear regression shown. (b) The distribution of the residuals from the regression line.

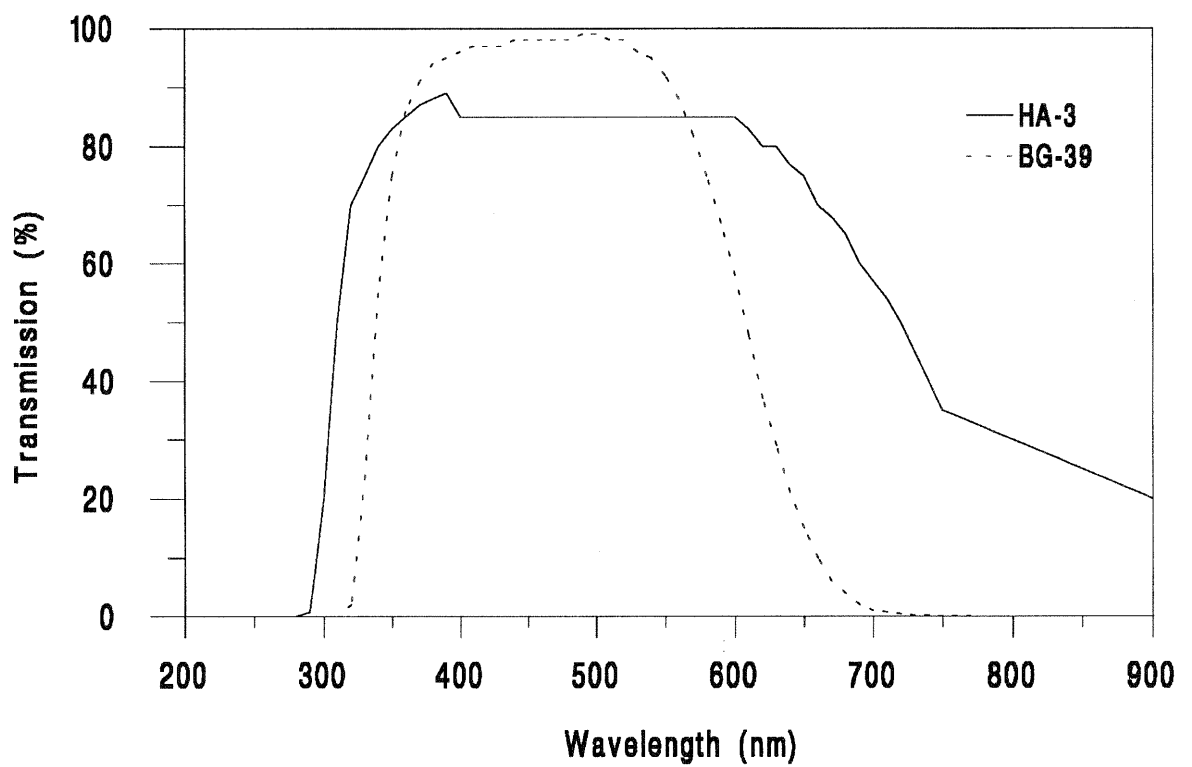


Figure 4.3.1: Transmission characteristics for the Schott BG-39 and Chance-Pilkington HA-3 filters (data taken from catalogues).

### 4.3.2 Emission and Absorption Characteristics for Feldspars

Huntley *et al* (1991) demonstrated that potassium rich feldspars show a distinct emission peak at 400nm when stimulated using IR wavelengths (figure 4.3.2(a)). This contrasts with plagioclase feldspars that have their peak emission at 570nm. In theory it should be possible to eliminate the plagioclase feldspar signal using a filter centred at around 400nm. However, Prescott, Akber and Gartia (1990) showed that some plagioclase feldspars give emissions one to two orders of magnitude greater than potassium rich feldspars. Thus even though their peak emission is at 570nm it is likely that, if present, plagioclase feldspars may contribute significantly at 400nm.

To investigate the spectral emission of separated potassium rich feldspars from New Zealand, 8 groups of 4 discs of GDNZ 17 were glowed and the TL observed through a series of narrow pass interference filters supplied by Daybreak Inc. These were spaced at approximately 50nm intervals from 340 to 700nm, with bandwidths of approximately 40nm (see table 4.3.2).

Table 4.3.2

Characteristics of narrow pass interference filters supplied by Daybreak Inc., and the calculation of correction factors to allow for variations in filter bandwidth and transmission, and photomultiplier tube sensitivity.

<u>Filter</u> <sup>(a)</sup>	<u>Wavelength</u> (nm) <sup>(b)</sup>	<u>Bandwidth</u> (nm) <sup>(b)</sup>	<u>Transmission</u> (%) <sup>(b)</sup>	<u>QE(%)</u> <sup>(c)</sup>	<u>Correction</u> <u>Factor</u> <sup>(d)</sup>
1	340	50	55	26	5.594
2	400	40	38	27	9.747
3	450	40	48	26	8.013
4	500	40	54	22	8.418
5	550	40	54	15	12.346
6	600	40	54	6	30.864
7	650	40	54	2	92.593
8	700	40	54	0.5	370.370

Notes:

(a) "Filter 1" is a UG-11 combined with a 3mm BG-38. Filters 2-8 are a set of visible bandpass filters supplied by Corion.

(b) Peak wavelength, bandwidth and transmission data were supplied by Corion.

(c) The Quantum Efficiency for the PMT was taken from data supplied by EMI. However, the data were not obtained for the specific tube used, and so the data are only approximate.

(d) The correction factor was obtained by the equation,

$$\text{Correction factor} = \frac{40}{\text{Transmission} \times \text{QE} \times \text{Bandwidth}}$$

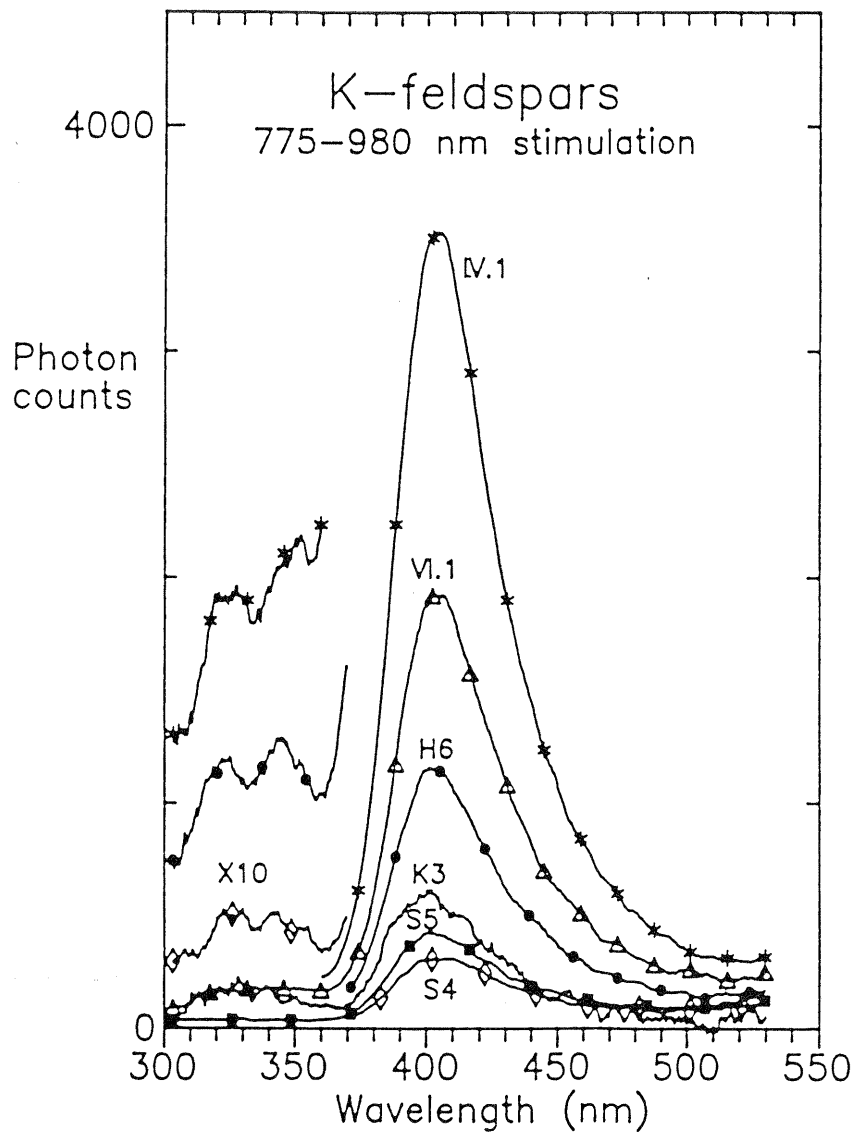


Figure 4.3.2(a): Emission spectra for potassium feldspars obtained using infrared diode stimulation, from Huntley *et al.* (1991). Samples H6, S4, S5, IV.1 and VI.1 are potassium feldspar grains separated from  $\sim 10^5$  year old sediments, while K3 is a museum specimen of potassium feldspar.

The variation in the efficiency with which emissions were detected by each filter combination was compensated for using the data in table 4.3.2. Figure 4.3.2(b) shows the TL glow curves for the different filters corrected for the response of the system, and figure 4.3.2(c) the same data plotted as intensity versus wavelength. It is clear that there is a major emission peak at 400nm. Additionally, the 340°C TL peak is particularly prominent at this wavelength. The thermal stability of this peak has been shown to be far greater than that of the 265°C peak by Strickertsson (1985).

The fall in emission below 400nm is similar to that found in previous studies on potassium rich feldspars (e.g. figure 4.3.2(a)). However, recent work by Wintle and Duller (1991) has suggested that this may be an artefact of the self-absorption of wavelengths below 400nm by the feldspar grain itself, and not a true feature of its emission spectrum. Figure 4.3.2(d) compares the absorption spectra for smoky sanidine (from Hofmeister and Rossman, 1983), the TL emission spectrum for a potassium feldspar (Orthoclase K3 from Huntley *et al.*, 1988) and the transmission characteristics of filters commonly used in TL dating studies. Hofmeister and Rossman (1983) consider this absorption to be caused by charge transfer from oxygen to a cation (probably  $\text{Fe}^{3+}$ ). It is characterized by a very steeply rising absorption edge. In their review Hofmeister and Rossman (1983) gave several examples of feldspars exhibiting this response (orthoclase, labradorite and amazonite). It has yet to be proven that this type of self-absorption does occur with the feldspar grains used for TL dating.

Calculations of the dose rate for feldspar grains assume that luminescence from all parts of the grain is detected equally efficiently. If self-absorption of the type seen in figure 4.3.2(d) occurred then luminescence below 400nm would be predominantly from the surface of the feldspar grain rather than the grain as a whole. Hence the internal dose rate would be smaller than that calculated. This may in part be the explanation of the severe underestimation of TL ages found by Balescu *et al.* (1991) and Dijkmans and Wintle (1991) when using a UG-11 filter. The magnitude of this type of effect would be highly variable from one sample to another, and the simplest solution is to use an optical filter that transmits primarily above 350-400nm.

### 4.3.3 Filter Characteristics

Blue filters, centred around 400nm, have been preferred by Mejdahl for many years (e.g. Kolstrup *et al.* 1990), in contrast to the use of the UG-11 by Dijkmans and Wintle (1991) and Balescu *et al.* (1991). Balescu and Lamothe (1992) have recently shown that significant ED under-estimation occurs when using the UG-11 with potassium feldspars,

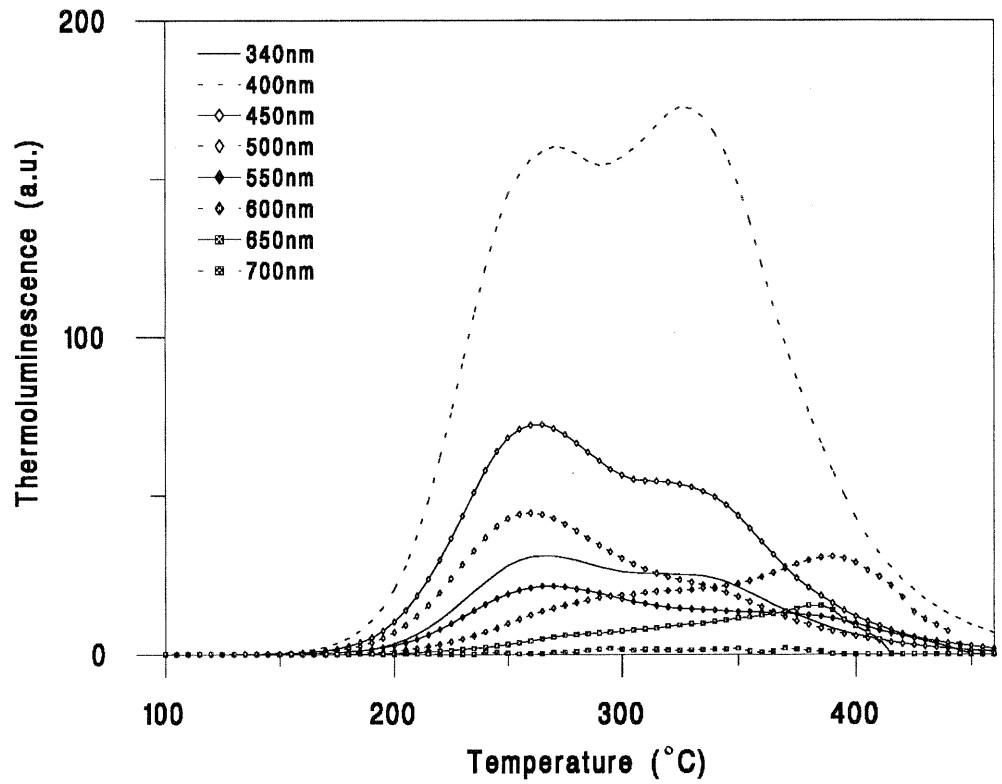


Figure 4.3.2(b): TL glow curves for sample GDNZ 17 when viewed through narrow bandpass filters. The peak wavelength of each filter is given.

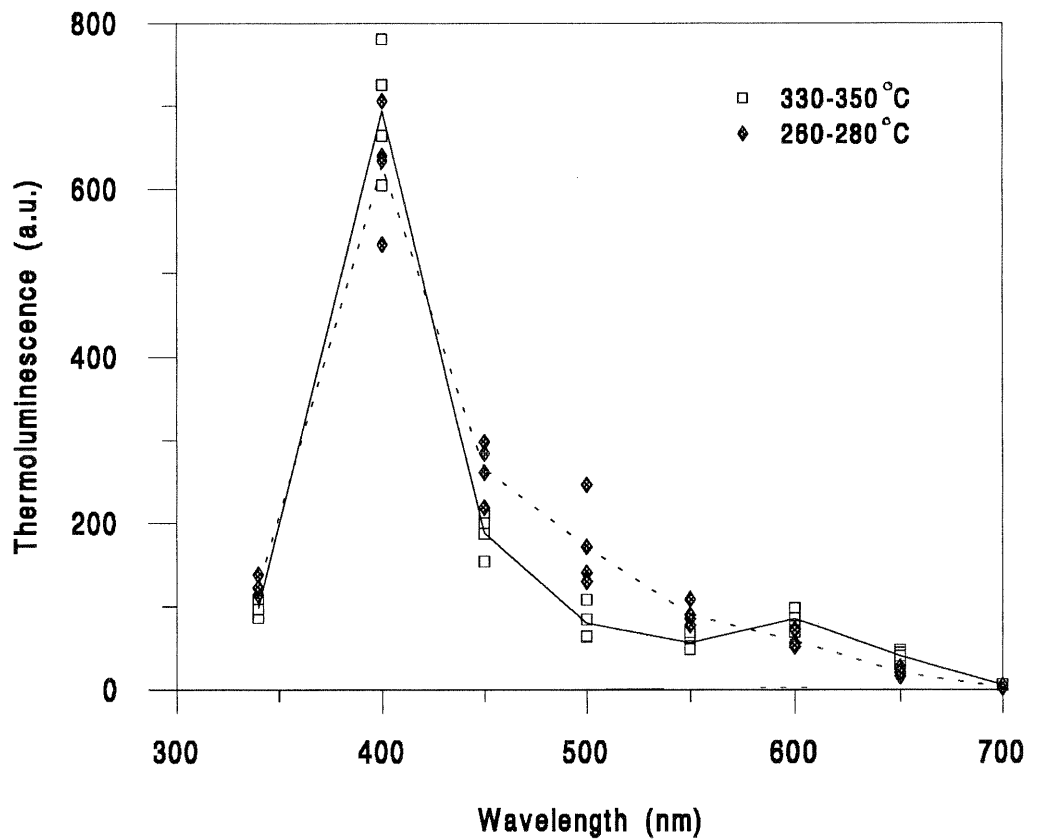


Figure 4.3.2(c): TL emission intensity as a function of detection wavelength for the data in figure 4.3.2(b).

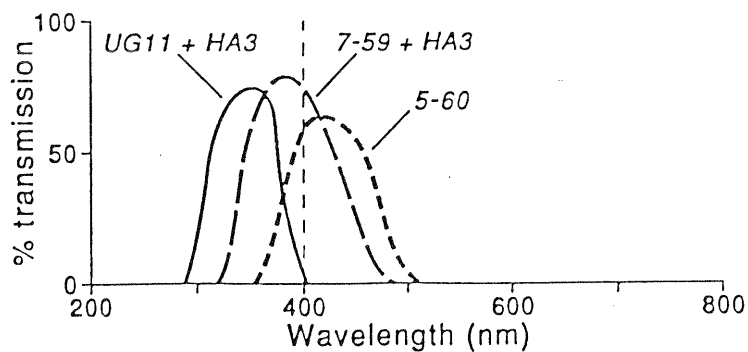
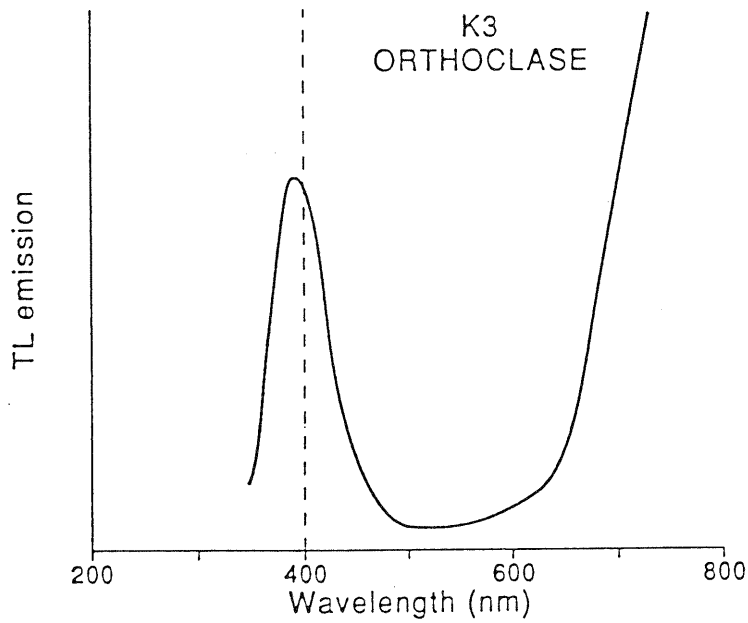
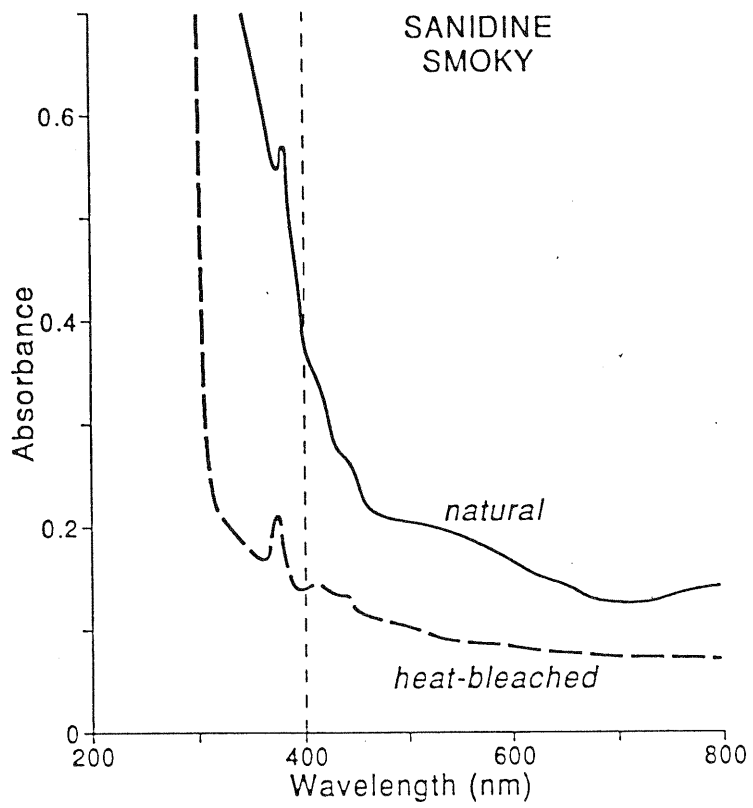


Figure 4.3.2(d): From Wintle and Duller (1991). Top - Absorption spectra for smoky sanidine from Hofmeister and Rossman (1983). Middle - TL emission spectrum for potassium feldspar (K3 orthoclase) from Huntley *et al.* (1988). Bottom - Transmission characteristics of filters commonly used in luminescence dating studies. The vertical dashed line at 400nm indicates wavelengths below which absorption is likely to affect luminescence measurements.

and this may be due to the self-absorption that occurs within grains at these wavelengths, as discussed above.

The filters chosen for this work are designed to cover the emission peak of potassium rich feldspars at 400nm, and hence to reduce the contribution from plagioclase feldspars which may be present in small quantities as contaminants. All the TL data have been taken using a Corning 5-60 and HA-3 combination, and the IRSL single aliquot data (chapters 6 and 7) using a 5-58 and BG-39 combination (figure 4.3.3). All the IRSL data in chapter 5 were taken just using a BG-39.

#### 4.4 Bleaching

A Hönle SOL2 solar simulator was used to bleach samples in the laboratory. This was preferred to using natural sunlight because of its reproducibility and reliability. The spectrum of the simulator is specifically designed to mimic that of natural sunlight (figure 4.4), and so should be a good analogue for the bleaching that the samples received in nature.

#### 4.5 Irradiation

Samples were irradiated with one of two  $^{90}\text{Sr}/^{90}\text{Y}$  beta sources. The Daybreak unit is capable of irradiating up to 20 discs under computer control and has a source strength of  $3.81 \pm 0.12$  Gy/min (see appendix II) to feldspar grains (180-211 $\mu\text{m}$ ) on aluminium discs. The other source used is mounted in the Risø automated TL reader and was used for second glow normalization and single aliquot work. This has been calibrated to  $1.24 \pm 0.04$  Gy/min (see section 6.8 and appendix II) for the same sample conditions.

#### 4.6 Sample Normalization

Variations in the mass of the samples and in intrinsic brightness are inevitable, and where many discs are to be compared these differences must be corrected for by some method of normalization. This was of most importance when determining EDs using standard TL and IRSL techniques, which required up to 60 discs to be normalised. Three methods of normalization were evaluated, those of weight normalization, natural normalization and second glow normalization. Figure 4.6 is a flow diagram of the processes involved in ED

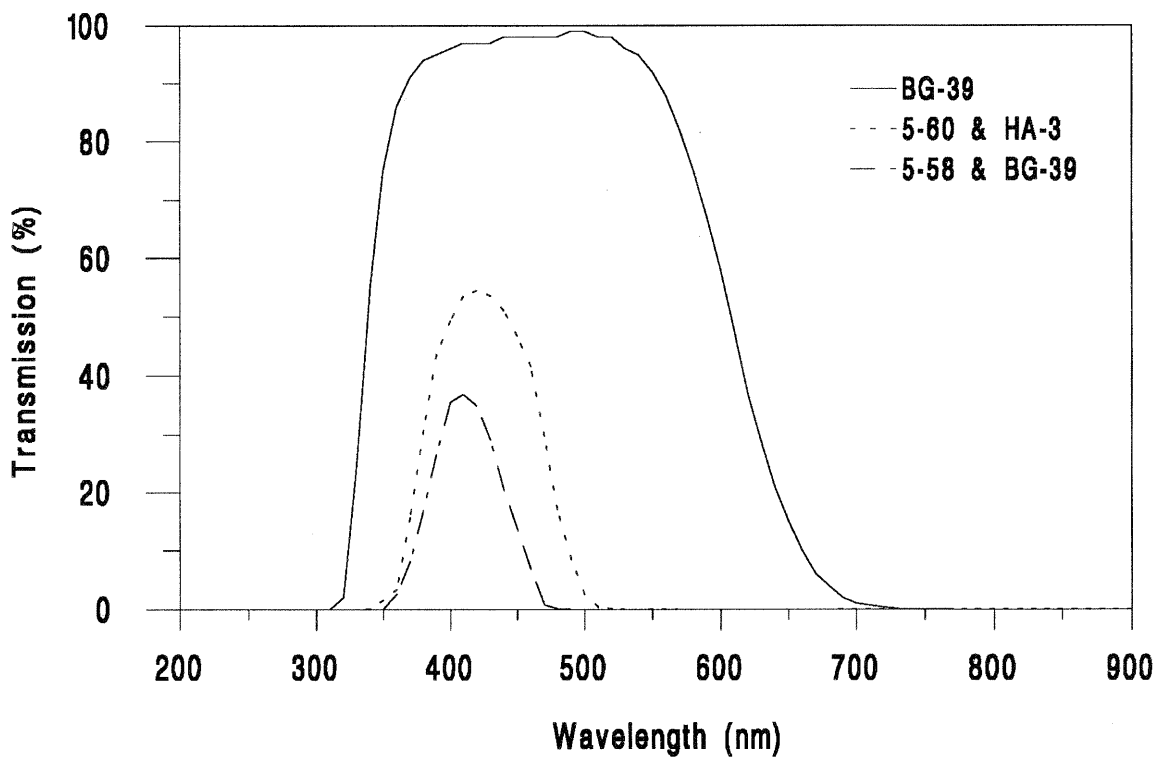


Figure 4.3.3: Transmission characteristics for various filter combinations used in this thesis (data taken from catalogues).

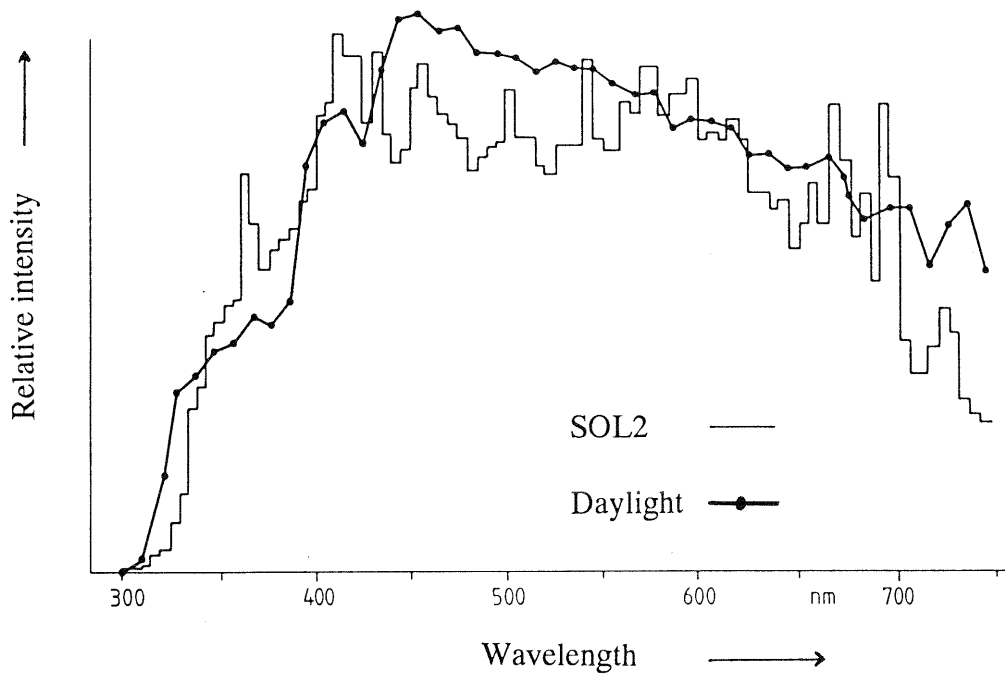


Figure 4.4: Comparison of the spectral distribution of emission from the Höhle SOL2 solar simulator and natural sunlight (data from the manufacturers specifications).

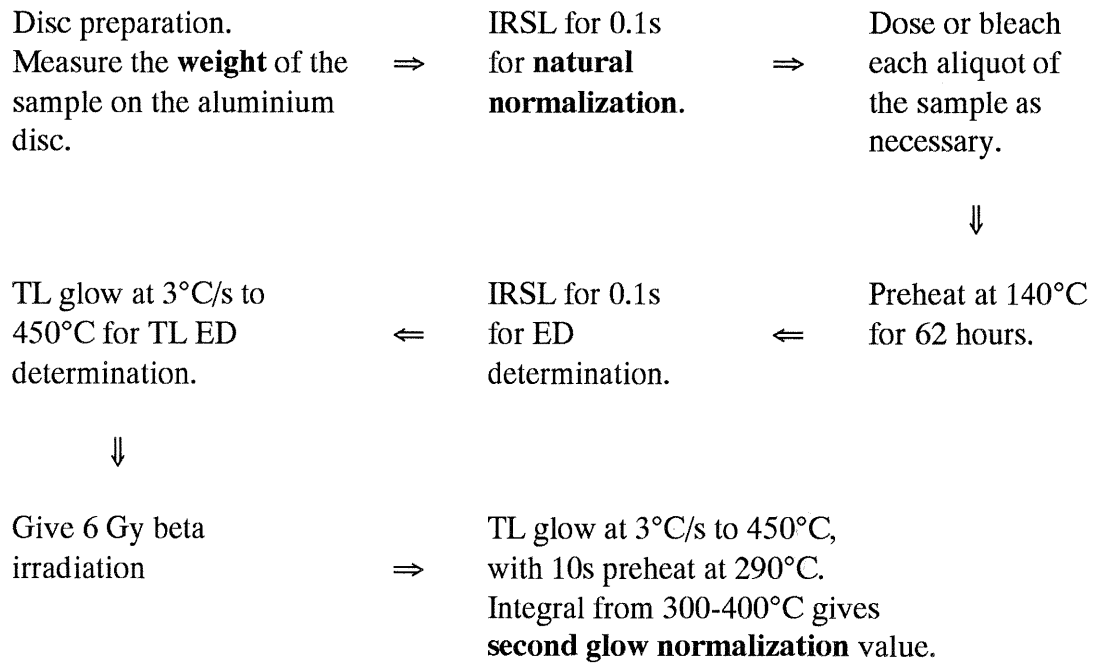


Figure 4.6: Flow diagram of the procedure adopted for routine dating of samples using multiple aliquot methods (see chapter 5). The occasions when normalization measurements are made are in bold.

evaluation as used in chapter 5. It clearly shows where normalization measurements are made, and where the 'data' measurements that they are applied to are made. All methods assume that no material is lost from the discs in the time between when the normalization measurement is made, and when the main luminescence measurements are made.

However, all these methods also make other assumptions which affect how successful they are. The methods and their relevant assumptions will be discussed in turn. Table 4.6(a) and 4.6(b) contain additive dose data sets for samples GDNZ 1 and GDNZ 17 showing the scatter when the three different normalization methods are used.

#### 4.6.1 Weight Normalization

This is perhaps the simplest form of normalization. The weight of feldspar on each disc is measured when mounting the sample. In theory, the greater the mass of feldspar, the greater the luminescence signal that it will give. However, this assumes either that all grains have the same luminescence sensitivity per unit mass, or that there are a sufficiently large number of grains that any variations will be masked by the large sample size. It is clear from both table 4.6(a) and (b) that while weight normalization reduces the scatter compared with no normalization, the improvement is minimal.

#### 4.6.2 Natural Normalization

Using this method the natural luminescence of the material is measured using a short IRSL measurement (typically 0.1s) made as soon as the sample has been mounted on an aluminium disc. This is then taken to be a measure of the relative brightness of the material. This method assumes that all grains have received the same environmental dose, and implicit to this, the same degree of resetting when they were deposited. This method is unsatisfactory for young samples since they have insufficient signal to give a reproducible measurement. For the examples in table 4.6 natural normalization reduces the scatter, especially for the IRSL data. The smaller error sum for the IRSL data compared with the TL data may be due to the fact that both the normalization and the 'measurement' are stimulating precisely the same traps, or it may be because the two measurements are made relatively closely together (figure 4.6) and so there is less likelihood of grains dropping off the discs.

Table 4.6(a)

Comparison of normalization methods for sample GDNZ 1. The figures in ordinary type are the mean values of the discs used for each point. The figures in bold are the coefficients of variation, calculated as 100% x (standard deviation/mean).

**TL Data, integrated from 283-367°C**

<u>Data Point</u>	<u>Number of discs</u>	<u>Type of Normalization</u>			
		<u>None</u>	<u>Weight</u>	<u>Natural</u>	<u>Second Glow</u>
Natural	6	472,630 <b>11.4%</b>	490,698 <b>8.3%</b>	470,046 <b>7.8%</b>	486,249 <b>4.0%</b>
N+19 Gy	6	708,680 <b>14.1%</b>	668,018 <b>9.9%</b>	640,488 <b>7.1%</b>	676,293 <b>5.2%</b>
N+38 Gy	6	855,890 <b>21.5%</b>	845,371 <b>16.4%</b>	806,329 <b>16.8%</b>	859,805 <b>4.5%</b>
N+76 Gy	6	1,276,809 <b>9.5%</b>	1,274,166 <b>11.2%</b>	1,223,548 <b>9.5%</b>	1,190,515 <b>3.4%</b>
N+133 Gy	9	1,625,555 <b>9.1%</b>	1,627,917 <b>5.9%</b>	1,800,404 <b>11.4%</b>	1,593,703 <b>6.1%</b>
N+229 Gy	6	2,441,328 <b>9.9%</b>	2,264,288 <b>6.8%</b>	2,308,405 <b>9.2%</b>	2,142,428 <b>7.4%</b>
<b><u>Error sum</u></b>		<b>75.5</b>	<b>58.5</b>	<b>61.8</b>	<b>30.6</b>
N+6m SOL2	5	128,595 <b>16.9%</b>	143,507 <b>13.2%</b>	152,177 <b>7.3%</b>	149,941 <b>5.6%</b>
N+60m SOL2	6	68,547 <b>6.6%</b>	68,762 <b>6.8%</b>	66,361 <b>13.0%</b>	68,160 <b>5.8%</b>
N+600m SOL2	6	37,263 <b>11.3%</b>	37,434 <b>8.0%</b>	38,393 <b>4.4%</b>	41,750 <b>9.2%</b>
<b><u>Error sum</u></b>		<b>34.8</b>	<b>28.0</b>	<b>24.7</b>	<b>20.6</b>

Table 4.6(a) continued

**IRSL Data, 0.1s measurement**

<u>Data Point</u>	<u>Number of discs</u>	<u>Type of Normalization</u>			
		<u>None</u>	<u>Weight</u>	<u>Natural</u>	<u>Second Glow</u>
Natural	6	7,303 <b>9.6%</b>	7,584 <b>6.2%</b>	7,274 <b>7.7%</b>	7,559 <b>9.8%</b>
N+19 Gy	6	11,133 <b>15.4%</b>	10,476 <b>10.3%</b>	10,044 <b>7.5%</b>	10,596 <b>4.1%</b>
N+38 Gy	6	12,748 <b>19.8%</b>	12,589 <b>14.0%</b>	11,943 <b>11.0%</b>	12,944 <b>13.0%</b>
N+76 Gy	6	19,838 <b>15.5%</b>	19,855 <b>18.1%</b>	18,909 <b>11.7%</b>	18,397 <b>7.8%</b>
N+133 Gy	9	25,283 <b>8.8%</b>	25,296 <b>3.6%</b>	27,936 <b>8.9%</b>	24,880 <b>10.5%</b>
N+229 Gy	9	38,204 <b>12.5%</b>	35,633 <b>9.4%</b>	37,362 <b>7.8%</b>	35,163 <b>9.0%</b>
<b><u>Error sum</u></b>		<b>81.6</b>	<b>61.6</b>	<b>54.6</b>	<b>54.2</b>
N+6m SOL2	6	120 <b>42.4%</b>	138 <b>35.7%</b>	145 <b>25.3%</b>	143 <b>27.8%</b>
N+60m SOL2	6	88 <b>28.2%</b>	90 <b>34.4%</b>	87 <b>36.1%</b>	88 <b>31.8%</b>
N+600m SOL2	6	55 <b>43.6%</b>	56 <b>46.1%</b>	58 <b>46.5%</b>	64 <b>50.4%</b>
<b><u>Error sum</u></b>		<b>114.2</b>	<b>116.2</b>	<b>107.9</b>	<b>110.0</b>

Table 4.6(b)

Comparison of normalization methods for sample GDNZ 17. The figures in ordinary type are the mean values of the discs used for each point. The figures in bold are the coefficients of variation, calculated as 100% x (standard deviation/mean).

**TL Data, integrated from 283-367°C**

<u>Data Point</u>	<u>Number of discs</u>	<u>Type of Normalization</u>			
		<u>None</u>	<u>Weight</u>	<u>Natural</u>	<u>Second Glow</u>
Natural	12	230,499 <b>25.0%</b>	272,170 <b>14.1%</b>	253,717 <b>12.0%</b>	267,959 <b>9.2%</b>
N+19 Gy	6	273,750 <b>9.7%</b>	470,943 <b>10.5%</b>	475,779 <b>13.2%</b>	443,154 <b>9.1%</b>
N+38 Gy	4	608,827 <b>20.0%</b>	594,624 <b>13.5%</b>	668,243 <b>10.9%</b>	600,080 <b>6.8%</b>
N+76 Gy	5	918,823 <b>11.9%</b>	1,007,273 <b>14.4%</b>	971,978 <b>12.7%</b>	948,374 <b>3.8%</b>
N+133 Gy	6	1,327,312 <b>8.7%</b>	1,572,382 <b>8.3%</b>	1,549,595 <b>11.1%</b>	1,462,216 <b>2.2%</b>
N+229 Gy	7	2,264,326 <b>18.9%</b>	2,365,164 <b>11.5%</b>	2,291,975 <b>8.3%</b>	2,048,450 <b>4.3%</b>
<b><u>Error sum</u></b>		<b>94.2</b>	<b>72.3</b>	<b>68.2</b>	<b>35.4</b>
N+6m SOL2	6	95,384 <b>14.9%</b>	79,428 <b>5.7%</b>	80,806 <b>12.5%</b>	78,354 <b>2.3%</b>
N+60m SOL2	4	51,031 <b>4.9%</b>	45,278 <b>9.5%</b>	45,600 <b>10.9%</b>	45,650 <b>4.5%</b>
N+600m SOL2	5	38,808 <b>6.1%</b>	35,863 <b>14.2%</b>	31,330 <b>12.9%</b>	32,979 <b>11.3%</b>
<b><u>Error sum</u></b>		<b>25.9</b>	<b>29.4</b>	<b>36.3</b>	<b>18.1</b>

Table 4.6(b) continued

**IRSL Data, 0.1s measurement**

<u>Data Point</u>	<u>Number of discs</u>	<u>Type of Normalization</u>			
		<u>None</u>	<u>Weight</u>	<u>Natural</u>	<u>Second Glow</u>
Natural	15	3,329	3,578	3,403	3,556
		<b>32.5%</b>	<b>17.5%</b>	<b>9.1%</b>	<b>8.8%</b>
N+19 Gy	6	3,687	6,335	6,381	6,001
		<b>10.8%</b>	<b>9.7%</b>	<b>9.6%</b>	<b>14.4%</b>
N+38 Gy	6	8,828	8,563	8,831	8,492
		<b>30.8%</b>	<b>26.4%</b>	<b>7.8%</b>	<b>16.3%</b>
N+76 Gy	6	14,242	15,488	14,864	14,737
		<b>13.1%</b>	<b>14.0%</b>	<b>10.6%</b>	<b>12.9%</b>
N+133 Gy	6	20,490	24,257	23,818	23,301
		<b>9.4%</b>	<b>8.0%</b>	<b>6.5%</b>	<b>7.1%</b>
N+229 Gy	7	38,503	39,235	38,780	34,794
		<b>20.6%</b>	<b>12.2%</b>	<b>6.0%</b>	<b>7.9%</b>
<b><u>Error sum</u></b>		<b>117.2</b>	<b>87.8</b>	<b>49.6</b>	<b>67.4</b>
N+6m SOL2	6	93	76	76	73
		<b>46.8%</b>	<b>38.1%</b>	<b>34.0%</b>	<b>33.3%</b>
N+60m SOL2	6	25	24	25	25
		<b>140.0%</b>	<b>140.4%</b>	<b>138.0%</b>	<b>144.7%</b>
N+600m SOL2	6	15	13	11	12
		<b>107.3%</b>	<b>105.7%</b>	<b>101.1%</b>	<b>105.0%</b>
<b><u>Error sum</u></b>		<b>294.1</b>	<b>284.2</b>	<b>273.1</b>	<b>283.0</b>

### 4.6.3 Second Glow Normalization

Following TL measurement up to 450°C in the Risø reader, all discs are given a 6 Gy test dose and then immediately glowed again to 450°C, with a preheat at 290°C for 10 seconds to isolate a single peak for integration (300-400°C in this study). Smith and Prescott (1984) suggested that samples should be left at least 24 hours after irradiation, preheating or bleaching, before being glowed. This was based on observations of quartz which appeared to show far higher scatter if it was glowed out within 24 hours of being irradiated.

Initially all discs were irradiated for second glow analysis and then left for 24 hours. However, this was very inconvenient because the reader had to stand idle and so 24 discs of GDNZ 1 and two sets of 18 discs of GDNZ 59 were used to compare second glow measurements made immediately after irradiation with those left 24 hours after irradiation before being glowed out. After their first TL measurement ( $N$ ,  $N+\beta$  or  $I_0$ ), the sample discs were given the 6 Gy test dose and immediately glowed as described above. They were then given the same 6 Gy test dose and left for 24 hours before being glowed a third time. For GDNZ 1 the ratio of the 2nd to the 3rd glow was  $0.979\pm 0.033$ , while for the two samples of GDNZ 59 the ratio was  $1.019\pm 0.014$  and  $0.982\pm 0.021$ . The small standard deviation shows that there was no significant increase in the scatter of the data, and so for most of the samples described in chapter 5, second glow normalization was performed with no delay after irradiation.

Second glow normalization assumes that no dose dependent or light-exposure dependent sensitivity change occurs. These problems have previously been reported for quartz (Rhodes 1990, figure 5.2), but not for potassium feldspar. To test for this the ratio of the natural normalization (nat. norm.) factor over the second glow normalization (s.g.) factor was plotted for eight samples analyzed in chapter 5. These were plotted as a function of dose for the additive dose and regeneration data sets, and bleaching time for the residuals (figure 4.6.3). Least squares linear regression lines were fitted to the additive dose and regeneration data sets (table 4.6.3). The slope of the line was significantly different from zero for all apart from three of the data sets analyzed. No clear relationship can be seen between the slope of these lines and the equivalent dose of the samples.

The additive dose data sets all show a drop in the ratio of (nat. norm.)/(s.g.) with dose except for GDNZ 10. The implication of this is that the growth curves generated using second glow normalized data will be more curved than those using natural normalization, and hence will probably underestimate the ED.

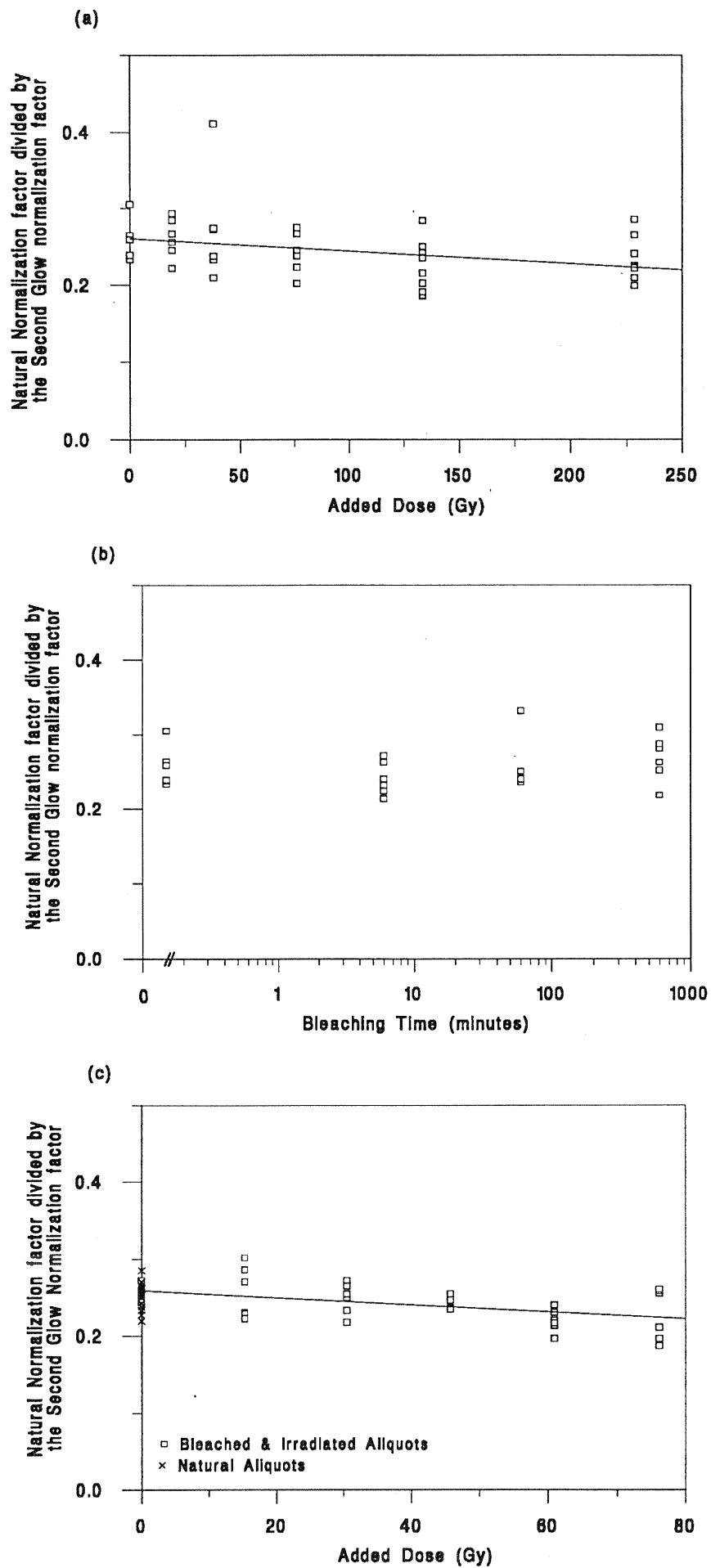


Figure 4.6.3: The ratio of the natural normalization factor divided by the second glow normalization factor for aliquots used (a) to construct an additive dose growth curve, (b) to define the residual levels and (c) used to determine the ED by the regeneration method. Data are shown for sample GDNZ 1, and the ratios are plotted as a function of dose in (a) and (c), and as a function of the length of exposure to the SOL2 solar simulator in (b).

All samples show a significant rise in the ratio of (nat.norm.)/(s.g.) with bleaching time except GDNZ 1, 13 and 17 which show no significant change. An increase in this ratio implies that residuals corrected using second glow normalization will be larger than those using natural normalization. This will tend to cause an underestimation of the ED.

Table 4.6.3

The slope<sup>(a)</sup> of a straight line regression through a plot of the ratio of the natural normalization factor divided by the second glow normalization factor against dose. The equivalent dose of each sample, determined in chapter 5, is also shown.

<u>Sample</u>	<u>Additive Dose</u>	<u>Regeneration</u> <sup>(b)</sup>	<u>Equivalent Dose (Gy)</u> <sup>(c)</sup>
GDNZ 1	-1.85 ± 0.79	-6.63 ± 2.07	40.7 ± 2.3
GDNZ 5	-0.76 ± 0.44	-2.02 ± 1.96	44.3 ± 1.6
GDNZ 10	2.69 ± 0.79	-0.87 ± 2.73	361.3 ± 19.0
GDNZ 13 <sup>(d)</sup>	-0.21 ± 0.08	-1.85 ± 0.55	44.3 ± 4.3
GDNZ 17	-0.88 ± 0.39	-0.59 ± 3.01	21.0 ± 1.3
GDNZ 51	-2.24 ± 0.90	0.91 ± 1.72	121.3 ± 14.6
GDNZ 52	-0.60 ± 0.52	-5.03 ± 2.61	83.0 ± 6.1
GDNZ 59	-1.68 ± 0.63	-2.24 ± 0.93	358.7 ± 33.2

Notes

- (a) All slopes are multiplied by 1000 for clarity.
- (b) The natural points were not used in determination of the slope for the regeneration data sets.
- (c) Equivalent dose determined using the regeneration method based on TL measurements (see table 5.4.5).
- (d) GDNZ 13 had its IR natural normalization values determined on a different instrument from the other samples, and hence its absolute slope cannot be directly compared with the other samples.

With the exception of GDNZ 51 and 52, for which the scatter on the data is very high, for any given sample the regeneration data sets show similar patterns of sensitivity change as the additive dose data sets. This is in spite of the fact that the regeneration discs had been bleached prior to dosing. In general there is little difference in the ratio of natural normalization factor to second glow normalization factor between discs retaining their 'natural' signal and those that have been bleached and not irradiated. The effect of dose dependent changes in sensitivity upon ED determination using regeneration is dependent upon the spacing of the doses in relation to the ED.

Tables 4.6(a) and (b) show that the least scatter is seen when normalizing TL data using second glow normalization, and IRSL data using natural normalization. This may reflect

the fact that it is better to use similar luminescence measurements for both normalization and data measurement, or it may simply be due to the fact that in this way there is least opportunity for grains to drop off an aliquot between normalization and data measurement. Table 4.6.3 shows that a dose dependent sensitivity change does occur for some samples. However, the magnitude of such a change is so small that it does not make a significant difference to the equivalent dose determined. In chapter 5 TL data are normalized using the second glow method, and the IRSL data using natural normalization in order to minimize the scatter between aliquots.

## 4.7 Preheating

Artificial irradiation of minerals in the laboratory induces signals with a wide range of stabilities. In thermoluminescence measurements the less stable signals are normally associated with lower temperature peaks. Thus it is possible to analyze a more stable signal by looking at the higher temperature TL signal. However, with the use of an optically stimulated signal (in this study IRSL) no such distinction can be made during measurement. Thus it is vital to remove the components of the luminescence signal that are unstable over the time period that one is dating. This is achieved by preheating the sample prior to luminescence measurement.

A satisfactory preheat should remove all components of the luminescence signal that are unstable over the time period being dated, and should be independent of dose. In practice two methods have been used to test the efficacy of preheat treatments.

1) One method is to plot a graph of the equivalent dose determined versus the preheat time or temperature used. This has been attempted for the preheat used in the single aliquot approach (section 4.7.3) since ED determination is relatively rapid. However the results from this type of analysis are very dependent upon the type of curve fitting routine used, and the quality of the data.

2) The alternative approach is to plot the ratio of signals from a 'Natural' and a 'Natural+ $\beta$ ' set of discs using different preheats. While the N+ $\beta$  discs retain an unstable signal increasingly severe preheats will reduce their signal at a faster rate than for the natural discs. Thus at the point where the ratio of (N+ $\beta$ )/N becomes a plateau both sets of discs are losing signal at the same rate, and hence the preheat is affecting the luminescence signals similarly, irrespective of whether they have received a laboratory dose or not. This second approach has been attempted for three preheats, at 100°C (section 4.7.1), 140°C (section 4.7.2) and 220°C (section 4.7.3).

The natural luminescence signal is likely to contain both a component which is stable over the time period being dated, and a component which has undergone some decay during this time period. Strickertsson (1985) showed that the 270°C TL peak in potassium feldspars has a relatively low stability (insufficient for dating over the time range considered here) and so this peak must also be removed by a preheating procedure. In sections 4.7.4 and 6.6.4 it is shown that there is an IRSL signal associated with the trapped charge giving rise to the 270°C TL peak. Thus any successful preheat must not only satisfy at least one of the methods described above, but must also isolate the 330°C TL peak to the greatest possible degree. Thus while both the tests above can be performed using either TL or IRSL, one must check the form of the glow curve to be sure that the 330°C TL peak is isolated. Thus although preheat tests can be performed solely using IRSL it is also essential to use TL to check that the 270°C TL peak is removed.

#### 4.7.1 Preheating at 100°C

Seventy-two discs of sample GDNZ 17 were used to examine the effectiveness of preheating at 100°C. The discs were divided into 18 groups of 4, with nine of the groups just retaining their natural TL signal (ED about 22 Gy), and the other nine groups receiving an additional 38 Gy. Pairs of groups (irradiated and naturals) were preheated at 100°C for periods of 0, 1, 6, 10, 24, 48, 96, 168 and 336 hours. Twenty-four hours after completion of all the preheating the discs were glowed to 450° at 3°C/sec. They were then second glow normalized.

Figure 4.7.1(a) shows the TL glow curves that were produced. For periods longer than 24 hours the 180°C peak has been removed from the irradiated samples and both the irradiated and natural aliquots show loss of the 270°C peak.

Figure 4.7.1(b) plots the ratio  $(N+\beta)/N$  for the TL integral from 0 to 450°C against the length of the preheat. The irradiated samples show considerable loss of luminescence associated with the removal of the 180°C peak and this causes an initial reduction in the ratio. After 48 hours the ratio remains constant implying that any loss in signal for the natural is matched by a loss in signal for the irradiated samples.

However, preheating at 100°C seems unable to remove the TL peak at 270°C and so is considered unsuitable for dating. Preheating at 140°C was studied using the same method.

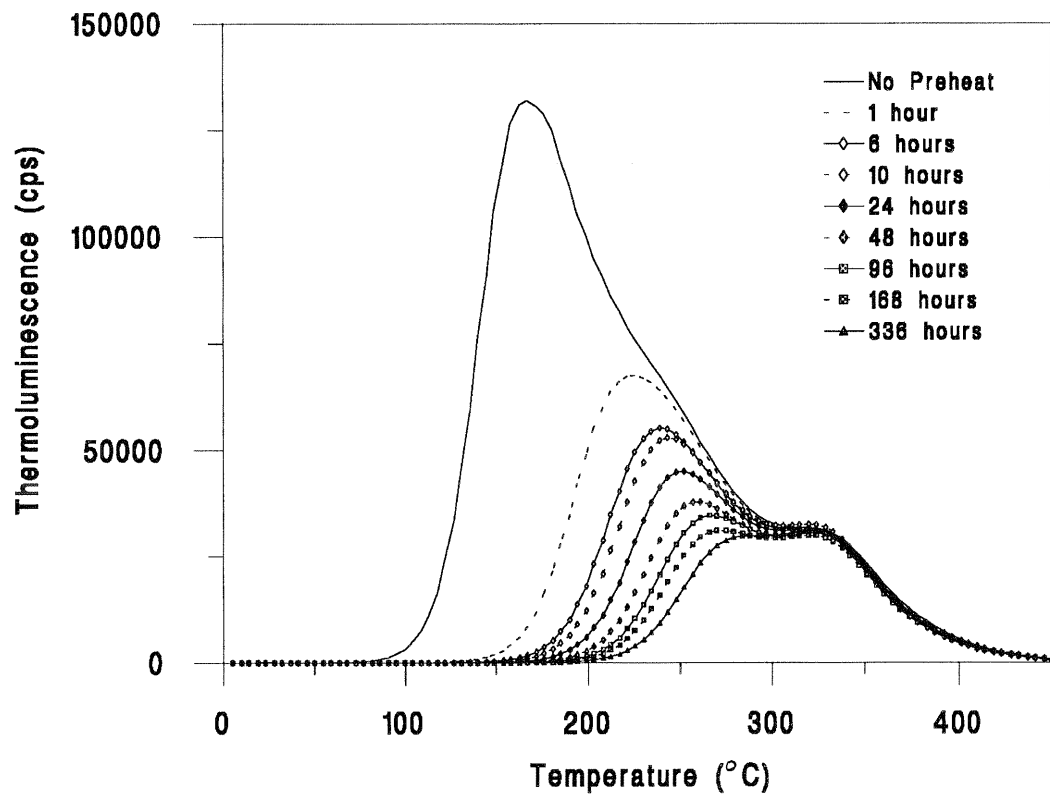
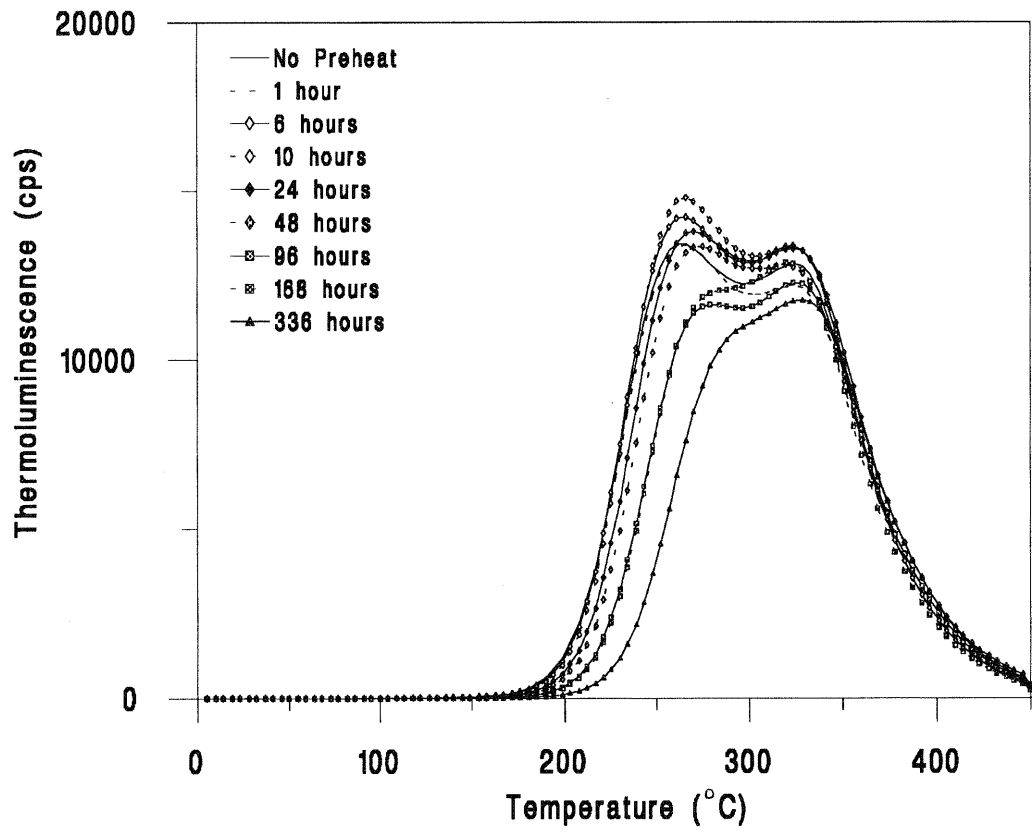


Figure 4.7.1(a): The effect of preheating at  $100^{\circ}\text{C}$  upon un-irradiated (above) and irradiated (bottom) aliquots of GDNZ 17 for different periods of time.

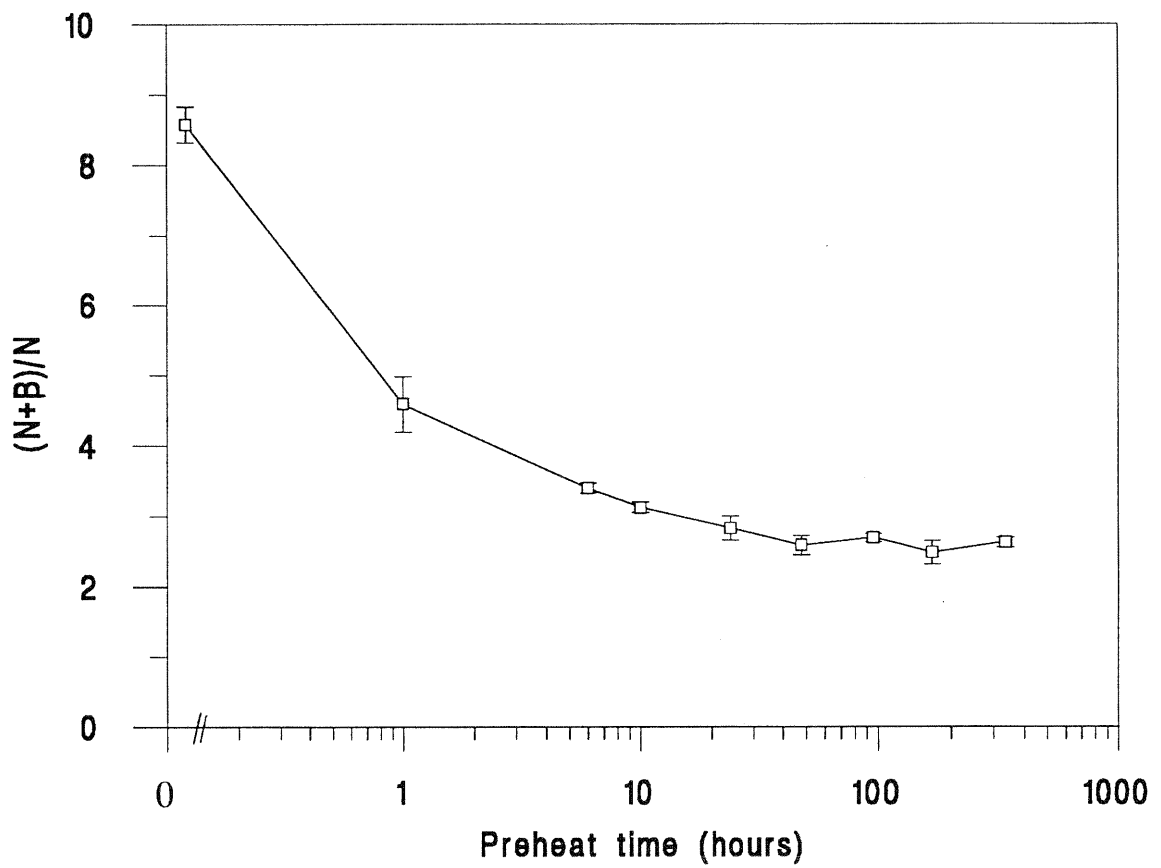


Figure 4.7.1(b): The ratio of the TL integral (0-450°C) of irradiated and un-irradiated aliquots of GDNZ 17 as a function of the length of preheating at 100°C.

### 4.7.2 Preheating at 140°C

Once more, seventy-two discs of sample GDNZ 17 were prepared and sub-divided as above. Since the preheat is at a higher temperature the lengths of time are correspondingly shorter. Different groups were heated at 140°C for 0, 1 and 10 minutes, and 1, 4, 12, 58 and 72 hours. Their TL signals were then measured as described for the 100°C preheat.

Figure 4.7.2(a) shows the glow curves for the various groups and figure 4.7.2(b) plots the ratio  $(N+\beta)/N$  for the TL integral from 0 to 450°C. After 4 hours, when the 180°C peak has been completely removed from the irradiated discs, this ratio remains constant, within errors, fulfilling the first of the two criteria necessary for a preheat. However, from figure 4.7.2(a), the 330°C peak is not isolated until 58 hours have elapsed. In this study a preheat of 62 hours at 140°C has been used for all the multiple disc equivalent dose determinations (chapter 5). This meets both requirements for a preheat as laid out in section 4.7.

This preheat is ideal for multiple disc methods, but is useless for ED determinations on single aliquots because of the time involved, so a preheat with a higher temperature for a shorter time was tested.

### 4.7.3 Preheating for single aliquots

When using the single aliquot method (chapters 6 and 7) one requires a preheat that can be performed in the Risø reader, and within a limited period of time. Experiments were initially started using a preheat of 220°C for 10 minutes. However, the work that Li (1991a) did to establish the validity of this preheat used an argon-ion laser to stimulate the luminescence. To ensure that this preheat was also applicable to IRSL, two experiments were performed. First, a similar analysis to that described above was used. Then an ED plateau was calculated using ten minute preheats at different temperatures.

The first experiment used ten discs of sample GDNZ 32. Samples were natural normalised, and five were then given an additional dose of 31 Gy on top of their ED of about 32 Gy. Pairs of natural and irradiated discs were then preheated at 220°C in the Risø reader for 0, 1, 5, 10 and 20 minutes. After IRSL measurement the discs were then TL glowed to 450°C at 3°C/s. A 5-58 and BG-39 filter were used. All discs were then second glow normalized.

Figure 4.7.3(a) shows the TL glow curves for the ten discs. The ratio of  $(N+\beta)/N$  for the TL integrals from 0 to 450°C are plotted in figure 4.7.3(b). After one minute preheating the

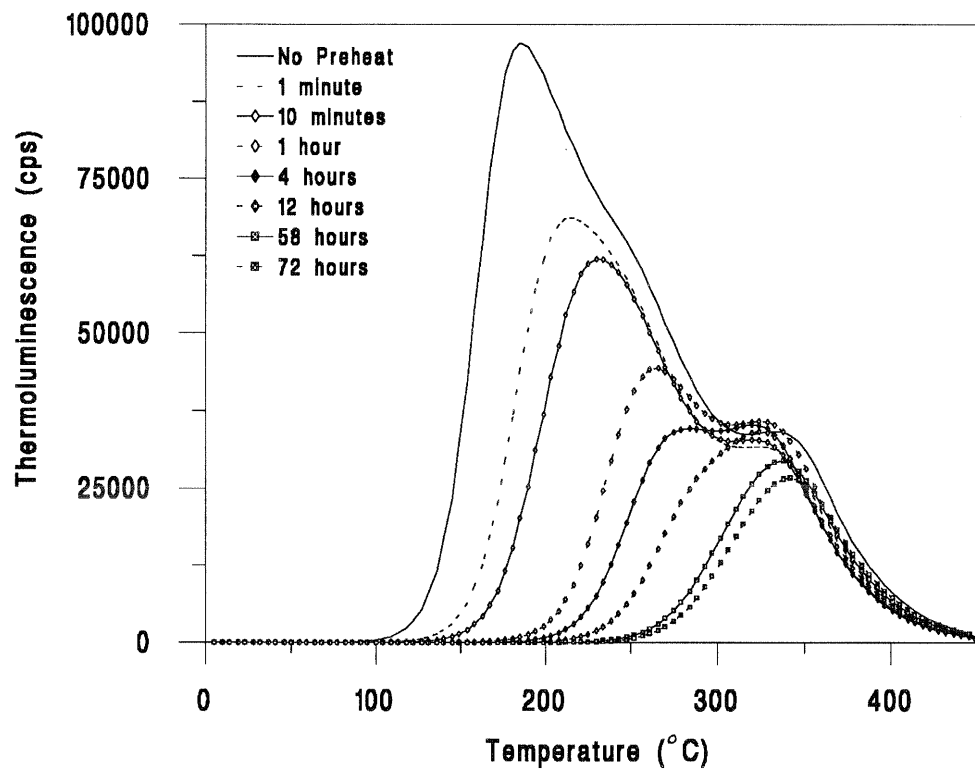
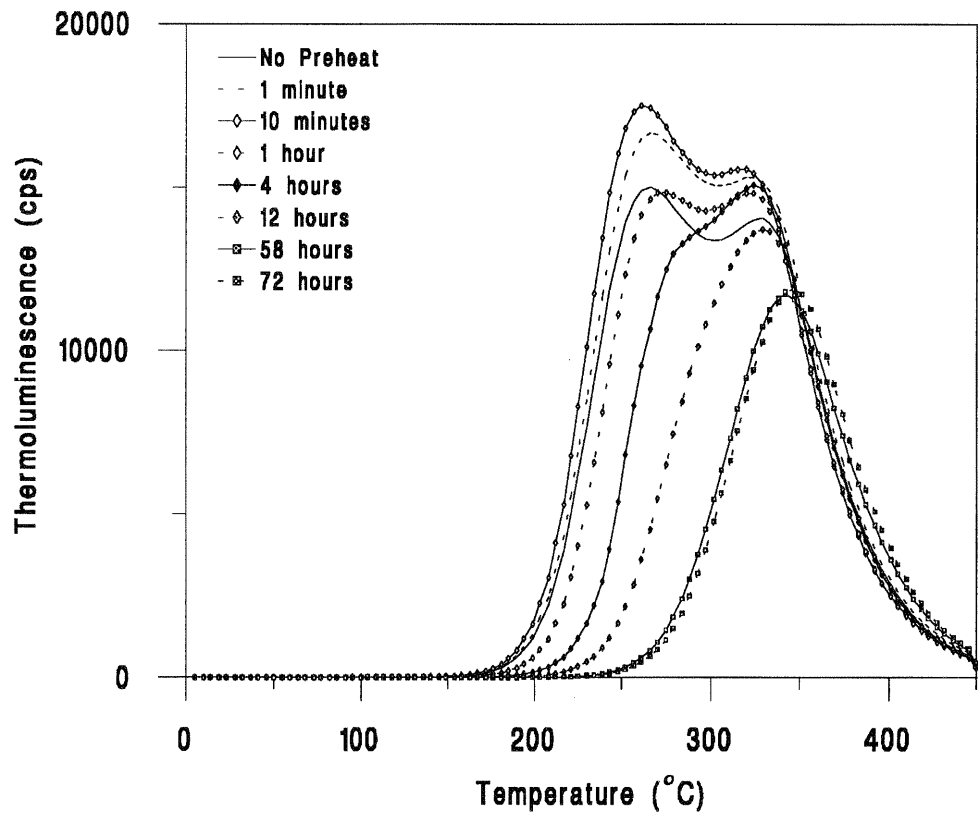


Figure 4.7.2(a): The effect of preheating at 140°C upon un-irradiated (above) and irradiated (bottom) aliquots of GDNZ 17 for different periods of time.

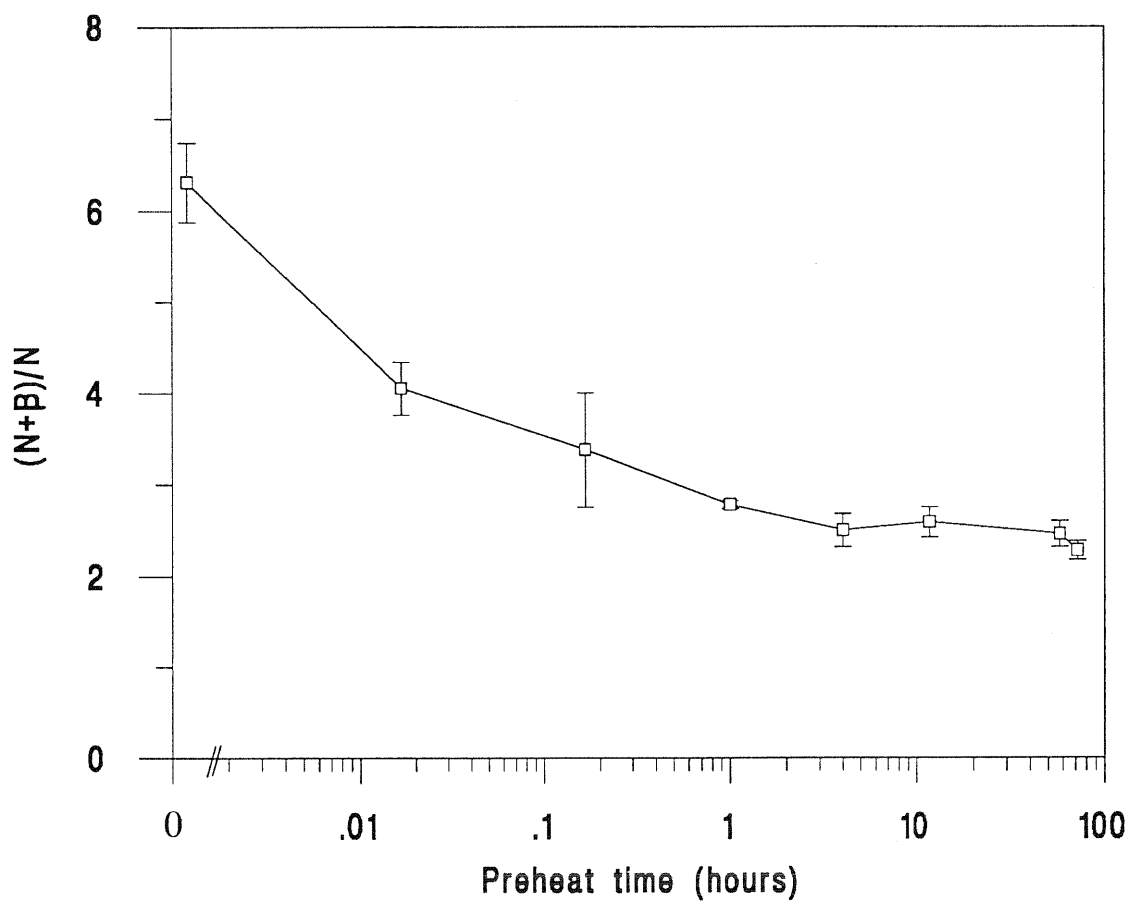


Figure 4.7.2(b): The ratio of the TL integral (0-450°C) of irradiated and un-irradiated aliquots of GDNZ 17 as a function of the length of preheating at 140°C.

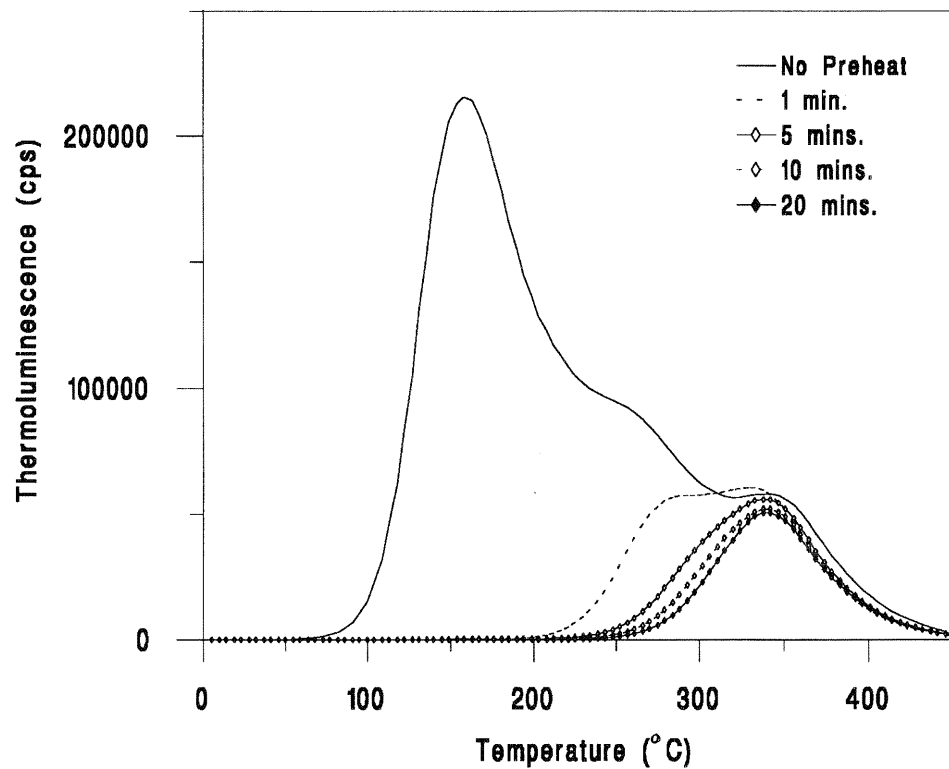
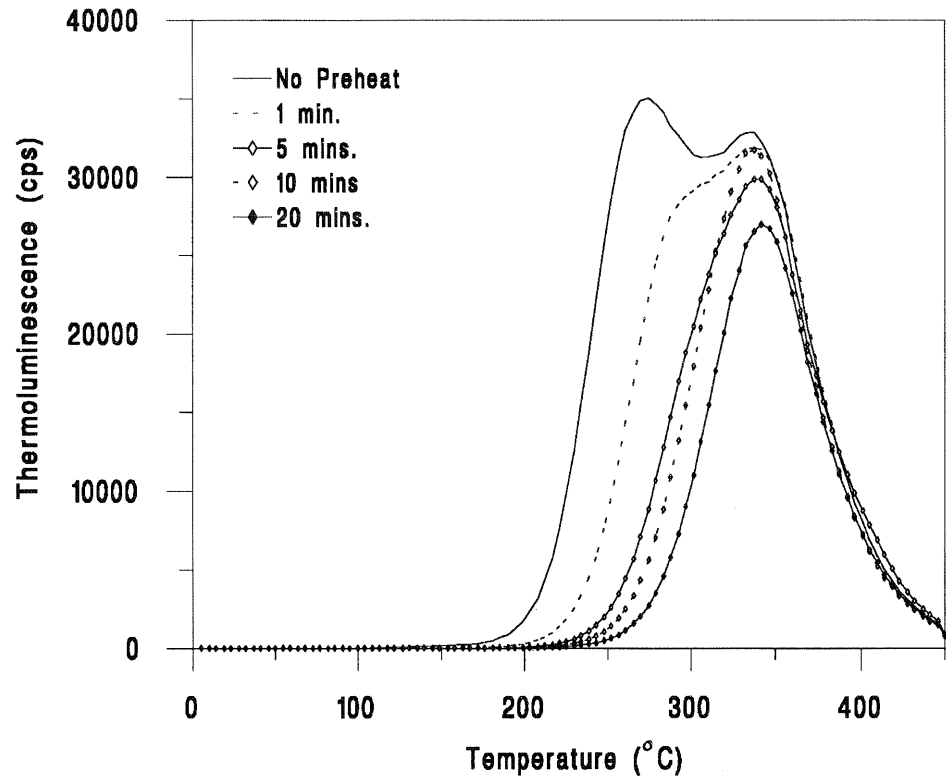


Figure 4.7.3(a): The effect of preheating at 220°C upon un-irradiated (above) and irradiated (bottom) aliquots of GDNZ 32 for different periods of time.

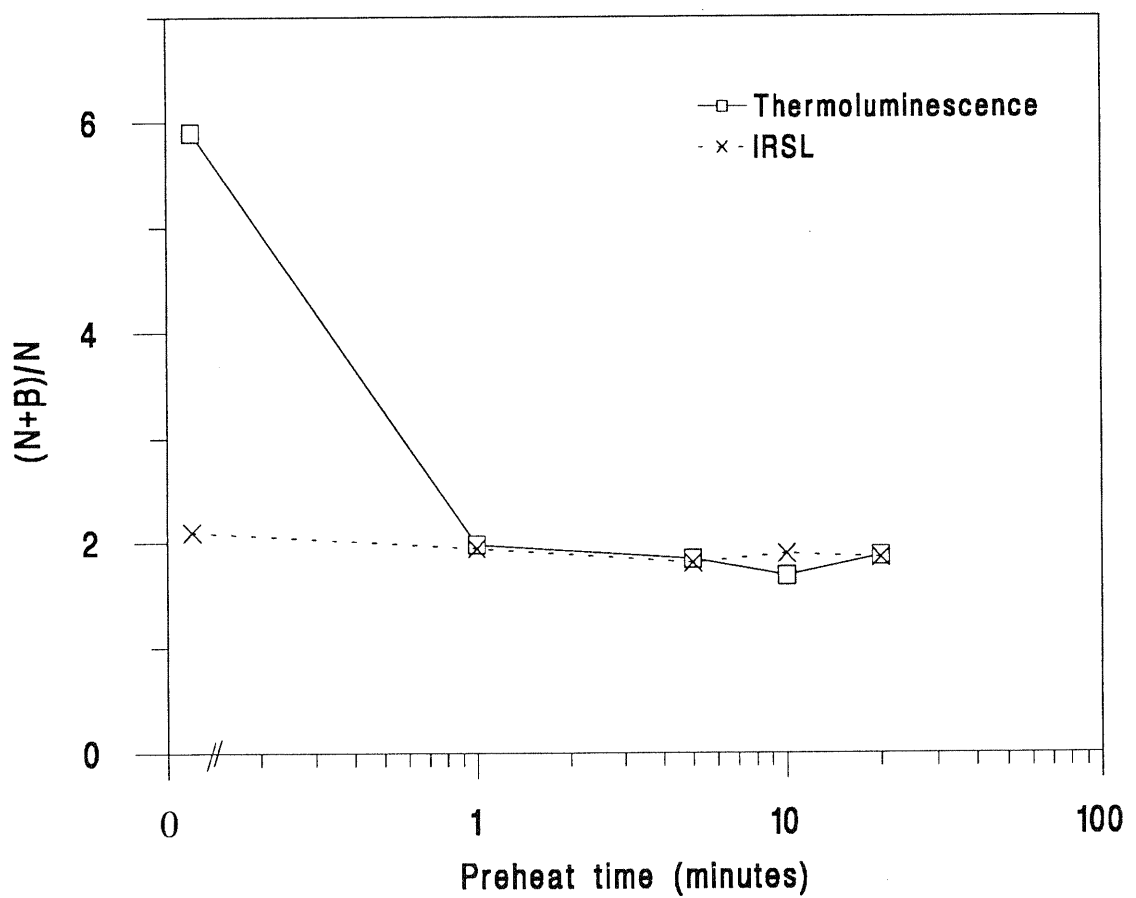


Figure 4.7.3(b): The ratio of the luminescence signals from irradiated and un-irradiated aliquots of GDNZ 32 as a function of the length of preheating at 220°C. TL data have been integrated from 0-450°C, and the IRSL data have been obtained using a 0.1s IRSL measurement.

ratio  $(N+\beta)/N$  as measured by TL remains constant, and from figure 4.7.3(a) a preheat of 5, 10 or 20 minutes isolates the 330°C TL peak. Figure 4.7.3(b) also shows the  $(N+\beta)/N$  IRSL results for the same ten discs. In contrast to the TL results the ratio of  $(N+\beta)/N$  as measured by IRSL remains almost constant over the whole period studied in the experiment. This strongly suggests that little or no IRSL is associated with the TL peak seen at 180°C and that for this sample there has been negligible loss of any IRSL signal associated with the 270°C peak over the period since the sample was deposited (sample age is  $11.7 \pm 0.8$  ka, table 8.3(b)).

The second experiment used a single aliquot additive dose method (see section 7.3.2 for the method) to provide data to calculate an ED plateau for GDNZ 13 using preheats for 10 minutes at room temperature, 100, 150, 200, 220 and 250°C. Four discs were used for ED determination and two for preheat calibration at each temperature. In addition 18 results using the 220°C preheat are shown, as determined in the routine dating of the sample. Figure 4.7.3(c) shows the growth curves generated for each different preheat temperature. The lower slope at higher preheat temperatures is due to the increasing loss of signal. Figure 4.7.3(d) suggests that while the EDs determined using no preheat are significantly lower than for other temperatures, there is very little difference in the EDs when using preheats of 100° and 150°C. The differences seen from 100 to 250°C are small and thought to be negligible.

The effect of the preheats at room temperature, 100°C, 150°C, 200°C, 220°C and 250°C on the TL signal were evaluated by glowing the discs used for their characterisation. In addition to the two discs that just retained their natural signal, used for preheat calibration of data in figures 4.7.3(c) and (d), at each temperature discs that had been bleached for 24 hours in the SOL2 and had 43 Gy added were preheated and subsequently glowed. Figure 4.7.3(e) shows the TL glow curves of the natural discs after 10 cycles of preheating, and the glow curves for the  $I_0+43$  Gy discs. Preheating for 10 minutes at 200°C or above is needed to isolate the 330°C peak.

On the basis of all the experiments reported in this section a preheat of 220°C for 10 minutes was used for all single aliquot analyses described in this study. Preheats at higher temperatures are unsuitable since the size of the signal is reduced by such a large fraction. This preheat is needed not to remove the 180°C TL peak, which appears to contribute very little, or not at all, to the IRSL signal, but to remove any prompt luminescence, and to isolate the 330°C peak from the 280°C peak which is believed to be less stable. IRSL alone is not capable of distinguishing a suitable preheat and TL must always be used as well.

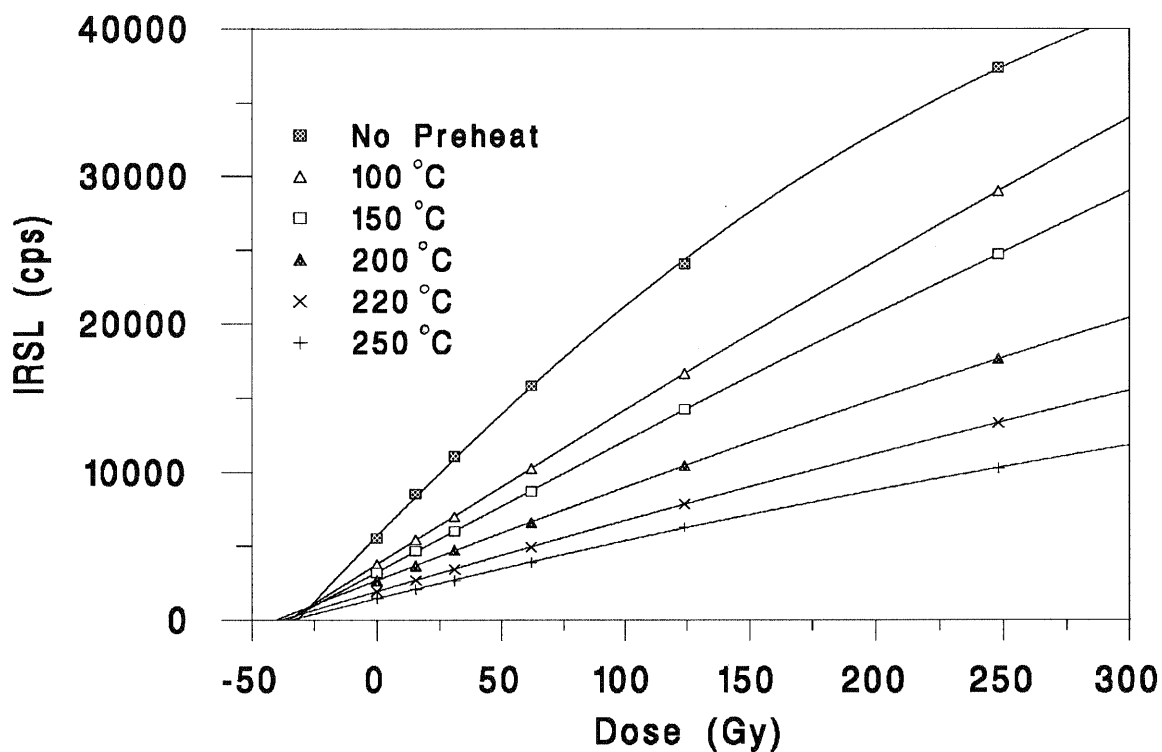


Figure 4.7.3(c): Single aliquot growth curves for GDNZ 13 using preheating at various temperatures for 10 minutes. Data have been corrected using luminescence correction method B (see section 7.3.2).

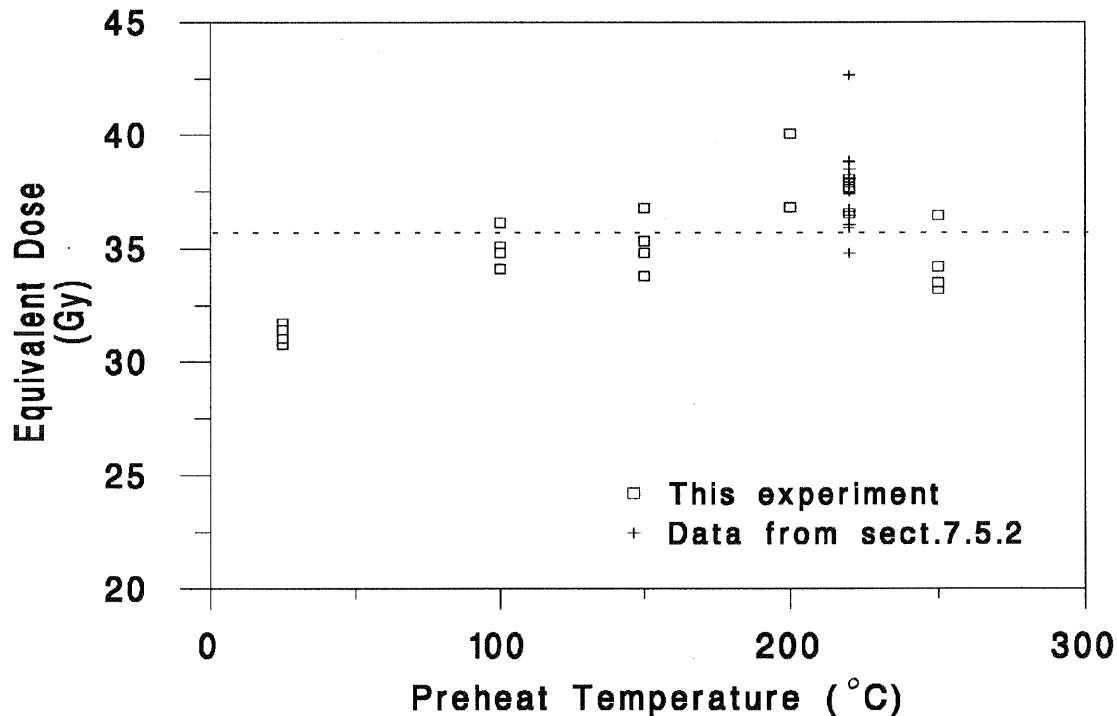


Figure 4.7.3(d): The relationship between equivalent dose and preheat temperature using single aliquots of GDNZ 13.

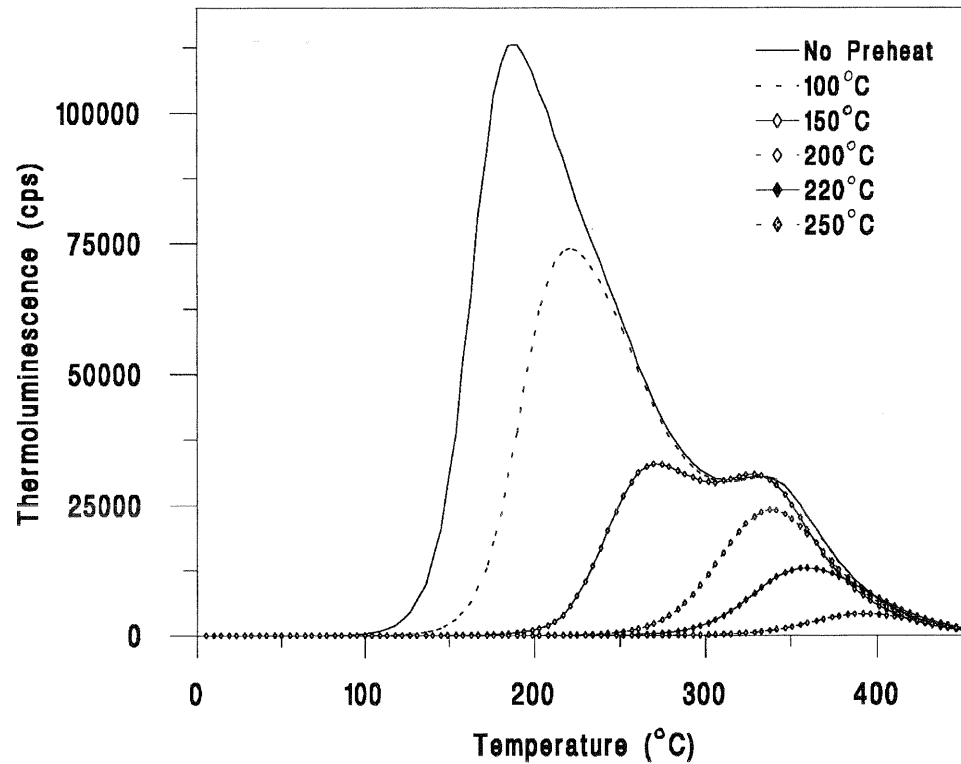
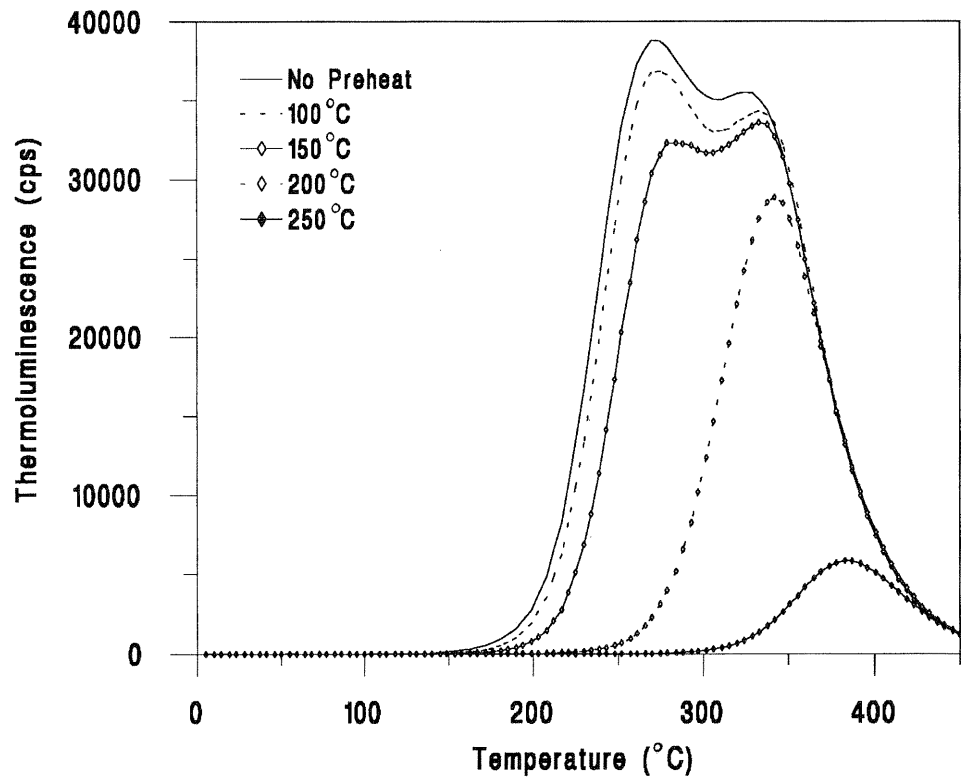


Figure 4.7.3(e): TL glow curves of un-irradiated (above) and irradiated (bottom) aliquots of GDNZ 13 after 10 cycles of preheating for 10 minutes at various temperatures.

Hütt and Jungner (1992) are of the opinion that there is little or no contribution to the IRSL from unstable components, and that only the 'phosphorescence' needs to be removed. This is the prompt luminescence due to highly unstable signals. Hütt and Jungner (1992) suggest that this is best removed by leaving at room temperature for 3 weeks. On the basis of the results in figure 4.7.3(d), heating to 100°C for 10 minutes is sufficient to remove such signals, but is not able to remove the relatively unstable 270°C TL peak (Strickertsson 1985). Figure 4.7.4 (in the next section) demonstrates that there is an IRSL signal associated with the TL peak at 270°C, and so the preheat at 220°C for 10 minutes is preferred since it effectively removes all of this TL peak.

#### 4.7.4 Implications of preheating experiments for our understanding of the relationship between IRSL and TL

Figure 4.7.4 plots the TL integral from 0 to 450°C for the results from figure 4.7.3(e) against the IRSL signal that they gave. All discs, with the exception of the irradiated discs that had received no preheat, or a preheat at 100°C, lie on a straight line. These two groups of samples are the only ones to have a significant TL signal below 200°C. This implies a very close relationship between the TL integral from about 250°C to 450°C and the IRSL signal when samples are preheated. Such a relationship would indicate that IRSL for this sample cannot be related to only a single charge trap as proposed by Hütt *et al.* (1988) and Hütt and Jaek (1989), and that the charge responsible for the two luminescence signals responds to preheating in similar ways. This would imply that similar traps are being probed by the two measurements. These results contrast with the striking differences in the behaviour of the two luminescence signals when exposed to light (see table 5.4 and figures 6.6.2 and 6.6.3). The relationship between the IRSL and TL signals from potassium feldspars will be discussed further in chapter 6.

### 4.8 Laser Ablation Inductively Coupled Plasma Mass Spectrometry

Dose rate determination has been attempted by a variety of methods. The majority of these are standard techniques in luminescence dating, and are discussed briefly in chapter 5. However, a new technique has been used for the determination of the potassium content of the potassium feldspar separated as described in section 3.2.1.

The most common method of determination of the internal beta dose due to the potassium within the grain involves dissolving the grains using a hydrofluoric-perchloric acid digestion technique, and subsequent potassium determination using flame emission

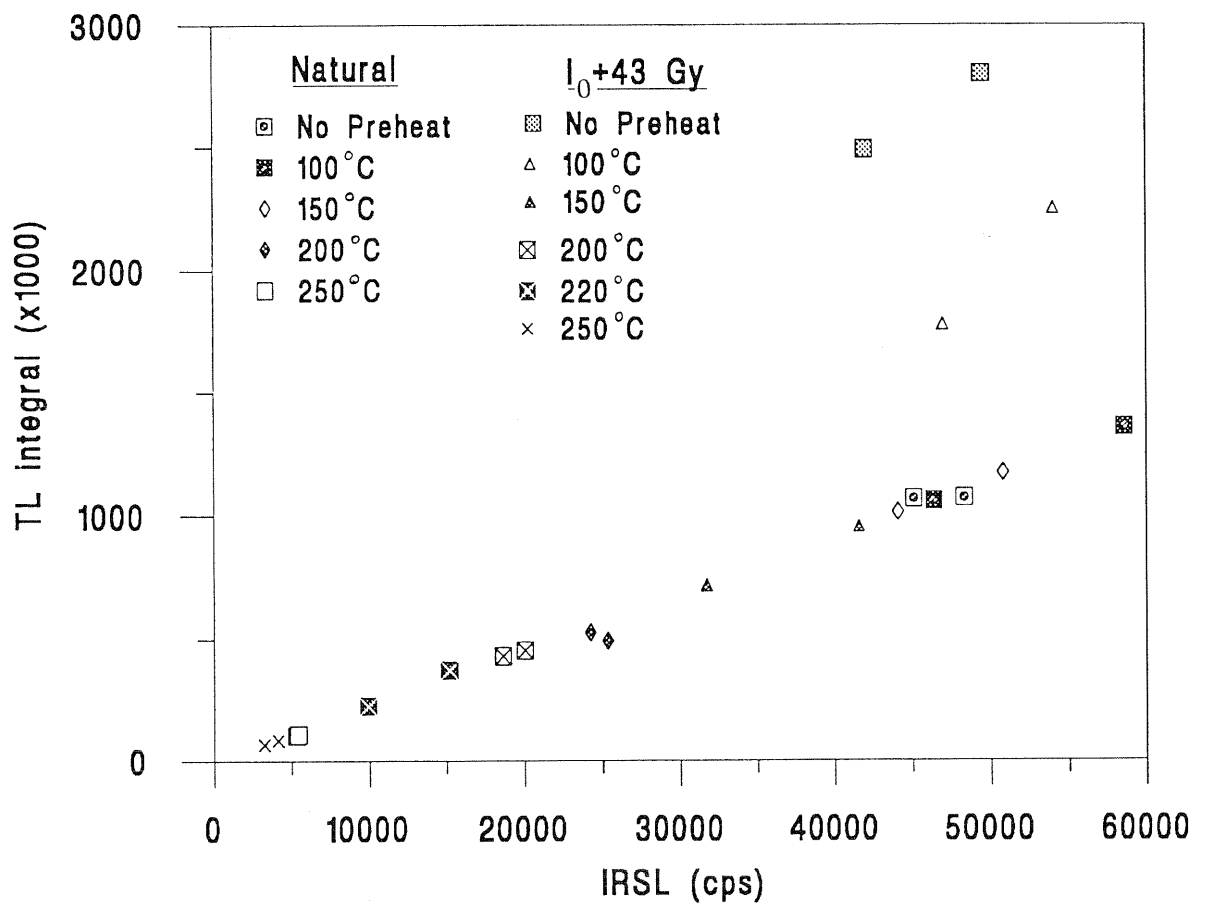


Figure 4.7.4: The relationship between the TL integral (0-450°C) and the IRSL signal (0.1s IRSL measurement) for the aliquots shown in figure 4.7.3(e). Each curve in figure 4.7.3(e) was the average from two aliquots and so there are double the number of data points in the diagram above.

spectrophotometry (FES). However, digestion of the feldspar involves the use of dangerous acids and is time consuming. An alternative method based upon laser ablation inductively coupled plasma mass spectrometry (LA-ICP-MS) has been described by Pearce *et al.* (1992) where the only pretreatment involved is to grind samples (to less than 20µm) and to press them into 'pellets' (normally 0.5cm in diameter and 0.5cm in height).

A VG Instruments Laserlab system, based around a Nd:YAG laser operating at 1064nm is used to ablate material from the surface of the pellets. The material is then introduced into the ICP-MS (VG Instruments PQII+ ICP-MS) where it is ionized in an argon plasma. The mass spectrometer can then be tuned to measure the concentration of specific ions with atomic mass from lithium (A=6) to uranium (A=238).

Using ICP-MS (or LA-ICP-MS) it is not possible to use the raw count data for an element to compare peak areas directly against standard samples to produce concentrations since variations in the amount of material ablated, or changes in the sensitivity of the instrument will cause the response to vary with time. When analyzing material in solution the normal procedure is to introduce an internal standard of known concentration for calibration. The concentration of this element varies with changes in operating conditions and can be used to normalize the data. When analyzing material in a solid form the major problem is the choice of an internal standard. In the case of alkali feldspars aluminium appears to be a suitable internal standard since it forms a major constituent of the crystal lattice, and it constitutes a relatively constant proportion of the total molecular mass (table 4.8).

Table 4.8 Concentrations of potassium and aluminium for standard reference feldspars used to calibrate the ICP-MS.

<u>Reference Material</u> <sup>(a)</sup>	<u>K(%)</u>	<u>Al(%)</u>
GSJ JF-1	8.36	9.52
GSJ JF-2	10.88	9.75
BCS-CRM-375	0.66	10.48
BCS-CRM-376	9.30	9.37
Mix A <sup>(b)</sup>	3.23	10.16
Mix B <sup>(c)</sup>	5.80	9.84

Notes:

- (a) Reference materials are from the Geological Survey of Japan (GSJ) and British Chemical Standards (BCS).
- (b) Mixture A consisted of two parts BCS-375 to one part JF-1 (by weight).
- (c) Mixture B consisted of two parts JF-1 to one part BCS-375 (by weight).

A number of standard reference feldspars were used to calibrate and verify this method. They are listed in table 4.8. The standards tended to have either very high, or very low potassium contents, and so two mixtures of these standards were used to provide intermediate values. Figure 4.8(a) shows the relationship between the ratio of the potassium divided by the aluminium content versus the potassium content for all the standards used to calibrate the instrument, calculated using published values.

Figure 4.8(b) shows the results of analysis of these standards using the Nd:YAG laser at a repetition rate of 1.7Hz. Two data points have been excluded from the analysis as they are obvious outliers. The remaining data give a regression coefficient ( $r^2$ ) of 0.9912. This method was used to determine the potassium content of all the feldspar separates analyzed in this thesis (see section 5.3.4).

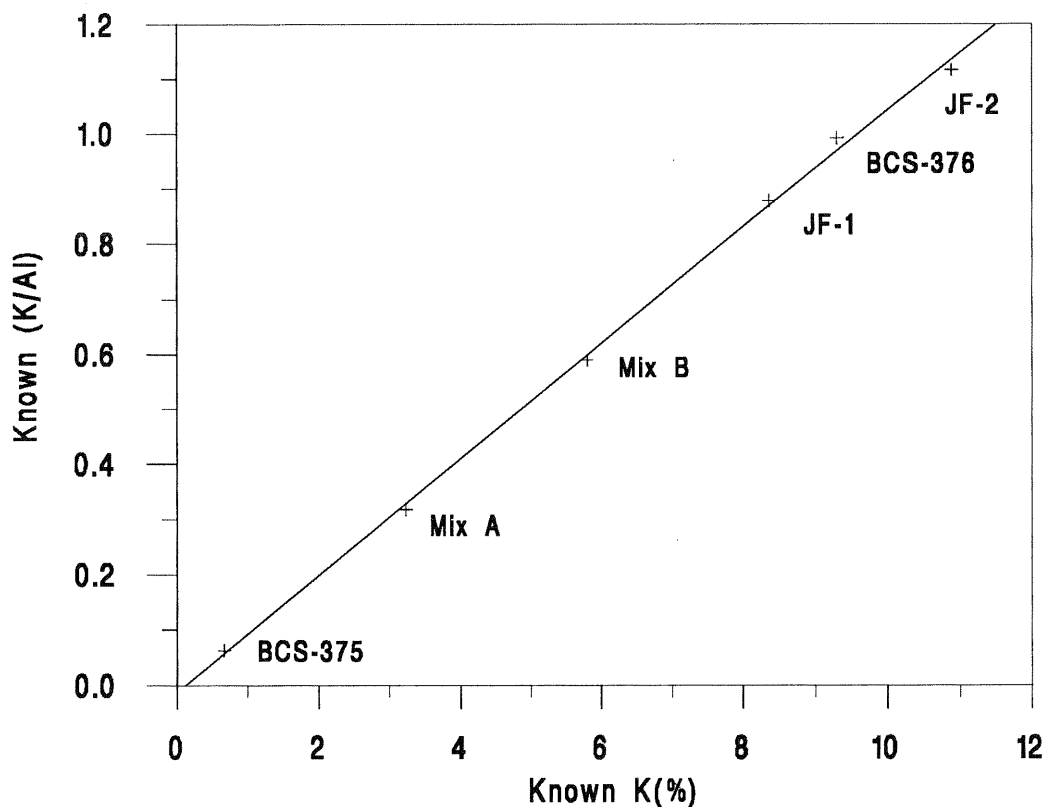


Figure 4.8(a): The ratio of potassium/aluminium (weight percent) as a function of potassium for a number of standard reference feldspars using quoted values (see table 4.8).

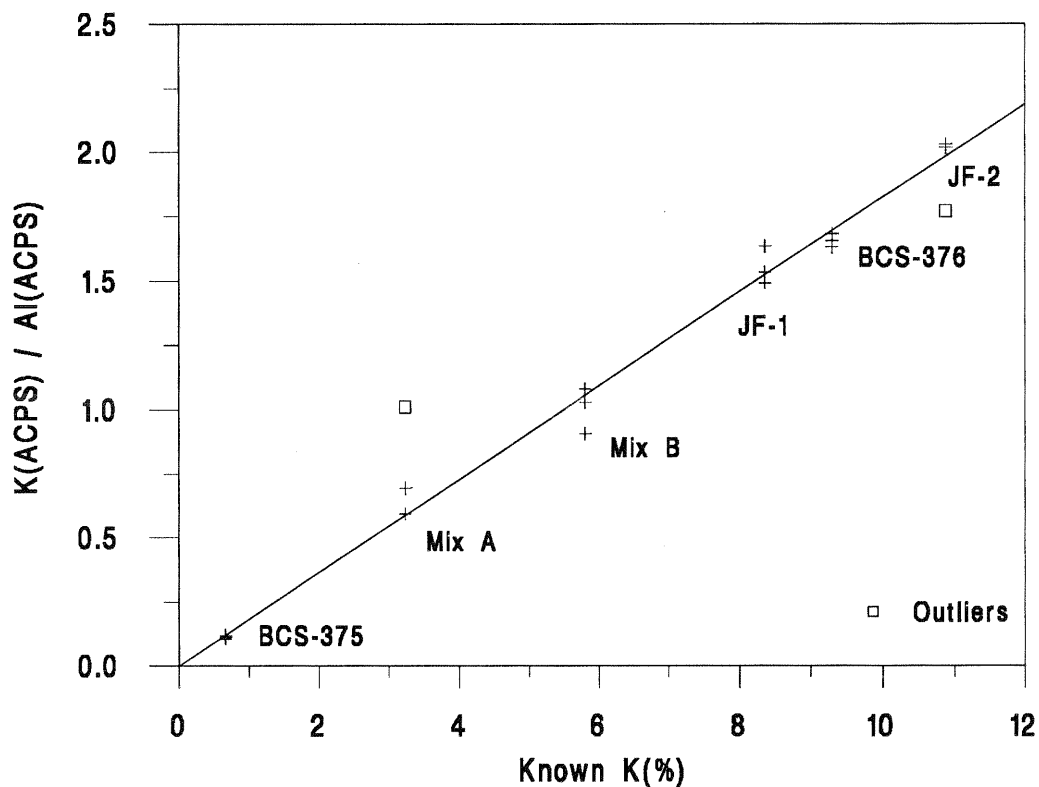


Figure 4.8(b): The ratio of potassium/aluminium, measured in area counts per second (ACPS) on the ICP-MS, as a function of known potassium concentration for a number of standard reference feldspars.

## **CHAPTER 5: The application of standard methods of equivalent dose determination to samples of known age.**

No geochronological method should be used without testing it on samples of known age. In practice this means comparing with another, preferably independent, dating method. The aim of this chapter is to date a variety of samples of dune sand from south-west North Island New Zealand, using luminescence methods based upon potassium feldspar as the dosimeter, and to compare the results with other age estimates for the sites concerned. The independent age control is provided by both radiocarbon and fission track dates. The geological setting from which the samples were taken is described in chapter 2.

### 5.1 Previous attempts to compare luminescence dating methods based upon potassium feldspar with known age samples.

Previous attempts to test luminescence dating based upon the use of coarse grain potassium feldspars have produced equivocal results. Only a single comprehensive dating study using IRSL has been published (Edwards (1993)) and no independent age control was available for any of the samples. The majority of studies on potassium feldspars have used thermoluminescence measurements and many have analyzed material that may not have been well bleached at deposition (e.g. Jungner *et al.* (1989) dating sandur). This leads to large uncertainties in the residual level and may cause overestimation of the age if the sample is overbleached in the laboratory. Where determination of the residual level has been especially difficult (e.g. Kolstrup and Mejdahl (1986) dating frost wedge cast infills, and Jungner (1987) dating sands intercalated with peat) a variety of techniques have been adopted to overcome it. Uncertainties in the residual level will have a particularly significant effect upon the age of young samples which are most frequently used for comparison with other dating methods.

Kolstrup *et al.* (1990) found good agreement between TL ages based upon quartz and potassium feldspars from Danish cover sands, while in a parallel study on the same samples Grün *et al.* (1989) found underestimation of the luminescence age by 20-40% when using potassium feldspars. Dijkmans and Wintle (1991) and Dijkmans *et al.* (1992) also found that luminescence ages measured using potassium feldspars underestimated the expected age of Dutch cover sands, and Balescu *et al.* (1991) found an apparently consistent 40% age underestimation for a suite of samples from raised beaches around NW Europe (figure 5.1). In this latter study, determination of the residual level for such beach material may have introduced some uncertainties but since the majority of samples were

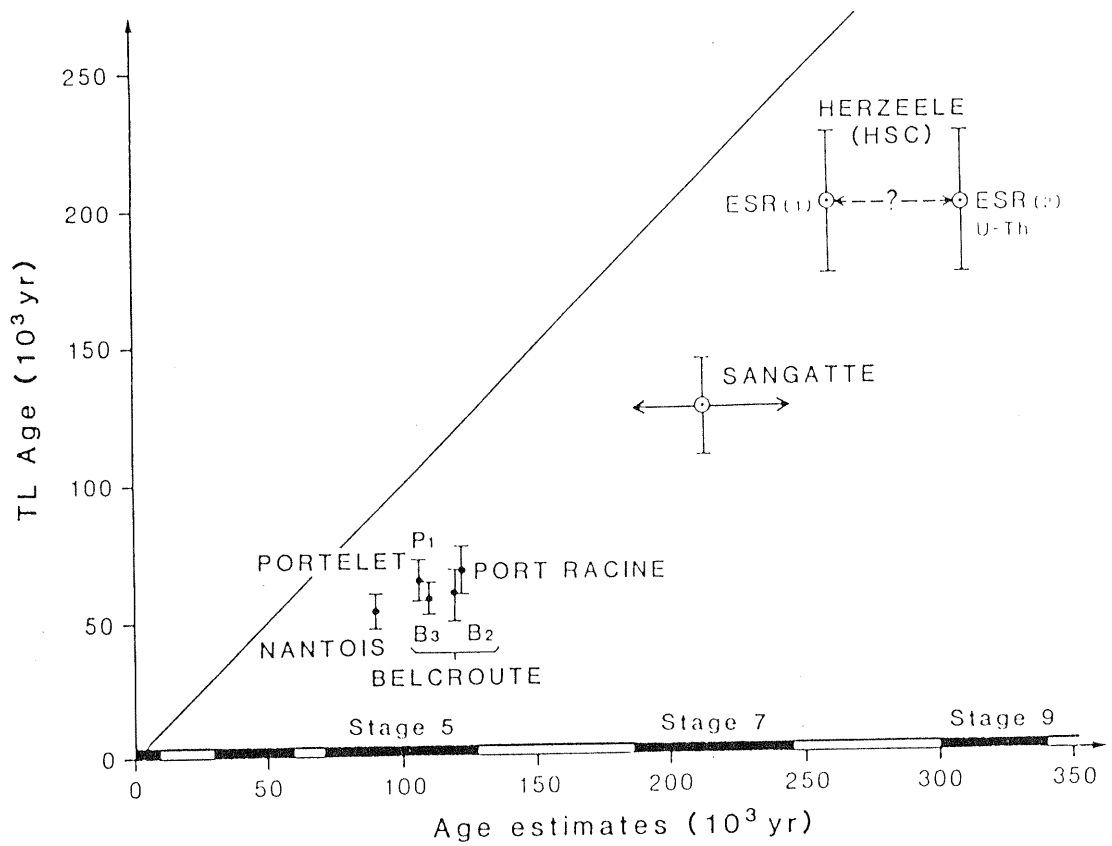


Figure 5.1: Comparison of geological age estimates and thermoluminescence age estimates (determined using potassium feldspars) for beach and dune sands from NW Europe (from Balescu et al. 1991).

100ka or older the effect upon the final age would be minimal. There was also a problem with the age control of the oldest sample used in the study since it was correlated to the Holsteinian interglacial. Whether the Holsteinian represents oxygen isotope stage 7 or 9 has been the subject of much debate (i.e. Sarnthein et al. 1986 and Schwarcz and Grün 1988) and still remains uncertain.

Balescu and Lamothe (1992) and Wintle and Duller (1991) suggested that the underestimation observed by many workers may relate to the use of a UG-11 filter which transmits primarily in the ultra-violet (see discussion in section 4.3.2). Those studies where a filter transmitting primarily in the blue was used (i.e. Kolstrup et al. (1990), Mejdahl (1992) and Balescu and Lamothe (1992)) produced ages that were closer to the expected results. Mejdahl (1992) also found severe supralinearity in several samples of dune sands from central Sweden of late-glacial age (amounting to as much as 20% of the ED) which would cause underestimation of the age if the additive dose technique were used.

Mejdahl (1988) suggests that another cause of age underestimation for samples over 100ka is a long term loss of signal at ambient temperature. This would imply that samples would exhibit a higher saturation luminescence signal when irradiated in the laboratory compared with that achieved in nature. A correction procedure is suggested by Mejdahl (1988), but the magnitude of the correction is thought to be dependent upon the mean ambient temperature.

Grün et al. (1989) suggested another possible explanation of the discrepancies between the expected ages and those determined using luminescence methods based upon potassium feldspar. An assumption of using potassium feldspars to date sediments is that the potassium content measured from all the grains separated for equivalent dose determination, and hence used in the dose rate calculation, represents the potassium content of those grains that yield the luminescence signal. By analysis of single grains Grün et al. (1989) showed that a large proportion of the total luminescence signal arises from a relatively small proportion of the grains separated for ED determination. They were unable to demonstrate any correlation between the magnitude of the luminescence signal and the potassium content of the grain. However, this assumption is important since the potassium content of separated 'potassium-rich feldspar' may vary from as low as 1.2% (Dijkmans et al. 1992) to as high as 13.0% (Dijkmans and Wintle 1991). Where the internal beta dose rate is a significant proportion of the total dose rate, such a variation would have an enormous effect upon the calculated luminescence age. Where no attempt was made to separate a potassium-rich feldspar fraction, because of the low feldspar content of the material, but all the material lighter than  $2.62 \text{ g cm}^{-3}$  was used (Rendell et

al. 1991 and Rendell 1992) concordant ages were obtained using the quartz and feldspar fractions. Potassium contents within these separated feldspar fractions were in the range 3-4.5%. In such a mixture of grains, with differing potassium contents, it is impossible to state whether the luminescence signal that is measured originates from grains with a high or a low internal beta dose rate, and thus a systematic error may be introduced.

On the basis of published data it is still unclear why there is such a discrepancy between the ability of different authors to match luminescence ages determined using potassium feldspars and expected geological ages. Large discrepancies are apparent between various studies in the ability to separate a potassium-rich feldspar fraction from sediments and this will have a significant impact upon the annual dose rate where the external dose rate is low. Additionally, the determination of the TL residual level has proved complex for many samples, and errors in this measurement have a profound effect upon the ED determined, especially for young samples.

The aim of this study is to use TL and IRSL measurements to date well bleached dune sands from the Wanganui and Manawatu regions of New Zealand using potassium feldspar. The use of IRSL, and the selection of dune sands, rather than waterlain sands, is intended to reduce the uncertainty in the residual level. Within this area dune sands can be found with ages from modern to about 350ka (Pillans, 1988), with a range of independent age controls against which the luminescence ages can be compared. Section 5.2 gives a brief description of the samples chosen and the age control upon them.

## 5.2 Description of samples analyzed

A suite of twelve samples were chosen for TL and IRSL dating using standard, multiple disc, methods of equivalent dose determination (described in section 5.4). They were chosen to give a broad age range, and to have some form of independent age control. Site descriptions can be found in appendix I and their locations are marked on figure 5.2. A brief description is given below of the age control on each sample. Samples are listed in order of increasing age.

### GDNZ 21: Hokio Beach

This sample was taken from the surface of an active slip face of a modern dune ridge 10m behind the beach. As along all of the coastline of this part of New Zealand, the sand is grey to black in colour due to the high content of mafic minerals.

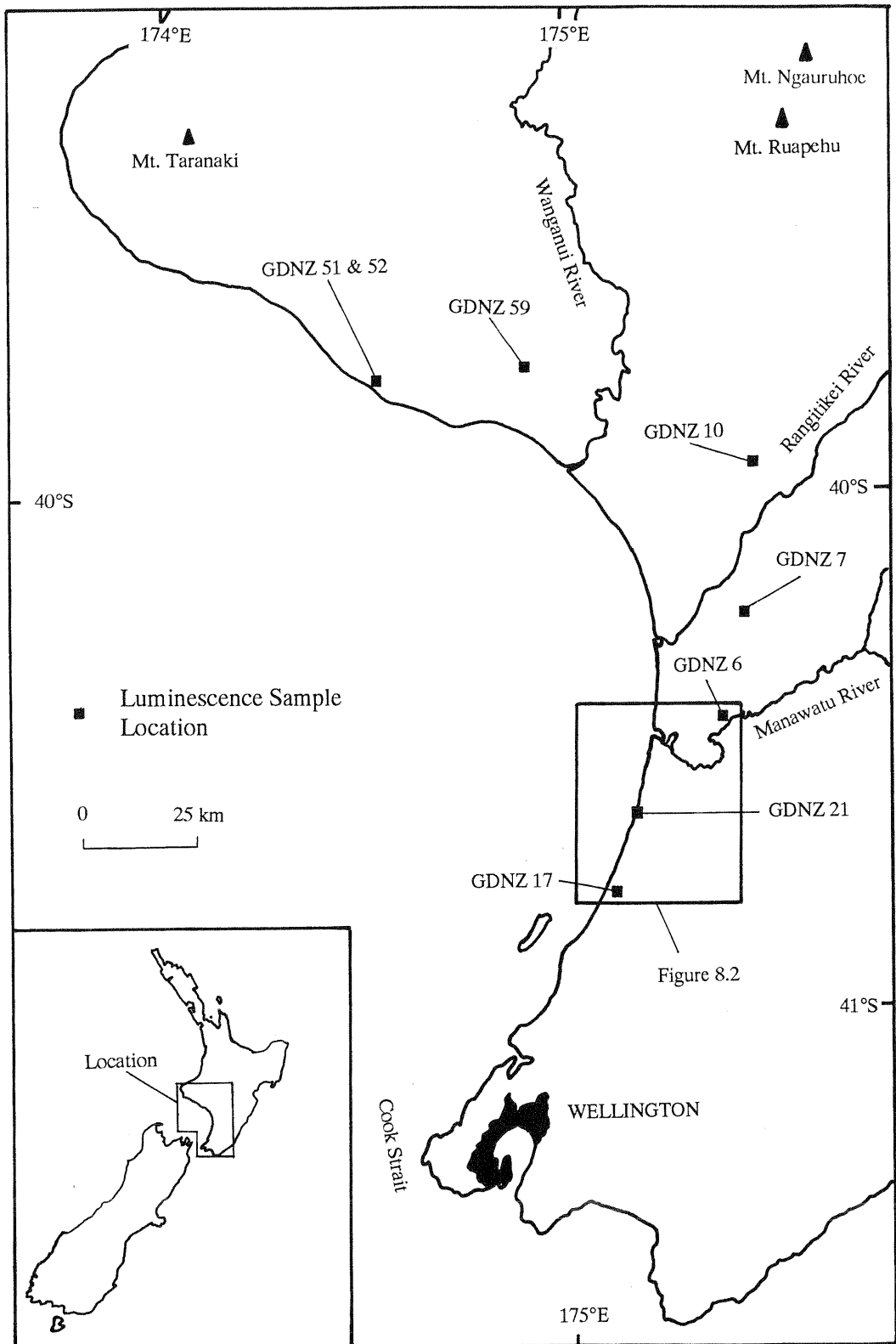


Figure 5.2: Map showing the location of samples collected for luminescence dating from sections with some age control. The relative position of figure 8.2 is also shown, and the locations of samples GDNZ 1, 5, 13 and 45 are marked on that figure.

### GDNZ 6: Manawatu River

A mafic rich dune sand was collected from between two peat units in a section exposed by river erosion. Radiocarbon ages for the peats are  $1860 \pm 65$  years BP and  $2380 \pm 110$  years BP (NZ5221 and NZ5220 respectively, from Shepherd and Lees (1987) corrected for secular effects). GDNZ 6 was taken from the middle of the 0.5-0.6m gap between the two peats.

### GDNZ 17: Te Waka road

A small group of dunes are found south of the Otaki river, west of State Highway One. At this site 3.1m of dune sand overlies fan gravels. GDNZ 17 was collected 0.7m from the crest of the dune where it was exposed in a road cutting. Both the alluvial fan and the dunes have been truncated on the seaward side by the post-glacial sea level maximum. Palmer *et al.* (1988) gave an age of 6,500yrs BP - 10,000yrs BP for these dunes. The maximum age is given by the date at which the alluvial fan is believed to have ceased to form. This is inferred by Palmer *et al.* (1988) from radiocarbon dating of similar aggradation surfaces in the Rangitikei valley (Milne and Smalley 1979), though the method of correlation between the two areas is not given. The lower age limit can be inferred from the cutting of a cliff into the fan and dune sand by marine action that is presumed to relate to the post-glacial sea level maximum. The post-glacial sea level maximum has been dated at circa 6,500yrsBP (Gibb, 1986 and Ota *et al.*, 1988) in this area.

### GDNZ 1: McLeavy road

GDNZ 1 was taken from a dune designated as part of the Koputaroa dune phase on the basis of the degree of soil development upon its surface and the presence of Kawakawa tephra. The sample was taken approximately 30cm above the Aokautere ash (a distal member of the Kawakawa tephra). The tephra thus gives a maximum age of  $22,590 \pm 230$   $^{14}\text{C}$  yrs BP for the dune above it (Wilson *et al.* 1988). As discussed in chapter 2, Bard *et al.* (1990) have shown that during this time period radiocarbon dates would underestimate the calendar age of the sample by approximately 2,500 years, and so the calendar age for the Kawakawa tephra would be 24 ka.

### GDNZ 5 & GDNZ 45: Paiaka road

Cowie (1963) first described this site, where dune sand overlies the Tokomaru marine terrace, which is thought to be last interglacial in age (Hesp and Shepherd, 1978). Kawakawa tephra occurs within the dune at this site as a layer of fine grey ash approximately 1-2cm in thickness. There is no indication of any weathering above or below the tephra to suggest any hiatus between deposition of the dune and the tephra. Sample GDNZ 5 was taken 0.5m above the ash and GDNZ 45 from 0.3m below, giving age constraints of <24 ka and >24 ka respectively as discussed above.

### GDNZ 13: Koputaroa road

Cowie (1963) first described this site that lies 2km south-west of the Paiaka road site. A more complex sequence is exposed at the Koputaroa road site (as described in appendix I), but once again Kawakawa tephra occurs within a dune sand. GDNZ 13 was taken 0.3m below the ash, and so should be >24 ka.

### GDNZ 51 & GDNZ 52: Whenuakura River

At this site a marine cut surface is overlain by pebbly marine sands, a lower mafic dune sand (GDNZ 51), loess (L4), an upper mafic dune sand (GDNZ 52), and then three loess units (L3, L2 and L1) (Palmer pers.comm.). Age control comes from dating of the pebbly marine sands using amino-acid racemization on wood fragments (Pillans 1983), and correlation of the loess units with the loess stratigraphy across the Wanganui basin (Pillans 1988). The amino-acid racemization results, together with correlation to other terrace fragments on the basis of altitude (see figure 2.1(c), part (iii)), indicate that the cut surface at the base of the section may be the Rapanui marine terrace which formed at the maximum of oxygen isotope stage 5e (O.I.S. 5e) (Pillans 1983). The precision of amino-acid racemization measurements is poor and so the correlation of the marine cut surface with O.I.S. 5e may be over optimistically precise, and the surface may have been cut during any part of O.I.S. 5. However, on the basis that the surface is the Rapanui marine terrace it is thought that loess unit L4 was deposited during O.I.S. 5d and that subsequently, the upper mafic dune sand (GDNZ 52) was deposited, during the interval from O.I.S. 5c to 5a, before deposition of loess units L3, L2 and L1 starting in O.I.S. 4 (Palmer pers.comm.). Using the timescale derived by Martinson *et al.* (1987), this interpretation gives age constraints for the two samples of 110-130ka for GDNZ 51 and 74-103ka for GDNZ 52. However given the uncertainty in the age of the cutting of the terrace, these can only be considered as maximum ages for the samples.

### GDNZ 7: Penny road

Separating the flood plains of the Rangitikei and Manawatu rivers, Mt. Stewart has been uplifted by block displacement of the basement. This has preserved a dune sand underlying three loess units (Berryman and Hull, 1984). The age of the sand is estimated only by counting loess units overlying the sand. Porewa, Rata and Ohakea loess overlie the dune sand, and Kawakawa tephra has been found within the Ohakean loess. No evidence exists regarding what part of O.I.S. 5 the dune sand may be from, so only the loosest of age constraints can be used (74-130ka, Martinson *et al.* 1987).

### GDNZ 10: Mt Curl Tephra type Site

Milne (1973) defined the type section for the Mt Curl Tephra. At the site a slightly mafic dune sand (Brunswick Dunesand) overlies the tephra, though there is some evidence of weathering in the upper part of the tephra implying a hiatus in deposition. Recent evidence has shown this tephra to be correlative with the Rangitawa Pumice and to have a fission track age of  $350\pm 40$  ka (Kohn *et al.* 1992, section 2.1.3). On this basis the age of the Brunswick Dunesand is thought to be less than 350ka.

### GDNZ 59: Rangitatau East road (Bushy Park Section)

In a small cutting on Rangitatau East road tephra can be seen within a dune sand. The tephra can be correlated with Rangitawa Pumice in a nearby site (Rangitatau East, Pillans 1988), where the tephra has been fission track dated, "by tephra mineralogy, loess stratigraphy and dune sand position in relation to tephra and loess" (Pillans, pers. comm.). The fission track dates that have been obtained for this tephra have been discussed in chapter 2 (section 2.1.3). On this basis GDNZ 59, which was taken from immediately above the Rangitawa Pumice is younger than  $350\pm 40$ ka. No sign of weathering or any other indication of a hiatus was apparent and so it is unlikely that a long time interval elapsed between deposition of the tephra and the dune sand sampled for GDNZ 59.

As discussed in chapter 1, two parameters, the annual dose rate and the equivalent dose, have to be determined in order to produce the age of the sample by luminescence dating. Measurements to determine the annual dose rate are discussed in section 5.3, while those concerning the equivalent dose are discussed in section 5.4.

## 5.3 Dosimetry

The annual dose rate to the sample can be divided into three parts, that derived from the bulk sediment matrix (the external dose), that derived from within the grains that are used for luminescence measurement (the internal dose), and a contribution from cosmic rays. The external dose rate was determined for the twelve samples listed in section 5.2 (and those listed in section 8.2) using a variety of methods. These are divided into direct counting of the radioactivity (alpha and beta counting, section 5.3.1) and determination of the concentration of radioactive nuclides within the sediment (section 5.3.2). The internal dose rate determination will be discussed in section 5.3.4.

### 5.3.1 Emission Counting

Three methods were used to determine the external dose rate for the 17 samples analyzed: thick source alpha counting, GM-beta counting and thick-source beta counting. Table 5.3.1 contains data derived by emission counting. No gamma-spectrometry was available when the samples were taken. However, care was taken to sample from homogeneous units, at least 30cm from the nearest lithological boundary, to ensure that there was no heterogeneity in the gamma dose rate.

Alpha counting was undertaken using a Daybreak 582 alpha counting system on subsamples that had been dried and then ground in a ball mill to less than 20 $\mu$ m diameter. Samples were counted until at least 4,000-5,000 counts and more than 100 slow pairs had been measured. The slow pairs counted are derived from the decay of  $^{220}\text{Rn}$  to  $^{216}\text{Po}$ , a daughter product of  $^{232}\text{Th}$ . The number of pairs counted, compared with the total number of alpha particles counted, can be used to determine the thorium and uranium concentrations (see table 5.3.1, Huntley and Wintle (1981) and Aitken (1985)). There is a relatively large error associated with the determination of the concentration of the two elements because of the low number of pairs counted. However, Aitken (1990) has shown that the effect of errors in the proportion of uranium to thorium derived by alpha counting makes less than 5% error on the final dose rate calculated. Thus it is preferable to use the alpha counting results to determine the total specific activity associated with both uranium and thorium decay chains (assuming secular equilibrium).

Radon is a gaseous decay product in both the uranium and thorium decay chains. The three isotopes of radon have half-lives of 55.6s ( $^{220}\text{Rn}$ ), 3.83 days ( $^{222}\text{Rn}$ ) and 3.96s ( $^{219}\text{Rn}$ ). In certain samples this gas has been found to migrate through the interstices of the matrix and to cause disequilibrium in the decay chain (Aitken 1985). A substantial part of the

radioactivity associated with the decay chains of uranium and thorium is derived from daughter products that occur after radon. Alpha counting can be used to check for radon loss by comparing alpha count rates for sealed and unsealed samples. The results are shown in table 5.3.1 for eight samples and indicate that this is not a problem for these samples.

Table 5.3.1

Results of emission counting measurements for the samples listed in sections 5.2 and 8.2.

<u>Sample (GDNZ)</u>	<u>U (ppm)</u>	<u>Alpha Counting results</u>			<u>Beta Counting Gy/ka<sup>(b),(c)</sup></u>
		<u>Th (ppm)</u>	<u>Bq/kg<sup>(a)</sup></u>	<u>Sealed/Unsealed ratio</u>	
21	1.68±0.22	7.37±0.73	51.91		1.737±0.024
6	1.31±0.13	4.95±0.43	37.23		1.494±0.018
17	1.13±0.10	3.86±0.32	30.44	0.94±0.05	1.223±0.016
5	1.18±0.12	4.37±0.39	33.17	0.95±0.05	1.193±0.030
1	1.20±0.18	4.72±0.58	34.86	1.02±0.05	1.413±0.014
45	1.33±0.14	4.40±0.45	35.24		1.129±0.029
13	2.03±0.19	4.50±0.62	44.75	1.02±0.04	1.320±0.034
52	0.66±0.12	4.02±0.37	24.98		0.606±0.013
51	1.10±0.11	3.35±0.34	27.97		0.769±0.030
7	0.62±0.10	3.79±0.32	23.52		0.649±0.010
10	0.90±0.11	3.52±0.35	26.06		0.827±0.012
59	0.70±0.09	3.40±0.30	22.97	1.01±0.05	0.667±0.013
14	0.96±0.19	6.79±0.61	40.18	1.05±0.05	1.132±0.109
15	2.41±0.25	7.77±0.82	63.03	0.98±0.03	1.490±0.067
16	1.78±0.20	4.86±0.64	42.97		1.246±0.107
24	1.29±0.16	5.72±0.50	40.11		1.269±0.064
32	1.28±0.26	8.93±0.86	53.07	0.94±0.04	1.507±0.045

Notes

- (a) Specific activity is calculated from the uranium and thorium values derived from alpha counting. Values of 4.08 Bq/kg/ppm <sup>232</sup>Th and 13.0 Bq/kg/ppm U have been taken from Aitken (1985).
- (b) All samples have been measured when dry and are values for the beta dose to an infinite matrix. No correction has been made for moisture content in this table.
- (c) Samples GDNZ 13, 14, 15, 16, 24 and 32 were counted using TSBC at Aberystwyth. All other samples were counted using a GM-Beta counter at Risø, Denmark. Samples GDNZ 1, 17, 21, 45 and 52 were counted on both systems. The ratio of the TSBC/GM-Beta counter results for these samples is 0.96±0.05.

Beta counting was undertaken by Dr.V. Mejdahl on a number of samples using a GM multicounter system at Risø, Denmark (Bøtter-Jensen and Mejdahl, 1988). Four 1g sub-samples of each sample were counted simultaneously and the beta dose rate was calculated

as the mean of these values. The remainder of the samples were counted at Aberystwyth using a Thick Source Beta Counter (TSBC) built at East Kilbride (Sanderson 1988), using MgO as a blank, and Shap Granite as a standard source. Each sample and standard (15g) was measured for a period of an hour, alternating samples and standards. The sample was analyzed three times, and each of the standards twice, during a day. The compatibility of the results from the two systems was checked by measuring five samples using both systems. The ratio of the beta activities as determined on the two systems was  $0.96 \pm 0.05$ . In both cases the samples were dried and crushed before having their beta activity measured.

### 5.3.2 Element Concentrations

In addition to determining the external dose rate by emission counting, it was also estimated by determination of the elemental concentrations of potassium, uranium and thorium within the sediment surrounding the sample. Following a perchloric ( $\text{HClO}_4$ )-hydrofluoric (HF) acid digestion, samples were analyzed for potassium using flame emission spectrophotometry (FES), and thorium and uranium using a VG-Plasmaquad Inductively-Coupled Plasma Mass Spectrometer (ICP-MS). Samples were analyzed in semi-quantitative mode on the ICP-MS. This involves setting up a response curve for the instrument over the entire mass range from  $^7\text{Li}$  to  $^{238}\text{U}$  using a tuning solution containing known concentrations of  $^9\text{Be}$ ,  $^{24}\text{Mg}$ ,  $^{59}\text{Co}$ ,  $^{115}\text{In}$ ,  $^{139}\text{La}$ ,  $^{208}\text{Pb}$  and  $^{238}\text{U}$ . Sample solutions are 'spiked' with 100ppb of  $^{115}\text{In}$  for use as an internal standard to correct for minor fluctuations in instrument running. The  $^{115}\text{In}$  response for each sample is then used, together with the response curve, in the calculation of element concentration. Table 5.3.2 gives values for the various elements derived using these methods.

### 5.3.3 Comparison of dosimetric methods

Using the techniques described in the previous two sections, the external alpha, beta and gamma dose rates can be determined for each sample by several different methods. However, each measurement technique has certain inherent problems. Comparison of the results from the different techniques is designed to clarify the veracity of the data.

Comparison of the uranium and thorium values derived by alpha counting and ICP-MS is best achieved by plotting the specific activity (Bq/kg) for each sample (figure 5.3.3(a)). As explained in section 5.3.1, alpha counting is relatively poor at determining uranium and thorium concentrations, but good at measuring the specific alpha activity of both decay chains. From figure 5.3.3(a) it can be seen that samples with low activity are

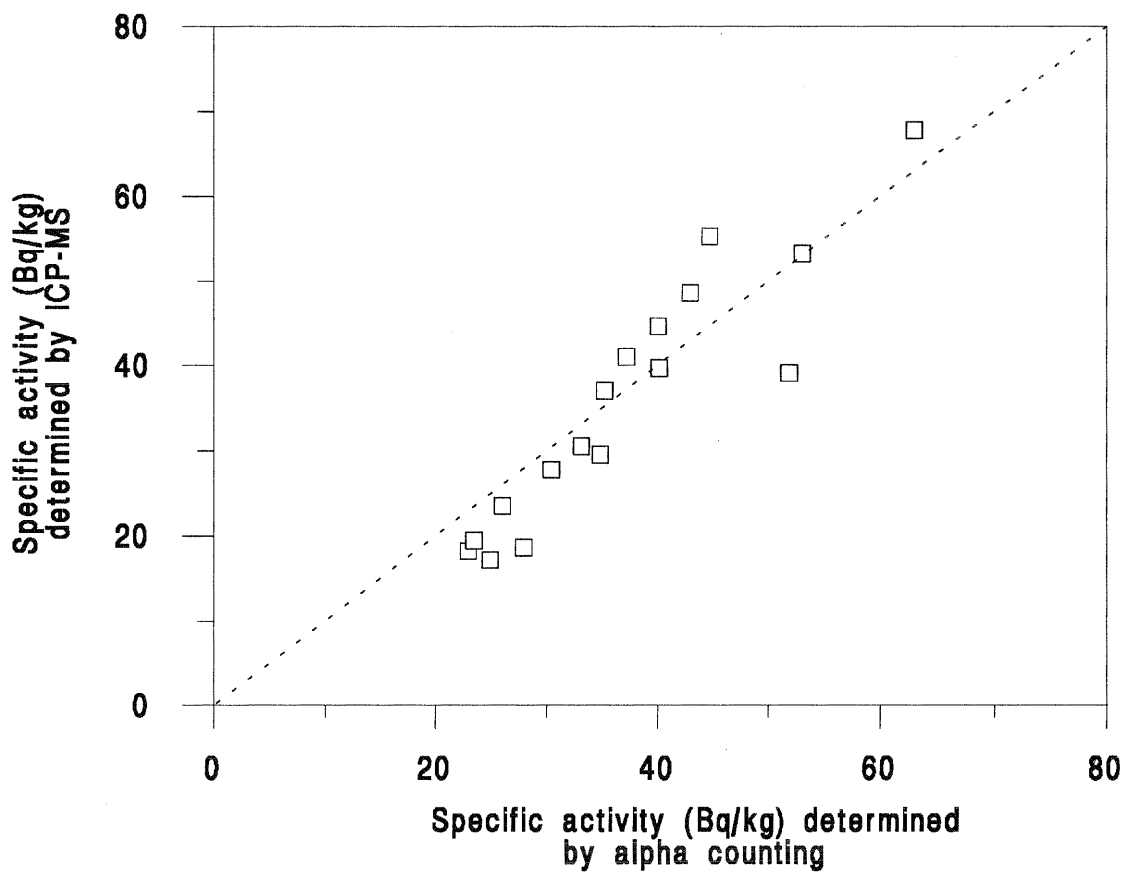


Figure 5.3.3(a): Comparison of specific alpha activity derived by alpha counting and ICP-MS. The dotted line is the 1:1 line.

underestimated by ICP-MS, and this may reflect the detection limit of the instrument, while samples with high activity are overestimated. Given the large analytical error associated with operating the ICP-MS in semi-quantitative mode it seems likely that this data set is the more likely of the two to be in error. Hence that derived by alpha counting is used for age calculation.

Table 5.3.2

Determination of the concentration of uranium, thorium and potassium contributing to the external dose rate for all the samples described in sections 5.2 and 8.2.

<u>Sample</u> (GDNZ)	<u>Uranium</u> (ppm) <sup>(a)</sup>	<u>Thorium</u> (ppm) <sup>(a)</sup>	<u>Specific</u> <u>Activity</u> <sup>(b)</sup> (Bq/kg)	<u>Potassium</u> (%)
21	0.81	7.00	39.09	1.59
6	0.93	7.08	40.98	1.51
17	0.63	4.80	27.77	1.18
5	0.59	5.60	30.52	1.12
1	0.63	5.24	29.57	1.28
45	0.65	7.00	37.01	1.07
13	2.41	5.87	55.28	1.36
52	0.37	3.02	17.13	0.58
51	0.37	3.38	18.60	0.77
7	0.33	3.71	19.43	0.66
10	0.38	4.56	23.54	0.83
59	0.45	3.02	18.17	0.68
14	1.64	4.47	39.56	1.28
15	2.66	8.13	67.75	1.40
16	1.94	5.72	48.56	1.53
24	1.80	5.20	44.62	1.35
32	2.25	5.89	53.28	1.36

Notes

- (a) Analysis using the ICP-MS was performed in semi-quantitative mode using  $^{115}\text{In}$  as an internal standard. The manufacturers, VG-Elemental, give the general figure of  $\pm 30\%$  accuracy in this mode. Repeat analyses, and analysis of standards suggest that this figure is closer to  $\pm 10\%$ .
- (b) Specific activity is calculated from the uranium and thorium values determined by ICP-MS. Values of 4.08 Bq/kg/ppm  $^{232}\text{Th}$  and 13.0 Bq/kg/ppm U have been taken from Aitken (1985).

The beta dose rate measured by TSBC and GM-beta counting can be compared with that derived from elemental analysis of potassium (by FES) and uranium and thorium (by alpha counting). Figure 5.3.3(b) compares the beta dose rate determined in these two ways, after

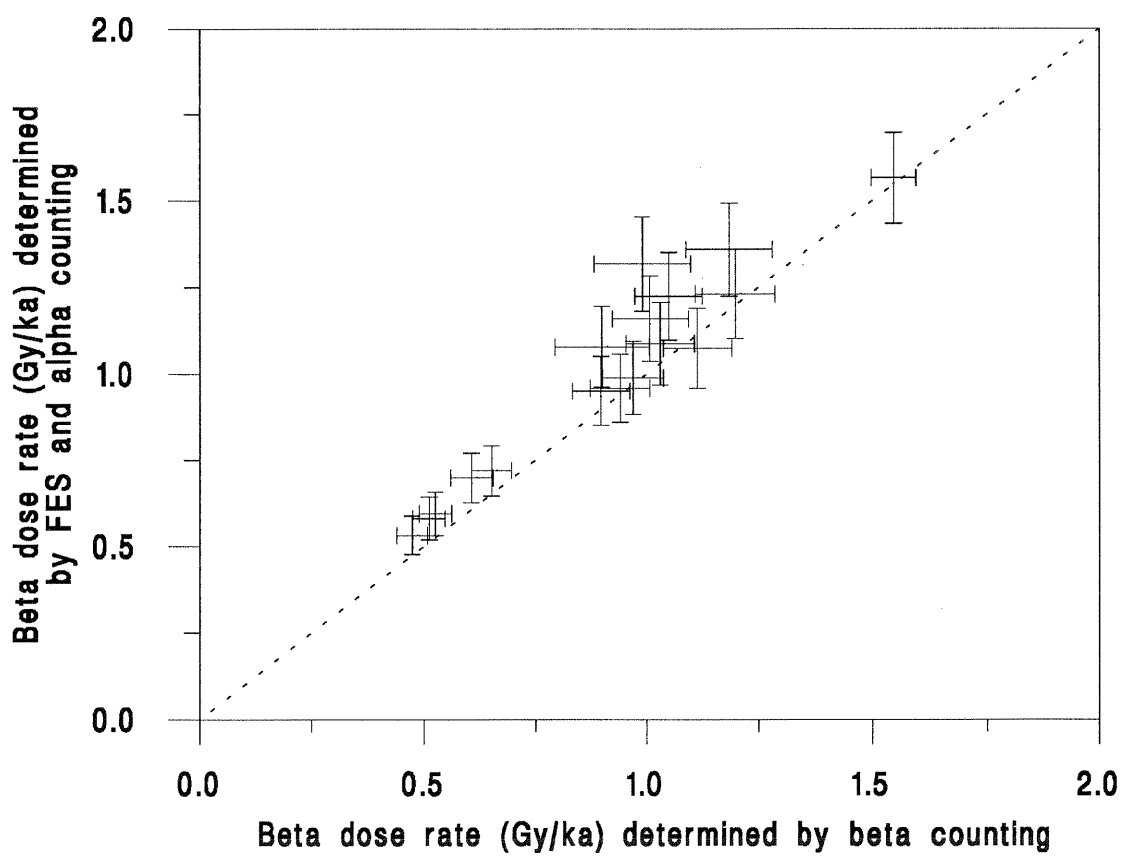


Figure 5.3.3(b): Comparison of external beta dose rates determined by beta counting and by a combination of FES (for potassium) and alpha counting (for uranium and thorium). The dotted line is the 1:1 line.

adjustment for water content and grain size. The values derived by beta counting tend to be approximately 10% smaller than those determined by elemental analysis. This may reflect a systematic error in the standards used for potassium determination by FES, though this would seem unlikely. The beta dose rate determined by emission counting is used in preference to that determined by measurement of the potassium concentration and the alpha counting results since the former is a direct measure of the beta dose to which the samples are exposed.

Table 5.3.3 lists the external dose rates for each sample corrected for grain size and water content. The alpha dose rate has been estimated assuming an alpha efficiency of  $0.2 \pm 0.1$  (Dijkmans and Wintle, 1991). As expected, samples that have not been etched, designated NE, have significantly higher external alpha dose rates compared with those that have been etched.

In the absence of field gamma spectrometry measurements the external gamma dose rate has been estimated using the values for the concentrations of uranium, thorium and potassium (uranium and thorium determined by alpha counting and potassium by FES). This method was not used to estimate the beta dose rate since a preferable alternative existed.

All the sites from which samples were taken were road cuttings, or sections exposed by erosion within the past 100 years. In the majority of cases it was impracticable to collect the sample from further than 0.3m back from the original face of the section. The permeable nature of dune sand means that in all cases it is likely that any water content measured today would not be a realistic average of the water content of the sample since deposition. For all samples, except GDNZ 21 and 6, a water content of  $10 \pm 5\%$  has been estimated. Sample GDNZ 21, a modern dune sand, has negligible water content (estimated at  $2 \pm 2\%$ ), while sample GDNZ 6 was taken from above a peaty aquaclude and so a water content of  $25 \pm 5\%$  has been used.

The cosmic ray dose has been estimated using the data of Prescott and Hutton (1988) and the thickness of the overburden above the sample. However, the average depth of burial since deposition cannot always be accurately estimated and so relatively large errors have been put on these estimates.

Table 5.3.3

External dose rates calculated using the AGE program of Grün, including water content, grain size and cosmic dose.

<u>Sample</u> (GDNZ)	<u>Grain</u> <u>Size</u> ( $\mu\text{m}$ )	<u>Water</u> <u>Content</u> (%)	<u>Alpha</u> <u>Dose rate</u> (Gy/ka)	<u>Beta</u> <u>Dose rate</u> (Gy/ka)	<u>Gamma</u> <u>Dose rate</u> (Gy/ka)	<u>Cosmic</u> <u>Dose rate</u> (Gy/ka)	<u>Total External</u> <u>Dose rate</u> (Gy/ka)
(a)	(b)		(c)	(d)	(e)	(f)	(g)
21	152 $\pm$ 27	2 $\pm$ 2	0.152 $\pm$ 0.117	1.546 $\pm$ 0.049	0.938 $\pm$ 0.062	0.300 $\pm$ 0.010	2.936 $\pm$ 0.142
6(NE)	195 $\pm$ 15	25 $\pm$ 5	0.120 $\pm$ 0.062	0.954 $\pm$ 0.075	0.560 $\pm$ 0.052	0.160 $\pm$ 0.010	1.794 $\pm$ 0.111
17	180 $\pm$ 30	10 $\pm$ 5	0.067 $\pm$ 0.052	0.969 $\pm$ 0.068	0.546 $\pm$ 0.046	0.160 $\pm$ 0.010	1.742 $\pm$ 0.098
5	195 $\pm$ 15	10 $\pm$ 5	0.068 $\pm$ 0.052	0.940 $\pm$ 0.068	0.562 $\pm$ 0.047	0.140 $\pm$ 0.010	1.710 $\pm$ 0.098
1	195 $\pm$ 15	10 $\pm$ 5	0.072 $\pm$ 0.055	1.113 $\pm$ 0.076	0.614 $\pm$ 0.057	0.130 $\pm$ 0.010	1.929 $\pm$ 0.110
45(NE)	195 $\pm$ 15	10 $\pm$ 5	0.146 $\pm$ 0.075	0.897 $\pm$ 0.065	0.567 $\pm$ 0.049	0.140 $\pm$ 0.010	1.750 $\pm$ 0.111
13(NE)	195 $\pm$ 15	10 $\pm$ 5	0.185 $\pm$ 0.096	1.049 $\pm$ 0.075	0.705 $\pm$ 0.063	0.130 $\pm$ 0.010	2.069 $\pm$ 0.138
52	215 $\pm$ 35	10 $\pm$ 5	0.047 $\pm$ 0.036	0.473 $\pm$ 0.034	0.377 $\pm$ 0.034	0.140 $\pm$ 0.010	1.037 $\pm$ 0.061
51	195 $\pm$ 15	10 $\pm$ 5	0.057 $\pm$ 0.044	0.606 $\pm$ 0.047	0.431 $\pm$ 0.037	0.110 $\pm$ 0.020	1.204 $\pm$ 0.077
7	195 $\pm$ 15	10 $\pm$ 5	0.049 $\pm$ 0.037	0.511 $\pm$ 0.036	0.379 $\pm$ 0.033	0.140 $\pm$ 0.010	1.079 $\pm$ 0.062
10	195 $\pm$ 15	10 $\pm$ 5	0.054 $\pm$ 0.041	0.651 $\pm$ 0.045	0.432 $\pm$ 0.037	0.140 $\pm$ 0.025	1.277 $\pm$ 0.075
59	195 $\pm$ 15	10 $\pm$ 5	0.047 $\pm$ 0.036	0.525 $\pm$ 0.037	0.374 $\pm$ 0.032	0.090 $\pm$ 0.030	1.036 $\pm$ 0.068
14(NE)	195 $\pm$ 15	10 $\pm$ 5	0.166 $\pm$ 0.086	0.899 $\pm$ 0.106	0.679 $\pm$ 0.061	0.140 $\pm$ 0.010	1.884 $\pm$ 0.150
15(NE)	195 $\pm$ 15	10 $\pm$ 5	0.260 $\pm$ 0.134	1.184 $\pm$ 0.096	0.903 $\pm$ 0.078	0.140 $\pm$ 0.010	2.487 $\pm$ 0.183
16(NE)	195 $\pm$ 15	10 $\pm$ 5	0.178 $\pm$ 0.092	0.990 $\pm$ 0.108	0.733 $\pm$ 0.066	0.130 $\pm$ 0.010	2.031 $\pm$ 0.157
24(NE)	195 $\pm$ 15	10 $\pm$ 5	0.165 $\pm$ 0.085	1.008 $\pm$ 0.085	0.684 $\pm$ 0.059	0.160 $\pm$ 0.010	2.017 $\pm$ 0.134
32(NE)	195 $\pm$ 15	10 $\pm$ 5	0.219 $\pm$ 0.113	1.197 $\pm$ 0.088	0.834 $\pm$ 0.076	0.160 $\pm$ 0.010	2.410 $\pm$ 0.162

Notes

- (a) Samples for which the potassium feldspar was not etched with HF acid prior to luminescence measurements are marked NE.
- (b) Etching using 10% hydrofluoric acid for 40 minutes is designed to remove the outer layer of the grain that has been affected by alpha radiation (Mejdahl and Winther-Nielsen, 1982) and this is estimated to be a 5 $\mu\text{m}$  shell. The figures quoted here are prior to etching.
- (c) Alpha dose rate calculated assuming an alpha efficiency of 0.2 $\pm$ 0.1.
- (d) Beta dose rate derived by beta counting and corrected for the moisture content of the sediment.
- (e) Gamma dose rate estimated from uranium and thorium concentrations determined by alpha counting, and the potassium concentration measured using FES.
- (f) Cosmic dose rate estimated from sample depth using data from Prescott and Hutton (1988).
- (g) Error calculated as the square root of the sum of the squares of the errors on the individual dose rate components.

5.3.4 Internal dose rate determination

One of the advantages of using potassium feldspars for luminescence dating (section 1.2.1) is that a significant part of their annual dose rate originates from within the grain, due to the large potassium content. This internal dose is not affected by variations in the water

content of the sediment as is the external dose rate (section 5.3.3). Using density separation (section 3.2.1) a potassium-rich feldspar fraction can be separated from the sediment, but it is impossible to isolate a single feldspar species, or to be sure that all the grains that have been separated have an equal potassium content. An assumption of the use of potassium-rich feldspars for dating is that the potassium content that is measured for the grains (an average for many thousands of grains) is representative of the potassium content of the grains that give the majority of the luminescence signal. Grün *et al.* (1989) analyzed single grains from a potassium-rich feldspar separate to see whether there was a correlation between potassium content (and hence internal dose rate) and thermoluminescence signal. If it could be shown that grains with a large potassium content gave a small luminescence signal then this would have serious implications for dating. They did find that a large proportion of the TL signal originated from a relatively small number of grains, but there was no evidence for any relationship between luminescence intensity and potassium content.

Mejdahl (1987) suggested that in addition to the decay of potassium (primarily by emission of beta radiation), a significant internal alpha dose may originate from uranium and thorium within the potassium-rich feldspar fraction. However, it was not clear from this study where the uranium and thorium that were detected were located within the potassium feldspar fraction and this problem has not been addressed by any subsequent study. There are four possible locations for the uranium and thorium detected by Mejdahl (1987) and other workers (see table 5.3.4(b)). Firstly the uranium and thorium may be found only in grains of a non-feldspathic mineral (that may give no luminescence) that has not been separated on the basis of density and is a contaminant. Secondly, the uranium and thorium may be found in micro-inclusions within predominantly feldspar grains. Thirdly, the two elements may have been precipitated along cleavage planes or other lines of weakness within the feldspar crystals. Finally, they may be located within the framework lattice of the feldspar, and would be most likely to be located at crystal defects where the ions could most easily be accommodated. The location of uranium and thorium detected from potassium-rich feldspars has important dosimetric implications. If it is primarily located in contaminant grains, within micro-inclusions, or along cleavage planes, then the alpha dose will be very localised around these sites, and the resulting effect upon the luminescence signal is likely to be relatively small. Only if the uranium and thorium are distributed evenly within the feldspar grains will the internal alpha dose have a significant effect upon the luminescence signal.

Table 5.3.4(a)

Internal dose rates for all samples using potassium values determined by LA-ICP-MS and uranium, and thorium values determined by semi-quantitative analysis using the ICP-MS.

Sample (GDNZ)	Grain Size <sup>(a)</sup> ( $\mu\text{m}$ )	Element Concentrations			Internal Dose Rates		Total Dose Rate <sup>(b)</sup> (Gy/ka)
		K (%)	U (ppm)	Th (ppm)	Alpha (Gy/ka)	Beta (Gy/ka)	
21	152±27	8.25	0.46	2.75	0.610±0.310	0.391±0.084	3.327±0.165
6(NE)	195±15	8.43				0.460±0.057	2.254±0.125
17	180±30	11.82	0.40	2.10	0.497±0.252	0.649±0.130	2.391±0.163
5	195±15	5.01	0.32	2.09	0.456±0.231	0.296±0.044	2.006±0.107
1	195±15	8.05	0.30	2.53	0.506±0.256	0.475±0.070	2.404±0.130
45(NE)	195±15	7.47				0.408±0.051	2.158±0.122
13(NE)	195±15	8.93				0.487±0.061	2.556±0.151
52	215±35	6.25				0.403±0.081	1.440±0.101
51	195±15	6.55				0.386±0.057	1.590±0.096
7	195±15	8.28	0.53	4.21	0.858±0.435	0.488±0.072	1.567±0.095
10	195±15	8.07	0.36	3.06	0.610±0.310	0.476±0.070	1.753±0.103
59	195±15	7.15	0.22	1.70	0.350±0.177	0.422±0.062	1.458±0.092
14(NE)	195±15	8.99				0.490±0.061	2.374±0.162
15(NE)	195±15	6.16				0.336±0.042	2.823±0.188
16(NE)	195±15	9.57				0.522±0.065	2.553±0.170
24(NE)	195±15	10.50				0.573±0.071	2.590±0.152
32(NE)	195±15	7.33				0.400±0.050	2.810±0.170

Note

- (a) Grain size prior to any HF etching. Samples marked NE have not been etched. All other samples are assumed to have had a 5 $\mu\text{m}$  shell removed from the grains by etching.
- (b) Total internal and external dose rate not including the internal alpha dose rate.

Table 5.3.4(a) presents the internal dose rate data obtained for the samples described in sections 5.2 and 8.2. Potassium has been determined using laser ablation ICP-MS as described in section 4.8. For seven of the samples the uranium and thorium content has been measured using semi-quantitative ICP-MS, as described in section 5.3.2, following a perchloric-hydrofluoric acid digestion.

Potassium contents are generally 8% or higher, indicating an effective separation of grains of potassium rich feldspar from the bulk sample. However, some samples, notably GDNZ 5, have much lower potassium contents and this reflects the problem of separating minerals from a solid solution series on the basis of density alone (see discussion in section 5.1). With no other evidence available, the potassium content measured from the separated

feldspar fraction must be assumed to approximate the average potassium content of all the grains from which luminescence is measured.

Table 5.3.4(b)

Concentrations of uranium and thorium in potassium-rich feldspars reported in previous studies. Where applicable the internal alpha dose rate is also given.

<u>Study</u>	<u>Sample Area</u>	<u>Internal Alpha Dose rate<sup>(a)</sup></u> (Gy/ka)	<u>Uranium range</u> (ppm)	<u>Thorium range</u> (ppm)	<u>Measurement Method<sup>(b)</sup></u>
Jungner 1985	Finland	n.d.	n.d.	n.d.	
Kolstrup and Mejdahl 1986	Denmark	0.16-0.24	0.15-0.23	n.d.	DNAA *
Jungner 1987	Finland	n.d.	n.d.	n.d.	
Lundqvist and Mejdahl 1987	Sweden	0.12-0.18	0.11-0.34	n.d.	DNAA *
Mejdahl 1987	Unknown	n.a.	0.1-0.4	0.1-1.0	NAA, DNAA
Dijkmans <u>et al.</u> 1988	Netherlands	0.05-0.07	n.d.	n.d.	TSAC
Godfrey-Smith <u>et al.</u> 1988	Canada	n.d.	n.d.	n.d.	
Hütt <u>et al.</u> 1988	NW USSR	n.d.	n.d.	n.d.	
Balescu <u>et al.</u> 1989	NW Europe	n.d.	n.d.	n.d.	
Grün <u>et al.</u> 1989	Denmark	n.d.	n.d.	n.d.	
Jungner <u>et al.</u> 1989	Norway	n.d.	n.d.	n.d.	
Kronborg and Mejdahl 1989	Denmark	0.10-0.18	-	n.d.	DNAA *
Kolstrup <u>et al.</u> 1990	Denmark	0.05-0.18	-	n.d.	DNAA *
Balescu <u>et al.</u> 1991	NW Europe	n.d.	n.d.	n.d.	
Dijkmans and Wintle 1991	Netherlands	0.06	n.d.	n.d.	TSAC
Rendell <u>et al.</u> 1991	UK	n.d.	n.d.	n.d.	
Balescu and Lamothe 1992	NW Europe & Italy	n.d.	n.d.	n.d.	
Balescu <u>et al.</u> 1992	N.France	n.d.	n.d.	n.d.	
Dijkmans <u>et al.</u> 1992	Netherlands	0.06	n.d.	n.d.	TSAC
Ervanne <u>et al.</u> 1992	Peru	n.d.	n.d.	n.d.	
Hütt and Jungner 1992	Russia	n.d.	n.d.	n.d.	
Mejdahl 1992	Scandinavia	0.03-0.28		n.d.	DNAA *
Rendell 1992	UK	n.d.	n.d.	n.d.	
Edwards 1993	SW USA	0.19-0.36	0.19-0.38	0.77-1.37	ICP-MS

Notes

- (a) Alpha dose rate calculated for the grain size used in the study, and assuming an alpha efficiency of  $0.2 \pm 0.1$ .
- (b) The method used for determining the internal activity. NAA - Neutron Activation Analysis, DNAA - Delayed Neutron Activation Analysis, TSAC - Thick-source alpha counting, ICP-MS - Inductively-Coupled Plasma Mass Spectrometry. Those marked with a (\*) have had their uranium content measured and the thorium content estimated using the relationship derived by Mejdahl (1987).

Table 5.3.4(b) lists all the publications since 1985 that have reported luminescence dating of Quaternary sediments using potassium feldspars as the dosimeter. For each publication the internal alpha dose rate is given, together with the internal concentrations of uranium and thorium where figures are quoted. The table shows that of the 24 publications, only 10 have made any attempt to quantify the internal alpha dose rate due to uranium and thorium. Where an attempt has been made, the dose rates have generally been under 0.2 Gy/ka.

The seven samples for which uranium and thorium have been measured in this study give internal alpha dose rates varying from 0.35 to 0.86 Gy/ka. All these values exceed the largest previous internal alpha dose rate reported for potassium feldspars (Edwards 1993). The most likely explanation of the high uranium and thorium values found here is that the potassium feldspar separated from the samples was contaminated with some other mineral fraction, and hence the measured uranium and thorium values do not relate to the uranium and thorium content within the feldspar crystal lattice. As noted in the sample descriptions (section 5.2), many of the samples appear very dark in colour due to the presence of a large proportion of mafic minerals such as hypersthene, augite and titanomagnetite (Shepherd pers.comm.). Although density separation was able to remove the majority of these dark minerals, the potassium-rich feldspar fraction that was used for luminescence measurements, and then for these measurements of internal potassium, uranium and thorium, still contained a proportion of dark coloured grains. For this reason the total dose rate quoted in table 5.3.4(a) does not include any internal alpha dose rate contribution.

## 5.4 Equivalent Dose determination

Equivalent doses (EDs) were determined for the twelve samples listed in section 5.2 using two standard methods; regeneration (Wintle and Proszynska, 1983) and additive dose (Singhvi *et al.* 1982). A major source of uncertainty in the use of TL for the dating of sediments is the residual level to which the TL signal is reduced at deposition. All the samples analyzed here had their luminescence measured both by TL and IRSL. The IRSL signal from a potassium feldspar falls more rapidly than the TL signal when it is exposed to light. Analysis using the total bleach method involved the determination of three different residual levels; following exposure to the SOL2 solar simulator for 6, 60 and 600 minutes. Table 5.4 compares the TL and IRSL residual levels for all the samples analyzed. The residual levels determined during ED determination by the regeneration method (60 minutes SOL2) are also shown for comparison.

Table 5.4. Residual levels, expressed as a proportion of the natural signal, for samples analyzed using standard multiple aliquot techniques. Samples are listed in order of increasing age.

<u>Sample</u> (GDNZ)	TL			IRSL		
	<u>6 mins</u>	<u>60 mins</u>	<u>600 mins</u>	<u>6 mins</u>	<u>60 mins</u>	<u>600 mins</u>
21	0.967	0.613 <b>0.638</b>	0.316	1.193	0.927 <b>0.871</b>	0.869
6	n.d.	n.d. <b>0.540</b>	n.d.	0.105	0.085 <b>0.070</b>	0.099
17	0.292	0.170 <b>0.180</b>	0.123	0.022	0.007 <b>0.000</b>	0.003
5	0.295	0.162 <b>0.135</b>	0.081	0.021	0.014 <b>0.010</b>	0.010
1	0.305	0.139 <b>0.151</b>	0.085	0.020	0.012 <b>0.011</b>	0.008
45(NE)	0.336	0.168 <b>0.156</b>	0.091	0.020	0.010 <b>0.013</b>	0.004
13(NE)	0.494	0.190 <b>0.178</b>	0.104	0.031	0.012 <b>0.016</b>	0.006
52	0.290	0.120 <b>0.108</b>	0.057	0.017	0.016 <b>n.d.</b>	0.013
51	0.267	0.118 <b>0.110</b>	0.055	0.022	0.008 <b>0.015</b>	0.002
7	0.284	0.092 <b>0.108</b>	0.043	0.012	0.004 <b>0.006</b>	0.000
10	n.d.	n.d. <b>0.066</b>	n.d.	0.018	0.007 <b>0.008</b>	0.004
59	0.273	0.084 <b>0.081</b>	0.030	0.014	0.004 <b>0.007</b>	0.001

Note:

Figures for the regeneration method are in bold type. All TL data have been integrated from 285°C to 365°C. For the IRSL signals a background signal was subtracted. Its magnitude is normally about 150 cps, of which 130 cps is PMT dark count. Samples marked (NE) have not been etched using hydrofluoric acid.

The TL signals for the three residual levels show considerable variation. After 6 minutes exposure to the SOL2 approximately 30% of the natural TL signal remains, for all apart from the modern dune, and after 600 minutes exposure only 5-10% of the TL signal remains. In contrast the IRSL signals remaining after the three bleaching times show relatively little difference. The residual level after 6 minutes exposure to the SOL2 is typically 2% of its initial level, while after 600 minutes exposure it has fallen to 0.5-1.5%. The implication of this is that where it is difficult to estimate the length of time for which a

sample was exposed at deposition, the residual level determined using TL may be as much as 20% in error, while using IRSL the error is likely to be less than 1% of the natural signal.

The residual levels for sample GDNZ 21 show that the TL signal of a modern sample can still be bleached, while the IRSL signal is proportionately reduced far less. Sample GDNZ 6 has a relatively weak luminescence signal because it is young and so the TL and IRSL residual signals are a larger proportion of the natural signal compared with the other samples.

#### 5.4.1 Additive Dose Method

The additive dose method involves adding radiation dose on top of that which the sample has acquired in nature in order to characterise the response of its luminescence signal to irradiation, and fitting a linear or saturating exponential regression line to the data points (figure 5.4.1). It is then possible to extrapolate this 'growth curve' to determine the radiation dose that the sample had received in nature. However, since the luminescence signal at the time of deposition may not have been zero (especially if one is using TL measurements) it is necessary to determine the luminescence signal after exposure of the sample to light (the residual level). The radiation dose that the sample received since deposition (its equivalent dose) can then be found by extrapolating the growth curve to this residual level.

Sixty discs of each sample were prepared and their IRSL signal measured for 0.1s to normalize them. They were then divided into ten groups, with six discs per group. Three of these groups were used to define residual levels after 6, 60 and 600 minutes exposure to the SOL2, one group to define the natural signal, and the remaining six groups were given radiation doses. All discs were left for a period of at least 24 hours after irradiation or bleaching. After preheating at 140°C for 62 hours their IRSL signal was measured for 0.1s and normalized using the measurement made prior to any treatment. Their TL signal was then measured by heating the samples to 450°C at a rate of 3°C/s in a pure argon atmosphere. The samples were then given 6 Gy irradiation within the Risø reader and had their TL signal remeasured. They were heated to 450°C at a rate of 3°C/s, pausing at 290°C for 10s. The effect of this pause was to produce a single peak between 300 and 400°C that could be used for normalization of the TL signal. Equivalent doses were determined for each of the three residual levels, using both IRSL and TL measurements.

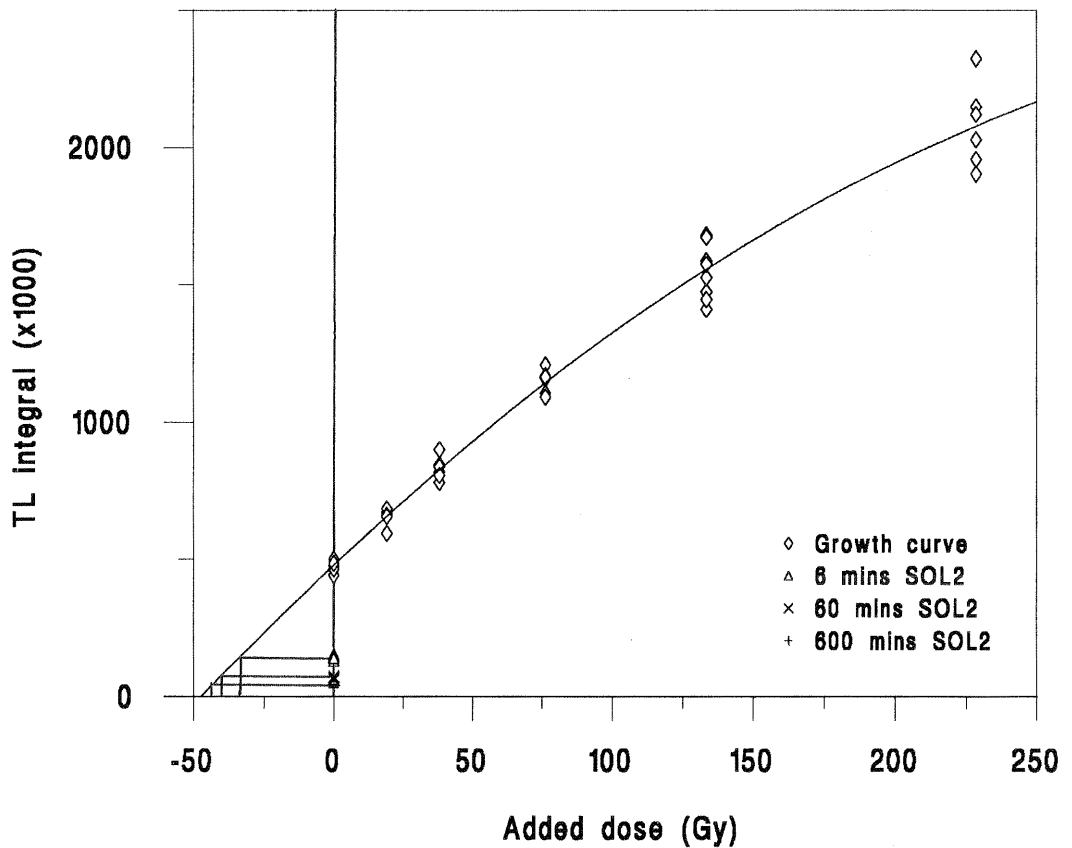
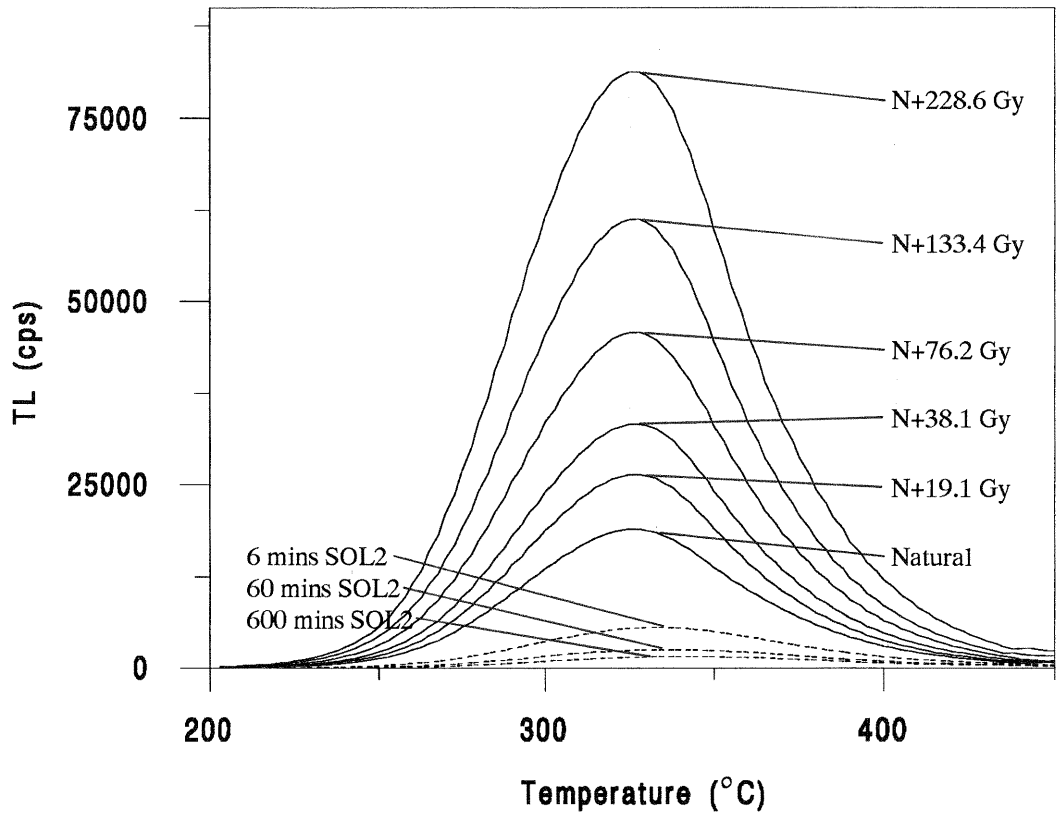


Figure 5.4.1: Top - TL glow curves used for equivalent dose determination of sample GDNZ 1 using the additive dose method. Bottom - Additive dose growth curve constructed using TL integrals (285-365°C) from glow curves shown above.

### 5.4.2 Regeneration Method

In the regeneration method the sample is exposed to light to attempt to mimic the reduction of the luminescence signal to a residual level that occurred at deposition. Radiation doses are given to samples that have been bleached in this way and the response of the material to radiation is characterised by fitting either a linear or saturating exponential regression line. The equivalent dose of the material is found by comparing the 'natural' luminescence signal from a group of unbleached aliquots of the sample with the growth curve generated following bleaching (figure 5.4.2).

The sequence of disc preparation, normalization, bleaching, irradiation, preheating and measurement was similar to that used for the additive dose method and described in the previous section. However, only a single residual level (60 minutes SOL2) was used. Forty-eight discs of each sample were prepared, twelve to define the natural level, and the remaining thirty-six divided into six groups of six discs. These six groups were all bleached for 60 minutes in the SOL2 solar simulator, and then irradiated for different times.

### 5.4.3 Temperature shifting of TL data

Measurement of the thermoluminescence signal gives a plot of luminescence as a function of sample temperature (a 'glow curve'). As discussed in section 1.2.2, the higher the sample temperature during TL measurement the deeper the trap from which charge can be evicted. In theory the deeper the trap in which charge is stored, the less likely it is that charge will be lost over time when stored at ambient temperatures. For each temperature ordinate of the TL 'glow curves' shown in figures 5.4.1 and 5.4.2 it is possible to construct a growth curve and determine an ED. A plot of ED as a function of temperature is known as a plateau test. For those temperatures where traps of similar stability, or those with a stability significantly greater than the age of the sample, are being evicted, an ED plateau should be seen (Aitken 1985). Mejdahl (1988) has used this plateau test as the basis for determining the correct bleaching time to use in order to determine the residual level reached at deposition.

TL glow curves were measured on the Risø TL reader at a heating rate of 3°C/sec. This relatively low heating rate was used in order to minimize problems associated with thermal lag between the hotplate and the sample. If such a lag occurs it results in shifting of the TL glow curve peak along the temperature axis.

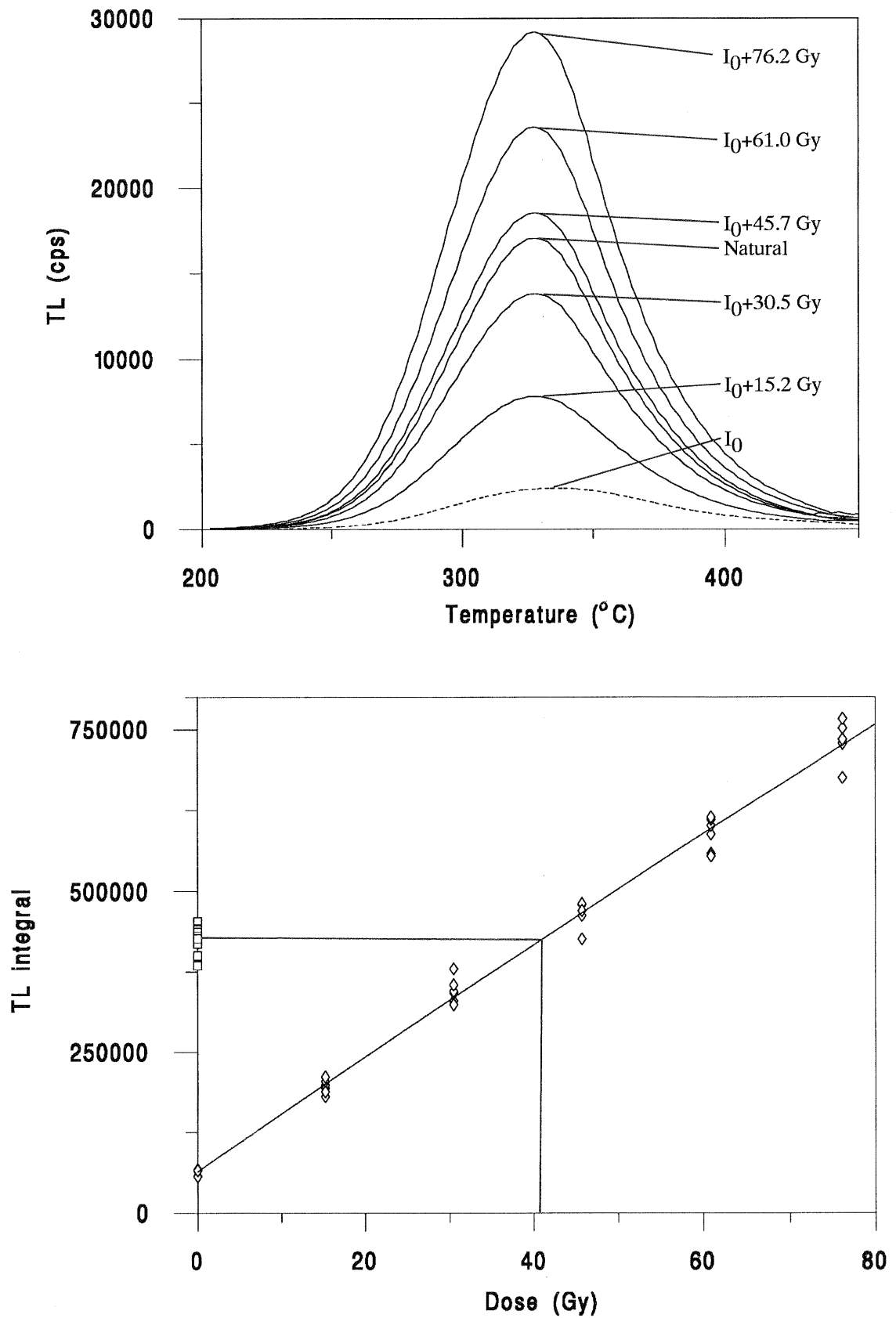


Figure 5.4.2: Top - TL glow curves used for equivalent dose determination of sample GDNZ 1 using the regeneration method. Bottom - Regeneration growth curve constructed using TL integrals (285-365°C) from glow curves shown above.

In spite of all attempts to reduce this problem small variations in peak temperature are seen in the TL data obtained in this study. These are normally under 20°C, but when such data are used to determine an ED, the ED plateau is very poor (figure 5.4.3(a)). Preheating at 140°C for 62hrs produces what appears to be a single peak at around 330°C (see figure 4.7.2(a)). A computer program was written that automatically aligns the peaks to a chosen 'standard' curve. Normally an 'average' natural glow curve was used as this standard. Only natural and dosed glow curves are shifted, not residuals which would be expected to have glow curve peaks at different temperatures.

Figure 5.4.3(b) shows the same data as in figure 5.4.3(a) but after alignment of the TL glow curves. The greatest temperature shift for this data set is 24°C, but on average the curves were moved only 6°C (a resolution of 4°C per channel was used during analysis). For all of the samples analyzed it was seen that the temperature shifting greatly improves the ED plateau.

This shows that merely looking for a plateau within a data set is an unreliable means for determining the ED, since it is very sensitive to small changes in TL peak positions. A far more robust method of analysis is using integrals over the main TL glow peak, as suggested by Frechen (1992), and this is used in table 5.4.5. Temperature shifting makes very little difference to the ED determined using an integral.

#### 5.4.4 Fading tests

Anomalous fading describes the loss over short time periods (a matter of minutes to months) of a luminescence signal generated by laboratory irradiation that on the basis of trap lifetimes should be stable over far longer time periods. The effect was first described by Wintle (1973) in the TL signal from volcanic feldspars and has more recently been described by Spooner (1992). In this more recent study he found that the TL and IRSL signals faded to a similar extent, and that where fading was detected it frequently continued indefinitely over the time period studied in the laboratory with no sign of a 'non-fading' residual component after prolonged storage.

For this study samples were tested to see whether they exhibited fading using IRSL measurements a month apart. Eight aliquots of each sample were prepared. Four of the aliquots were bleached in the SOL2 solar simulator for 24 hours to remove the natural luminescence signal. After a further period of 24 hours these were then given beta irradiations equivalent to their EDs. All eight aliquots of each sample were then preheated at 140°C for 62 hours, using the same procedure as that used for dating of the samples.

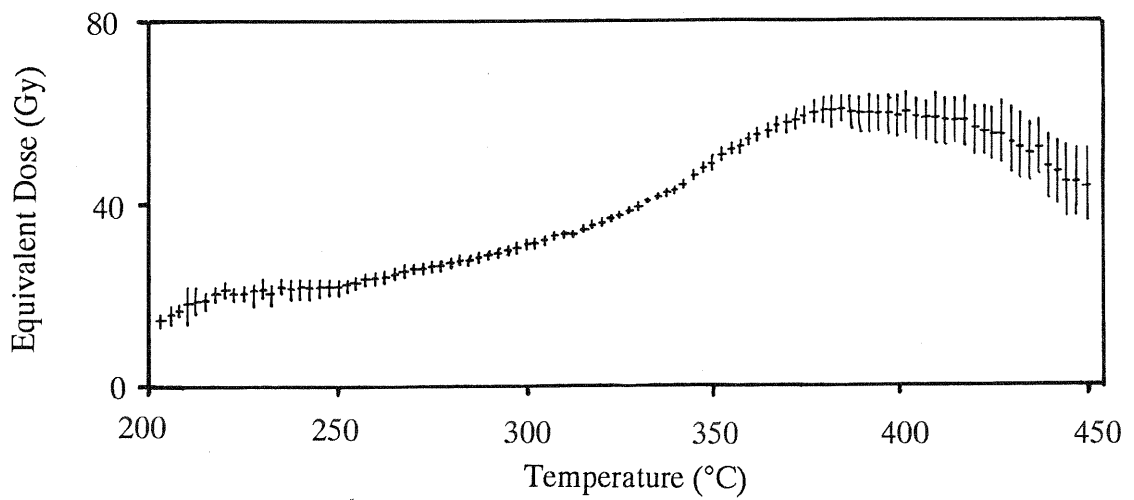
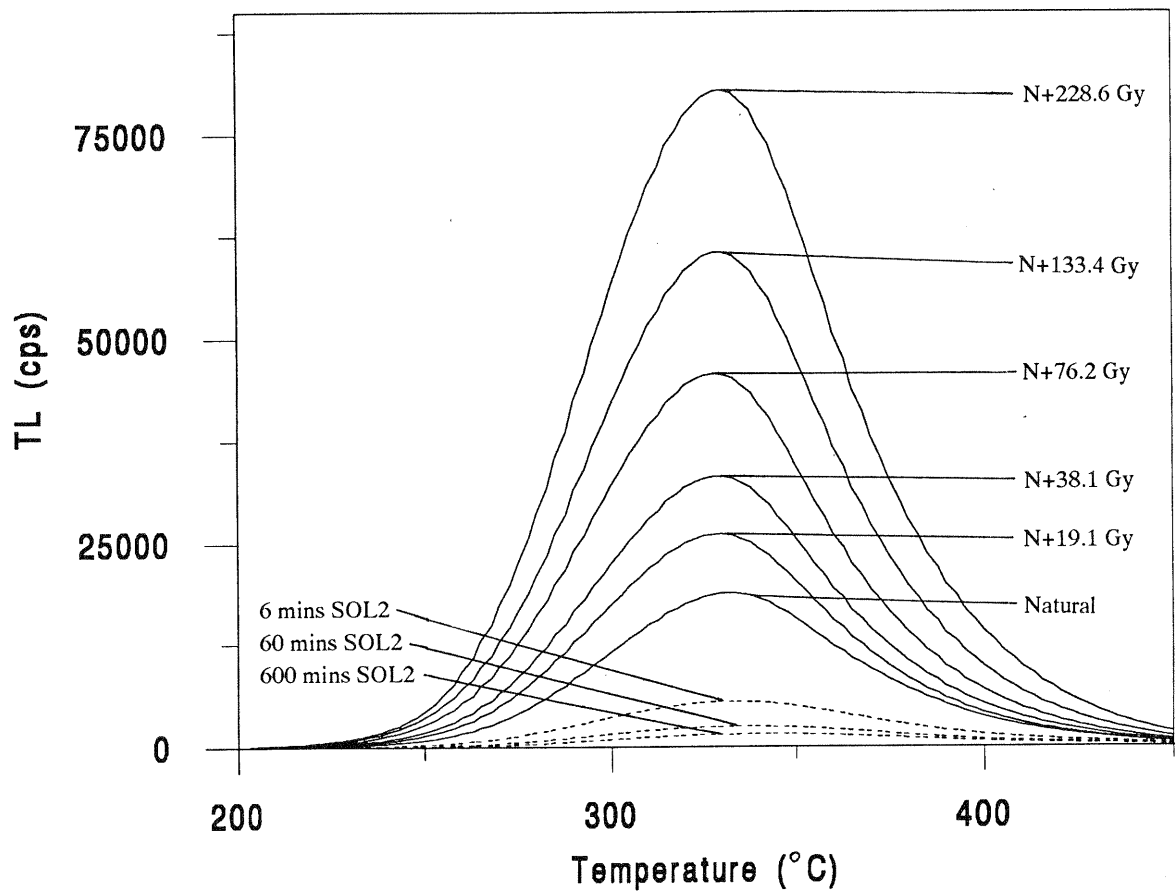


Figure 5.4.3(a): Top - Glow curves from GDNZ 1 used for equivalent dose determination using the additive dose method. Data has been second glow normalized. Bottom -Equivalent dose as a function of glow curve temperature for sample GDNZ 1 using the data set above (bleaching time 60 minutes SOL2).

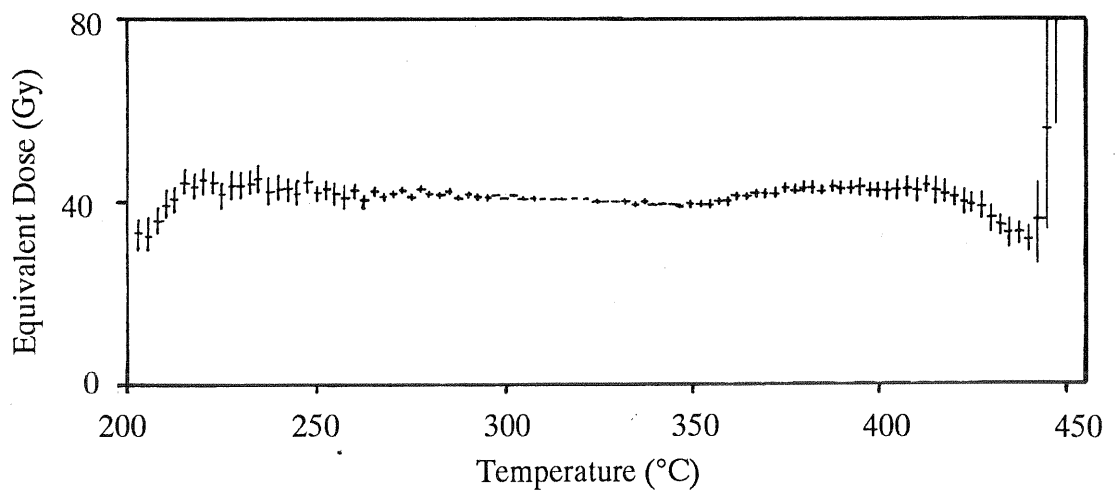
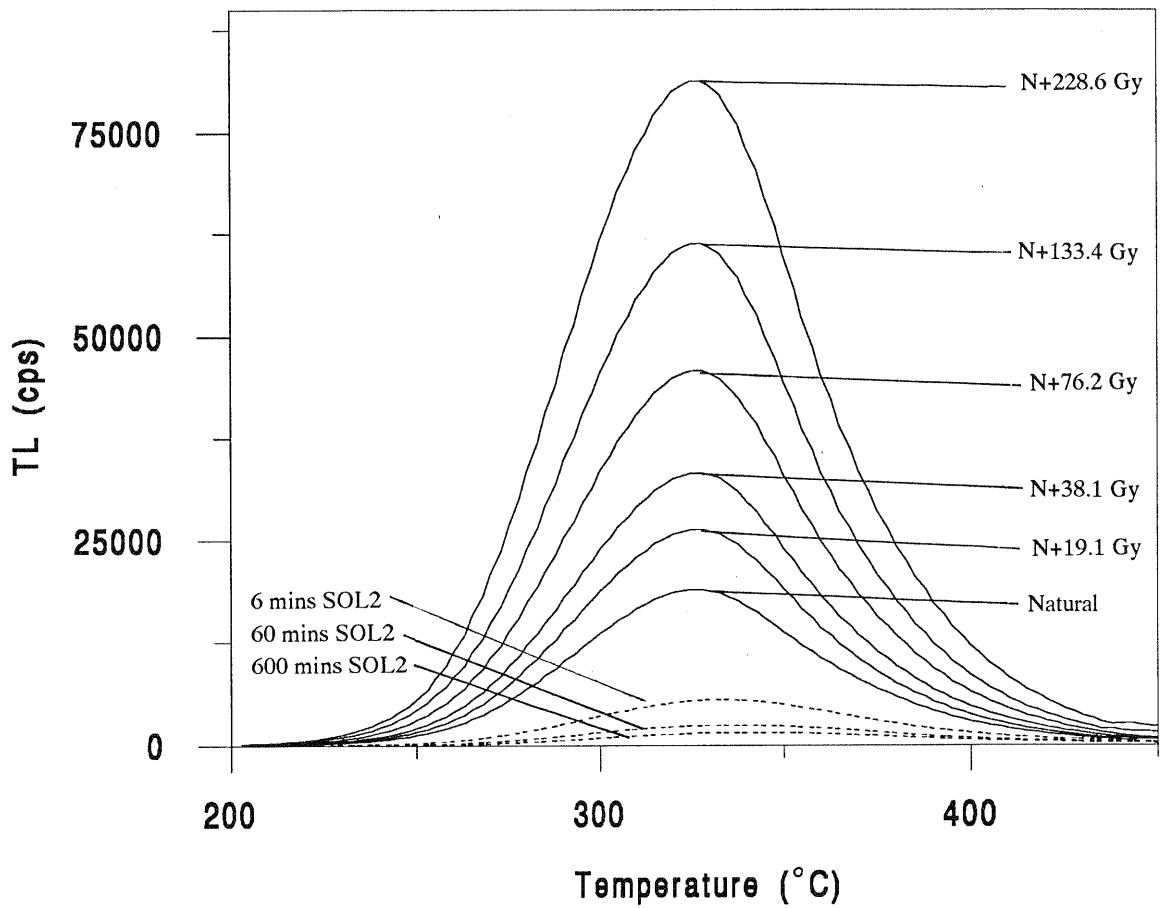


Figure 5.4.3(b): Top - The same glow curves as shown in figure 5.4.3(a) after temperature shifting to align the peaks of the individual glow curves. The maximum temperature shift is 24°C. The residual signals were not re-aligned. Bottom - Equivalent dose as a function of glow curve temperature for the sample GDNZ 1 using the data set above (bleaching time 60 minutes SOL2).

IRSL measurements were made on all aliquots 24 hours after finishing the preheat and they were then stored for a period of a month before repeating the IRSL measurements. Fading could then be calculated by comparing the ratio of the IRSL signals measured before and after the month's storage for the natural and the irradiated aliquots. Table 5.4.4 lists the samples analyzed, the test doses given to samples after bleaching, the proportion by which the IRSL signal from the irradiated samples has faded in comparison with that from the natural samples, and the error on the degree of fading.

The samples show fading of between 0.9 and 4.2% over the month during which they were stored. Samples GDNZ 13 and 17 show a degree of fading that did exceed the calculated error for each specific sample. However, the error on these fading measurements, due to scatter between aliquots and loss of grains during the period of storage, varies between 0.4% and 5.9%, and so taken as a group, no samples exhibit fading that exceeds the experimental error.

Table 5.4.4

Results from anomalous fading test for the samples described in section 5.2.

<u>Sample</u> <u>(GDNZ)(a)</u>	<u>Test Dose</u> <u>(Gy)(b)</u>	<u>Fading</u> <u><math>(I_0+B)/N</math>(c)</u>	<u>Error</u>	<u>Fading</u> <u>(%)</u>
21(d)	n.a.	n.d.	n.d.	n.d.
6(NE)	3	0.982	0.032	1.8
17	22	0.981	0.015	1.9
5	37	0.985	0.021	1.5
1	37	0.982	0.029	1.8
45(NE)	37	0.980	0.044	2.0
13(NE)	37	0.958	0.029	4.2
52	84	0.991	0.059	0.9
51	122	0.975	0.021	2.5
7	152	0.984	0.010	1.6
10	381	0.987	0.004	1.3
59	381	0.968	0.013	3.2

Notes

- (a) Samples that were not etched using HF acid prior to analysis are marked NE.
- (b) The test dose is the irradiation given to the aliquots after bleaching in the SOL2 for 24 hours.
- (c) The degree of fading is calculated as the proportion by which the IRSL signal from the irradiated aliquots has dropped compared with the signal from the aliquots retaining their natural luminescence signal.
- (d) No fading test was undertaken for sample GDNZ 21 because its natural IRSL signal was too low.

### 5.4.5 Comparison of EDs determined using various methods

Table 5.4.5 lists all the EDs determined for the twelve samples listed in section 5.2. Additive dose EDs have been calculated using all three bleaching times. The errors that are given are those produced by the analysis software used (written by Dr R.Grün). The estimation of the error in the ED is particularly difficult when extrapolating a saturating exponential (as in the additive dose method). The values for the uncertainties shown in table 5.4.5 are minimum values, and a figure of  $\pm 10\%$  is probably more realistic. However, the errors quoted by the analysis software are given here since they give an impression of the fit of the data to the equation.

The TL results show a large variation in the calculated EDs depending upon the bleaching time used. The effect is especially marked for the young samples where the residual level is large compared with the natural TL. However, even for older samples there is at least 20% difference between the TL EDs calculated using the 6 and the 600 minute residual level. This contrasts with the IRSL results where the difference in ED between those calculated using the shortest and the longest residual time is approximately 1%. The rapid bleaching of the IRSL signal under sunlight means that the uncertainty in the residual level, and hence the uncertainty in the ED, is greatly reduced, even for these relatively well bleached dune sands.

In figure 5.4.5(a) the EDs determined using IRSL are plotted against those obtained using TL, and in figure 5.4.5(b) the EDs determined using the additive dose method (using the 60 minute SOL2 residual level) are plotted against those using the regeneration method. The TL and IRSL signals from potassium feldspars have quite different bleaching characteristics (table 5.4, and Godfrey-Smith *et al.* 1988), and are believed to originate from different trapped charge populations (section 6.6.5). However, it is not known whether the trapped charge populations that are probed (after preheating at 140°C for 62 hrs) have similar thermal stabilities. One method of testing this is to plot EDs determined using TL against those using IRSL (figure 5.4.5(a)). The majority of results fall very close to the 1:1 line. The modern sample (GDNZ 21) gave a very high TL ED, using both the regeneration and additive dose methods, though the IRSL ED was negligible. It is possible that bleaching of this sample was inhibited by the high proportion of mafic minerals present and so the TL signal was not well bleached although the IRSL was. The two oldest samples (GDNZ 10 and 59) gave larger regeneration EDs using IRSL than when using TL, though the difference may not be significant given the large uncertainty in these results. This data set suggests that the IRSL and TL signals remaining after the 140°C preheat have

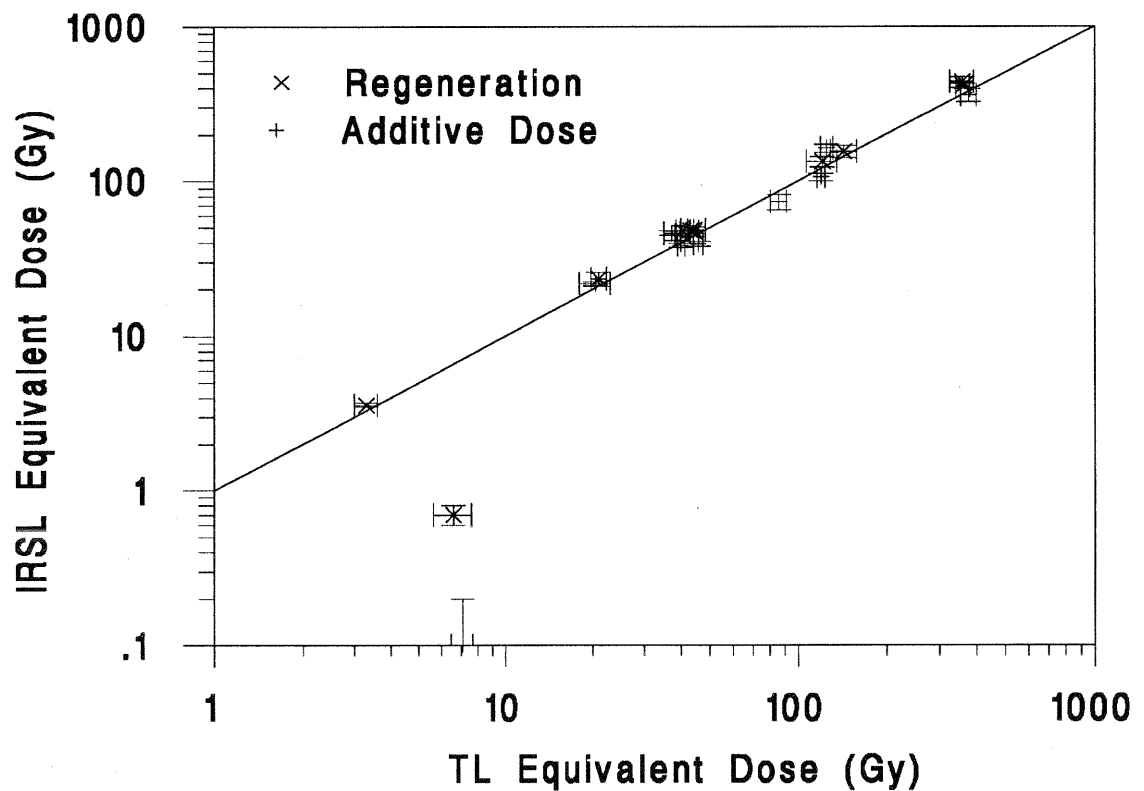
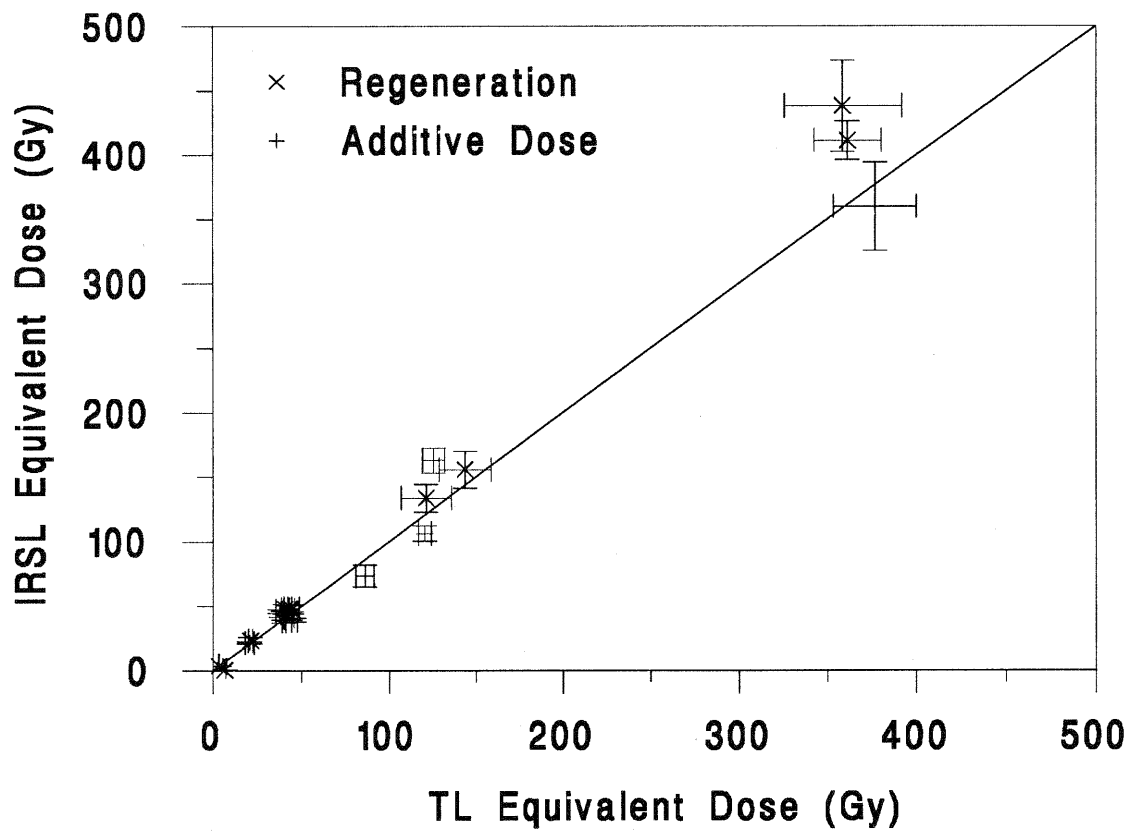


Figure 5.4.5(a): Comparison of equivalent doses determined using TL measurements with those using IRSL. The data are plotted on a linear scale (above) and a log-log scale (bottom).

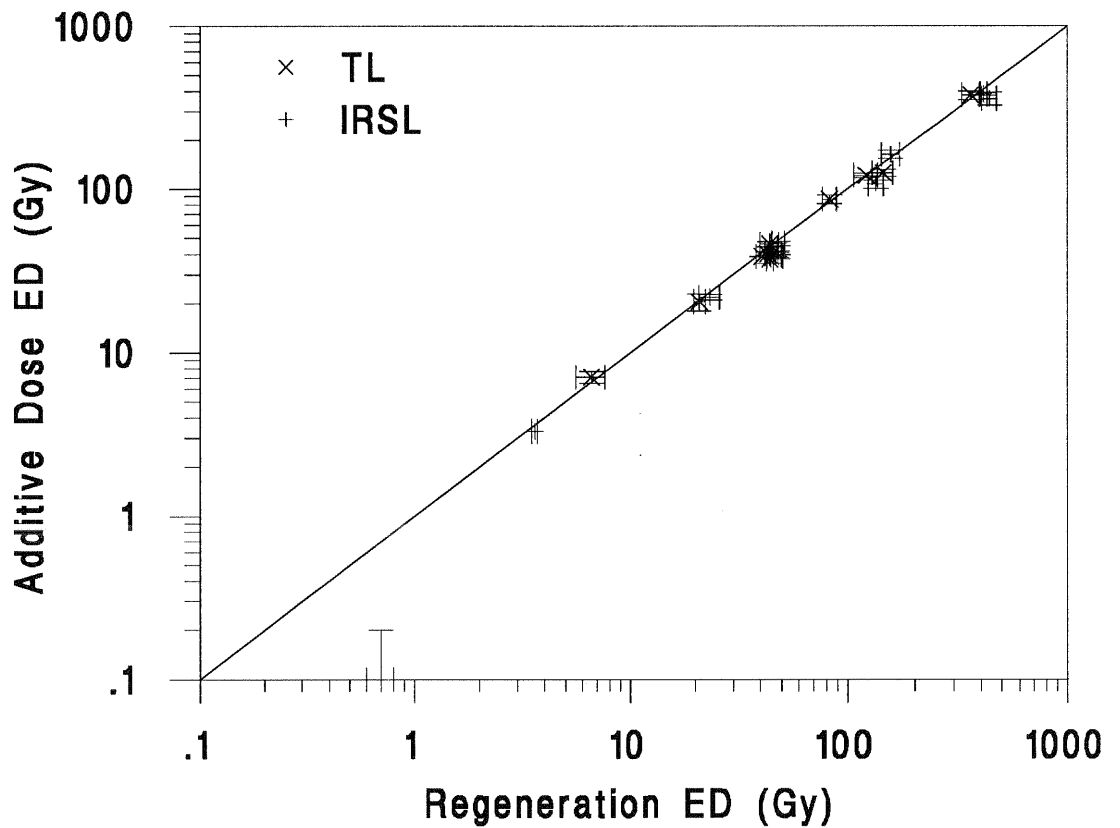
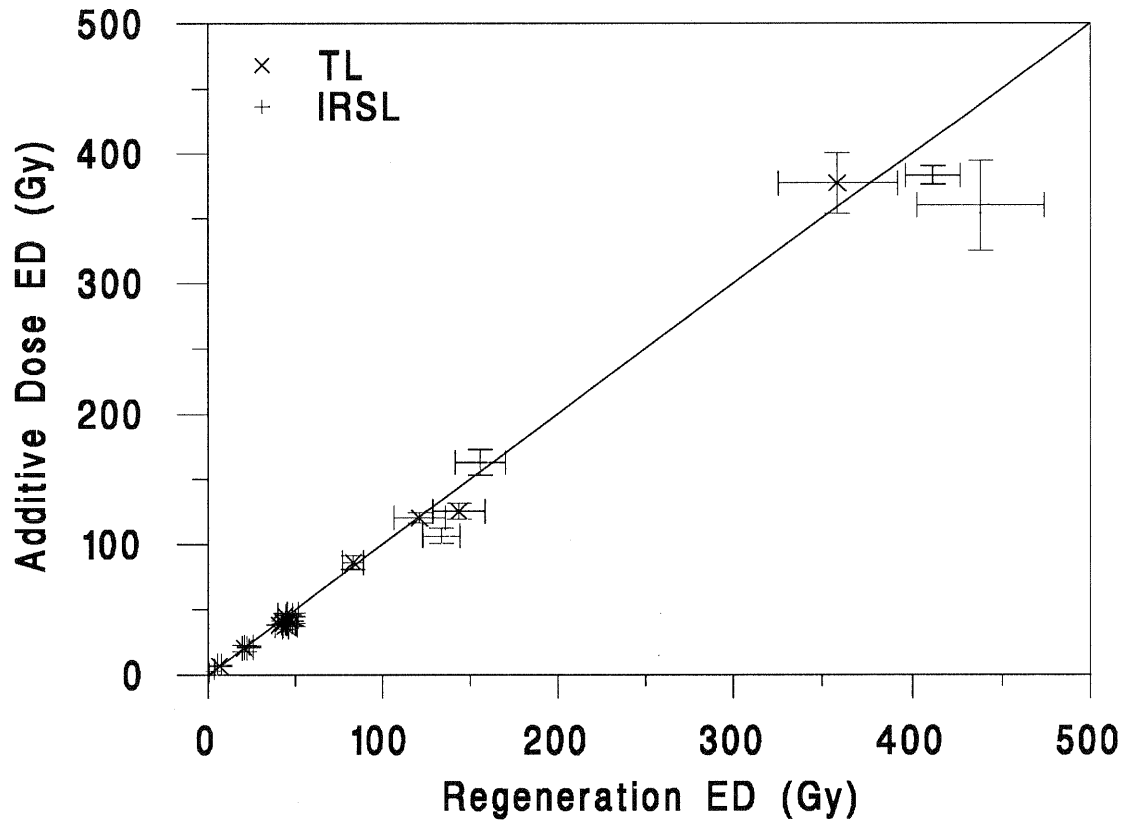


Figure 5.4.5(b): Comparison of equivalent doses determined using the additive dose method with those using regeneration. The data are plotted on a linear scale (above) and a log-log scale (bottom).

a similar thermal stability over the period of time represented by the samples here (0-350 ka).

Table 5.4.5

Equivalent doses calculated using the additive dose and the regeneration method, using TL and IRSL measurements. Additive dose results are calculated using three residual levels; after 6, 60 and 600 minutes exposure to the SOL2 solar simulator. The regeneration results are in bold type, irradiation occurring after 60 minutes exposure to the SOL2. All EDs are in grays. The errors quoted are those associated purely with the mathematical fit of the data to the regression line.

<u>Sample</u> (GDNZ)	<u>TL</u>			<u>IRSL</u>		
	<u>6 mins</u>	<u>60 mins</u>	<u>600 mins</u>	<u>6 mins</u>	<u>60 mins</u>	<u>600 mins</u>
21	0.7±0.4	7.1±0.6 <b>6.6±1.0</b>	12.4±0.6	0.3±0.1	0.1±0.1 <b>0.7±0.1</b>	0.2±0.1
6	n.d.	n.d. <b>3.3±0.3</b>	n.d.	3.2±0.0	3.3±0.0 <b>3.6±0.1</b>	3.2±0.1
17	17.5±2.4	20.5±2.5 <b>21.0±1.3</b>	21.7±2.5	21.5±0.8	21.8±0.8 <b>23.4±2.5</b>	21.9±0.8
5	32.4±2.1	37.3±2.2 <b>44.3±1.6</b>	40.3±2.3	46.1±1.6	46.3±1.6 <b>48.5±3.2</b>	46.5±1.6
1	31.4±0.2	38.4±0.2 <b>40.7±2.3</b>	40.8±0.2	44.3±3.0	44.7±3.1 <b>48.1±3.7</b>	44.9±3.1
45	32.1±1.1	40.0±1.2 <b>43.2±1.1</b>	43.5±1.2	38.1±1.2	38.5±1.2 <b>48.4±2.5</b>	38.7±1.2
13	30.1±1.5	45.8±1.7 <b>44.3±4.3</b>	50.1±1.8	38.5±1.5	39.5±1.4 <b>47.5±2.5</b>	39.6±1.5
52	70.9±5.3	86.1±5.4 <b>83.0±6.1</b>	92.2±5.3	73.5±8.4	73.8±8.5 <b>n.d.</b>	73.9±8.8
51	102.5±3.4	120.4±3.8 <b>121.3±14.6</b>	126.1±8	105.2±5.7	106.5±5.9 <b>133.7±10.6</b>	107.1±5.7
7	101.4±5.5	125.5±6.2 <b>143.6±14.9</b>	131.0±6.4	161.8±9.8	163.0±9.8 <b>155.8±14.4</b>	163.7±9.8
10	n.d.	n.d. <b>361.3±19.0</b>	n.d.	379.1±7.2	383.2±7.2 <b>411.4±14.9</b>	384.0±7.2
59	290.3±17.5	376.9±23.4 <b>358.7±33.2</b>	396.2±24.4	356.5±34.4	360.0±34.7 <b>438.0±35.4</b>	361.0±34.7

The regeneration method is preferable to the additive dose method for old samples since it uses interpolation rather than extrapolation. However, there is evidence from some studies of a change in sensitivity, due to bleaching prior to irradiation, causing under-estimation of EDs determined using regeneration (Rendell and Townsend 1988, and Li and Wintle 1992). Figure 5.4.5(b) shows no evidence of this phenomenon. However, the two oldest

samples give larger regeneration EDs than additive dose EDs when using IRSL measurements. These two results are substantially larger than those determined using any other method of ED determination and the explanation is not clear.

#### 5.4.6 Comparison between equivalent dose values and normalization factors

The methods used for age determination in this chapter (outlined in sections 5.4.1 and 5.4.2) are extremely time-consuming, and prevent large numbers of samples being processed in a reasonable length of time. Normalization factors were determined for all the discs analyzed in this chapter on the basis of sample weight, IRSL brightness (0.1s measurement prior to any irradiation or bleaching), and the TL intensity (300-400°C) after 6 Gy beta irradiation following TL readout. The IRSL normalization factor is proportional to the dose the sample has received in nature (the ED) and the luminescence sensitivity of the sample to irradiation. The second glow normalization factor is a measure of the sensitivity of the sample to irradiation. In theory, dividing the IRSL normalization factor by the second glow normalization factor should give a ratio that is proportional to the ED of the sample. Figure 5.4.6 plots the two normalization factors, and their ratio, as a function of sample ED as determined in section 5.4.5. The curvilinear relationship is due to the saturation of the luminescence signal at high EDs.

Potentially this 'master curve' could be used to interpolate sample EDs simply by determining the ratio of their natural normalization factor to their second glow normalization factor. The precision of this method is limited by the scatter seen in figure 5.4.6. However, other 'rapid' methods of ED determination are discussed in chapters 6 and 7 that have the potential to produce more precise results.

### 5.5 Comparison of luminescence and geological age estimates

Tables 5.5(a) and 5.5(b) list ages determined by TL and IRSL respectively, using both regeneration and additive dose methods. The calculated luminescence ages are compared with the expected ages of the samples based upon other dating methods (discussed in section 5.2) and the results are plotted in figure 5.5. As discussed in section 5.4.5, the EDs determined from TL and IRSL measurements using both the additive dose and the regeneration methods are generally very similar, and consequently there is little difference in the ages calculated.

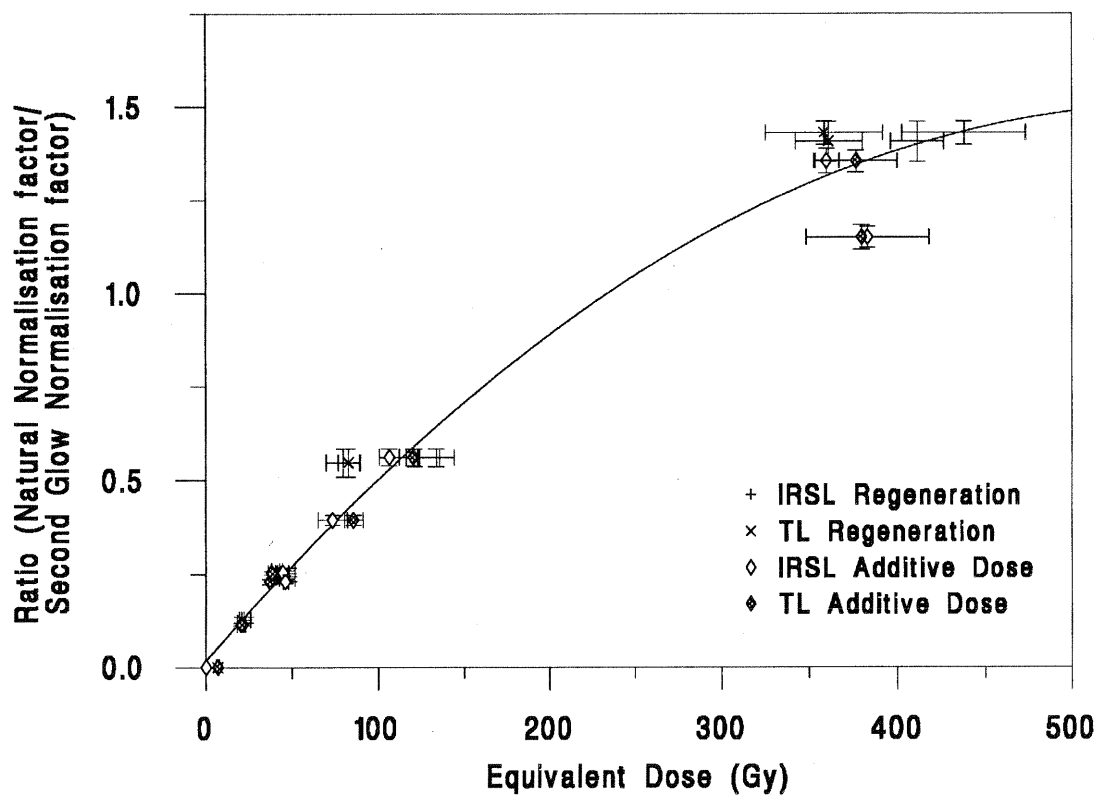


Figure 5.4.6: The relationship between the equivalent dose determined for a sample and the ratio of its natural normalization factor (0.1s IRSL measurement) divided by its second glow normalization factor (TL integral 300-400°C after a 6 Gy test dose).

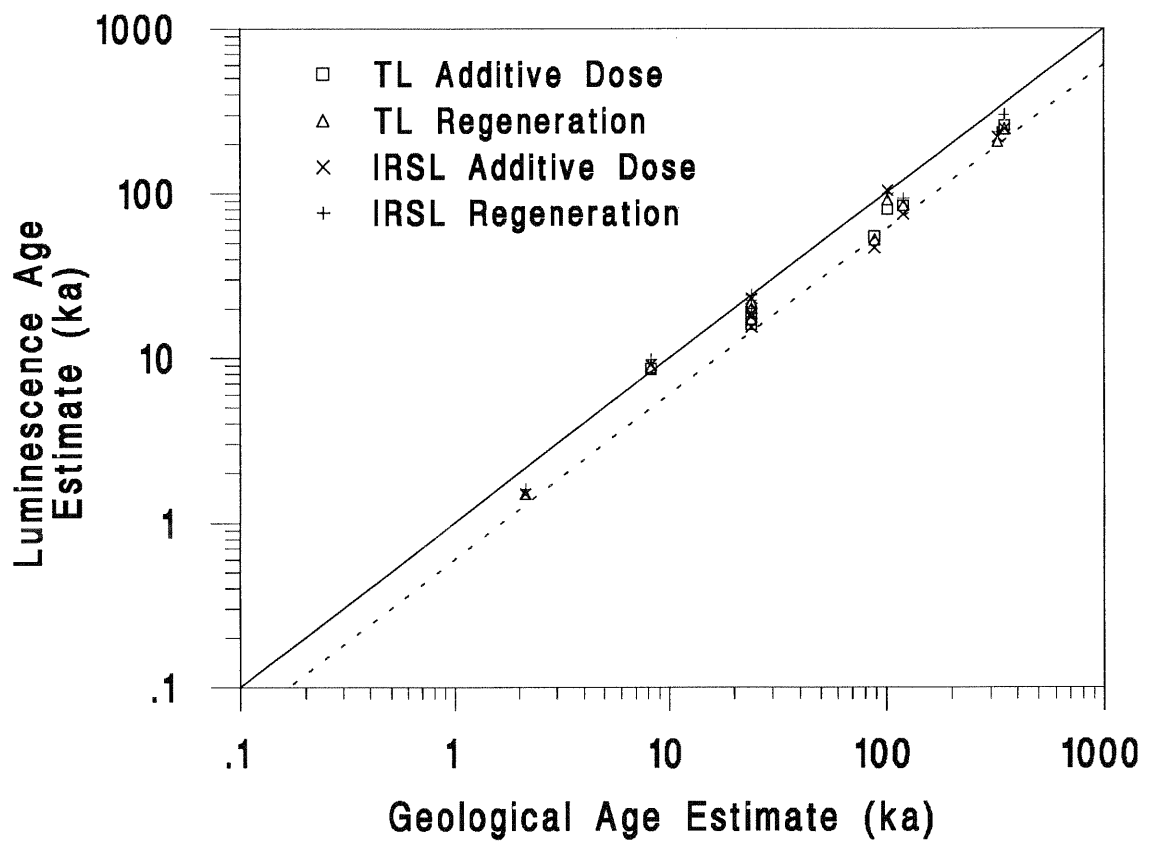
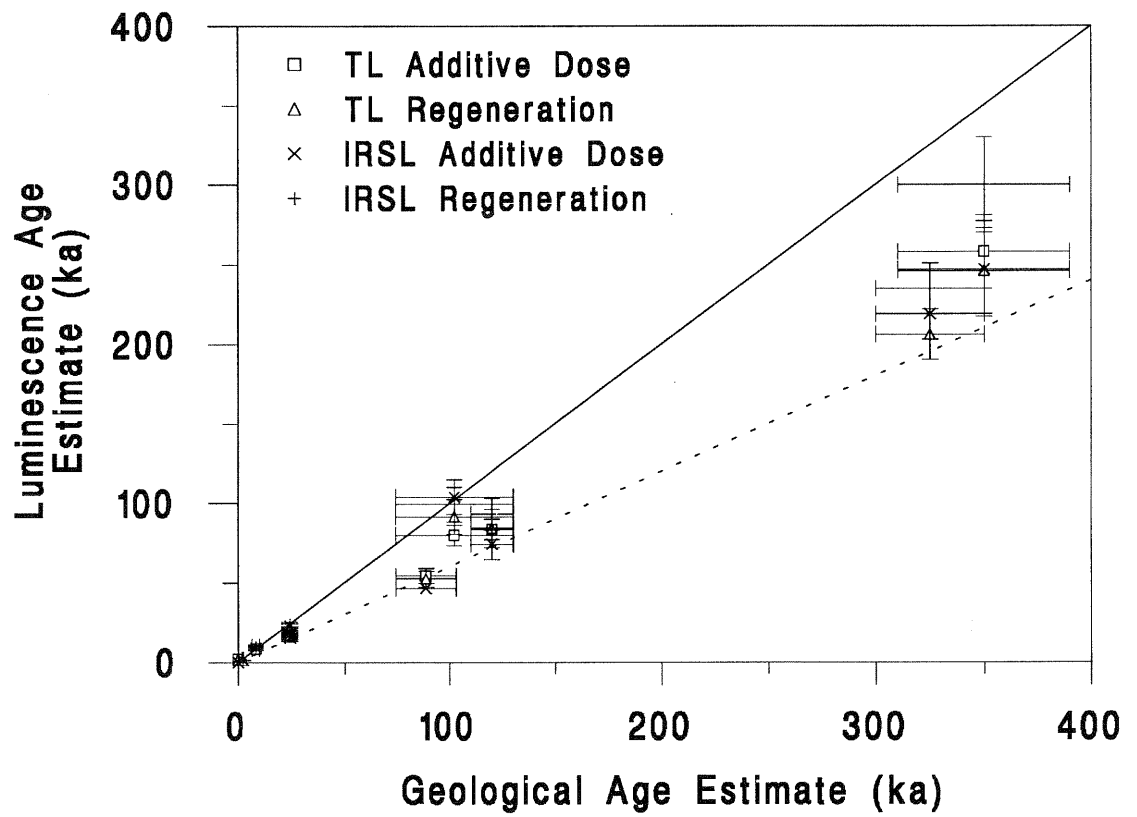


Figure 5.5: Comparison of luminescence age estimates with the expected geological ages determined by independent methods. The data are plotted on a linear scale (above) and a log-log scale (bottom).

Table 5.5 (a)

Comparison between thermoluminescence ages, determined using both the additive dose and the regeneration methods, and the expected geological age estimates.

<u>Sample</u> (GDNZ)	<u>Total Dose</u> Rate <sup>(a)</sup> (Gy/ka)	<u>Additive Dose</u>		<u>Regeneration</u>		<u>Expected</u> Age (ka)
		<u>ED</u> <sup>(b)</sup> (Gy)	<u>Age</u> (ka)	<u>ED</u> (Gy)	<u>Age</u> (ka)	
21	3.33±0.17	7.1±0.6	<b>2.1±0.2</b>	6.6±1.0	<b>2.0±0.3</b>	0
6	2.25±0.13	n.d.	<b>n.d.</b>	3.3±0.3	<b>1.5±0.2</b>	1.9-2.4
17	2.39±0.16	20.5±2.5	<b>8.6±1.2</b>	21.0±1.3	<b>8.8±0.8</b>	6.5-10
5	2.01±0.11	37.3±2.2	<b>18.6±1.5</b>	44.3±1.6	<b>22.0±1.4</b>	<24
1	2.40±0.13	38.4±0.2	<b>16.0±0.9</b>	40.7±2.3	<b>17.0±1.3</b>	<24
45	2.16±0.12	40.0±1.2	<b>18.5±1.2</b>	43.2±1.1	<b>20.0±1.2</b>	>24
13	2.56±0.15	45.8±1.7	<b>17.9±1.2</b>	44.3±4.3	<b>17.3±2.0</b>	>24
52	1.59±0.10	86.1±5.4	<b>54.2±4.8</b>	83.0±6.1	<b>52.2±5.0</b>	74-103
51	1.44±0.10	120±3.8	<b>83.6±6.4</b>	121±15	<b>84.2±12</b>	110-130
7	1.57±0.10	126±6.2	<b>79.9±6.4</b>	144±15	<b>91.5±11</b>	74-130
10	1.75±0.10	n.d.	<b>n.d.</b>	361±19	<b>206±16</b>	<350±40
59	1.46±0.09	377±23	<b>258±23</b>	359±33	<b>246±27</b>	<350±40

Table 5.5 (b)

Comparison between infrared stimulated luminescence ages, determined using both the additive dose and the regeneration methods, and the expected geological age estimates.

<u>Sample</u> (GDNZ)	<u>Total Dose</u> Rate <sup>(a)</sup> (Gy/ka)	<u>Additive Dose</u>		<u>Regeneration</u>		<u>Expected</u> Age (ka)
		<u>ED</u> <sup>(b)</sup> (Gy)	<u>Age</u> (ka)	<u>ED</u> (Gy)	<u>Age</u> (ka)	
21	3.33±0.17	0.1±0.1	<b>0.0±0.0</b>	0.7±0.1	<b>0.2±0.0</b>	0
6	2.25±0.13	3.3±0.0	<b>1.5±0.1</b>	3.6±0.1	<b>1.6±0.1</b>	1.9-2.4
17	2.39±0.16	21.8±0.8	<b>9.1±0.7</b>	23.4±2.5	<b>9.8±1.2</b>	6.5-10
5	2.01±0.11	46.3±1.6	<b>23.0±1.5</b>	48.5±3.2	<b>24.1±2.1</b>	<24
1	2.40±0.13	44.7±3.1	<b>18.6±1.6</b>	48.1±3.7	<b>20.0±1.9</b>	<24
45	2.16±0.12	38.5±1.2	<b>17.8±1.6</b>	48.4±2.5	<b>22.4±1.7</b>	>24
13	2.56±0.15	39.5±1.4	<b>15.4±1.1</b>	47.5±2.5	<b>18.6±1.5</b>	>24
52	1.59±0.10	73.8±8.5	<b>46.4±6.1</b>	n.d.	<b>n.d.</b>	74-103
51	1.44±0.10	107±5.9	<b>74.3±6.6</b>	134±11	<b>93.1±10</b>	110-130
7	1.57±0.10	163±9.8	<b>104±9.1</b>	156±14	<b>99.4±11</b>	74-130
10	1.75±0.10	383±7.2	<b>219±13</b>	411±15	<b>235±16</b>	<350±40
59	1.46±0.09	359±33	<b>246±27</b>	438±35	<b>300±30</b>	<350±40

Notes

- (a) Dose rate is taken from table 5.3.4(b) and does not include any internal alpha dose rate contribution.
- (b) The equivalent dose determined using the additive dose method is that using the residual level after 60 minutes of exposure to the SOL2 solar simulator.

As discussed in section 5.4.5 the TL results from the modern sample GDNZ 21 give a non-zero ED, and this corresponds to an apparent age of  $2.0 \pm 0.3$  ka. This is believed to be due to poor bleaching at deposition and the IRSL results, which are less dependent upon the extent of bleaching at deposition, give ages of  $27 \pm 19$  years using the additive dose method and  $206 \pm 34$  years using regeneration. The implication of the IRSL results for this modern sample is that it would not be feasible to date similar sediments younger than approximately 0.5 ka reliably. Edwards (1991) produced an age of  $40 \pm 17$  years for a surface sample from the Kelso dunefield (USA) using IRSL measurements, but this was aided by the high rates of solar insolation in the area, giving efficient bleaching of the luminescence signal, and a high dose rate (4.8 Gy/ka).

The discrepancy between ages determined using TL and IRSL measurements is not seen for sample GDNZ 6. All three of the age determinations for this sample are similar, but appear to underestimate the age estimated from the radiocarbon dating of the peats above and below it by at least 0.4 ka. A sample taken from the same position, and collected at the same time as GDNZ 6, by Dr M. Shepherd has been dated using TL measurements on quartz, and gave an age of  $3.0 \pm 0.5$  ka (Shepherd and Price 1990). This overestimate may relate to problems in determining the residual level for the quartz TL signal in this young sample.

The four luminescence age estimates for GDNZ 17 fall within the expected age range and give a mean age of 9.1 ka. The relationship of the group of dunes from which this sample was taken, south of Otaki, with those classified as belonging to the Koputaroa dune phase will be discussed in chapter 8.

Four samples were analyzed from immediately above or below the Aokautere ash (Kawakawa tephra). At Paiaka road there is little evidence for any hiatus in dune deposition above or below the ash. Sample GDNZ 5, from above the ash, gives an average age of 21.9 ka, while sample GDNZ 45, from immediately below the ash at the same site, gives an average age of 19.7 ka. While the ages determined for GDNZ 5 are completely in agreement with the radiocarbon dates on the ash, those for GDNZ 45 appear to be underestimated by about 4 ka. Shepherd and Price (1990), using quartz as the dosimeter, analyzed an identical sample to GDNZ 45 and produced a TL age of  $24.0 \pm 3.7$  ka completely in agreement with the expected result. GDNZ 1 and 13 were the other two samples which were taken from around the Aokautere ash. GDNZ 1, from above the ash at McLeavy road, gave an average age of 17.9 ka while GDNZ 13, from below the ash at Koputaroa road, gave an average age of 17.3 ka. The age of GDNZ 1 is compatible with the stratigraphy of the site. The underestimation of the age of GDNZ 13 may be due, in

part, to an underestimate of the water content of the sample. The site today consists of a narrow strip of ground (about 8m wide) remaining between a cutting for a railway on one side, and a road on the other. Estimation of the past water content is very difficult, but it is conceivable that it may have been substantially higher than the figure of  $10\pm 5\%$  used in table 5.3.3 for the majority of the period of burial of the sediment.

Three samples were taken from sands believed to date from the last interglacial: GDNZ 7, 51 and 52. No evidence was available to constrain which part of oxygen isotope stage (O.I.S.) 5 sample GDNZ 7 was from. The average luminescence age of 94 ka lies comfortably within O.I.S 5. The two other samples GDNZ 51 and 52 were collected from the Whenuakura river site where a maximum age for the samples, of 130 ka, was provided by amino-acid racemization results on wood found within the marine sands on the wave cut surface. As discussed in section 5.2 the lower age limits for the samples were derived from correlation of the loess units overlying the sand units with other loess units within this part of the Wanganui basin (Pillans 1988). The average luminescence ages of the two samples are 83.8 ka (GDNZ 51) and 50.9 ka (GDNZ 52). These ages are younger than those expected on the basis of the amino-acid racemization results and analysis of the stratigraphy (110-130 ka and 74-103 ka respectively), although there was doubt as to the quality of this age control (see section 5.2). The luminescence ages imply that the lower dune sand was deposited during O.I.S. 5a (74-91 ka) and the upper dune sand during the warmest phase of O.I.S. 3 (44-59 ka, substages 3.13 to 4.0 of Martinson *et al.*, 1987). This chronology implies that the loess above the upper dune sand was deposited over the past 51,000 years, during which period Pillans (1988) suggests that only two periods of loess accumulation have occurred. Identification of periods of loess deposition at this site was hampered by the lack of clearly defined palaeosols, and re-investigation of the site may show that only two loess units can be identified. It is difficult to use the data from samples GDNZ 51 and 52 to judge whether the luminescence dates are correct given the uncertainties that are involved in the independent age control on these samples.

When samples were collected for this study the Mt Curl Tephra was dated at  $240\pm 50$  ka and the Rangitawa Pumice at  $340\pm 40$  ka by fission track dating (Milne 1973, Pillans and Kohn 1981). Subsequently it has been shown that the two tephra are correlative and have a fission track age of  $350\pm 40$  ka (Kohn *et al.* 1992). Samples GDNZ 10 and 59 were taken from dune sands overlying the tephra at the Mt Curl Tephra type site and at Rangitatau East road (Bushy Park section) respectively. Allowing for the possibility of a hiatus between deposition of the tephra and the dune sand at the Mt Curl site the two luminescence ages are very similar (220 ka and 263 ka respectively) and support the idea that the two are correlative. However they underestimate the fission track age by as much

as 30% (depending upon what period of time is thought to have elapsed between deposition of the tephra and the dune sand). This may relate to the type of long term fading described by Mejdahl (1988, 1989) for which he predicts that for samples with an annual dose rate of 1.5 Gy/ka, luminescence ages of 250 ka would be obtained from samples whose true age is close to 320 ka (very close to the expected age of these two samples). This type of long term fading would cause less than 5% underestimation of samples aged 100 ka and so would not be seen in samples GDNZ 7, 51 and 52.

## 5.6 Conclusions

The comparison of luminescence ages with those determined by other methods always involves an implicit reliance upon the validity of those other methods. The seven samples analyzed in this chapter with expected ages less than 30 ka show good agreement between the luminescence age estimated and those determined by other methods. However, if the expected ages for samples GDNZ 51 and 52 are accepted at face value then the implication is that the luminescence methods used in this study suffer from underestimation by about 35% at 100-130 ka, although this is not the case for GDNZ 7. A more consistent relationship can be proposed if the chronology of the Whenuakura river section is altered to place the lower dune sand in O.I.S. 5a and the upper dune sand in O.I.S. 3. On this basis the extent of any underestimation up to 100 ka cannot be distinguished from the errors inherent to the luminescence method. No samples were analyzed in this study with ages between 130 and 300 ka. The two samples with expected ages of about 300-350 ka showed underestimation by up to 30% which is consistent with the behaviour described by Mejdahl (1988, 1989).

Thus the conclusion of this part of this study is that accurate luminescence ages may be determined using potassium feldspars as the dosimeter in the age range from 0.5-100 ka. The lower age threshold can only be reliably approached using IRSL measurements, but in the range 1.5-100 ka no systematic differences could be seen between ages measured using TL and those using IRSL. Additionally, no consistent differences between ages determined using the additive dose and the regeneration method could be seen over the entire time range studied here for these relatively well bleached sediments.

## CHAPTER 6: Regeneration using a single aliquot

The standard methods of equivalent dose (ED) determination for sedimentary material (additive dose method - Singhvi *et al.* 1982; regeneration method - Wintle and Proszynska 1983; and partial bleach method - Wintle and Huntley 1982) involve the preparation of many aliquots of the sample. This is inevitable given the changes of sensitivity that occur upon heating during TL measurements and the fact that one has to destroy the whole luminescence signal in order to measure it. Each aliquot can only be measured once. Problems arise concerning normalisation between these different aliquots, and the large number of aliquots that are required necessitates the processing of large amounts of sample.

Southgate (1985) attempted to use TL measurements on single feldspar grains to determine the equivalent dose of beach and dune sands, but no final results were presented, and only one measurement could be made on each grain because of the changes in sensitivity that occurred upon TL readout.

The use of optically stimulated luminescence (OSL) offers a less destructive method of sampling the trapped charge concentration (Huntley *et al.* 1985). The aim of the work presented in this chapter and the next, is to investigate methods of equivalent dose determination based upon using OSL measurements on a single aliquot of sample. In this chapter the regeneration method is used, and in the next chapter a technique based upon the additive dose method is explored.

Smith *et al.* (1986) mention the use of a single aliquot of quartz or zircon for ED determination using OSL (stimulating with an argon-ion laser), but give no details or results. Rhodes (p.90, 1990) pursued the possibility, but stated that such a method was impracticable because of the change in sensitivity that occurred upon exposure to the laser. The large amount of labour involved was also prohibitive since no automation was available.

The Risø automated TL reader, together with an infrared stimulated luminescence (IRSL) add-on unit (Bøtter-Jensen *et al.* 1991), provides all the facilities that are required to carry out ED determination on single aliquots of feldspar. Computer control of a radioactive source, a heating strip, and an infrared diode array means that all measurements and treatments can be carried out automatically, without the need for constant operator supervision.

## 6.1 Advantages of using a single aliquot

Despite the problems found when using the argon-ion laser to stimulate quartz (Rhodes 1990), the advantages of using only a single aliquot are clear:

(a) Precision - Since all measurements for the equivalent dose are made on a single aliquot there is no need for normalisation between measurements due to variations in sample weight or sample mineralogy. Although IR will only stimulate luminescence from feldspathic minerals, variations in potassium feldspar mineralogy are a problem in multiple aliquot procedures. A potassium feldspar separate from a sedimentary sample contains a variety of minerals (mainly orthoclase, sanidine and microcline). These are unlikely to behave similarly in terms of dose response and in normal luminescence methods of ED determination (either TL or IRSL) some means of normalisation is required. If the saturation doses of the individual minerals were different then standard ED determinations would be seriously compromised (Li 1991b). In particular when high doses are given, with some minerals approaching their saturation dose and others not, the scatter between measurements increases. This effect will not be a problem using a single aliquot.

(b) Multiple determinations - By running many single aliquots the true variability in the ED of the minerals in a particular grain size can be assessed. Small variations in the ED can be seen and an average value calculated together with the standard deviation. Using standard techniques it is very time consuming to make repeat ED determinations, and where only one determination is made the error is estimated purely in terms of the mathematical fit of the data to a linear or exponential regression. The errors obtained in this way are highly dependent upon the exact method of error analysis and are not representative of the variability in mineral response (Berger and Huntley, 1989).

(c) Effort - Standard luminescence techniques require at least 30 measurements to be made in total to ensure reproducible behaviour even for well-behaved material. In many cases, where greater precision is required, or for older samples, this number may easily exceed 60, each measurement needing a separate aliquot. Using a smaller number of aliquots would mean that smaller samples could be used (particularly important in archaeological sites and where field access is difficult), less effort is required to extract sufficient potassium feldspar, and less time taken to mount the sample.

The greatest economy in effort is in the ED determination where ALL sample treatment - irradiation, preheating, bleaching, and measurement - is undertaken automatically within the Risø reader.

## 6.2 Advantages of using Regeneration

Regeneration is intrinsically the simplest method used to determine the equivalent dose. For TL the method was described originally by Wintle and Proszynska (1983); it relies upon the ability to bleach the sample to its residual level, mimicking its signal at deposition. Using IRSL, all measurements to build up a growth curve can be performed on a single aliquot. Since the method relies upon interpolation, and not extrapolation, the analytical error will be relatively small. The IRSL signal can be measured over a long time period, say 100 seconds, in order to improve the signal-to-noise ratio.

## 6.3 Description of the method

All measurements needed for ED determination are performed by the Risø reader automatically (using the software package SINGLE). A single aliquot of the sample is preheated at 220°C for 600s to remove the relatively unstable potassium feldspar TL peak at 270°C (section 4.7.3). The IRSL signal is then measured for 100s to produce a decay curve which is stored for analysis. Once a residual level has been achieved the aliquot can be irradiated, preheated and remeasured. Bleaching back to the residual level can then be followed by as many irradiations as required to build up a growth curve.

An ED can be calculated by integrating the IRSL signal from the various measurements over the whole 100s period, or by using the IRSL signal obtained during each of the 100 seconds of the measurements. Calculating an ED for each second of the 100s of measurement, the results can then be plotted against the measurement time to form an ED plateau plot analogous to that plotted for TL data (see section 5.4.3). It is thought that the initial IRSL signal obtained represents the charge from the most light-sensitive traps, and that as the measurement continues progressively harder-to-bleach components are measured (Rhodes, 1990). Deviations from a flat plateau may be caused by, amongst other reasons, the use of a bleaching procedure in the regeneration method that does not accurately mimic that experienced at the time of deposition of the sample. However, little work has been published about the significance of this type of plot. After IRSL measurement further infrared (IR) exposure is used to reduce the IRSL signal from the aliquot to a residual level. During this time the IRSL signal is constantly monitored. The sample can be exposed to IR for a fixed time, or until the IRSL signal falls below a preset count rate to achieve the residual level required.

## 6.4 Application to GDNZ 5

Sample GDNZ 5 was used to undertake some preliminary tests on the method outlined above. The sample was chosen since it gave a large IRSL signal, yet its ED was such that irradiation times using the beta source mounted on the Risø (1.24Gy/min for 180-211µm grains) would not be prohibitive.

### 6.4.1 Reproducibility of results

Figure 6.4.1 shows the IRSL decay curves, growth curve and associated plateau for a single aliquot of GDNZ 5. Six aliquots were run at the same time, all yielding plateaux similar to that in figure 6.4.1. Using an integral over the full 100s of IRSL measurement six independent EDs were determined (table 6.4.1). These give a weighted mean of 32.8 ±0.6 Gy, a precision of 1.7%.

Table 6.4.1

Equivalent doses obtained using single aliquots of GDNZ 5. See text for details.

<u>Aliquot Number</u>	<u>Equivalent Dose (Gy)<sup>(a)</sup></u>	<u>Analytical Error (Gy)<sup>(b)</sup></u>
1	32.3	1.3
2	32.8	1.4
3	32.5	1.4
4	33.2	1.4
5	32.7	1.4
6	33.7	1.4

**Note:**

- (a) After measurements of the natural IRSL the ED was determined measuring the residual level first, and then giving successively larger irradiation doses. Samples were exposed to IR between each measurement until their IRSL signal fell below 600 cps.
- (b) The analytical error quoted here is that resulting purely from the uncertainty in the regression analysis, performed by Rainer Grün's software.

### 6.4.2 Comparison with standard methods of ED determination

Table 6.4.2 compares ED values for sample GDNZ 5 determined using a variety of methods. The first four EDs have been measured using multiple aliquot methods (section 5.4.5). Clearly the regeneration method using a single aliquot has underestimated the true ED, even though a greater precision was achieved.

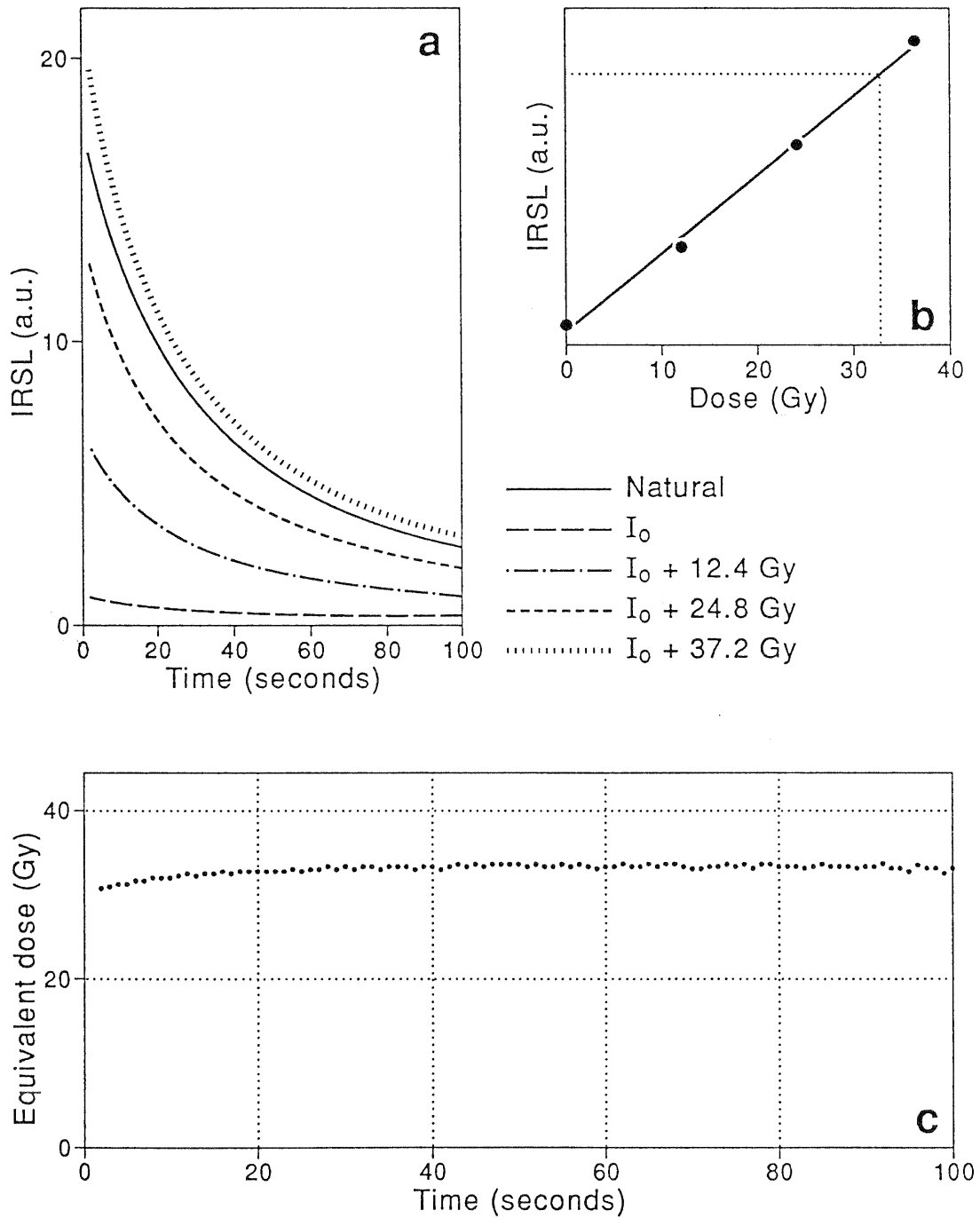


Figure 6.4.1: The IRSL decay curves (a), growth curve obtained by integrating the IRSL signal for all 100s of measurement (b) and the variation in equivalent dose as a function of the period of measurement (c), for sample GDNZ 5. After measurement of the natural signal the smaller doses were given first.

Table 6.4.2

Comparison of equivalent doses determined for GDNZ 5 using a variety of multiple aliquot methods and the single aliquot regeneration method.

<u>Method of Determination</u>		<u>Equivalent Dose</u> (Gy)
Regeneration	TL	44.3 ± 1.6
	IRSL	48.5 ± 3.2
Additive Dose	TL	37.3 ± 2.2
	IRSL	46.3 ± 1.6
Single Aliquot	IRSL (regen.)	32.8 ± 0.6

### 6.4.3 Effect of progressive changes in sensitivity

Since the sample is bleached between each measurement it might be expected that there is no special reason why the regeneration curve has to be built up in any specific order (e.g. smaller doses given first as in section 6.4.1).

Figure 6.4.3(a) shows IRSL data for another aliquot of GDNZ 5 measured using similar parameters as for the sample in figure 6.4.1. The only difference is that after measuring the natural signal the largest irradiations were given first. The difference in the shape of the growth curve is obvious. An equivalent dose of  $36.2 \pm 1.6$  Gy was obtained, far closer to the EDs determined using standard 'multiple aliquot' methods.

For the same aliquot the response to the largest dose and the residual level were remeasured after the points in figure 6.4.3(a) were taken (figure 6.4.3(b)). As more measurements are taken the signal increases. This is not simply due to an unbleachable component building up; the signal increase from the sample after it has been bleached and given 37.2 Gy is far larger than that for the residual. As more measurements are taken there is a progressive increase in sensitivity. This explains why the shape of the two growth curves in figures 6.4.1 and 6.4.3(a) are so different. This would also cause the ED to be underestimated, with the effect being most severe if a large number of doses were given before that which most closely approximates to the ED (cf. figures 6.4.1 and 6.4.3(a)).

The significant exception to this behaviour was shown for a colluvial sample from South Africa (Li and Wintle, 1991) for which the natural (TL) signal was close to saturation.

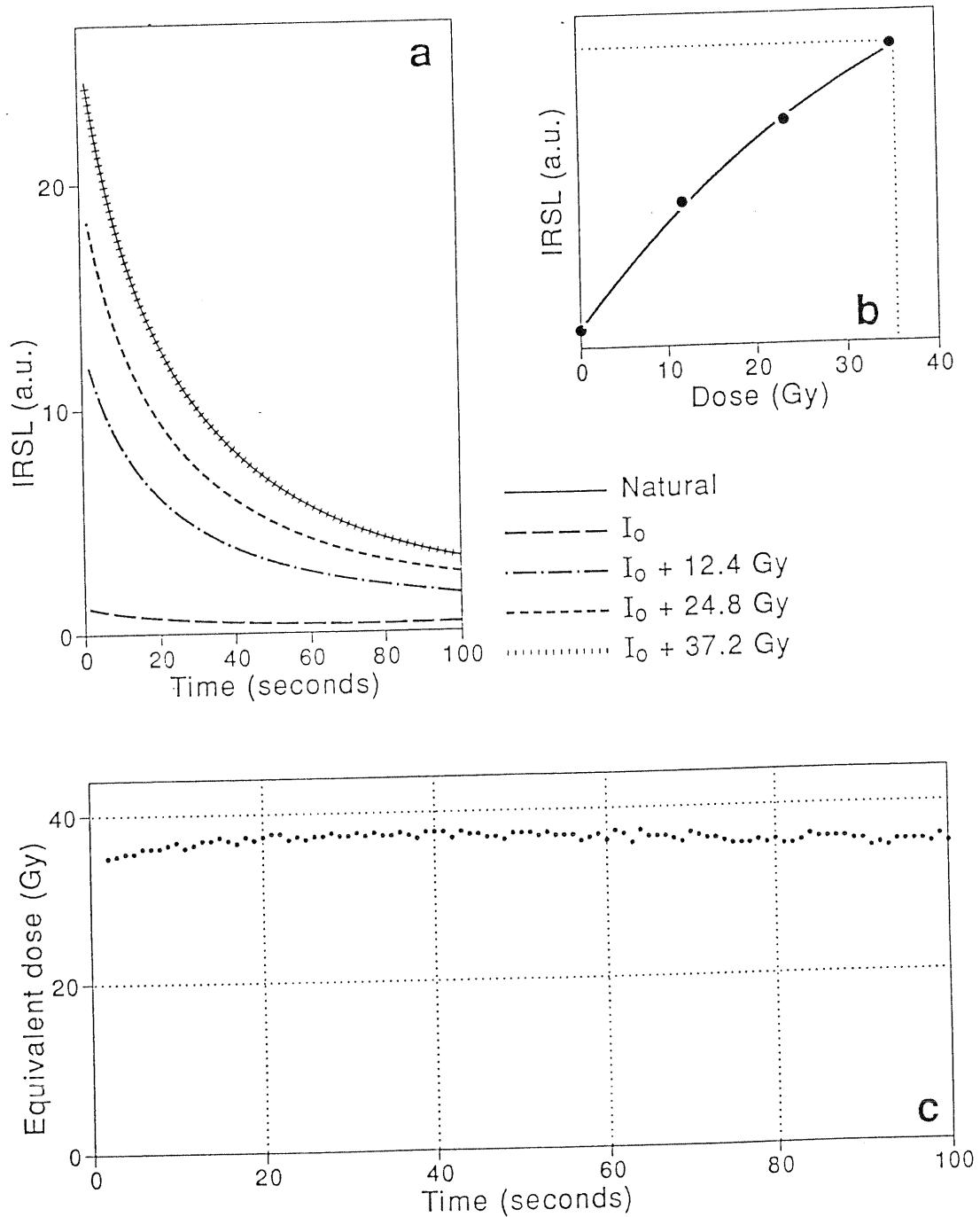


Figure 6.4.3(a): The IRSL decay curves (a), growth curve obtained by integrating the IRSL signal for all 100 seconds of measurement (b) and the variation in equivalent dose as a function of the period of measurement (c), for sample GDNZ 5. After measurement of the natural signal the largest dose was given first, followed by successively smaller ones.

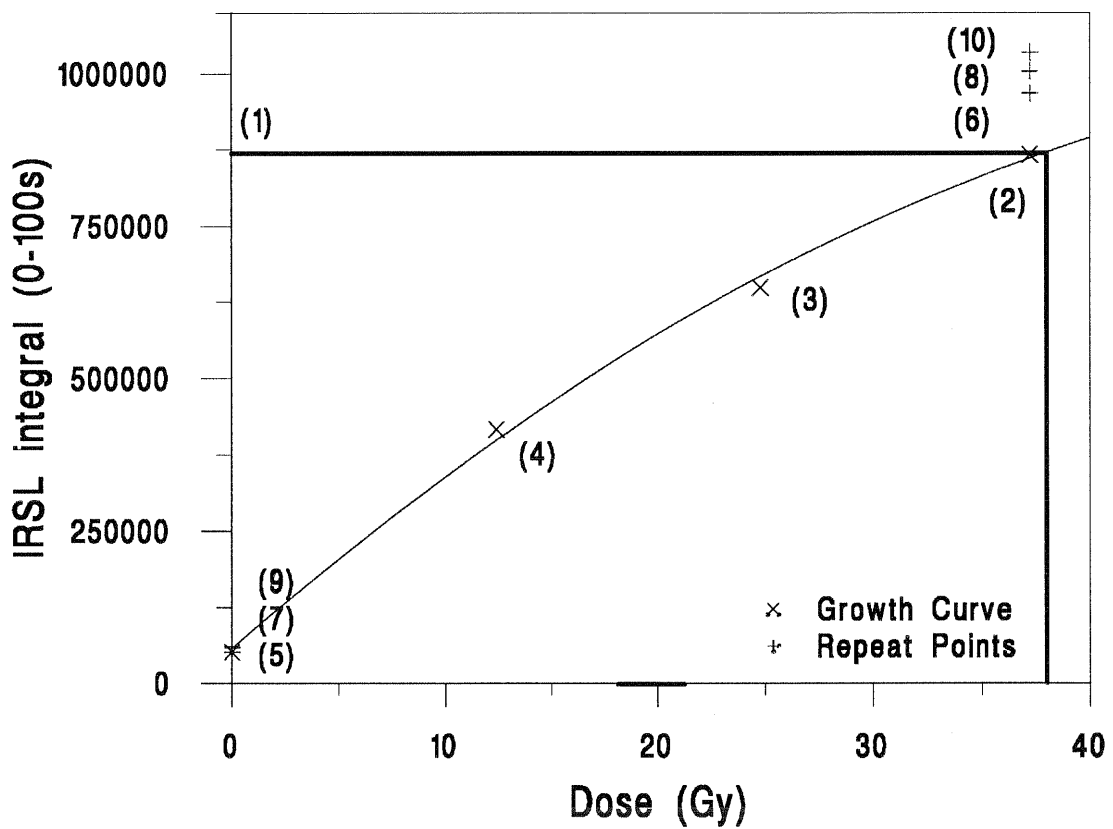


Figure 6.4.3(b): The IRSL growth curve for the aliquot of GDNZ 5 shown in figure 6.4.3(a). The order in which measurements were made is indicated by the numbers in brackets. Repeat measurements were made of the  $I_0$  and  $I_0+37.2$  Gy points.

Several repeat measurements were made using a large dose, close to that of the ED, and very little change in signal was seen.

## 6.5 Effect of elevated temperatures on IRSL

The progressive change in sensitivity seen for sample GDNZ 5 (figure 6.4.3(b)), and all others analyzed, is thought to be due to the incomplete removal of the electrons in light sensitive traps by exposure of the sample to infrared. Li and Aitken (1989) and Duller and Wintle (1991) have shown that at room temperature only a small proportion of the trapped charge responsible for the TL signal is affected by exposure to IR. Here it is hypothesised that by raising the temperature of the sample while it is exposed to IR, the proportion of the trapped charge that can be removed will be increased, and hence changes in sensitivity during regeneration using a single aliquot will be reduced. A series of experiments are described below to test this hypothesis.

The nature of the IRSL from a sample varies with temperature in a complex way. Discussion of the behaviour will be divided into three sections for clarity. The first discusses how changes in temperature affect the rate at which the IRSL signal is generated. The second looks at the effect upon the magnitude of the IRSL residual of exposing a sample to IR for long periods of time at different temperatures. The third looks at the same data, but analyzing the TL residual after exposure to IR.

### 6.5.1 Effect of temperature upon the IRSL signal

To investigate the effect of temperature upon the magnitude of the IRSL signal, the Risø reader was programmed to perform a rapidly alternating sequence of TL and IRSL measurements while heating the sample (program name TOL). In this way the TL component of the IRSL signal could be accurately subtracted to show the change in IRSL with temperature. The experiment is similar to that performed by Hütt and Jaek (1989), except that IR diodes are used here instead of a pulsed excimer dye laser (set to 866nm); this experimental procedure also permits subtraction of the TL signal directly, so giving greater precision in the measurement than was available previously.

Samples of GDNZ 17 were heated at 5°C/s in a pure argon atmosphere to 450°C. During this heating the luminescence from the sample was monitored every 10°C. A 0.1s measurement of TL was made with no infrared stimulation, followed immediately by another 0.1s measurement with infrared stimulation. This sequence allowed the TL

component to be subtracted. Measurement of the IRSL for 0.1s causes a signal reduction of about 0.5% at room temperature.

The total luminescence, the net IRSL (with the TL and dark count subtracted) and the TL signals are plotted as a function of temperature in figure 6.5.1(a). Above 50°C there appears to be a linear increase in IRSL up to 200°C; in fact the IRSL is increased by a factor of five between 50 and 200°C. Beyond this temperature thermal eviction reduces the charge population that the IR is stimulating. A second sample (figure 6.5.1(b)) had been preheated prior to these measurements to remove the TL below about 250°C, a procedure which extends the region of apparent linear growth of the IRSL signal up to a temperature of 260°C, before loss of the TL signal starts to reduce the IRSL.

Data obtained using a similar experimental method as that described above have been used by others to calculate an activation energy for the intermediate trap hypothesised in the Hütt *et al.* (1988) model for the IRSL process. A thermal activation energy of  $0.2 \pm 0.1$  eV was previously obtained for an unidentified alkali feldspar sample by Hütt and Jaek (1989) from a plot of  $\ln I/I_0$  versus  $T^{-1}$ , though no plot was given. Bailiff and Poolton (1991) obtained lower values for museum specimens of microcline ( $0.10 \pm 0.02$  eV), sanidine ( $0.09 \pm 0.02$  eV) and albite ( $0.08 \pm 0.02$  eV), but no experimental data were given. The data in figure 6.5.1(b) may be plotted in the form  $\ln I/n$  versus  $T^{-1}$ , where  $I$  is the IRSL intensity at temperature  $T$  (measured in kelvin) and  $n$  is the integrated IRSL signal remaining. This plot is linear in the temperature region from 50 to 180°C and gives a thermal activation energy of  $0.15 \pm 0.02$  eV (Duller and Wintle 1991), which is of the same order as the values given above. This type of analysis assumes that the IRSL signal that is measured at the various sample temperatures originates from a single trap population, and that as the sample temperature increases, the number of traps that are probed does not change.

To test this assumption 12 aliquots of potassium feldspar separated from GDNZ 1 were prepared and normalised using a 0.1s IRSL measurement. The aliquots were then divided into six pairs, and exposed to IR (at room temperature) from the built-in diode array on the Risø reader for different lengths of time (0, 10, 40, 100, 500 and 2000s). Each aliquot then had its TL and IRSL signals measured from 50 to 500°C using the method described above, but making measurements at 50°C intervals, rather than every 10°C. The IRSL signal from each pair of aliquots is shown in figure 6.5.1(c) as a function of temperature. Figure 6.5.1(d) plots the same data but shows the loss of IRSL (measured at 50°C intervals) as a function of IR exposure prior to measurement. The data is only shown for temperatures up to 350°C since above this temperature the scatter in the data is too large.

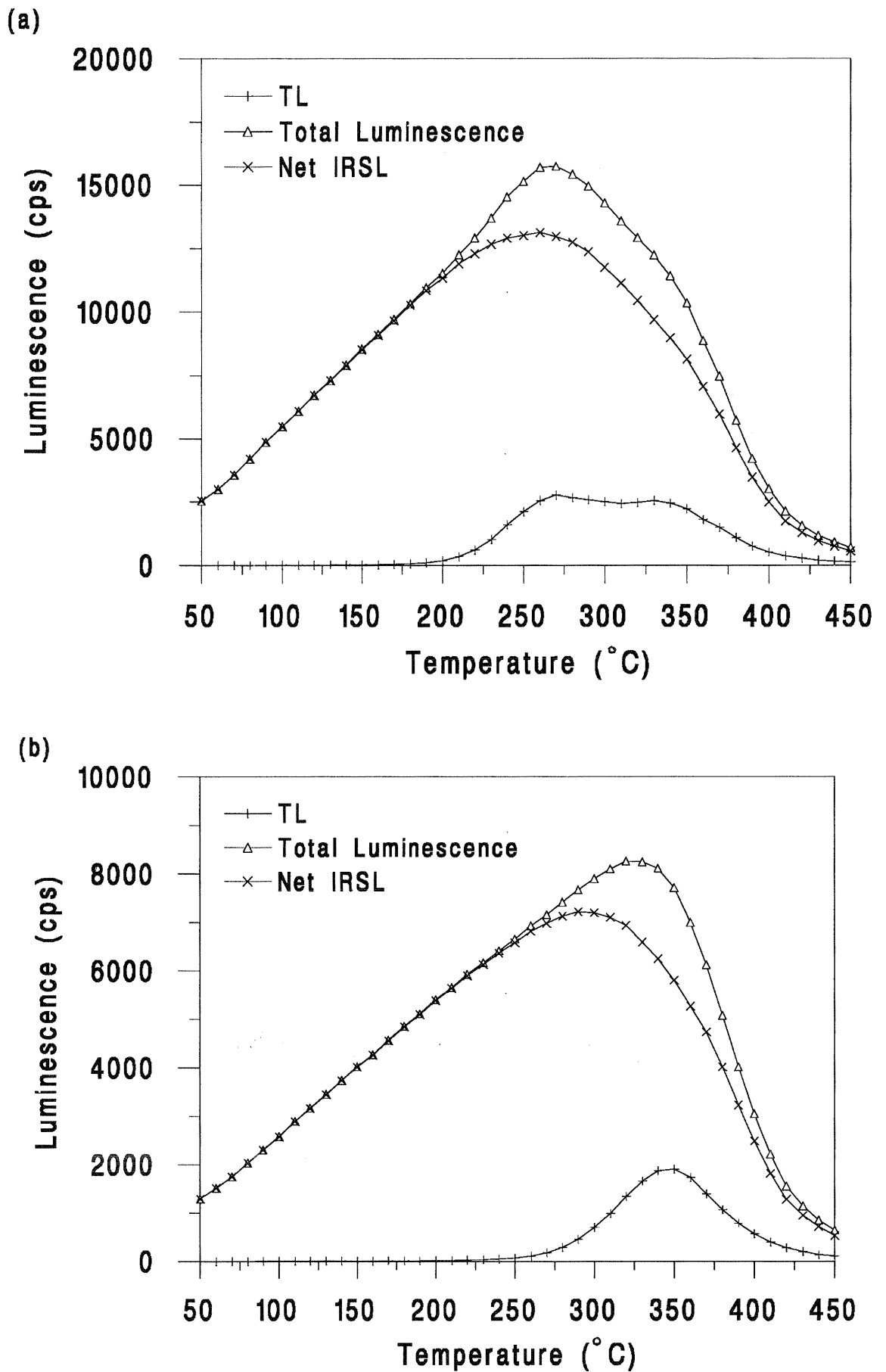


Figure 6.5.1: Near simultaneous measurements of the TL and IRSL signals from two samples of GDNZ 17, heating the sample from 50 to 450°C at 10°C/s. (a) is a natural sample and (b) has been preheated at 220°C for 10 minutes prior to analysis.

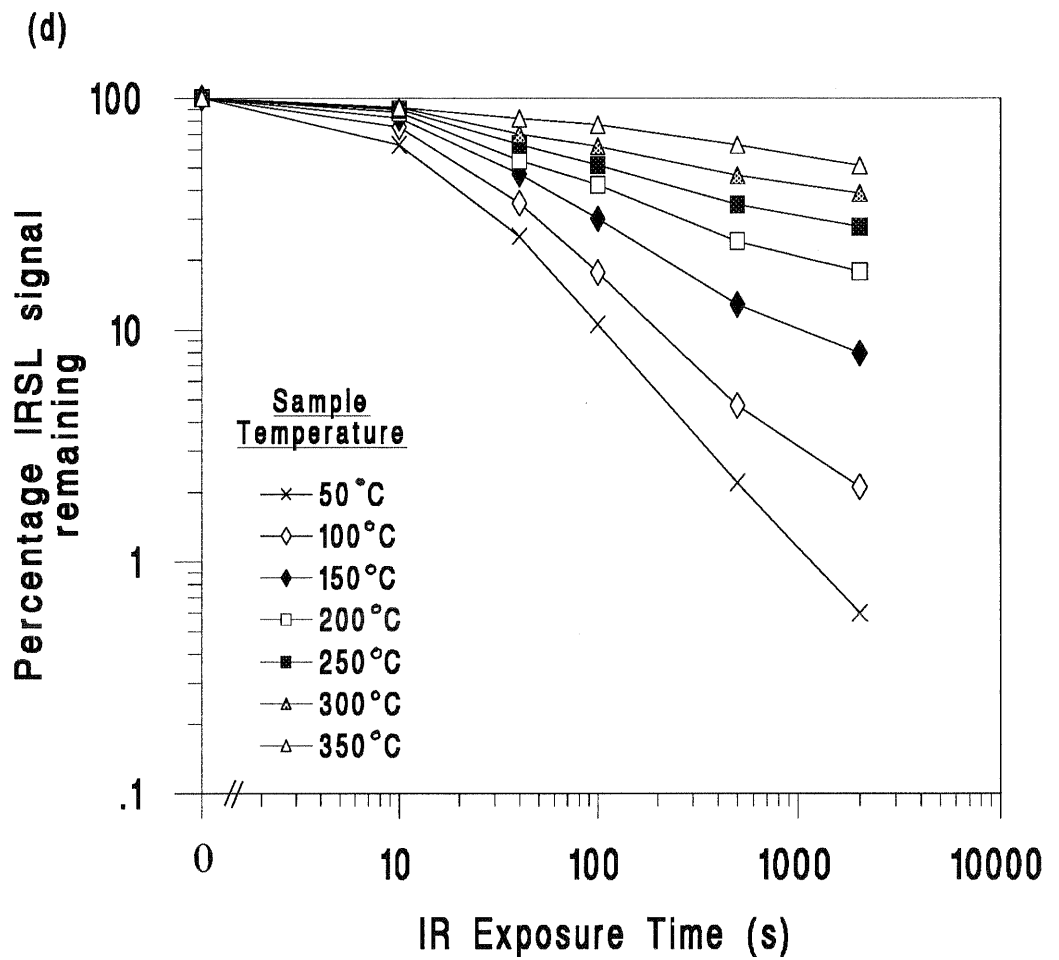
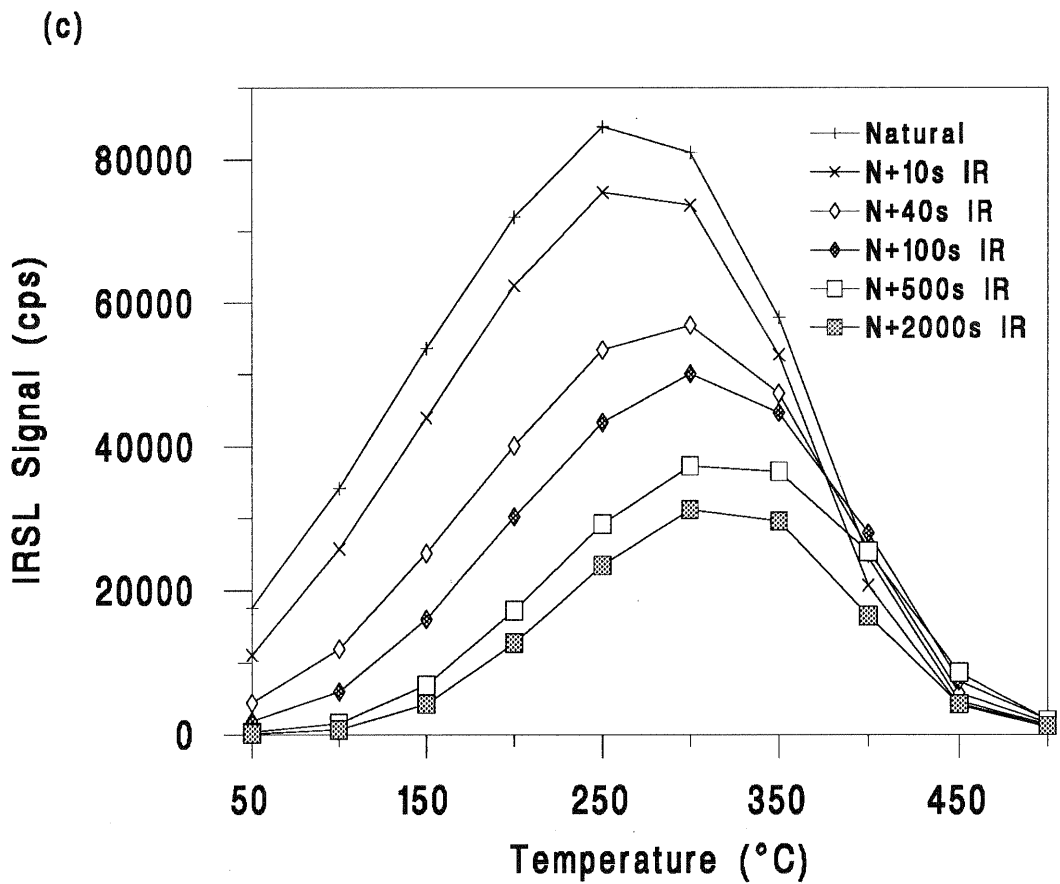


Figure 6.5.1: (c) Net IRSL signals from a number of aliquots that have been exposed to IR for varying lengths of time prior to analysis, measured using the TOL program. (d) The loss of the IRSL signal, measured at varying temperatures, due to exposure to IR within the Risø reader.

Figure 6.5.1(d) shows that although 2000s exposure to IR causes the IRSL signal measured at 50°C to be reduced to less than 1% of its initial level, when measured at 350°C the signal is only reduced to 51% of its initial level. The implication of figure 6.5.1(d) is that measurement of IRSL at 350°C probes a significant number of electron traps that are not probed when measurements are made at 50°C. This therefore invalidates the use of data such as that presented in figures 6.5.1(a) and (b) for the determination of an activation energy for the intermediate trap hypothesised by Hütt *et al.* (1988).

### 6.5.2 Effect of IR exposure at different temperatures upon the IRSL residual

In the previous section the IRSL was measured, without significantly reducing the trapped electron population, at elevated temperatures. Longer exposures to IR reduce the signal to levels which depend upon the total IR energy incident on the sample. For a thermo-optical process as proposed by Hütt *et al.* (1988), it might be expected that the temperature at which the sample is held during a long exposure will have an effect on the residual IRSL reached.

Twenty four samples of GDNZ 5 were mounted on aluminium discs. A control group of 4 aliquots were not bleached. The remaining twenty aliquots were split into five groups of four aliquots. The groups were bleached for 1000s using the infrared diode array in the Risø add-on unit, while being held at 25°C, 50°C, 100°C, 150°C and 200°C respectively. IRSL decay curves for the first 100s show that a significantly higher signal is obtained at higher sample temperatures (figure 6.5.2(a)) as would be expected as a result of the data given in section 6.5.1.

The total light emitted over the 1000s period and the residual level reached after 1000s (Table 6.5.2, column A) were measured at the different temperatures. Table 6.5.2 (column B) also shows the IRSL remaining after the bleaching treatments when the samples were measured at room temperature. There is an order of magnitude difference in the remaining signal as measured at room temperature whereas the remaining IRSL at elevated temperatures are the same within experimental error; this implies that bleaching at higher temperatures has removed a greater proportion of the IRSL signal as measured at room temperature.

From this data set it is impossible to calculate the total IRSL emitted at the different temperatures since it is unknown how much of the IRSL signal measured was due to thermal eviction. Thus a second set of aliquots, this time of sample GDNZ 17, were prepared.

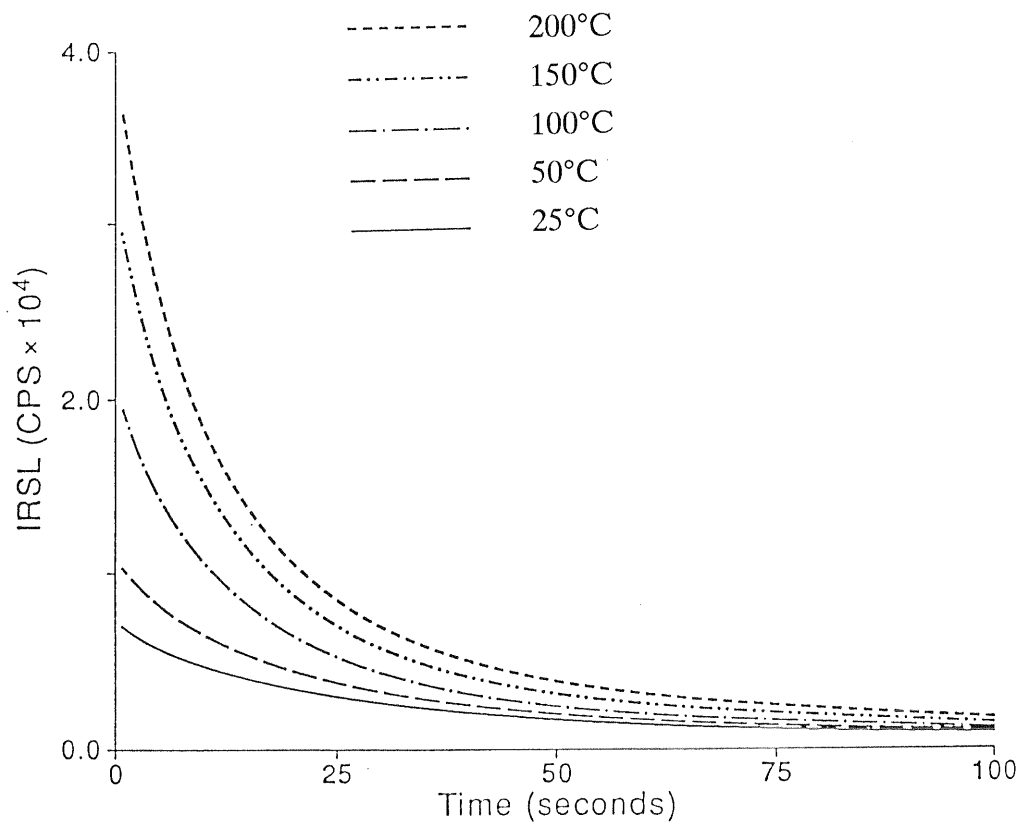


Figure 6.5.2(a): IRSL decay curves obtained while holding the sample at the stated temperatures showing the loss of signal over 100 seconds of measurement.

Table 6.5.2

IRSL signals remaining after 1000s of IR exposure at different sample temperatures. Column A contains measurements made at the respective elevated temperatures after 1000s of IR exposure, while those in column B were made at room temperature. The IRSL signal (1s IRSL measurement) from the unbleached samples is also shown for comparison. All measurements are the average of four aliquots ( $\pm 1\sigma$ ).

<u>Bleaching Temperature</u>	<u>Remaining IRSL (cps)</u> <b>COLUMN A</b>	<u>Remaining IRSL (cps)</u> <b>COLUMN B</b>
Room temp. (25°C)	84 ± 10	66 ± 15
50°C	73 ± 9	46 ± 24
100°C	80 ± 7	8 ± 1
150°C	72 ± 23	3 ± 2
200°C	107 ± 22	0 ± 1
Unbleached sample	-	3730 ± 15

These aliquots were also bleached by infrared stimulation while being held at various temperatures from 25°C to 200°C. However, once the hotplate had been stabilised at the appropriate temperature, an alternating sequence of measurements was made with and without IR stimulation. IRSL was measured for one second and the IR LEDs then turned off. After the IR stimulation the sample was left for half a second to allow phosphorescence to die away (Wheeler 1988), and then the luminescence signal was measured for half a second. This is defined as the isothermal TL. This signal was then doubled to give the contribution of the isothermal TL component over one second to the previous IRSL measurement. This cycle was repeated every two seconds until 1000s of IRSL had been measured.

Figure 6.5.2(b) shows the isothermal TL signals for the first 100s of measurement. During the first 2-5s the TL signal increases, probably related to build up of signal in shallow traps by phototransfer. Following this there is a steady decline. However the magnitude of the TL signal (30-700 cps) is very small compared with the IRSL (8,000-40,000 cps) and hence its subtraction makes little or no difference to the data shown in figure 6.5.2(a).

Subtracting the isothermal TL signal from the total luminescence signal, for the 1000 measurements, gave integrals for the total amount of IRSL signal evicted during the period. Figure 6.5.2(c) plots these data as a function of temperature. It clearly shows that the IRSL light sum increases with sample temperature.

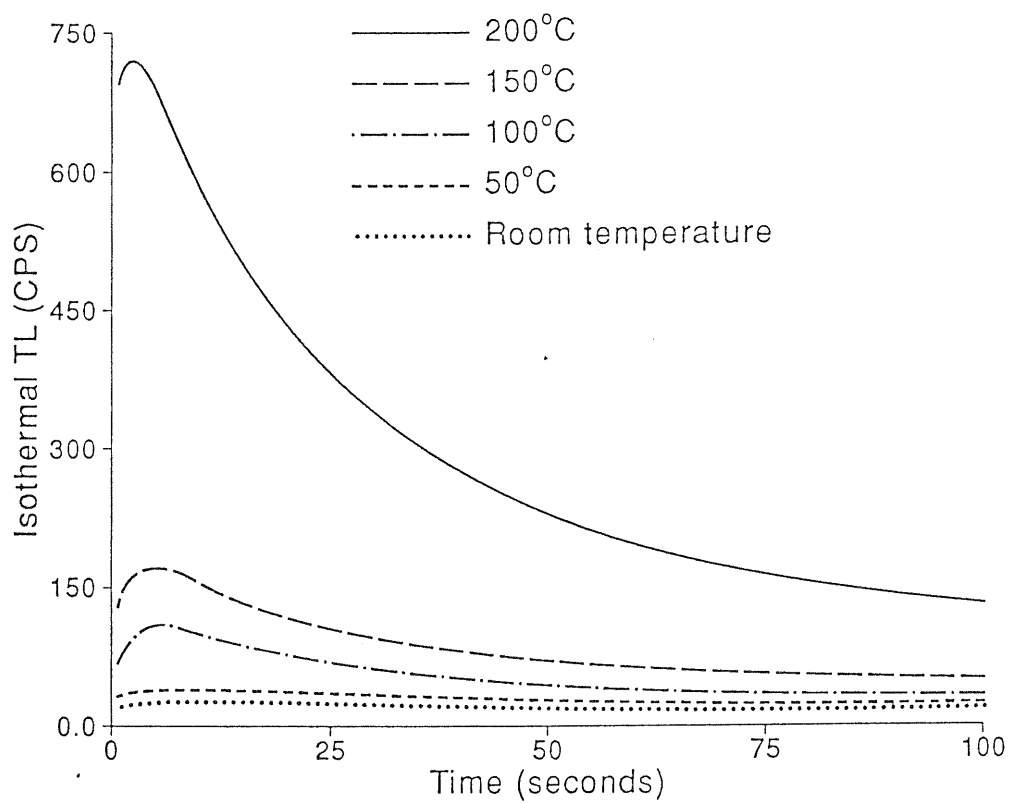


Figure 6.5.2(b): The isothermal TL signal obtained, using the method described in the text, for a set of aliquots whose IRSL decay curves were measured while holding the sample at various temperatures from 25°C (room temperature) to 200°C.

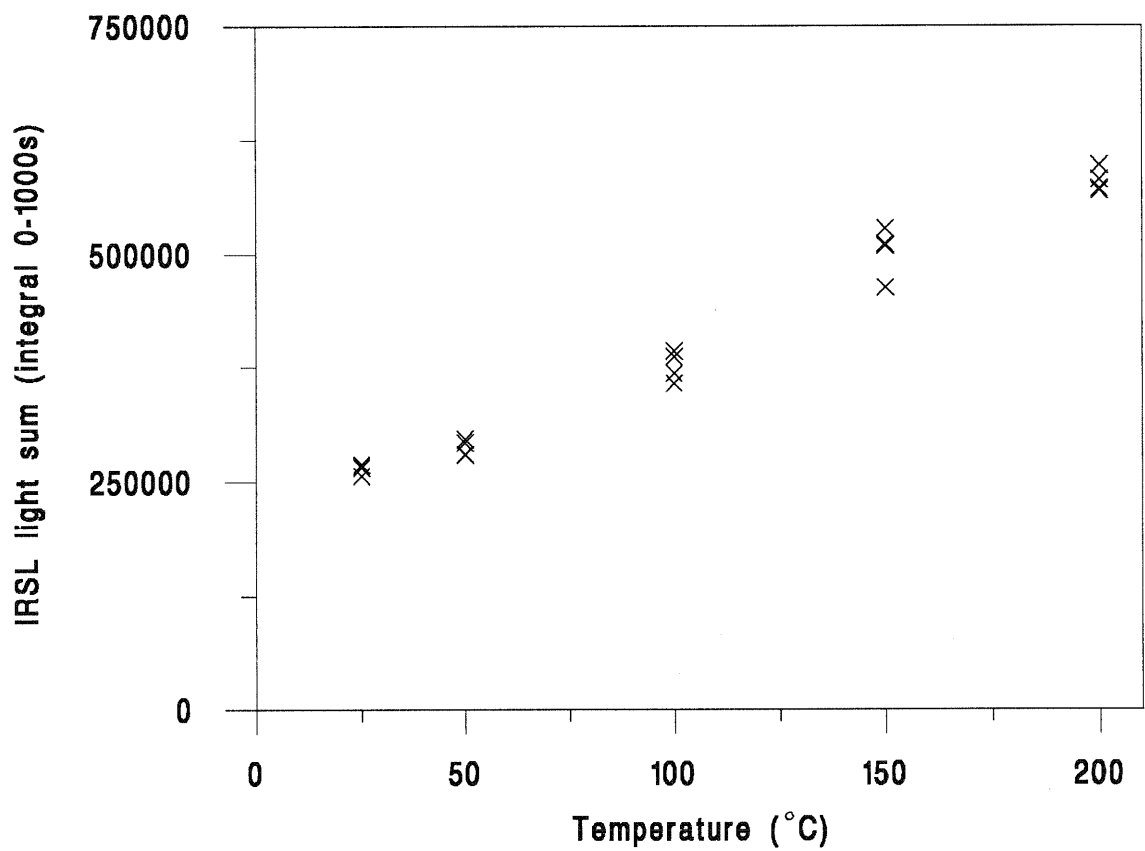


Figure 6.5.2(c): The IRSL light sum obtained over a 1000 second exposure to IR, with the isothermal TL signal subtracted, as a function of the temperature at which the sample was held during IR exposure.

### 6.5.3 Effect of IR exposure at different temperatures upon TL

The experiment described above analyzed the effect of IR exposure at different sample temperatures upon the IRSL residual. As was discussed previously (section 6.5), at room temperature only a small part of the TL signal is affected by exposure to IR. To understand the changes in sensitivity that are seen when using a single aliquot for regeneration it is also important to look at the effect of IR exposure at elevated temperatures upon the TL residual, and this is discussed below.

After exposure to IR at various temperatures (described in section 6.5.2) all 24 aliquots were heated to 450°C at a rate of 3°C/s and their TL glow curves recorded. They were then given a dose of 6 Gy and heated to 450°C with a preheat at 290°C for 10s. The peak integral from 300-400°C was used for normalization between glow curves.

Figure 6.5.3 shows the TL glow curves after IR exposure at the different temperatures, compared with the glow curves for samples which had received no bleaching. It is clear that for both TL peaks (270°C and 330°C) there is no significant difference in the signal remaining after bleaching at the various temperatures that cannot be explained purely by thermal eviction of charge (in particular for the bleach at 200°C). This shows that for the temperature range 25-200°C the proportion of the TL signal that can be affected by IR is independent of temperature.

Phototransfer occurs, as is shown by the increased TL signal between 100 and 200°C for glow curves B, C and D. However, when IR stimulation is carried out at temperatures above 150°C (curves E and F) no phototransferred signal is seen.

### 6.5.4. The relationship between IRSL, temperature and TL

The experiments described above show clearly that one cannot alter the amount of the TL signal removed by altering the temperature at which a sample is exposed to infrared radiation (figure 6.5.3). This implies that any single aliquot method using regeneration after bleaching with infrared is inevitably going to suffer from some form of sensitivity change that will cause an underestimation of the ED, unless the degree of bleaching when the sample was deposited was similar to that achieved by exposure to IR alone. It is possible that some form of numerical correction method may be devised, but this is not pursued here. The remaining alternatives to IR bleaching are discussed in sections 6.7 and 6.8.

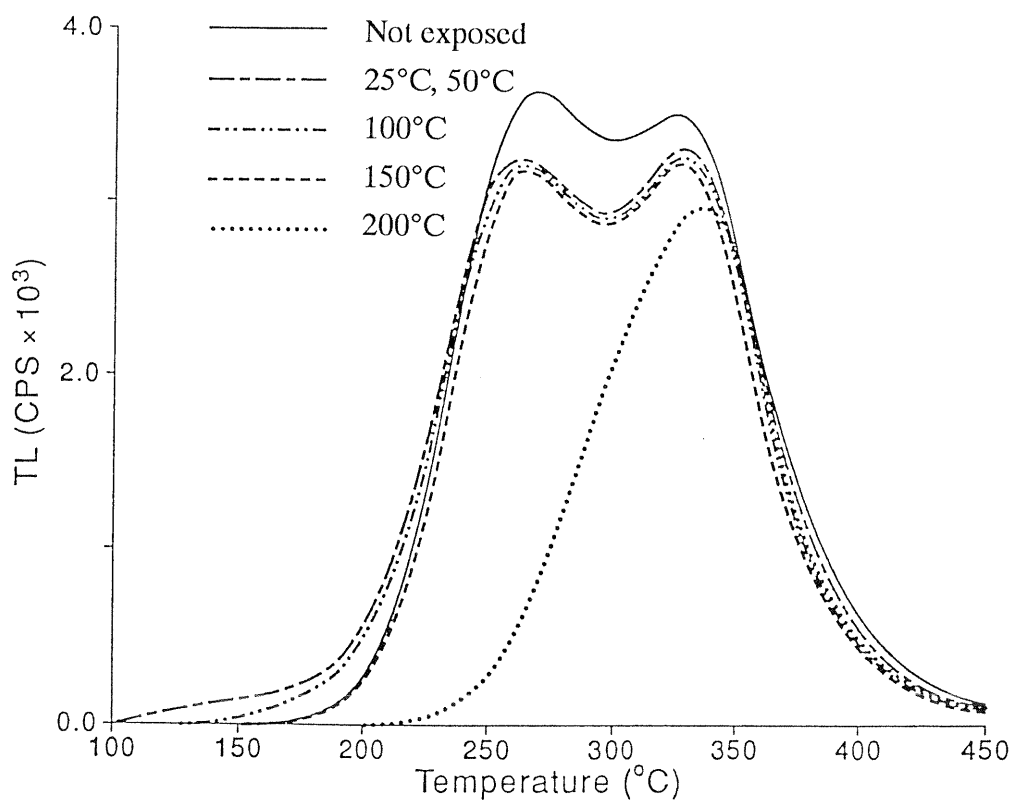


Figure 6.5.3: TL glow curves for aliquots that have been exposed to IR for 1000 seconds while being held at the temperatures shown.

The physical mechanism by which IRSL is generated from a potassium feldspar has not been completely defined. The results presented here indicate something of the nature of the relationship between IRSL, TL and temperature. Figure 6.5.1(a) shows that the IRSL signal can be increased by a factor of five by raising the sample temperature from 50°C to 200°C. Three mechanisms can be postulated for the increased IRSL signal at higher temperatures compared with the IRSL at room temperature - a larger trapped charge population being sampled, the same population being sampled but with a greater luminescence efficiency, or the same population being sampled but with an increased eviction efficiency per unit infrared power.

As discussed above, figure 6.5.3 suggests that by raising the sample temperature one cannot remove any greater proportion of the trapped charge population as measured by TL. Figure 6.5.1(d) suggested that at higher sample temperatures a larger population of IR sensitive traps is being measured which do not contribute to the TL signal. This suggestion is pursued further in section 6.6.

Wintle (1975) was able to determine the luminescence efficiency of quartz as a function of temperature by measuring its radioluminescence, but this experiment has not been performed on feldspar, and no facilities were available to undertake it in this study.

It is possible to examine the third mechanism by replotting the data for figure 6.5.2(a). Figure 6.5.4 shows the IRSL decay curves from the final experiment. They have had the isothermal TL component subtracted and have then been normalised to the same initial signal level. As the temperature of the sample increases the rate at which the IRSL signal decays also increases. This shows that at higher temperatures either the rate of eviction per unit IR power is higher, or a significantly larger population of IR sensitive traps are being probed.

From the data in table 6.5.2 (column B) it appears that at higher temperatures the rate of eviction per unit IR power is higher since as the temperature of the sample during bleaching increases, so the remaining signal, which is measured at room temperature, decreases. If the larger signal were due entirely to an increase in the efficiency of the luminescence centres at higher temperatures or a larger trapped charge population being probed, the remaining signal at room temperature would have remained constant. The decrease that we see implies that the higher temperature does increase the efficiency with which IR stimulation can evict trapped charge. However, this does not rule out the possibility that increasing the temperature at which samples are exposed to IR can also increase the number of traps that are probed as suggested by the data in figure 6.5.1(c). This is pursued in the next section.

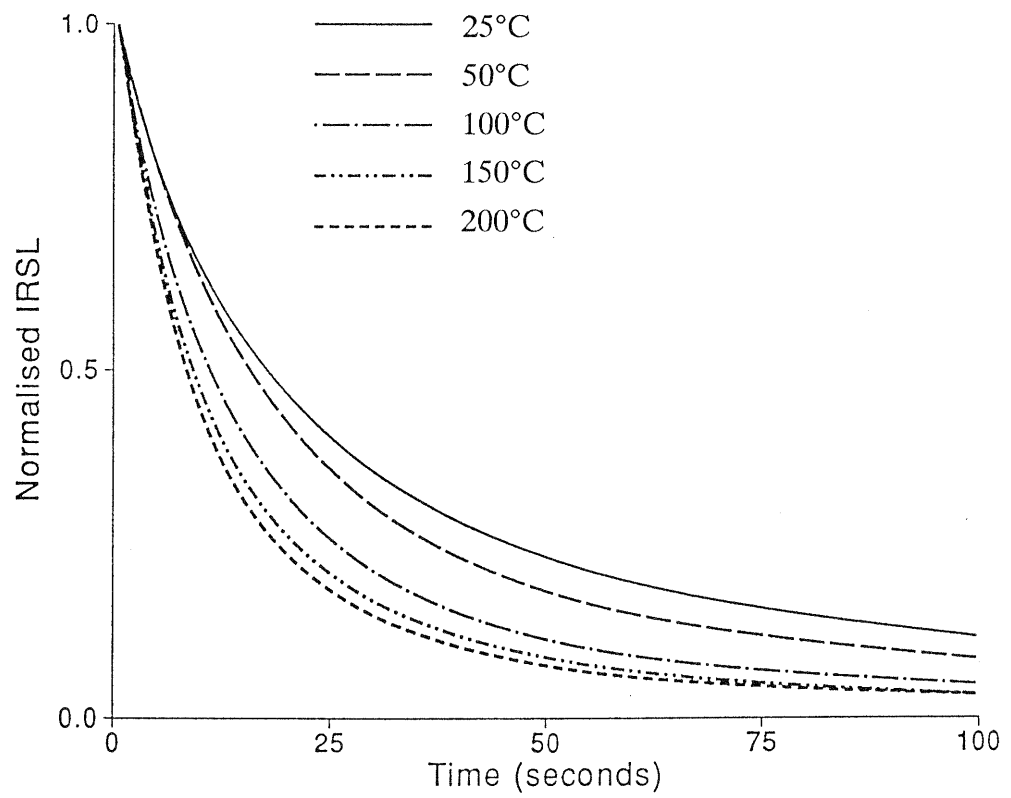


Figure 6.5.4: IRSL decay curves for aliquots held at the temperatures shown replotted by normalizing each curve to its initial IRSL signal level (data from figure 6.5.2(a)).

## 6.6 The relationship between TL, IRSL and GLSL signals from potassium feldspars

Figure 6.5.2(c) shows that by raising the temperature at which a sample is held while it is exposed to IR, a greater IRSL signal can be generated. However, figure 6.5.3 shows that the aliquots that have produced a larger IRSL signal do not appear to have a correspondingly smaller TL signal remaining, but figures 6.5.1(c) and (d) do suggest that at elevated temperatures a larger population of IR sensitive traps are being probed. The implication is that the TL and IRSL signals may not originate from the same traps. To investigate the behaviour of the two luminescence signals three experiments were performed using potassium feldspar from GDNZ 24, and a further experiment using GDNZ 1. In addition to analyzing the TL and IRSL signals, a third luminescence signal, GLSL (green light stimulated luminescence) was measured (see section 4.1.3) in the first three experiments to give additional information about the trapped charge population within the crystal.

### 6.6.1 The effect of preheating at different temperatures

The first experiment was similar to that described in section 4.7.3 and is primarily designed to give some information about the nature of the GLSL signal. Twenty-four aliquots of the feldspar were split into six groups of four aliquots each. All aliquots had their IRSL and GLSL signals measured for 0.1 and 0.5s respectively in order to provide 'natural normalisation' values. Two of the aliquots in each group were given doses of 36 Gy using the beta source within the Risø reader. The six groups were preheated for ten minutes at various temperatures (room temperature (no preheat), 100, 150, 200, 220 and 250°C) and left for 24 hours. The IRSL and GLSL signals were re-measured for 0.1 and 0.5s respectively, and the results normalised using natural normalisation values obtained prior to any treatment. The aliquots had their TL measured and these results were normalized by giving the aliquots a test dose of 9 Gy and measuring the TL integral from 300-400°C after preheating at 290°C for 10s.

This type of experiment may be used to determine the effect of different preheat treatments (cf. section 4.7.3 where a similar experiment was used, but varying the preheat time, not the temperature). Plots of  $(N+\beta)/N$  laser stimulated luminescence ratios versus preheat temperatures were shown by Li (1991a) to reach a constant value as the temperature was raised. This indicates that the trapped charge in the natural sample, which is assumed to be stable over the period to be dated, and that in the  $N+\beta$  sample is responding in the same way to the preheat, and thus only a stable component of the irradiated sample is left.

Figure 6.6.1 illustrates this for the TL, IRSL and GLSL data. For the TL data there is a large unstable component (associated with the 150°C peak) in the irradiated aliquots that have had no preheat, and this causes a large initial  $(N+\beta)/N$  ratio. However, the ratio drops with increasing preheat temperature, until at 200, 220 and 250°C a constant ratio of approximately 1.9 is seen. The GLSL also shows a drop in ratio with increasing preheat temperature, finding a constant value with preheats of 200°C or higher, though the change in ratio is not as great as for the TL. In contrast the IRSL ratio changes negligibly over the temperature range of the experiment.

### 6.6.2 The effect of IR exposure upon TL, IRSL and GLSL

For the second experiment a set of twenty-four aliquots of GDNZ 24 were prepared and natural normalised using IRSL and GLSL as in the previous section. The aliquots were divided into six groups and each group exposed to IR (from the diode array) for different periods of time (0, 10, 50, 100, 1000 and 6000s). The IRSL and GLSL signal remaining in each aliquot was then measured. Finally, each aliquot had its TL measured, and these results were then normalised by measuring the TL signal after administering a dose of 9 Gy. The experiment is similar to that described in section 6.5.1, but here all IRSL and GLSL measurements are made at room temperature so that the TL signal could also be accurately measured.

The remaining IRSL, GLSL and TL (at 270 and 330°C) signals are plotted in figure 6.6.2 as a function of exposure time to IR. The loss of IRSL simply follows the decay function when continuously measuring IRSL over a long period of time. The GLSL signal falls rapidly with exposure to IR, but consistently retains a higher proportion of its signal than the IRSL. The two TL peaks at 270 and 330°C fall to 90% of their initial value after 10s of exposure to IR, and do not change significantly over the next 5990s. Significant phototransfer occurs causing growth of the TL peak at 180°C after 50s. After 6000s exposure the IRSL signal has fallen to 0.3% ( $\pm 0.2$ ) of its initial level, while the GLSL retains 13% ( $\pm 0.6$ ) of its signal and the TL 90% ( $\pm 4$ ) at 270 and 89% ( $\pm 1$ ) at 330°C.

### 6.6.3 The effect of green light exposure upon TL, IRSL and GLSL

An identical experimental procedure was adopted as in section 6.6.2, but samples were exposed to green light (515-560nm from the Risø GLSL add-on unit) instead of IR. The remaining IRSL, GLSL and TL (at 270 and 330°C) signals are plotted in figure 6.6.3 as a function of exposure time.

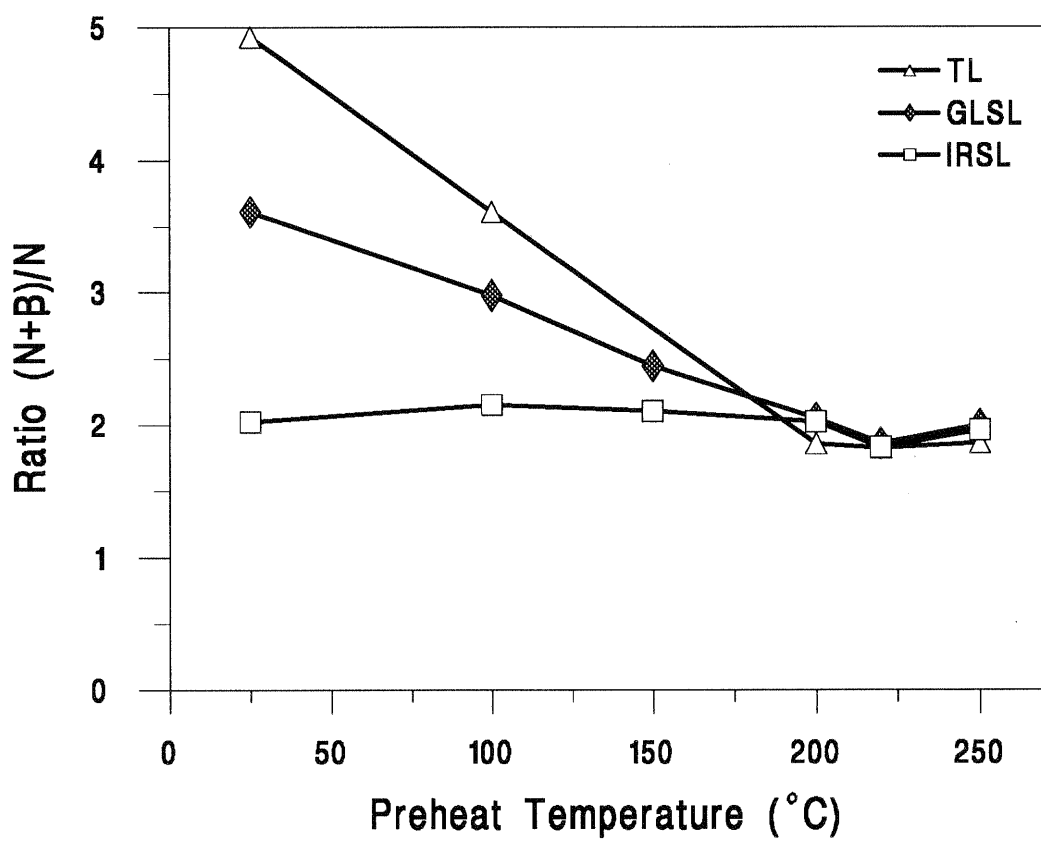


Figure 6.6.1: The ratio of the luminescence signals (TL, IRSL and GLSL) from irradiated and natural aliquots of GDNZ 24 after preheating for 10 minutes at various temperatures.

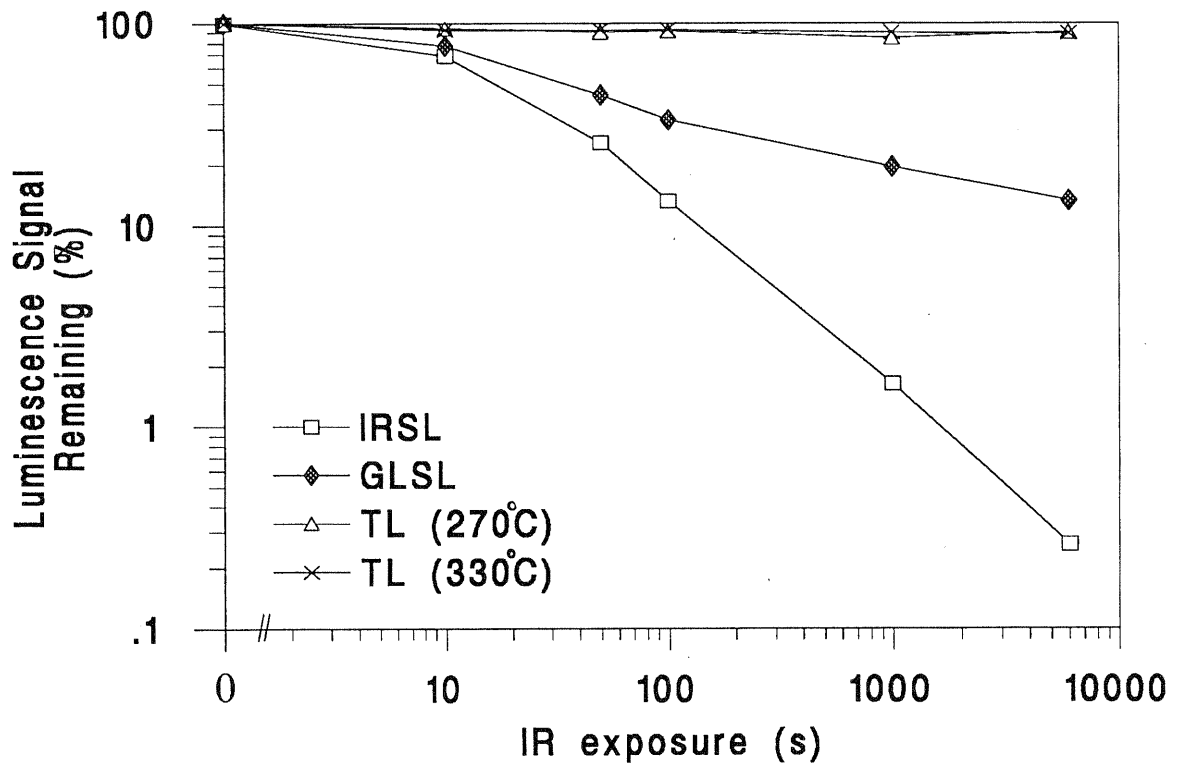


Figure 6.6.2: The loss of IRSL, GLSL and TL signals from aliquots that have been exposed to IR for varying periods of time. All the IRSL and GLSL measurements were made at 50°C (cf. figure 6.5.1(d)).

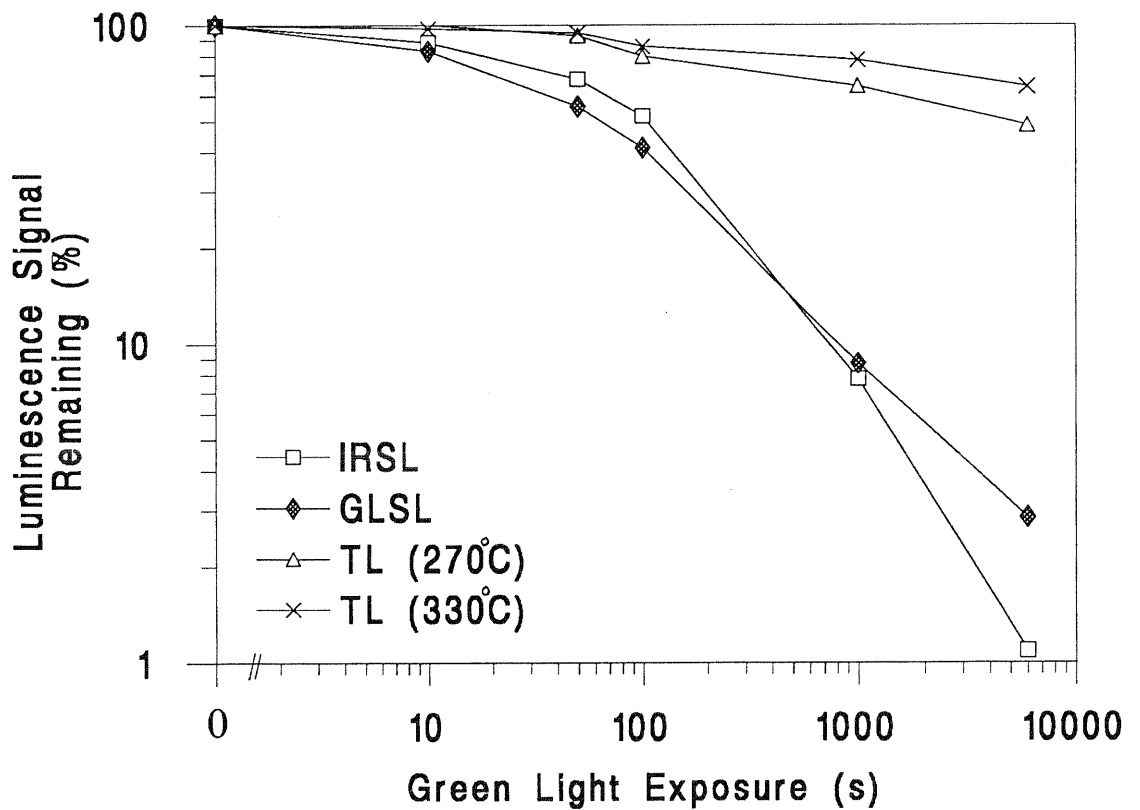


Figure 6.6.3: The loss of IRSL, GLSL and TL signals from aliquots that have been exposed to green light for varying periods of time. All the IRSL and GLSL measurements were made at 50°C.

The GLSL signal falls the most rapidly of the three initially, but with exposures over 1000s the IRSL signal is lower than the GLSL. The two TL peaks present in the natural signal are both bleached significantly by exposure to the green light, the 270°C peak falling to 49% ( $\pm 3$ ) after 6000s, and the 330°C peak to 64% ( $\pm 3$ ). Phototransfer to a peak at 180°C does occur, but the magnitude is far smaller than that seen during exposure to IR.

#### 6.6.4 Comparison of trapped charge distributions measured using IRSL and TL

The approach used here for the determination of the distribution of traps responsible for the TL and IRSL signals is based upon pulse-annealing. The procedure involves measuring the IRSL signal from a single sample aliquot following annealing to successively higher temperatures. A slightly modified procedure was used to enable TL measurements to be made that were compatible with the IRSL data. Samples were heated at 10°C/s to the appropriate annealing temperature and the TL signal measured for 0.1s while the sample was held at that temperature. The sample was then cooled for two minutes prior to measurement of the remaining IRSL signal. All IRSL measurements were made at 50°C for 0.1s using the 31 TEMT 484 IR diodes (880 $\Delta$ 80nm) in the Risø reader. Up to 40 IRSL measurements were made on each sample aliquot. The loss of IRSL during these measurements was corrected for by making repeat 0.1s IRSL measurements on two other aliquots, that were not subjected to any pulse annealing, to characterise the loss of signal. Luminescence measurements were made through a filter pack containing a Corning 5-58 and a Schott BG-39 filter.

In order to characterise the trap depth distribution of both stable and thermally unstable components of the IRSL signal, samples were treated in four ways prior to analysis. The first set had no treatment (Natural); the second were given a  $\beta$ -dose of 45 Gy 2 hours prior to analysis (N+45Gy); the third were preheated at 220°C for 10 minutes (N+ph); and the fourth were given the same beta dose (45Gy) and then preheated at 220°C for 10 minutes (N+45Gy+ph). Previously, pulse annealing measurements on potassium feldspars have been shown by plotting the percentage of the IRSL signal remaining after annealing at a given temperature (e.g. Bøtter-Jensen *et al.* 1991, using potassium feldspar separated from a Quaternary sediment; and Bailiff and Poolton 1991, using slices of hand specimens of feldspars). Figure 6.6.4(a) shows data for the four groups of aliquots plotted in this manner. While differences are clear between the data sets, it is impossible to draw many conclusions from this figure.

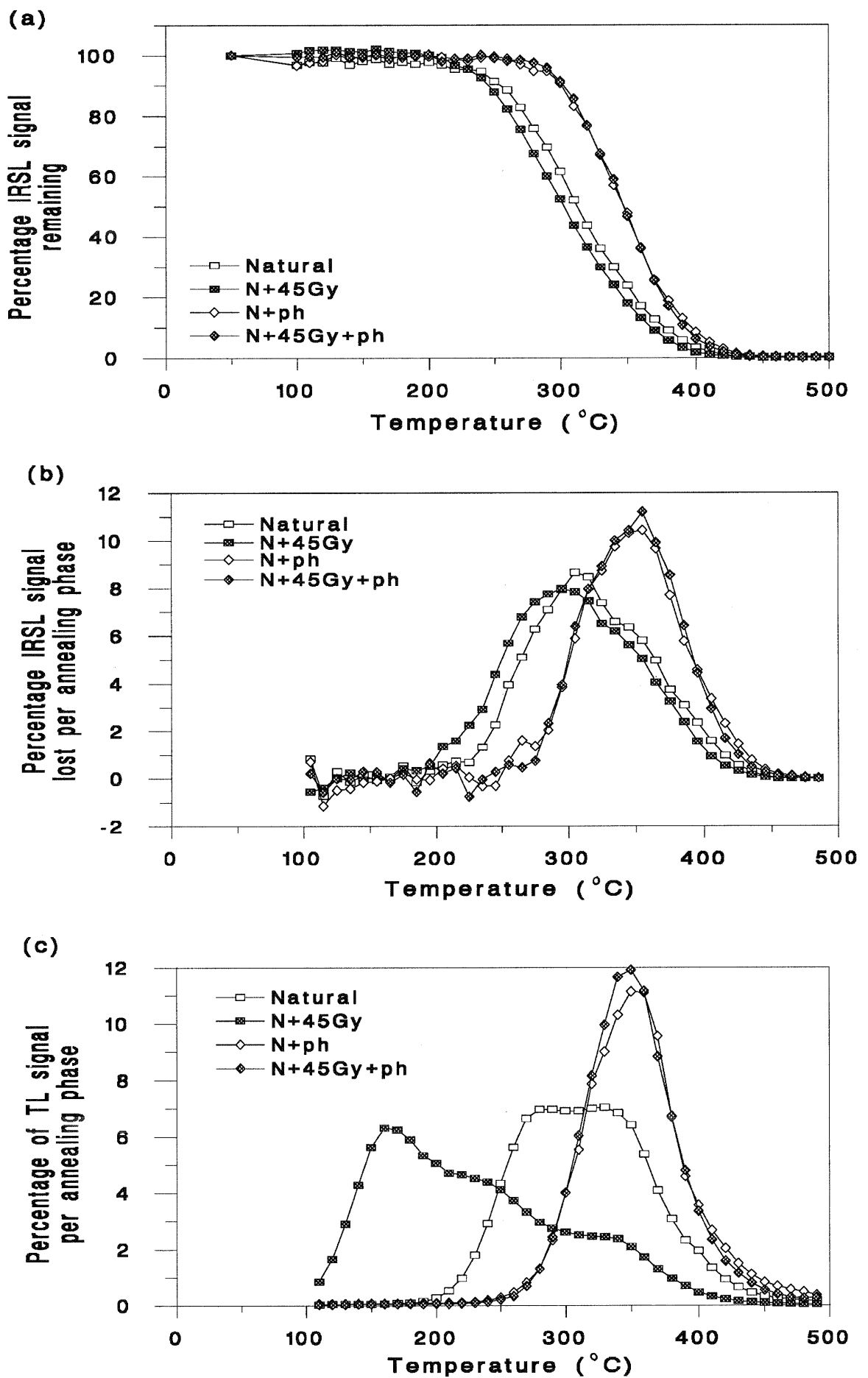


Figure 6.6.4: (a) The proportion of the IRSL signal, measured at  $50^{\circ}\text{C}$ , remaining after pulse annealing to progressively higher temperatures. (b) The percentage of the IRSL signal lost due to each pulse annealing displayed as a function of the temperature to which the sample was annealed. (c) The TL signal measured at a given temperature, plotted as a percentage of the sum of all the TL signals measured for that aliquot. Data in (b) and (c) have been smoothed using a 3-point running mean. All measurements made on the same aliquots of GDNZ 1.

An alternative way to display the data from figure 6.6.4(a) is shown in figure 6.6.4(b). Instead of calculating the percentage of the IRSL signal remaining after annealing at a given temperature, the percentage of the IRSL signal that is lost due to each annealing step is calculated and plotted against temperature. This type of plot shows how much of the IRSL signal is associated with traps emptied by annealing to a specific temperature. Figure 6.6.4(c) shows the TL data obtained from the same aliquots during the pulse annealing procedure. The TL signal, measured for 0.1s at the maximum temperature of each phase of annealing, has been plotted as a function of the annealing temperature. To make figure 6.6.4(c) comparable with figure 6.6.4(b) the TL signal at each temperature has been plotted as a percentage of the sum of all the TL measurements for that aliquot.

Figures 6.6.4(b) and (c) show the percentage of the luminescence signal (IRSL and TL) lost by each successive annealing of the samples. These plots show the distribution of trapped charge within the potassium feldspar that give IRSL and TL signals. The TL curves in figure 6.6.4(c) appear identical to TL glow curves, for similarly treated aliquots, that have been measured by continuous heating from room temperature to 500°C.

The aliquots that have had no treatment (Natural) have a broad TL peak from 280 to 330°C that may consist of two closely spaced peaks. The IRSL signal peaks at 300°C, with a small shoulder apparent at 340°C. It is not clear from this data whether the TL and IRSL traps are the same (but give different TL and IRSL ratios for the two peaks) or whether there are two different sets of traps, one set responsible for the TL signal and the other for the IRSL signal, but with similar trap depths. The data in figure 6.6.2 would suggest that the two are different (see discussion in section 6.6.5).

The aliquots that have been irradiated (N+45Gy) show a complex TL signal with a peak at 160°C and shoulders at 240 and 340°C. In contrast the IRSL signal appears very similar to that for the aliquots that were not treated, but with some additional IRSL component from 200 to 270°C in the irradiated sample. This marked contrast in the TL and IRSL trap depth distributions for irradiated samples has previously been observed indirectly (figures 4.7.3(b) and 4.7.4, Bøtter-Jensen *et al.*, 1991, Duller and Bøtter-Jensen, 1992). The small difference between the IRSL trap depth distributions for the natural and the irradiated aliquots (from 200 to 270°C) has been observed consistently for several similar samples. The difference in trap depth distributions between irradiated and unirradiated aliquots implies that some form of preheating is needed if IRSL is to be used for dating Quaternary sediments (as also suggested in section 4.7.4).

The remaining two groups of aliquots were both preheated at 220°C for 10 minutes as suggested by Li (1991a). The first group were just preheated (N+ph), while the second group had been irradiated (N+45Gy+ph). The trap depth distributions show a single peak at 350°C and are identical irrespective of whether the sample has been irradiated prior to preheating or not, and whether measured using IRSL or TL. This type of analysis enables, for the first time, the measurement of the temperature at which charge giving rise to an IRSL signal is evicted, and thus the trap depth distribution of that charge. Thus it is possible to ensure that a similar distribution of charge, from which an IRSL signal can be generated, remains in irradiated and unirradiated aliquots after a preheating treatment. This is particularly useful given the inability to differentiate between the effects of various preheats upon the IRSL signal using plots of the ratio of (N+β)/N (figure 4.7.3(b)), or by calculating EDs using the different preheats (figure 4.7.3(d)).

### 6.6.5 Implications for the relationship between the TL, IRSL and GLSL signals from potassium feldspar

Comparison of figures 6.6.4(b) and (c) show that the TL and IRSL trap depth distributions for the natural aliquots are similar, though not identical. Figure 6.6.2 shows that exposure of the sample to IR for 10s caused reduction of the TL signal at 270 and 330°C by 10%. Further exposure up to 6000s caused no further loss of TL. The IRSL signal after 10s of exposure to IR had fallen to 68% of its initial level, and after 6000s to 0.3%. Thus at least 68% of the electron traps that are responsible for the IRSL signal give no TL signal, under the measurement conditions used here.

Comparison of figures 6.6.2 and 6.6.3 shows that IR exposure for 6000s reduces the GLSL signal to 13% of its initial level while leaving 90% of the TL signals at 270 and 330°C intact. A similar reduction of the GLSL signal was achieved after approximately 500s exposure to green light, but with the loss of 30% of the 270°C TL peak and 20% of that at 330°C (figure 6.6.3). This strongly implies that the loss of the TL and GLSL signals represents the emptying of two populations of traps, not one.

The results of the experiments presented here suggest the following conclusions:-

a) The trapped charge responsible for generating the TL signal observed here are largely, if not wholly, distinct from those giving rise to the IRSL (and GLSL) signals. This explains why raising the temperature at which samples are held while exposed to IR does not affect the proportion of the TL signal that is removed (figure 6.5.3). The fact that a greater IRSL light sum is released as the sample temperature is increased (figure 6.5.2(c))

suggests that deeper electron traps are being stimulated and this is supported by the data in figure 6.5.1(d).

b) For unirradiated samples the TL and IRSL trap depth distributions are similar (figure 6.6.4(b)), though as noted above it seems that they represent different trap populations. When irradiated a large TL signal is generated at 150°C, but there is no corresponding IRSL signal (figures 6.6.4(b) and (c)).

c) The rate of IRSL trap filling (the sensitivity to dose) is dependent upon the electron population within the TL traps (figures 6.4.3(b) and 6.7(b) in the next section).

The implication of all these experiments is that a large proportion of the TL signal cannot be removed by exposure to IR. As a result the sensitivity of a sample being analyzed by the single aliquot method described in section 6.3 will progressively increase as measurements are made upon it because of the build up of trapped charge, due to successive irradiations of the aliquot, that cannot be removed by exposure to IR. This trapped charge does not contribute to the IRSL signal, but its presence causes the IR sensitive traps to fill more quickly upon irradiation because of competition effects, and hence the sensitivity of the aliquot, as measured by IRSL, increases.

## 6.7 Effect of using a solar simulator to produce a residual signal

Since the change in sensitivity of the sample to dose is thought to be related to the remnant trapped charge, using a SOL2 solar simulator, instead of IR, for bleaching, should reduce the magnitude of the problem since it will remove a larger proportion of this charge. Six samples of Dutch cover sands (Lutte 1, 2, 3, 8, 9 and 12, Dijkmans and Wintle (1991)) were analyzed, exposing them to the SOL2 solar simulator for 10 hours between each measurement.

Twelve samples from the aeolian sands of the Lutterzand area were dated by Dijkmans and Wintle (1991). The geological age estimates ranged from less than 1,000 yrs bp to more than 20,000 yrs bp. A novel TL technique, based upon method (a) of Wintle and Huntley (1980), was employed for determination of the ED since it was uncertain how much bleaching the samples had received at deposition. Six of these samples have been dated using the IRSL single aliquot regeneration method.

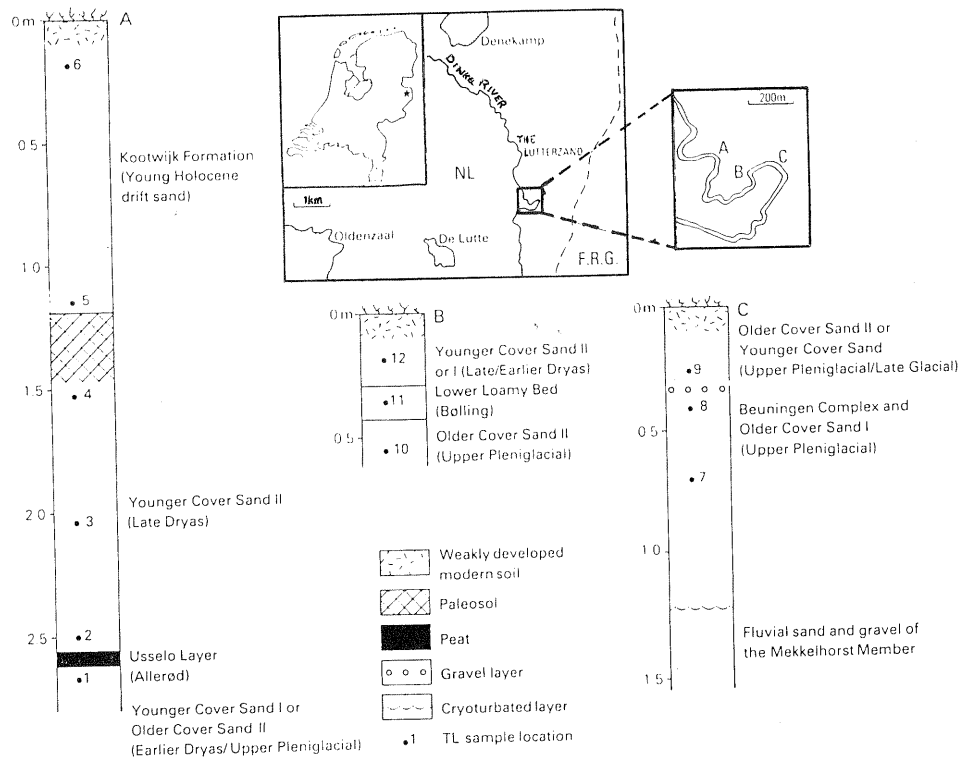


Figure 6.7(a): Location of the sections along the Dinkel valley in the Lutterzand area of The Netherlands from which samples Lutte 1, 2, 3, 8, 9 and 12 were taken, and their stratigraphic positions (from Dijkmans and Wintle, 1991).

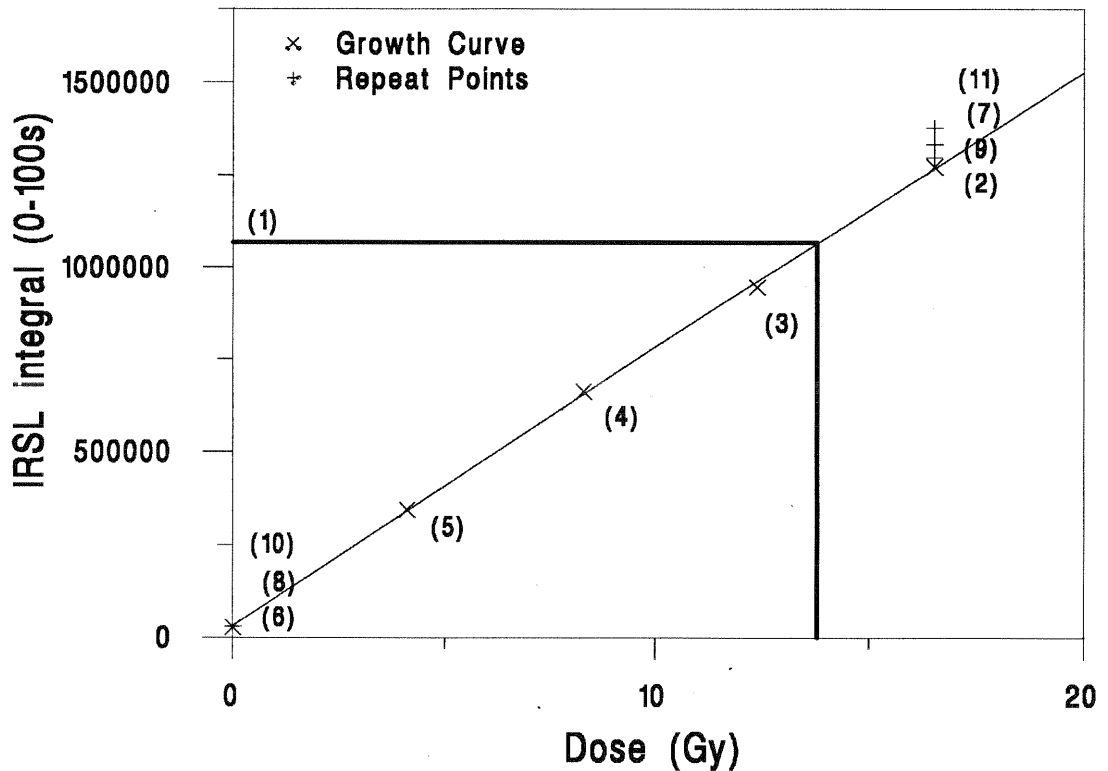


Figure 6.7(b): Single aliquot IRSL regeneration growth curve for sample Lutte 2. The order in which measurements were taken is indicated by the numbers in brackets. Repeat measurements were made of the signals from the lowest and highest dose points.

Lutte 1 and 2 were taken immediately below and above the Usselo layer (figure 6.7(a)) which has been dated by Van der Hammen and Wijmstra (1971) :GrN-4899 - 11,630±65 B.P. and GrN-4900 - 11,630±90 B.P. Lutte 2 and 3 are from the Younger Cover Sand II, and Lutte 12 was also taken from this unit, but at a different section. Finally, Lutte 8 and 9 are from immediately below and above the Beuningen gravel. The age control on this gravel is based upon a section at Staphorst (Northern Netherlands) where a gully is filled with material that is interpreted to be the Beuningen gravel. Organic material below this produced a date of 19,100±180 B.P. (Kolstrup, 1980, GrN-8594). However, based upon the work of Koster (1988), Dijkmans and Wintle (1991) suggest that the Older Coversand I unit below the gravel layer may have formed between 22.5-29 ka.

The growth curves for all samples were generated by giving the largest dose first (figure 6.7(b)). Measurements of the signal induced by the largest and smallest doses were repeated after the growth curve had been generated. For sample Lutte 8 the largest dose showed an increase in signal of 4.8% ( $\pm 2.3\%$  at  $1\sigma$ ,  $n=6$ ) and the residual an increase of 15.7% ( $\pm 2.9\%$  at  $1\sigma$ ,  $n=6$ ). EDs were determined for another six aliquots of Lutte 8 bleaching with IR between each phase for 750s instead of using the SOL2. Repeating the top dose showed an increase in signal of 16.2% ( $\pm 2.4\%$  at  $1\sigma$ ,  $n=6$ ) and the ED determined was  $24.6 \pm 1.2$  Gy ( $n=6$ ). Thus using the SOL2 had reduced, but not eliminated, the change in sensitivity.

The results for the six samples are compared with those given by Dijkmans and Wintle (1991) in table 6.7(a). Sample Lutte 2 is in close agreement, but the five other samples give significantly higher EDs, and ages, using the single aliquot regeneration method. All samples now give ages closer to the geological age estimates, though four of the six are still significantly underestimated.

Lutte 1 and 2 give bracketing ages for the Usselo Layer approximately 1.8ka younger than the uncorrected  $^{14}\text{C}$  age. Lutte 3 gives an age almost identical to that for Lutte 2.

The single aliquot age for Lutte 12 lies within the expected age range and by comparison with samples 1 and 2 would suggest that the unit correlates with the Younger Cover Sand I rather than II. Lutte 9 also lies within the expected age range but Lutte 8 is still far younger than expected. It is not clear whether this is due to an error in the luminescence dating, or the geological interpretation of the Beuningen Complex.

Table 6.7(a)

Comparison of equivalent doses and ages determined using a single aliquot regeneration method (bleaching for 10 hours using the SOL2 between measurements) and those published by Dijkmans and Wintle (1991), for six samples from the Lutterzand area of the Netherlands.

<u>Sample</u>	<u>Single Aliquot Regeneration ED (Gy)<sup>(a)</sup></u>		<u>Multiple Aliquot TL ED (Gy)</u>
Lutte 1	18.1±0.7	(4)	14.6 ± 0.4
Lutte 2	13.7±0.5	(8)	13.3 ± 0.3
Lutte 3	14.1±0.6	(4)	12.4 ± 0.3
Lutte 8	28.5±0.8	(6)	19.7 ± 0.2
Lutte 9	17.3±0.9	(4)	13.3 ± 0.4
Lutte 12	19.7±1.0	(8)	11.9 ± 0.6

<u>Sample</u>	<u>Single Aliquot Age (ka)<sup>(b)</sup></u>	<u>Multiple Aliquot TL Age (ka)<sup>(b)</sup></u>	<u>Geological Age Estimate (ka)</u>
Lutte 1	9.8 ± 0.4	7.9 ± 0.2	1.8-14
Lutte 2	9.1 ± 0.3	8.8 ± 0.2	10-11
Lutte 3	9.2 ± 0.4	8.1 ± 0.2	10-11
Lutte 8	14.9 ± 0.4	10.3 ± 0.1	±22.5-29
Lutte 9	11.9 ± 0.6	9.2 ± 0.3	10-14
Lutte 12	10.2 ± 0.5	6.1 ± 0.3	10-12

Note

- (a) The number of single aliquots run is in brackets. The ED quoted is the mean, and the error is the standard deviation of the means.
- (b) The error on the calculated age is derived solely from the uncertainty in the ED, and does not include any uncertainty in the dose rate.

The cause of the large difference in EDs for all samples, except Lutte 3, between the multiple and single aliquot methods is not clear. The original potassium feldspar separates produced by Dr.J.W.A. Dijkmans were used in these analyses, but here a 5-58 and BG-39 filter combination was used, rather than the UG-11 and HA-3 used by Dijkmans and Wintle (1991). No direct inter-calibration exists between the  $\beta$ -sources in Cambridge (used by Dijkmans and Wintle (1991)) and Aberystwyth, but both have been well calibrated against other sources. As discussed in section 4.3.2. the use of a UV filter may cause underestimation of the ED.

Given the uncertainty in the multiple aliquot ED derived from TL measurements it is impossible to gauge how accurate the single aliquot regeneration method is, but the change

in sensitivity that is apparent in figure 6.7(b) shows that the method will underestimate the ED to some extent.

The change in sensitivity is likely to be caused by a progressive build up of the trapped charge within the sample which affects the rate of subsequent trap filling when a sample is irradiated. Use of the SOL2 solar simulator reduces the severity of the problem because it removes a greater proportion of the signal, but apparently the problem still persists to some degree. This may reflect the fact that it is unlikely that the SOL2 would exactly mimic the trapped charge distribution at deposition.

The effect of a sensitivity change when bleaching with either IR or a solar simulator can be reduced if the ED of the sample is approximately known. Giving the dose that is nearest the ED first means that this will have the smallest error. However, the shape of the growth curve will be incorrect. Since the regeneration method relies upon interpolation, rather than extrapolation, the form of the growth curve away from the intercept with the natural is unimportant. However, the size of the systematic error, though small, is still unknown.

The procedure adopted to analyze the Lutte samples requires the operator to transfer the samples from the Risø reader to the SOL2 between each measurement. This is time consuming and thus somewhat negates the advantages of the method over standard equivalent dose techniques.

In conclusion, although the use of the regeneration method using a single aliquot seemed to be the simplest approach, the effect of progressive, and apparently irreversible, changes in sensitivity limits the technique. It would seem to be most applicable to very old samples, close to saturation, where these changes occur least, and for which the method is most useful anyway.

## 6.8 Use of regeneration for source inter-calibration.

### 6.8.1 Determination of the most appropriate method

To exemplify the problems of accuracy associated with using IR to bleach a sample between each regeneration step six aliquots of GDNZ 17 were used to calibrate the  $\beta$ -source within the Risø reader against itself. In this way the correct answer was known and so any inaccuracies could be seen easily.

The six aliquots were first heated to 450°C at 5°C/s. They were then given a  $\beta$ -dose for 600s (dose rate 1.24Gy/minute). After preheating at 220°C for 600s the samples had their IRSL measured for 100s at 50°C (filters used were a Schott BG-39 and Corning 5-60). They were then exposed to IR for 15 minutes (power approximately 40mW cm<sup>-2</sup>), while being held at 50°C, to reduce the IRSL signal to a residual level (<1% of the 'natural' signal due to 600s of  $\beta$ -dose) before being irradiated by the same Risø  $\beta$ -source, preheated (220°C for 10 minutes) and their IRSL remeasured. Further bleaching and adding of dose was repeated to build up a response curve. Doses of 0, 200, 400, 600, 800, 1000, 0, 600 and 1000s were used in this order. Figure 6.8.1(a) shows that the growth curve is supra-linear, and that the ED generated is significantly lower than the expected 600s (table 6.8.1(a)). The precision of the result is excellent (1%), but there is an overestimation of the source strength by 13%.

Table 6.8.1(a). Intercalibration of the first Risø  $\beta$ -source against itself using IR to reduce the IRSL signal to a residual level.

Aliquot No.	ED (secs) <sub>(a)</sub>	Source ratio
1	535	1.12
5	533	1.13
9	527	1.14
13	535	1.12
17	539	1.11
21	529	1.13
Average =		<b>1.13 ± 0.01</b>

Table 6.8.1(b). Intercalibration of the first Risø  $\beta$ -source against itself heating samples to 450°C to reduce the IRSL signal to a residual level.

Aliquot No.	ED (secs) <sub>(a)</sub>	Source ratio
4	604	0.99
8	565	1.06
12	596	1.01
16	587	1.02
20	583	1.03
24	592	1.01
Average =		<b>1.02 ± 0.02</b>

Note

(a) 'ED' is the irradiation time interpolated from the growth curve to be necessary to match the signal produced by the initial 600s irradiation with the Risø source.

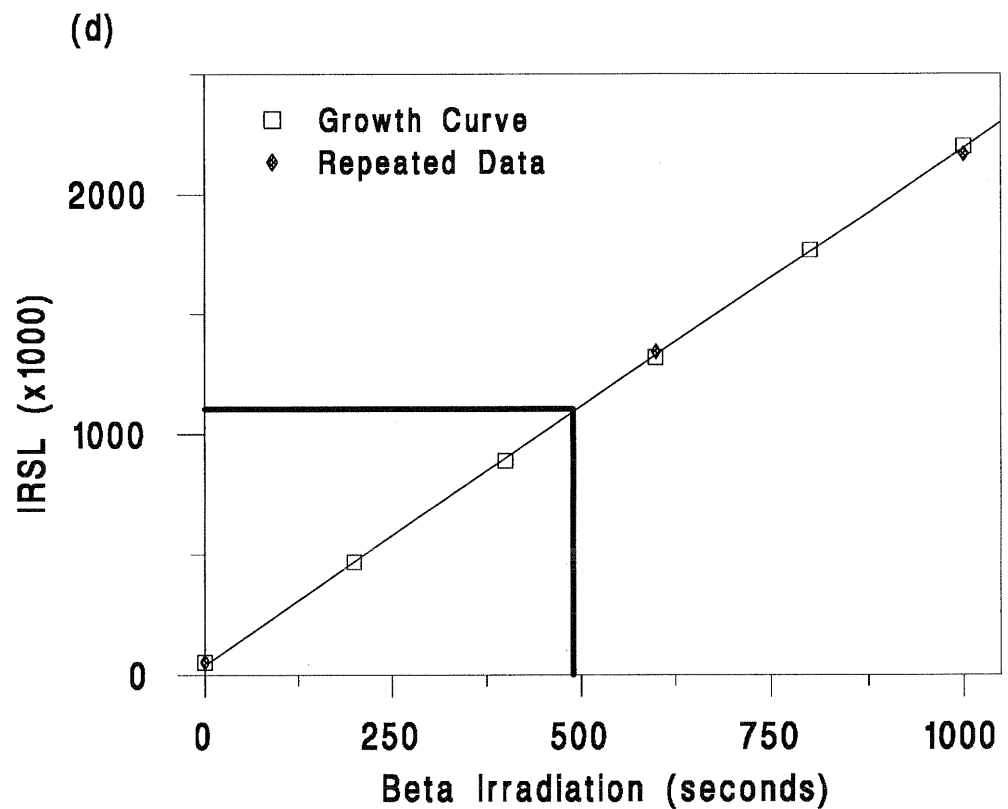
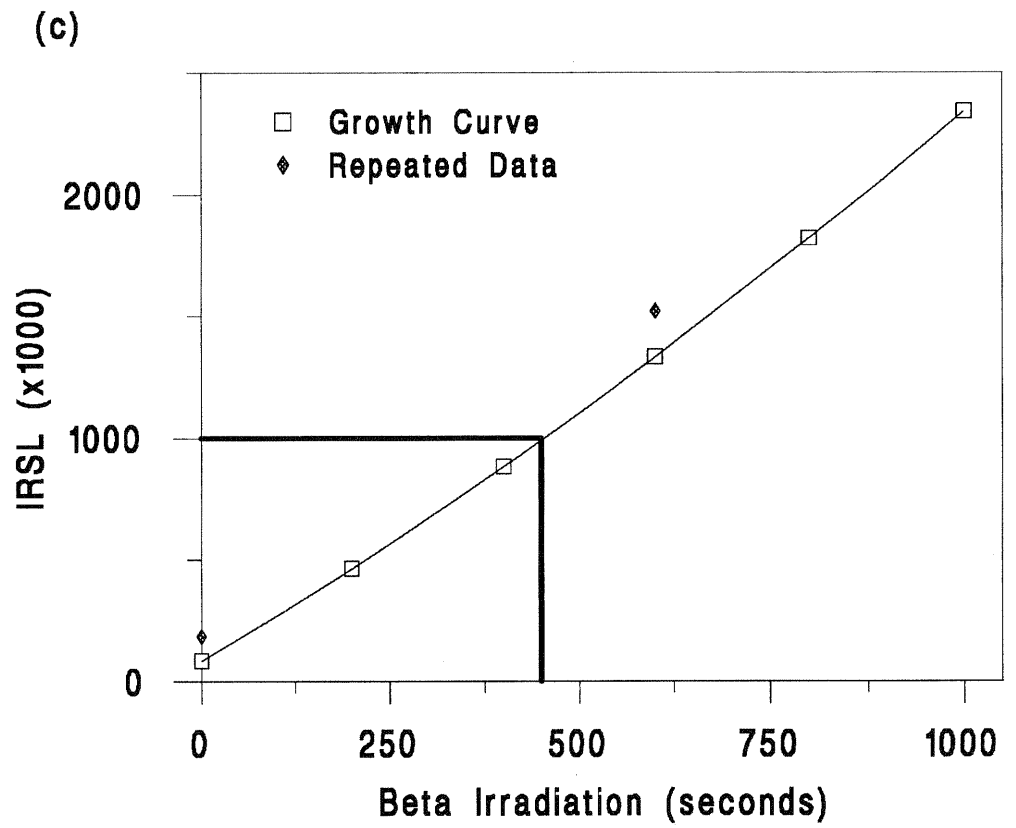


Figure 6.8.1: Intercalibration between the Risø I and Risø II  $\beta$ -sources (c) exposing the samples to 15 minutes IR and (d) heating the samples to 450°C at 5°C/s, between each phase of regeneration. The IRSL signal has been integrated over 100s of measurement. The data points at  $I_0$  and  $I_0+600s$  (also  $I_0+1000s$  for figure 6.8.1(d)) were repeated after all the other measurements were made.

An alternative approach is to heat the aliquots between each regeneration step in order to produce a residual level. Heating the sample to 450°C removes any residual TL or IRSL signal up to that temperature. Such an approach is clearly inappropriate when dating sediments, but may be used when inter-calibrating two radioactive sources. The  $\beta$ -source in the first Risø reader was calibrated against itself again, using this alternative method. Figure 6.8.1(b) shows a typical growth curve. The response to dose is now linear, and repeat measurements ( $I_0$ ,  $I_0+600s$  and  $I_0+1000s$   $\beta$ -irradiation) are almost identical. The 'ED' generated is  $588 \pm 13s$  (table 6.8.1(b)) within 1 sigma of the given time of initial irradiation.

An intercalibration between the  $\beta$ -source in the Risø reader used for all experiments in this thesis (Risø I) and a second Risø reader in Aberystwyth (Risø II) was performed both using IR and heating between each step to define the residual level. Figures 6.8.1(c) and 6.8.1(d) show the two growth curves generated.

The curve in figure 6.8.1(c) was generated using the same method as that used for figure 6.8.1(a). A  $\beta$ -dose of 600s was given on the first Risø reader, and irradiations of 0, 200, 400, 600, 800, 1000, 0, and 600s were given with the second Risø reader  $\beta$ -source. The form of the growth curve is supra-linear, and when the  $I_0$  and  $I_0+600s$  measurements were repeated (after all other measurements had been made) they showed a significant increase in IRSL signal. The precision of the results generated using this method is excellent (table 6.8.1(c)), but the accuracy poor.

The problem observed above is related to the remnant trapped charge. Heating the sample to 450°C removes any residual TL or IRSL signal and so no change in sensitivity is seen. Figure 6.8.1(d) shows a growth curve generated using identical analytical conditions to those for figure 6.8.1(c), except that the sample was heated to 450°C at 5°C/s between each regeneration phase instead of being exposed to IR. The growth curve is now linear, and when measurements are repeated (at 0, 600 and 1000s) they lie exactly on the growth curve. All samples gave a flat plot of 'ED' against IRSL exposure time for the 100s period analyzed. The signal from the irradiation on the first Risø  $\beta$ -source could be compared to the growth curve generated by the second  $\beta$ -source using the regeneration analysis program written by R.Grün. The precision here is also excellent (table 6.8.1(d)), but the result is significantly different from that in table 6.8.1(c). This second method is considered to give a reliable ratio between the two sources.

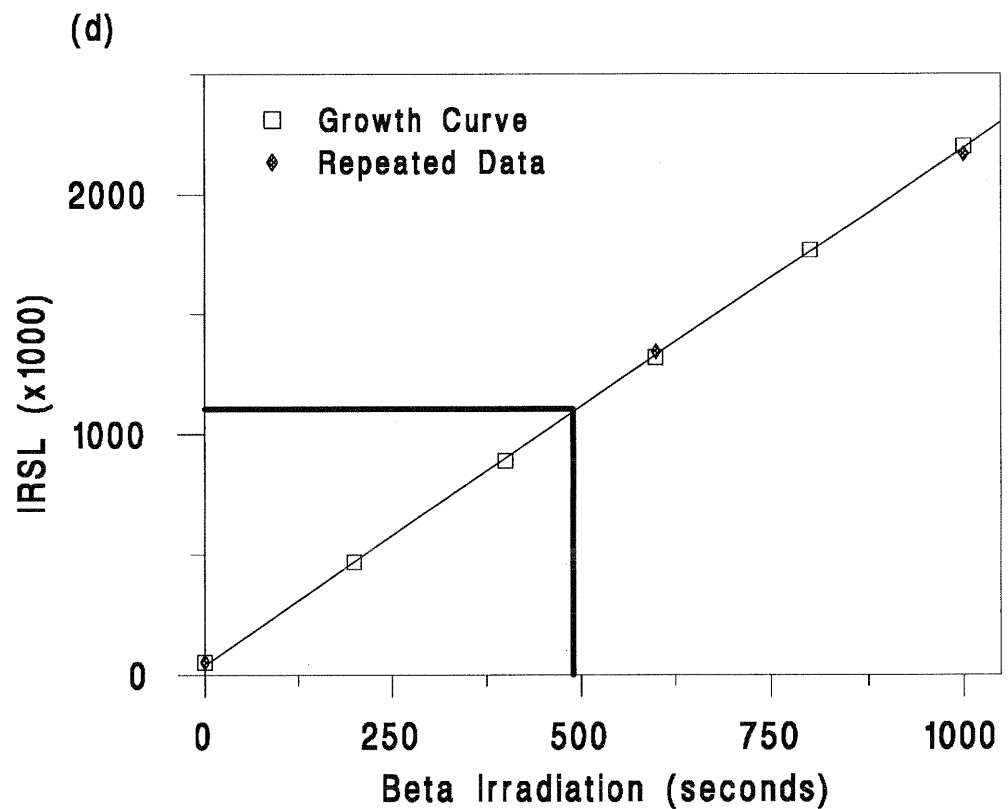
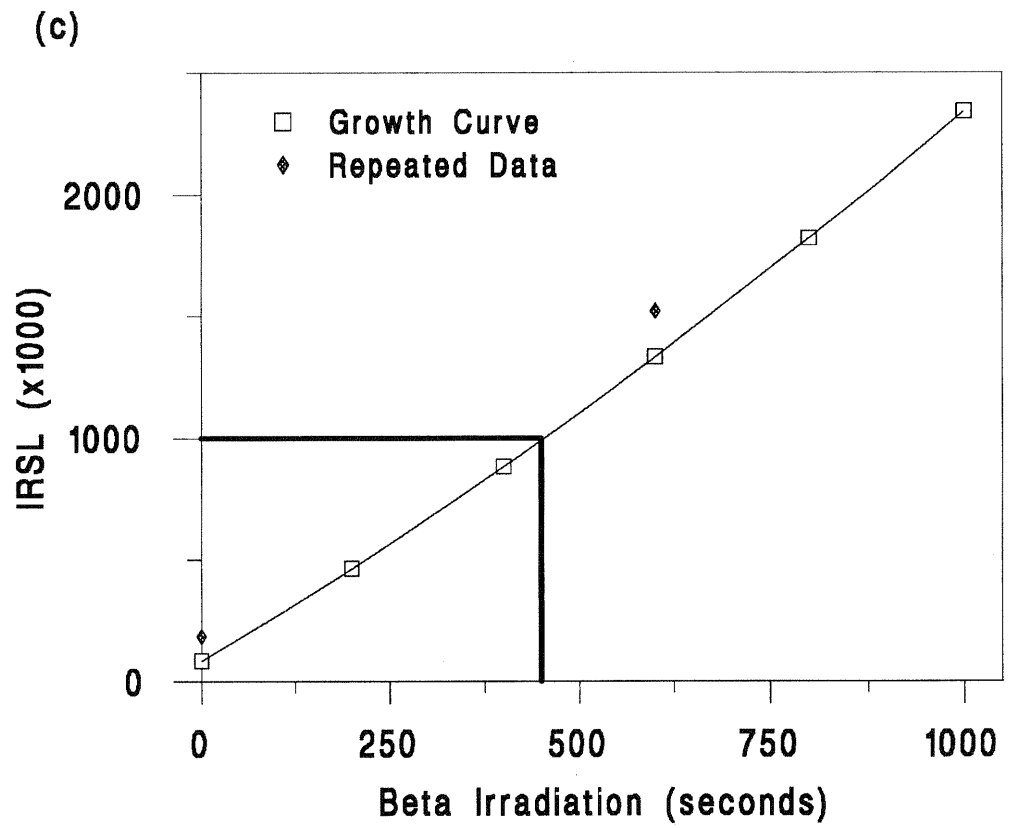


Figure 6.8.1: Intercalibration between the Risø I and Risø II  $\beta$ -sources (c) exposing the samples to 15 minutes IR and (d) heating the samples to 450°C at 5°C/s, between each phase of regeneration. The IRSL signal has been integrated over 100s of measurement. The data points at  $I_0$  and  $I_0+600s$  (also  $I_0+1000s$  for figure 6.8.1(d)) were repeated after all the other measurements were made.

Table 6.8.1(c). Intercalibration between the two Risø  $\beta$ -sources using IR to reduce the IRSL signal to a residual level.

<u>Aliquot No.</u>	<u>ED (secs)(a)</u>	<u>Source ratio(b)</u>
14	440	1.36
16	442	1.36
18	428	1.40
20	429	1.40
22	430	1.40
24	429	1.40
Average =		<b>1.39 <math>\pm</math> 0.02</b>

Table 6.8.1(d). Intercalibration between the two Risø  $\beta$ -sources heating samples to 450°C to reduce the IRSL signal to a residual level.

<u>Aliquot No.</u>	<u>ED (secs)(a)</u>	<u>Source ratio(b)</u>
1	505	1.19
5	515	1.17
9	494	1.22
13	493	1.22
17	483	1.24
21	488	1.23
Average =		<b>1.21 <math>\pm</math> 0.03</b>

Notes

- (a) 'ED' is the irradiation time using the second Risø source necessary to match the signal produced by 600s irradiation with the first Risø source.
- (b) The source ratio is the ratio of Risø II/Risø I source strengths.

6.8.2 Advantages of this method of intercalibration

Any sensitivity changes, that may result from heating the sample, occur before the 'test' dose is given to the sample. Subsequent heating of the sample causes no further changes in sensitivity and removes the residual trapped charge population within the crystal.

This method has two major advantages over normal methods of intercalibration, first it is very quick and simple to perform, and hence one may reasonably perform many determinations to get a precise value. Secondly, the calibration is determined for the actual material being dated, not for calcium fluoride or some other phosphor. Hence there is no need for further adjustment of the data.

The intercalibration between the Daybreak and Risø reader sources (appendix II) was made using this method on feldspar separated from sample GDNZ 6. Twelve aliquots were selected and heated to 450°C at 5°C/s in a pure argon atmosphere. They were then irradiated for 3 minutes with the Daybreak  $\beta$ -irradiator. A growth curve was generated for the Risø  $\beta$ -source, and the signals after irradiation with the two sources compared.

## 6.9 Conclusions

The method described above may be suitable for the dating of archaeological material that was reset by firing, but cannot be applied to Quaternary sediments unless it can be proved that no change in luminescence sensitivity occurs when the sample is heated to 450°C. The regeneration method is particularly sensitive to changes in luminescence sensitivity following bleaching. These are apparent in the methods outlined in this chapter when using either IR (section 6.3) or a solar simulator (section 6.7) to reduce the luminescence signal to a residual level.

The additive dose method does not involve repeated bleaching of the signal. A single aliquot method based upon this approach is described in chapter 7.

## **CHAPTER 7: Additive dose using a single aliquot**

### 7.1 Advantages of using the additive dose method

The IRSL signal from potassium feldspar bleaches so rapidly for material on the surface of a sand dune that there is effectively no residual signal at deposition. Hence the residual signal for a buried sample may be taken to be zero and an additive dose procedure adopted. The additive dose method involves no exposure to light (except for the very short IR exposure during readout) and hence there is no opportunity for changes in sensitivity such as those that affect the regeneration method. Finally, because there is no bleaching between irradiations, the measurement time is greatly reduced.

### 7.2 The effect of preheating

The sample is preheated at 220°C for 10 minutes prior to each measurement to ensure that only a stable signal is measured (see section 4.7.3). After measurement of the natural signal a beta dose is given and the sample preheated again. This is repeated for as many doses as required to generate a growth curve for a single aliquot.

The drawback with this procedure is that every preheat removes a part of the stable signal as well as all the unstable component (see figure 4.7.3(a)). After adding the first beta dose the preheat will remove all the unstable component induced by that dose, and a part of the stable natural signal. It is necessary to correct for the loss of part of the stable signal.

The loss of signal due to preheating can be assessed for each sample by taking a single aliquot and repeatedly preheating it and measuring its IRSL without irradiating between measurements. Figure 7.2(a) shows the loss of signal for sample GDNZ 15 during ten cycles of preheating and IRSL measurement. The scatter is thought to be due to the effect of small variations in the mineralogy of the grains making up each sub-sample.

Measurement of the IRSL signal can be made using very brief exposures to IR stimulation (e.g. 0.1 second). This causes negligible loss of signal. However the uncertainty in such a measurement may be relatively large, especially for samples with a low signal. A half second IR stimulation improves the reproducibility of the measurements and a correction for the loss of the IRSL signal during measurement is incorporated in the correction for preheat loss.

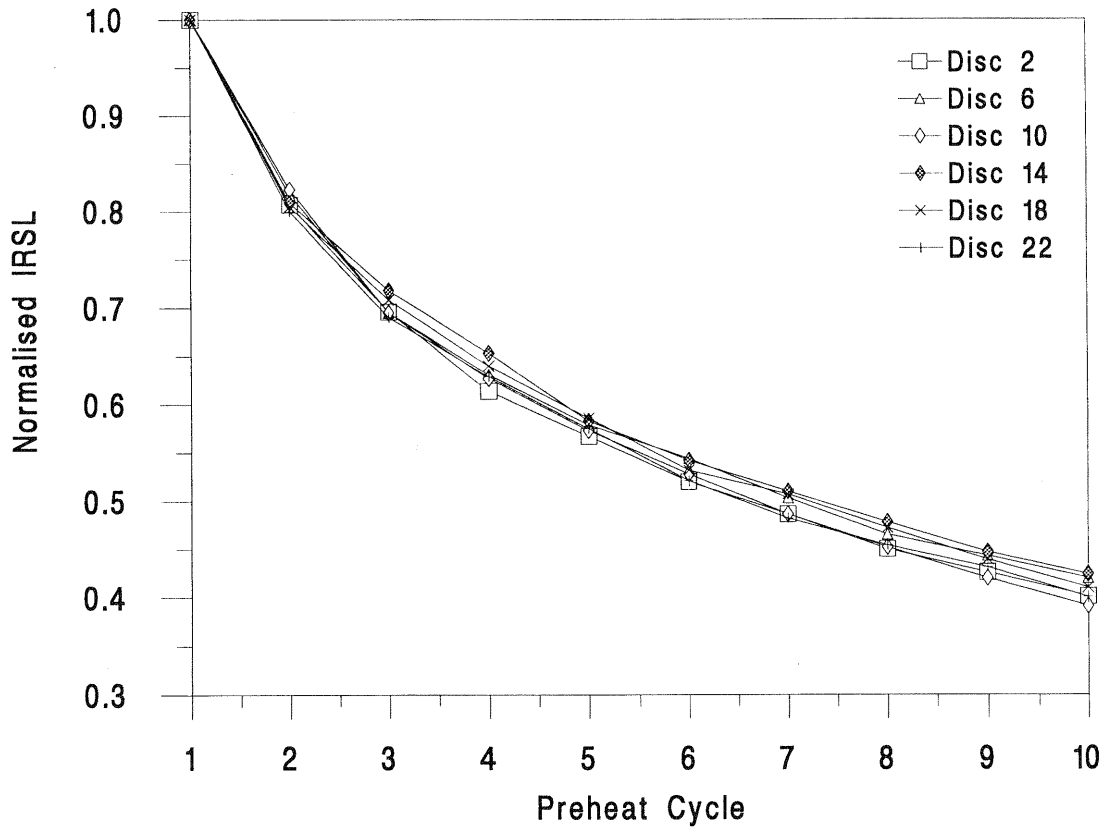


Figure 7.2(a): The proportion of the IRSL signal remaining after repeated preheating of sample GDNZ 15. The sample was preheated at 220°C for 10 minutes and the IRSL measured for 0.5 seconds at 50°C. The data for each of the six discs have been normalized to the IRSL signal remaining after the first preheat.

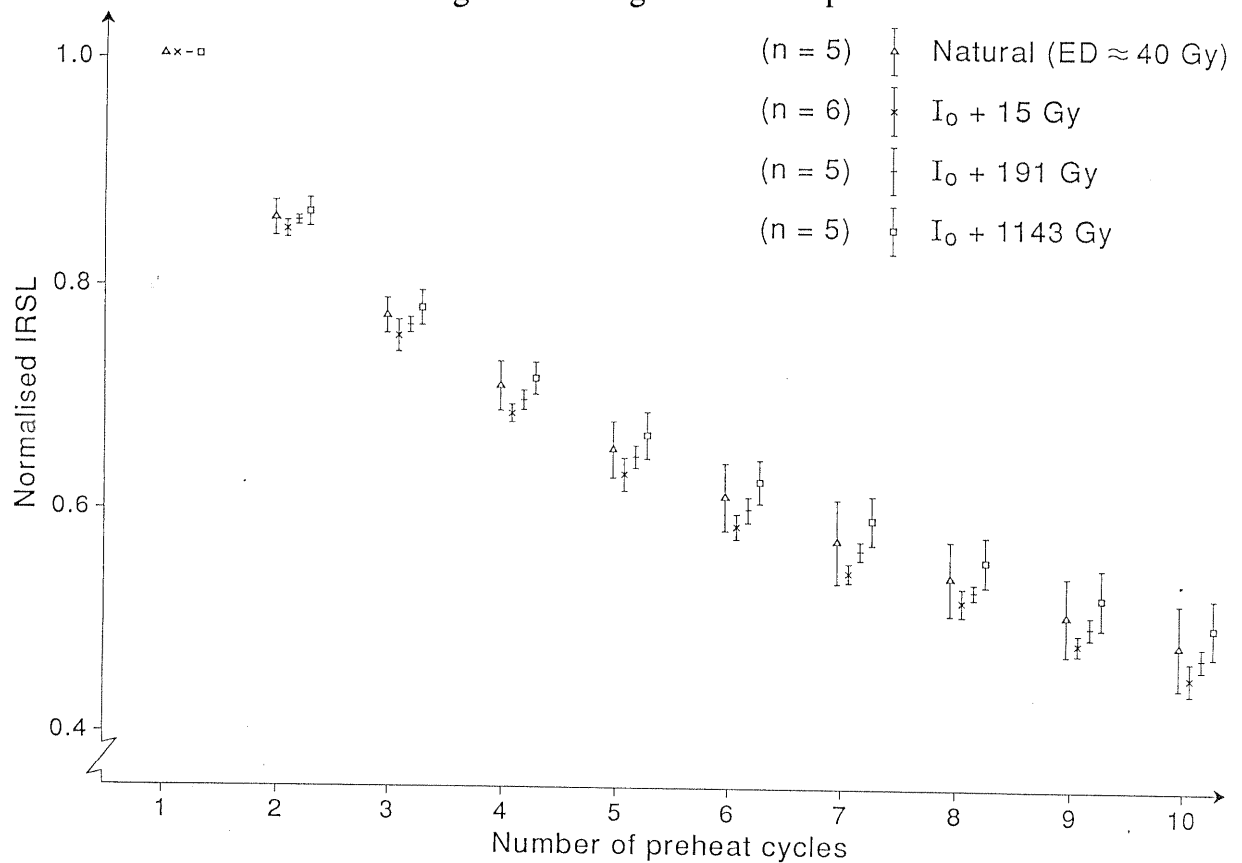


Figure 7.2(b): The proportion of the IRSL signal remaining after repeated preheating of sample GDNZ 5 at 220°C for 10 minutes. Four groups of aliquots, that had been treated in various ways, were analyzed. See text for details.

Table 7.2 shows the loss of signal due to the combination of preheating and IRSL measurement for all samples that were analyzed using this additive dose, single aliquot, method. In general, all samples responded to the preheating very similarly. GDNZ 5 appears to lose its signal more slowly than the other samples, but it is likely that this is because of changes in IR power between the time when this sample was run, and when all the others were run (approximately 25% of the initial signal is lost due to exposure to IR during the IRSL measurements themselves, see last column of table 7.2).

A central assumption of the method is that an IRSL signal induced by a beta dose decays during preheating in the same way as the natural signal. To test this twenty-one aliquots (split into four groups) of sample GDNZ 5 were exposed to ten cycles of preheating. After each preheat the IRSL signal was measured. One group still retained their natural signal (ED of about 40 Gy) while the other three groups had been bleached in a SOL2 solar simulator for 24 hours and then given beta irradiations of 15, 191 and 1143 Gy respectively. The results for all four groups of discs (figure 7.2(b)) lie within error limits. The implication is that for this preheat there is no significant difference in the way that the relevant natural and beta induced signals decay.

However in figure 7.2(b) it can be seen that the decay of the signal from samples which have had a beta dose show a consistent, but small, dose dependence, with the samples that have received the larger dose decaying more slowly than those that received the small dose.

Having characterised the effect of preheating upon a sample, it is then necessary to use these results to correct the additive dose data set. This can be done in two fundamentally different ways. The first considers the preheat as removing part of the stable luminescence signal. This can be corrected for by increasing the IRSL signal actually measured at each dose by an amount dictated by the results of the preheat characterisation. This approach is described in section 7.3.

Alternatively, the preheat can be viewed as having effectively removed a part of the signal that can be related to a received dose. Thus the total dose received by the sample is adjusted, rather than the signal it produces. This approach is described in section 7.4.

Table 7.2: Preheat characterisation results for all the New Zealand samples analyzed using the single aliquot additive dose method. The figures given are the ratio of the IRSL signal measured after 'n' preheats compared with the IRSL signal after the first preheat.

Preheat Cycle	GDNZ 1	GDNZ 5	GDNZ 6(a)	GDNZ 7	GDNZ 10	GDNZ 13	GDNZ 14	GDNZ 15	GDNZ 16
1	1.000	1.000	1.000	1.000	1.000	1.000	1.000	1.000	1.000
2	0.824	0.858	0.805	0.835	0.814	0.814	0.817	0.810	0.818
3	0.720	0.772	0.684	0.734	0.712	0.710	0.713	0.700	0.713
4	0.648	0.710	0.606	0.665	0.636	0.636	0.640	0.632	0.638
5	0.595	0.653	0.538	0.611	0.579	0.578	0.582	0.577	0.582
6	0.552	0.613	0.493	0.568	0.535	0.534	0.539	0.531	0.536
7	0.513	0.574	0.447	0.530	0.491	0.495	0.502	0.496	0.499
8	0.480	0.542	0.410	0.499	0.461	0.464	0.467	0.462	0.464
9	0.451	0.511	0.383	0.469	0.427	0.435	0.439	0.434	0.435
10	0.426	0.487	0.352	0.441	0.400	0.408	0.415	0.408	0.409

Preheat Cycle	GDNZ 17	GDNZ 21(a)	GDNZ 24	GDNZ 32	GDNZ 45	GDNZ 51	GDNZ 52	GDNZ 59	No Preheat(b)
1	1.000	1.000	1.000	1.000	1.000	1.000	1.000	1.000	1.000
2	0.816	0.791	0.810	0.808	0.805	0.807	0.810	0.825	0.962
3	0.719	0.684	0.705	0.698	0.691	0.706	0.712	0.728	0.924
4	0.641	0.588	0.633	0.635	0.618	0.630	0.637	0.651	0.894
5	0.586	0.539	0.576	0.585	0.561	0.579	0.583	0.592	0.868
6	0.538	0.494	0.532	0.543	0.514	0.530	0.534	0.546	0.843
7	0.501	0.458	0.493	0.515	0.476	0.495	0.493	0.508	0.814
8	0.469	0.426	0.462	0.485	0.447	0.461	0.464	0.470	0.791
9	0.438	0.393	0.434	0.461	0.420	0.430	0.428	0.442	0.769
10	0.411	0.373	0.408	0.433	0.393	0.402	0.398	0.419	0.745

Notes:

(a) Samples GDNZ 6 and GDNZ 21 had their IRSL signal measured at 50°C for 1.0s compared with 0.5s for the other samples.

(b) This sample of GDNZ 13 had its IRSL measured for 0.5s at 50°C, but with no preheat between each measurement. This shows the loss of IRSL signal simply due to the measurement itself.

## 7.3 Luminescence correction methods

There are two ways of applying a luminescence correction for the effect of preheating. They rely upon different assumptions concerning the way in which charge is distributed in a crystal when it is irradiated. They are designated methods A and B. The two procedures have been tested empirically using data sets from samples GDNZ 17, 5 and 7.

Samples were given five or six doses, and preheated and measured between each dose. The results are given in table 7.3, along with the results after application of the two methods of correction described below. The figures from the preheat characterisation for the samples are given in table 7.2. Growth curves were constructed from the uncorrected IRSL measurements in table 7.3 (curve 'a' in figures 7.3(a), 7.3(b) and 7.3(c)). The aliquots were then preheated again, with no dose added, and remeasured. This was repeated four or five times to repeat measurements of the top dose point. The IRSL signal became progressively smaller with the successive preheats for all three samples. Application of a successful correction procedure should be able to make these repeat measurements equal and this was the criterion used to determine the best method of luminescence correction.

### 7.3.1 Luminescence correction method A.

Method 'A' assumes that after irradiation the distribution of trapped charge will be similar irrespective of what preheats or irradiations have occurred previously. In this case each preheat will cause the previous signal to decay by the ratio between preheat 1 and 2 on the preheat characterisation (table 7.2), that is by a factor of 0.816 for GDNZ 17, 0.858 for GDNZ 5 and 0.835 for GDNZ 7.

Table 7.3 contains numerical examples of the corrections applied to the raw data using this assumption (columns 3 and 4). For GDNZ 5 the natural signal ( $S_{\beta 1} = I_1$ ) will decay to 0.858 of its initial level when the sample is preheated after the first  $\beta$  irradiation is added. When this value is subtracted from the luminescence measured after 15 Gy has been added to the natural ( $I_2$ ) it gives the signal induced just by the last  $\beta$  irradiation that was added ( $S_{\beta 2}$ , column 3). This is then added to the natural signal ( $S_{\beta 1}$ ) obtained in the first measurement.

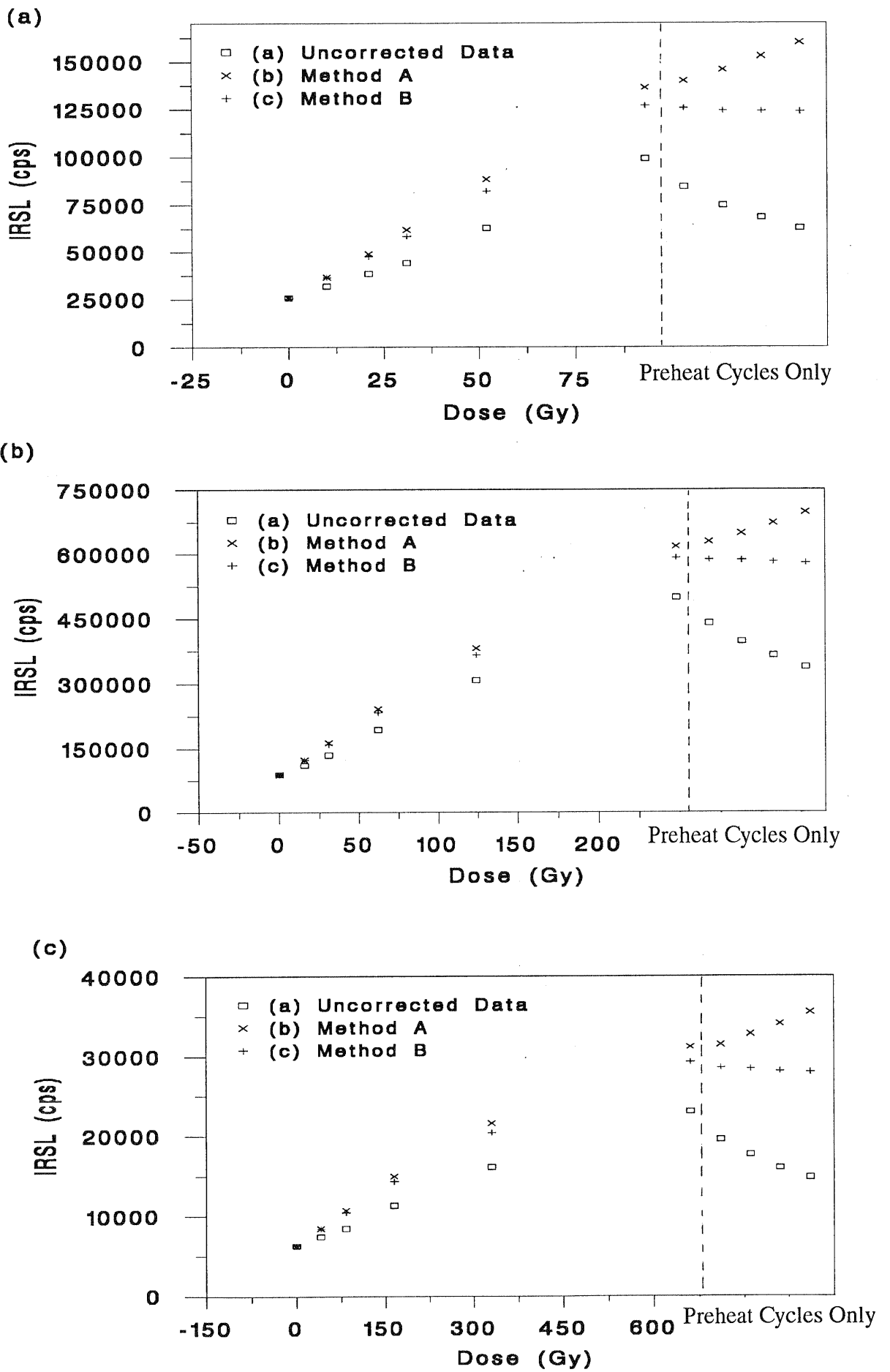


Figure 7.3: Single aliquot additive dose data, showing the uncorrected data, and the same data after application of correction methods A and B, for samples GDNZ 17 (a), GDNZ 5 (b) and GDNZ 7 (c).

Table 7.3:

Luminescence correction using two methods with different assumptions. Method 'A' assumes that the signal will decay in the same way irrespective of previous irradiations and preheats. Method 'B' assumes that each component of the trapped charge population behaves independently of the others. All values in columns 2-6 are luminescence measurements in counts per second.

GDNZ 17

<u>Total Dose</u> (Gy)	<u>Measured</u> <u>IRSL</u>	<b>Method A</b>		<b>Method B</b>	
		<u>IRSL due to</u> <u>last added</u> <u>dose</u>	<u>Corrected</u> <u>IRSL</u>	<u>IRSL due to</u> <u>last added</u> <u>dose</u>	<u>Corrected</u> <u>IRSL</u>
Natural	25641	(25641)	25641	(25641)	25641
N+10	31797	10874	36515	10874	36515
N+21	38292	12346	48861	10983	47498
N+31	44080	12834	61695	10864	58362
N+52	62575	26606	88301	23817	82179
N+93	99013	47952	136253	44560	126739
N+93	84351	3556	139809	-1230	125509
N+93	74661	5831	145640	-1390	124119
N+93	68111	7188	152828	-69	124050
N+93	62587	7008	159836	-391	123659

GDNZ 5

<u>Total Dose</u> (Gy)	<u>Measured</u> <u>IRSL</u>	<b>Method A</b>		<b>Method B</b>	
		<u>IRSL due to</u> <u>last added</u> <u>dose</u>	<u>Corrected</u> <u>IRSL</u>	<u>IRSL due to</u> <u>last added</u> <u>dose</u>	<u>Corrected</u> <u>IRSL</u>
Natural	88944	(88944)	88944	(88944)	88944
N+15	110950	34636	123580	34636	123580
N+31	134514	39319	162899	36154	159722
N+62	193288	77875	240774	72424	232146
N+124	306690	140849	381623	133938	366084
N+248	498718	235578	617201	225072	591156
N+248	439592	11692	628893	-4246	586910
N+248	396688	19518	648411	-6032	585124
N+248	364412	24054	672465	-3804	581320
N+248	337916	25251	697716	-2566	578754

Table 7.3 continued.

GDNZ 7

<u>Total Dose</u> (Gy)	<u>Measured</u> <u>IRSL</u>	<b>Method A</b>		<b>Method B</b>	
		<u>IRSL due to</u> <u>last added</u> <u>dose</u>	<u>Corrected</u> <u>IRSL</u>	<u>IRSL due to</u> <u>last added</u> <u>dose</u>	<u>Corrected</u> <u>IRSL</u>
Natural	6253	(6253)	6253	(6253)	6253
N+41	7399	2178	8431	2178	8431
N+83	8440	2262	10693	2031	10462
N+165	11292	4245	14938	3842	14304
N+331	16047	6618	21556	6079	20383
N+661	23005	9606	31162	8876	29259
N+661	19521	312	31474	-697	28562
N+661	17606	1306	32780	-141	28421
N+661	15970	1269	34049	-291	28130
N+661	14769	1434	35483	-127	28003

To calculate the signal induced by the second added  $\beta$  irradiation (16 Gy) the contribution of the natural and the first  $\beta$  irradiation have to be subtracted. These are found by multiplying the previous measurement taken at N+15 Gy ( $I_2$ ) by 0.858. This process was repeated for all ten measurements and is summarised in equation 1.

$$S_{\beta n} = I_n - (I_{n-1} \times 0.858) \quad \text{Equation [1]}$$

The corrected data are plotted as curve 'b' in figures 7.3(a), 7.3(b) and 7.3(c). All three samples clearly show that the correction procedure is not valid. The form of the growth curves up to the highest irradiation is reasonable, but the repeat measurements at this point are different and increase monotonically with successive preheating corrections.

7.3.2 Luminescence correction method B.

Method 'B' assumes that the trapped charge induced by each irradiation behaves independently of the others. For instance the natural signal decays in precisely the same way as shown in table 7.2 whether the sample is exposed to further  $\beta$  irradiation or not. Similarly, when the first  $\beta$  irradiation is added the trapped charge population that it produces will decay following the same pattern as in table 7.2. To correct for this type of effect one has to isolate each component of the signal and then use the decay curves in table 7.2 to calculate the loss of signal. By subtracting the contribution that all the previous irradiations make to the measured signal, one can calculate the part of the signal that must

be due to the last added  $\beta$  irradiation (column 6 in table 7.3). This can be described mathematically as,

$$S_{\beta n} = I_n - \sum_{i=1}^{n-1} (S_{\beta i} \times F_{(n-i+1)}) \quad \text{Equation [2]}$$

Where for measurement (n) the luminescence signal (S) due to that  $\beta$  irradiation ( $\beta n$ ) can be calculated by subtracting the sum of the components of the previous signals ( $S_{\beta i}$ ) (column 5, table 7.3) multiplied by the appropriate correction factors ( $F_{(n-i+1)}$ , table 7.2) from the measured luminescence  $I_n$  (column 2, table 7.3). Column 6 of table 7.3 has been corrected using this second assumption and the data are plotted as curve 'c' in figures 7.3(a), 7.3(b) and 7.3(c).

Table 7.3.2 shows a fully worked example of this type of correction. Working from the first measured luminescence signal (row 1, column 2), the luminescence signal due to each added  $\beta$  irradiation is calculated. Each figure in bold type is calculated by subtracting the sum of the luminescence contributions from previous irradiations from the luminescence measured at that point. For example the IRSL signal due to the 21Gy irradiation (from 31 to 52Gy) is calculated as  $62575 - (15026 + 6970 + 7897 + 8865) = 23817$ . Having established the IRSL signal due to each irradiation, the decay of that signal due to preheating can be calculated using the preheat characterisation values in table 7.2. Thus the 23817 counts due to the 21Gy of irradiation has decayed to  $(0.816 \times 23817) = 19435$  counts when the next measurement has occurred, and  $(0.719 \times 23817) = 17124$  counts after the next measurement.

For GDNZ 17 and 5 this correction method produces very similar measurements for the repeated readings. This is the more successful of the two correction methods. The repeat measurements after 93 Gy irradiation are not identical but are well within the error limits associated with the uncertainties in the preheat correction factors. This experiment was repeated eighteen times for each sample and in all cases a small, but consistent decrease in signal was seen for these five repeat measurements. For GDNZ 5 the corrected signal had dropped by 4.2% from the first to the last of these repeat measurements on average. For sample GDNZ 7, the correction method is less successful for these repeat measurements. However this is the luminescence correction method used in all subsequent analyses since it is the most successful of the two.

Table: 7.3.2.

Example of the application of luminescence correction (method B) to an additive dose data set for an aliquot of sample GDNZ 17.

$\beta$ Irrad. (Gy)(a)	Actual IRSL(b)	Signal Component.(c)								Corrected IRSL(d)			
		(1)	(2)	(3)	(4)	(5)	(6)	(7)	(8)		(9)	(10)	
0	25641	<b>25641</b>											25641
10	31797	20923	<b>10874</b>										36515
21	38292	18436	8873	<b>10983</b>									47498
31	44080	16436	7818	8962	<b>10864</b>								58362
52	62575	15026	6970	7897	8865	<b>23817</b>							82179
93	99013	13795	6372	7040	7811	19435	<b>44560</b>						126739
93	84351	12846	5850	6436	6964	17124	36361	<b>-1230</b>					125509
93	74661	12026	5448	5909	6366	15267	32039	-1004	<b>-1390</b>				124119
93	68111	11231	5100	5502	5845	13957	28563	-884	-1134	<b>-69</b>			124050
93	62587	10538	4763	5151	5443	12814	26112	-788	-999	-56	<b>-391</b>		123659

Notes:

- The total added  $\beta$  irradiation.
- The IRSL signal measured for 0.5s at 50°C.
- Figures in **bold** are the calculated IRSL signals due to the last  $\beta$  irradiation. These decay as subsequent measurements (and preheating cycles) occur, calculated using the figures in table 7.2.
- The corrected IRSL is the sum of the signal components in **bold**.

### 7.3.3 Testing luminescence correction method B.

Two further experiments were used to test the internal consistency and the precision of method 'B' outlined above. The first test was aimed at examining the efficacy of the correction technique for two samples - the first, GDNZ 17, exhibiting linear additive dose response (figure 7.3(a)) and the second, GDNZ 7, showing non-linear behaviour (figure 7.3(c)). The first test was designed to look for errors in luminescence correction method 'B' by comparing the ratio of the luminescence signals from an aliquot with just its natural signal, and its signal after additional irradiation, for two sets of aliquots. The first set were given a series of small irradiations, with the aliquot being preheated and its IRSL measured after each dose, while the second set were given a single large irradiation. The first set required many corrections, using luminescence correction method 'B', while the second set required only a single correction.

For this first test each of twenty aliquots of sample GDNZ 17 were given five irradiations to generate growth curves. Another set of six discs were just given a single irradiation (93 Gy), equivalent to the total dose received by the other twenty. The ratios between the signals for the natural and the N+93 Gy were calculated for both sets of discs. One set needed five 'phases' of correction, the other only one. If a problem exists with the correction method then there should be a significant difference between the two ratios. For the twenty discs given a sequence of irradiations, the ratio between the natural signal and that for N+93 Gy was  $5.14 \pm 0.27$ , while for the other six it was  $4.89 \pm 0.22$ . The two ratios lie within each other's error limits and suggest that there are no problems in the correction method that can be seen within the precision of this experiment ( $\pm 5\%$ ).

This test was also performed on sample GDNZ 7, whose single aliquot ED (using luminescence correction method B) is  $107.0 \pm 7.2$  Gy. For this sample a total irradiation of 661 Gy was used. For fifteen discs, five irradiations were added to generate a growth curve. The ratio of the corrected signals for (N+661Gy)/N was  $4.72 \pm 0.26$ . Seven discs were just given a single irradiation of 661 Gy, and for these discs the same ratio gave a value of  $4.01 \pm 0.18$ . These two ratios do not fall within error limits and suggest that the IRSL signal for the aliquots that have had many phases of corrections has been over-corrected to too high a value.

The second test involved repeat measurements of the ED for samples GDNZ 17, GDNZ 5 and GDNZ 7 to determine the precision of the analyses. Twenty samples of GDNZ 17 were given irradiations of 10, 21, 31, 52 and 93 Gy. A linear fit was found suitable for each

growth curve and a mean ED of 22.5 Gy was calculated. The standard deviation of the mean was 1.6 Gy, i.e. a precision of 7%.

Nineteen samples of GDNZ 5 were given the same irradiations as those in figure 7.3(b) and corrected using luminescence method B. ED determinations were calculated using an exponential fit to the data and only the first of the measurements after irradiation to N+248 Gy was included. The mean of the EDs was 34.5 Gy, the standard deviation of the mean being 1.2 Gy, i.e. a precision of 3%.

Eighteen samples of GDNZ 7 were given irradiations of 41, 83, 165, 331 and 661 Gy. Using an exponential fit a mean ED of 107 Gy was calculated. The standard deviation of the mean was 7.2 Gy, i.e. a precision of 7%.

The results presented above show that the additive dose single aliquot method using luminescence correction 'B' produces high precision results when repeat ED determinations are made for different aliquots of a sample. They also show that comparing the ratio of  $(N+\beta)/N$  for aliquots where the beta dose was given in a single dose with those where the same beta dose was given as the sum of five smaller doses (and hence where either one or five phases of correction were needed) the method was found to give accurate results for the young sample GDNZ 17, but not for the older sample GDNZ 7 where the correction method appeared to have boosted the IRSL signal to too great an extent. The implications of these results will be discussed in section 7.3.5.

#### 7.3.4 Comparison of equivalent doses determined using standard methods and single aliquot results corrected using luminescence correction method B

The most important test of the single aliquot method (using luminescence correction method B) is to compare the results obtained with those determined using standard methods of equivalent dose determination. All the samples whose EDs were determined using standard multiple aliquot methods in chapter 5 (table 5.4.5) have also had their ED determined using the single aliquot additive dose method and the results are listed in table 7.3.4 and plotted in figure 7.3.4. In addition, a number of samples from The Netherlands and from the southwestern United States of America have also had their EDs measured using the single aliquot additive dose method. These have had multiple aliquot EDs determined by other workers in other laboratories, and so any comparison of EDs is more uncertain because different radioactive sources, detection filters, preheats and analysis procedures have been used. The results are listed in appendix III.

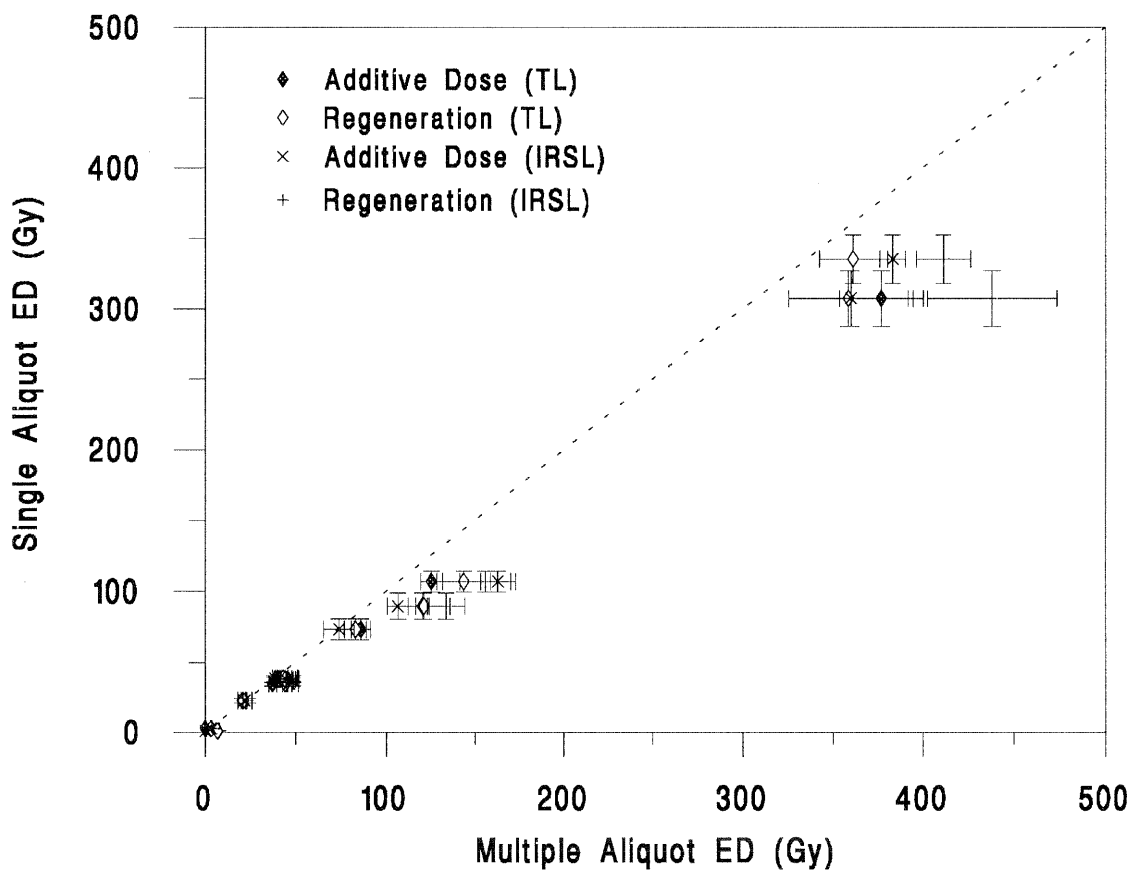


Figure 7.3.4: Comparison of equivalent doses determined using the single aliquot additive dose method, using luminescence correction B, with those determined using standard multiple aliquot methods, for samples collected from New Zealand.

Table 7.3.4

Comparison of equivalent doses determined using the single aliquot additive dose method with correction B (section 7.3.2) with those determined using multiple aliquot methods for samples collected from New Zealand (see table 5.4.5).

<u>Sample</u> <u>(GDNZ)</u> (a)	<u>Single</u> <u>Aliquot</u> <u>ED</u> (b)	<u>Multiple Disc Methods</u>			
		<u>Additive</u> <u>Dose (TL)</u> (b)	<u>Regeneration</u> <u>(TL)</u> (b)	<u>Additive</u> <u>Dose (IRSL)</u> (b)	<u>Regeneration</u> <u>(IRSL)</u> (b)
21	1.0± 0.1	7.1± 0.6	6.6± 1.0	0.1± 0.1	0.7± 0.1
6(NE)	2.8± 0.2	n.d.	3.3± 0.3	3.3± 0.0	3.6± 0.1
17	22.5± 1.6	20.5± 2.5	21.0± 1.3	21.8± 0.8	23.4± 2.5
5	34.5± 1.2	37.3± 2.2	44.3± 1.6	46.3± 1.6	48.5± 3.2
1	37.9± 1.7	38.4± 0.2	40.7± 2.3	44.7± 3.1	48.1± 3.7
13(NE)	37.7± 0.9	45.8± 1.7	44.3± 4.3	39.5± 1.4	47.5± 2.5
45	38.5± 1.9	40.0± 1.2	43.2± 1.1	38.5± 1.2	48.4± 2.5
52	73.4± 7.3	86.1± 5.4	83.0± 6.1	73.8± 8.5	n.d.
51	89.8± 9.2	120.4± 3.8	121.3±14.6	106.5± 5.9	133.7±10.6
7	107.0± 7.2	125.5± 6.2	143.6±14.9	163.0± 9.8	155.8±14.4
10	335.6±17.2	n.d.	361.3±19.0	383.2± 7.2	411.4±14.9
59	307.6±20.2	376.9±23.4	358.7±33.2	360.0±34.7	438.0±35.4

Notes:

- (a) Samples that were not etched, using 10% HF acid for 40 minutes, are indicated with an (NE).
- (b) All equivalent doses are in grays. Multiple disc samples were irradiated using the Daybreak irradiator (3.81 Gy/min), single aliquot samples using the Risø irradiator (1.24 Gy/min).

The majority of samples with an ED of less than 100 Gy show a good agreement between results from the luminescence corrected single aliquot method and the multiple aliquot methods, although the single aliquot results are typically at the lower end of the range of EDs produced by the multiple aliquot methods. For samples whose ED is greater than 100 Gy a significant underestimation, when using the single aliquot method, is apparent (e.g. GDNZ 10 and GDNZ 59).

In conclusion, application of luminescence correction method 'B' appears to give similar answers to those derived by standard methods of ED determination for samples with EDs less than 100 Gy, and whose response to dose is nearly linear. For samples whose response to additional irradiation is significantly non-linear, significant differences between the methods become apparent.

### 7.3.5 Problems when applying luminescence correction method B to non-linear growth curves

Analysis of many samples using the single aliquot (additive dose) method gives reproducible results as shown in section 7.3.3. The precision of this method is excellent, but its accuracy is poor for older samples, as shown above. In addition, from the results discussed so far several other problems are apparent for samples whose growth curves are non-linear.

Firstly, the experiment described in section 7.3.3 (comparing results after one or five phases of correction) showed that the correction method was not working correctly for GDNZ 7 since the signal measured after the addition of 661Gy depended upon the number of steps in which this irradiation was given (and thus the number of luminescence correction phases required). Additionally, for sample GDNZ 7, it was impossible to make repeat measurements of the IRSL at the highest irradiation point reproducible (see table 7.3 and figure 7.3(c)). This tendency was observed for the majority of the samples analyzed. Table 7.3.5 gives the average percentage 'loss' of signal at the first repeat measurement of the highest irradiation point for all the samples analyzed using luminescence correction method B. These data are plotted in figure 7.3.5(a).

Figure 7.3.5(a) shows that for samples with a higher ED the loss of IRSL signal also increases. This mirrors the underestimation of ED observed for older samples when compared with standard methods of ED determination (tables 7.3.4, AIII.1(a) & AIII.1(b)). It seems that the samples analyzed from the south-western USA exhibit larger losses of signal at a given ED than those from New Zealand and the Netherlands.

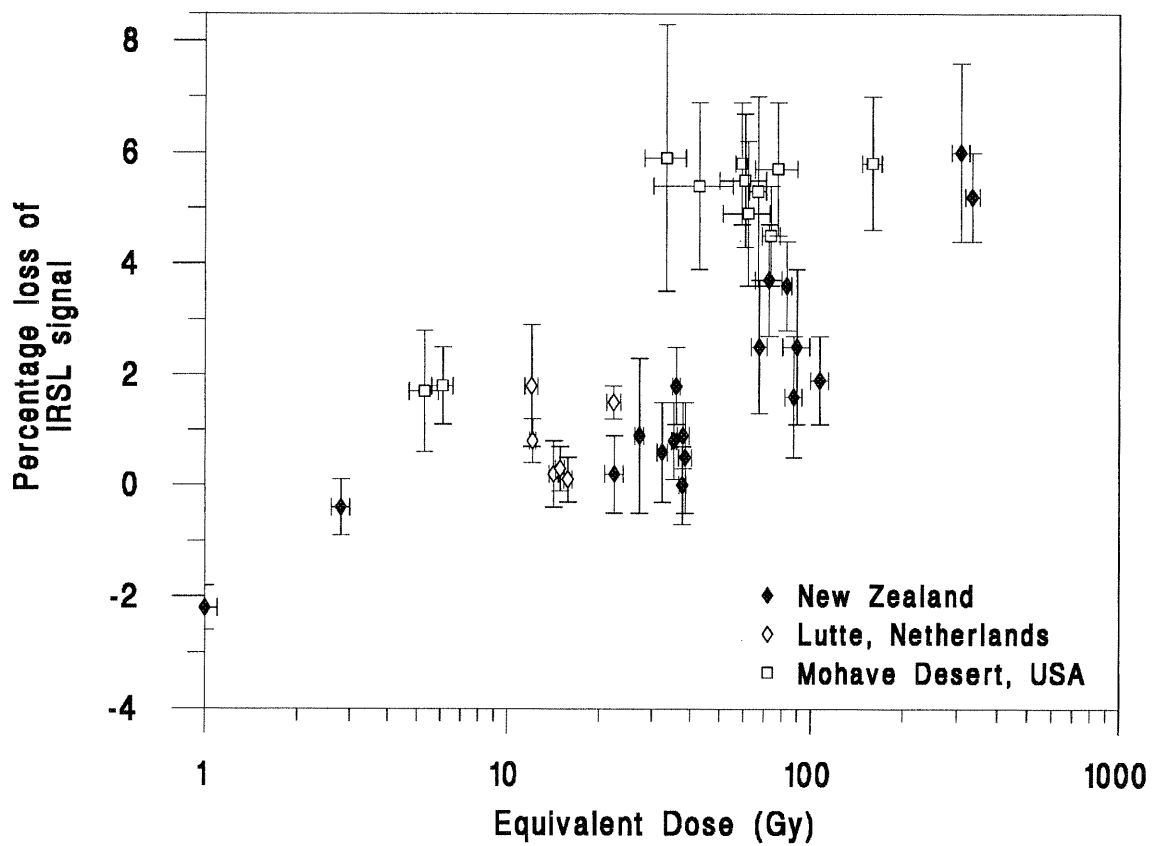


Figure 7.3.5(a): The relationship between the percentage drop in IRSL signal at the first repeat measurement of the highest irradiation point and the equivalent dose of a sample as determined by the single aliquot additive dose method, using luminescence correction B.

Table 7.3.5

Comparison of the equivalent dose of a sample and the loss of IRSL signal from individual aliquots, following application of luminescence correction method B, when repeat measurements were made of the aliquot after it had received the highest irradiation.

<u>Sample</u> <sup>(a)</sup>	<u>Single Aliquot</u> <u>ED (Gy)</u>	<u>Loss of Signal</u> <u>(%)</u> <sup>(b)</sup>	<u>Number of</u> <u>Samples</u>
GDNZ 21	1.0± 0.1	-2.2± 0.4	(7)
GDNZ 6(NE)	2.8± 0.2	-0.4± 0.5	(17)
GDNZ 17	22.5± 1.6	0.2± 0.7	(6)
GDNZ 24(NE)	27.2± 0.9	0.9± 1.4	(18)
GDNZ 32(NE)	32.4± 1.2	0.6± 0.9	(18)
GDNZ 15(NE)	35.4± 0.7	0.8± 0.7	(18)
GDNZ 5	34.5± 1.2	1.8± 0.7	(20)
GDNZ 1	37.9± 1.7	0.9± 0.6	(12)
GDNZ 13(NE)	37.7± 0.9	0.0± 0.7	(18)
GDNZ 45	38.5± 1.9	0.5± 1.0	(18)
GDNZ 16(NE)	83.2± 3.1	3.6± 0.8	(18)
GDNZ 14(NE)	87.8± 5.8	1.6± 1.1	(18)
GDNZ 52	72.7± 7.3	3.7± 1.0	(8)
GDNZ 51	89.8± 9.2	2.5± 1.4	(18)
GDNZ 7	107.0± 7.2	1.9± 0.8	(17)
GDNZ 10	335.6±17.2	5.2± 0.8	(18)
GDNZ 59	307.6±20.2	6.0± 1.6	(16)
Lutte 1	14.9± 0.5	0.3± 0.4	(6)
Lutte 2	12.0± 0.6	1.8± 1.1	(6)
Lutte 3	12.1± 0.3	0.8± 0.4	(6)
Lutte 8	22.4± 1.2	1.5± 0.3	(4)
Lutte 9	14.2± 0.5	0.2± 0.6	(6)
Lutte 12	15.8± 0.5	0.1± 0.4	(6)
CD01	77.8±12.5	5.7± 1.2	(4)
CD03	42.8±12.5	5.4± 1.5	(4)
CD04	66.9± 4.3	5.3± 1.7	(4)
CD07	33.4± 5.2	5.9± 2.4	(4)
DL01	159.0±11.6	5.8± 1.2	(6)
DL16	62.0±10.8	4.9± 1.3	(6)
DL17	56.9± 6.1	5.5± 1.2	(6)
DL18	73.8± 4.9	4.5± 0.9	(4)
DL19	59.1± 2.8	5.8± 1.1	(4)
DL22	37.9± 5.4	n.d.	
K30L	5.3± 0.6	1.7± 1.1	(18)
K31L	6.1± 0.5	1.8± 0.7	(17)

#### Notes

- (a) Samples prefixed GDNZ are those collected by GATD; Lutte are samples from Dijkmans and Wintle (1991); CD, DL and K are from Cat Dune, Dale Lake and Kelso in the Mohave desert, California (potassium feldspar provided by Dr H.Rendell). Single aliquot results for Lutte, CD, DL and K samples are in appendix III. Samples marked (NE) were not etched with HF before single aliquot analysis.
- (b) The loss of signal is calculated as the difference between the corrected IRSL signal after the largest irradiation and the corrected IRSL signal when no further dose is added, but the aliquot is preheated again, expressed as a percentage.

A possible explanation for the problems observed when the luminescence correction method is applied to growth curves with a non-linear response to irradiation is shown diagrammatically in figure 7.3.5(b). A hypothetical growth curve has been constructed and for convenience it has been divided into a linear and a non-linear section, as would be seen using multiple disc methods.

The crosses on the diagram indicate measurements made on a single aliquot. As the measurements are made, the signal observed (and hence the trapped charge population) at any particular dose becomes progressively lower than that measured in the multiple disc method because of the effect of the repeated preheats. It can be seen that the sample response remains in the linear growth region until dose  $D_B$ , whereas the 'true' response of the material has non-linear growth beginning at dose  $D_A$ . Both luminescence correction methods described above implicitly assume that no change in luminescence efficiency per unit dose will occur (i.e. that the sample remains linear). This is not the case for older samples and hence, beyond dose  $D_A$ , the corrected single aliquot signal is higher than the 'true' signal.

For a real sample where there is no clear boundary between linear and non-linear behaviour, the situation will be more complex, but of a similar nature. The trapped charge population within the sample after any given dose will always be lower than that for the same sample using a multiple disc method. Given an exponential form for the growth curve, the single aliquot will have a higher luminescence efficiency per unit dose than the multiple disc sample after the same irradiation. This results in the growth curve being steeper and more linear, giving an underestimate of the ED. Importantly, the effect will only become significant for samples whose growth curve is strongly curved. For these samples an alternative method is required that does not assume a constant luminescence efficiency. This is pursued in section 7.4.

## 7.4 Dose correction method

As discussed in the preceding section, inherent to the luminescence correction method is the assumption that the growth curve is linear. This assumption is implicit since one is adjusting the measured luminescence; hence it is essential to know the luminescence efficiency of the sample after any given irradiation (in effect, the luminescence efficiency must be constant).

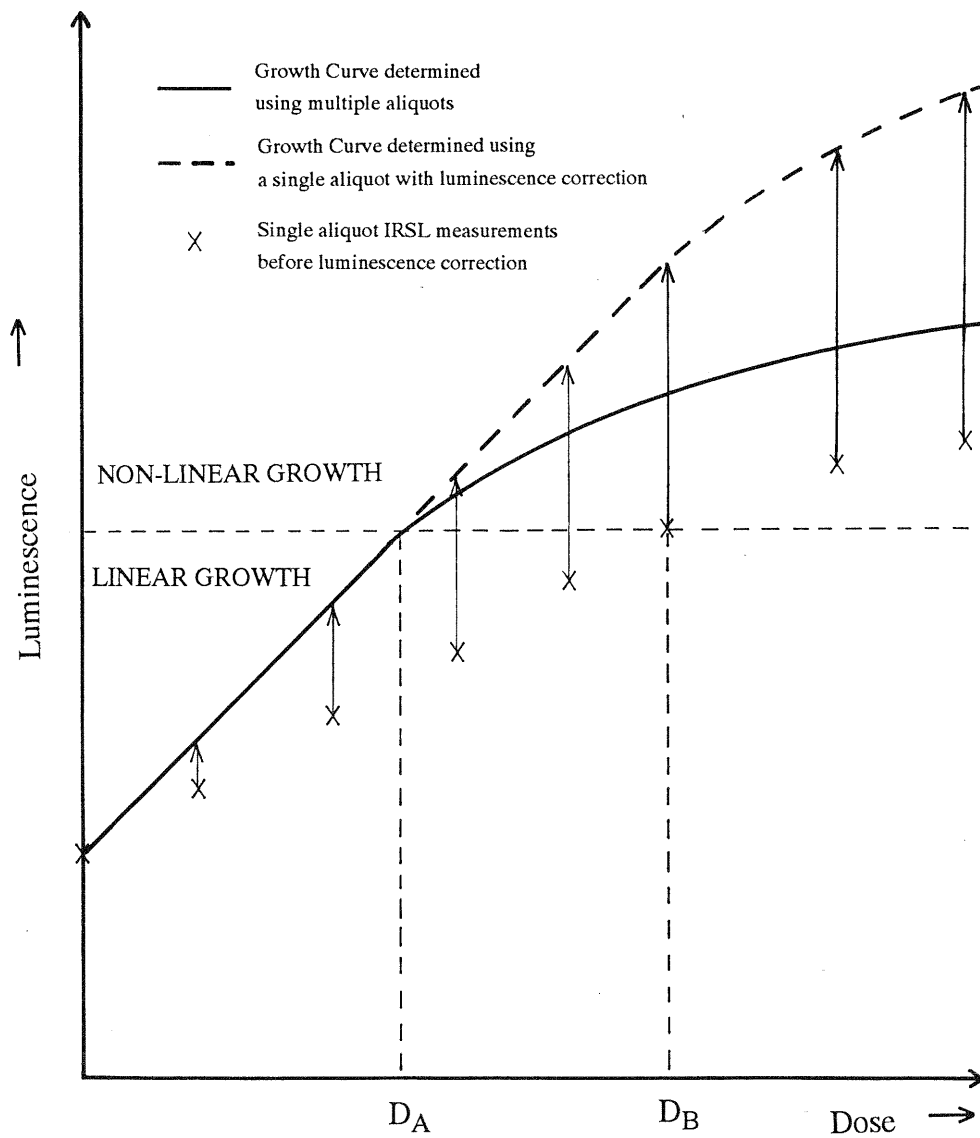


Figure 7.3.5(b): Schematic comparison of the growth curve derived using multiple aliquot methods with that derived using the single aliquot additive dose method with luminescence correction method B. In this figure it is assumed that the growth of the luminescence signal with dose is initially linear, and then becomes non-linear above a certain limit (marked by the horizontal dashed line).

An alternative approach is to correct for the loss of trapped charge from stable traps as a result of preheating by viewing this as an effective 'negative dose'. This approach makes the assumption that the loss of 'effective dose' per preheat remains constant.

#### 7.4.1 Description of the method

A similar procedure can be used as described by equation 2 (section 7.3.2). However, rather than adjusting the luminescence, it is the dose that is altered. Hence equation 2 becomes,

$$TAD_n = \sum_{i=1}^{n-1} (D_i \times F_{(n-i+1)}) - D_1 \quad \text{Equation [3]}$$

Where for measurement (n) the corrected 'total added dose' (TAD) can be calculated by subtracting the estimated ED ( $D_1$ ) from the sum of the previous component doses ( $D_i$ ) multiplied by the appropriate correction factors ( $F_{(n-i+1)}$ , from table 7.2). Table 7.4.1 shows a worked example of this type of correction. It is very similar to that illustrated in table 7.3.2 (and equation [2]), except that unlike the component signals, the component doses are all known precisely with the exception of the ED ( $D_1$ ). As with the luminescence correction method, the decay of each 'dose' component must be computed, including the natural dose. This is the dose when the sample is first measured (i.e. the equivalent dose). Thus one needs to know the ED before one can correct the data.

This seemingly catastrophic flaw can be overcome by using an iterative procedure. Starting with an ED estimate of zero, and using successive EDs calculated in this way, the result quickly converges. Figure 7.4.1 shows such a sequence of growth curves for sample GDNZ 17 generated using ED estimates from the previous correction cycle.

Figure 7.4.1 also shows repeat measurements of the highest dose point. Unlike the luminescence correction approach, where repeat measurements should lie on top of each other after correction, the dose corrected data all fall on the growth curve, but at different points along it.

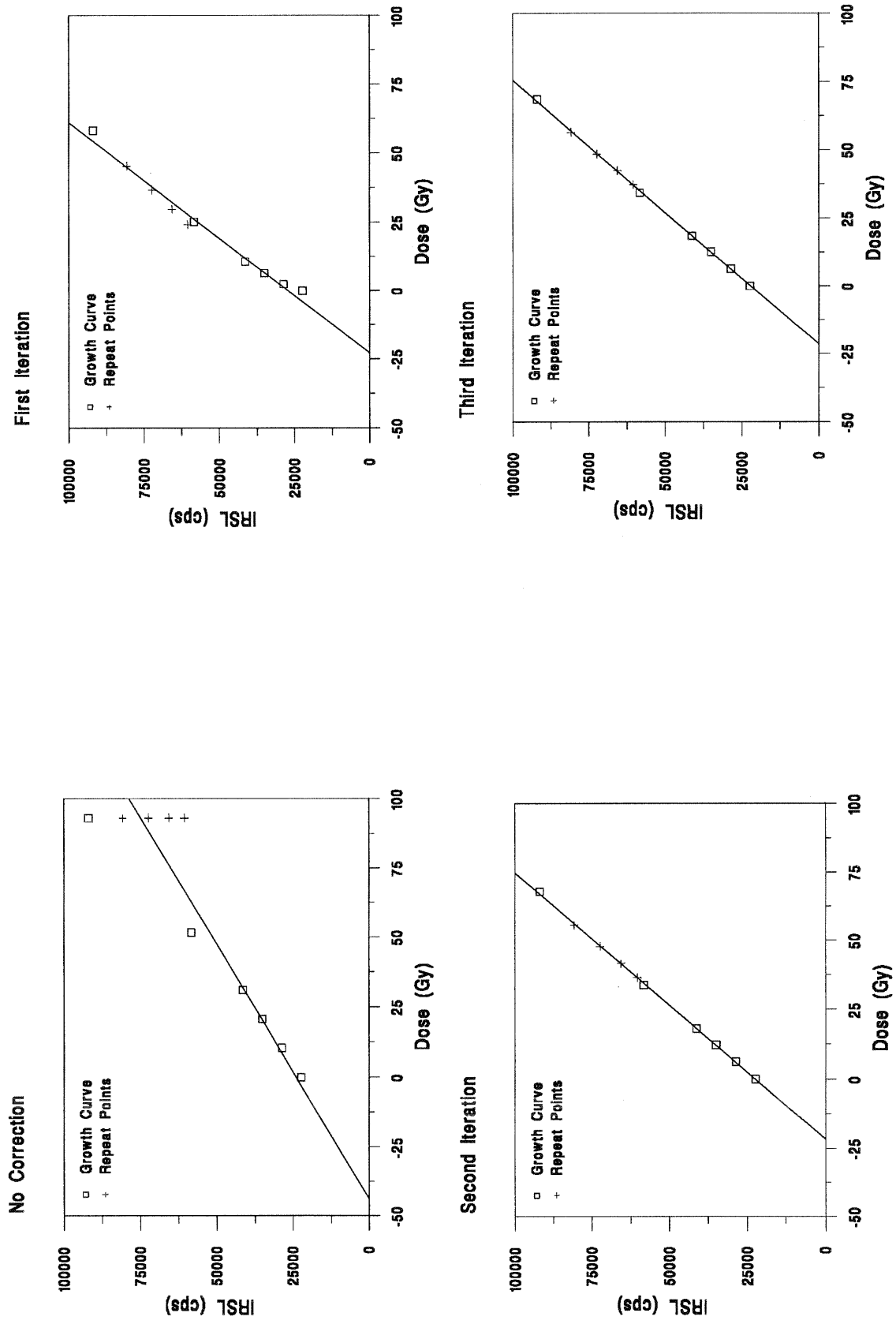


Figure 7.4.1: Four growth curves generated for a single aliquot of sample GDNZ 17 applying the dose correction method. Each iteration uses the equivalent dose derived from the previous iteration as its starting point.

Table: 7.4.1.

Example of the dose correction method for GDNZ 17 using the same data set as in table 7.3.2.

<u>IRSL(a)</u>	<u>Total Dose</u> <u>(Gy)(b)</u>	<u>Dose Components (Gy)(c)</u>										<u>Corrected</u> <u><math>\beta</math>-Dose (Gy)</u> <u>(e)</u>		
		(1)	(2)	(3)	(4)	(5)	(6)	(7)	(8)	(9)	(10)			
25641	(24.9)	24.9											24.9	0
31797	10.3	20.3	<b>10.3</b>										30.6	5.7
38292	20.7	17.9	8.4	<b>10.3</b>									36.7	11.8
44080	31.0	16.0	7.4	8.4	<b>10.3</b>								42.2	17.3
62575	51.7	14.6	6.6	7.4	8.4	<b>20.7</b>							57.8	32.9
99013	93.0	13.4	6.1	6.6	7.4	16.9	<b>41.3</b>						91.7	66.8
84351	93.0	12.5	5.6	6.1	6.6	14.9	33.7	<b>0</b>					79.3	54.4
74661	93.0	11.7	5.2	5.6	6.1	13.2	29.7	0	<b>0</b>				71.4	46.6
68111	93.0	10.9	4.9	5.2	5.6	12.1	26.5	0	0	<b>0</b>			65.1	40.2
62587	93.0	10.2	4.5	4.9	5.2	11.1	24.2	0	0	0	<b>0</b>		60.1	35.3

Notes:

- a) IRSL signal measured at 50°C for 0.5s with no correction.
- b) Figures for the total irradiation added to the sample. The value of 24.9 Gy is the ED estimated using the uncorrected data and this value has not been added to the figures in the rest of this column for clarity.
- c) The decay of each dose component (analogous to the signal components in table 7.3.2) has been calculated using the preheat characteristics in table 7.2. In this case all the component doses are known precisely (the figures in **bold**) except for the ED.
- d) The sum of all the dose components (i.e. all of that row, (1) to (10), in the table).
- e) The sum of all the dose components having subtracted the ED that was used in the calculation.

## 7.4.2 Testing the method on samples with linear growth

For samples whose response is linear there should be no significant difference in the ED calculated whether luminescence (method B) or dose correction is used. To test this, data for samples GDNZ 6 and 17 was analyzed by both methods. Table 7.4.2 shows the comparison of the EDs for GDNZ 17. Any repeat measurements have been included in the ED determinations by both methods. Figure 7.4.2 compares the results given by the two correction methods for a sample of GDNZ 17.

The ratio of the EDs calculated by dose and luminescence methods is  $0.994 \pm 0.023$  (n=18) for GDNZ 17 and  $0.986 \pm 0.023$  (n=17) for GDNZ 6. These figures show that within one standard deviation the two correction methods give the same results for samples whose growth curve is linear.

Table 7.4.2:

Comparison of equivalent doses determined for GDNZ 17 after application of the luminescence (method B) and dose correction methods. A linear fit was used in all cases.

<u>Sample Disc</u>	<u>Luminescence Correction ED (Gy)</u>	<u>Dose Correction ED (Gy)</u>	<u>Ratio of Dose Correction ED to Luminescence Correction ED</u>
1	25.1 ± 0.3	24.5 ± 0.7	0.9761
2	23.6 ± 0.4	23.2 ± 0.8	0.9831
3	22.1 ± 0.2	n.d.	-
5	24.9 ± 0.6	26.2 ± 2.0	1.0522
6	22.9 ± 0.3	22.3 ± 0.7	0.9738
7	22.3 ± 0.2	22.1 ± 0.3	0.9910
9	26.2 ± 0.6	25.6 ± 0.7	0.9771
10	20.9 ± 0.3	20.5 ± 0.5	0.9809
11	21.3 ± 0.2	21.3 ± 0.3	1.0000
13	22.4 ± 0.2	22.0 ± 0.5	0.9821
14	21.1 ± 0.4	20.8 ± 0.6	0.9858
15	21.8 ± 0.2	21.4 ± 0.5	0.9817
17	25.2 ± 0.6	25.8 ± 0.7	1.0238
18	21.3 ± 0.1	21.6 ± 0.2	1.0141
19	21.5 ± 0.1	21.8 ± 0.5	1.0140
21	22.3 ± 0.3	22.3 ± 0.5	1.0000
22	21.5 ± 0.2	21.9 ± 0.5	1.0186
23	21.7 ± 0.3	21.1 ± 0.7	0.9724
24	21.2 ± 0.6	20.4 ± 0.8	0.9623
25	20.9 ± 0.3	n.d.	-
<u>Mean ED (Gy)</u>	22.5 ± 1.6 Gy	22.5 ± 1.8 Gy	

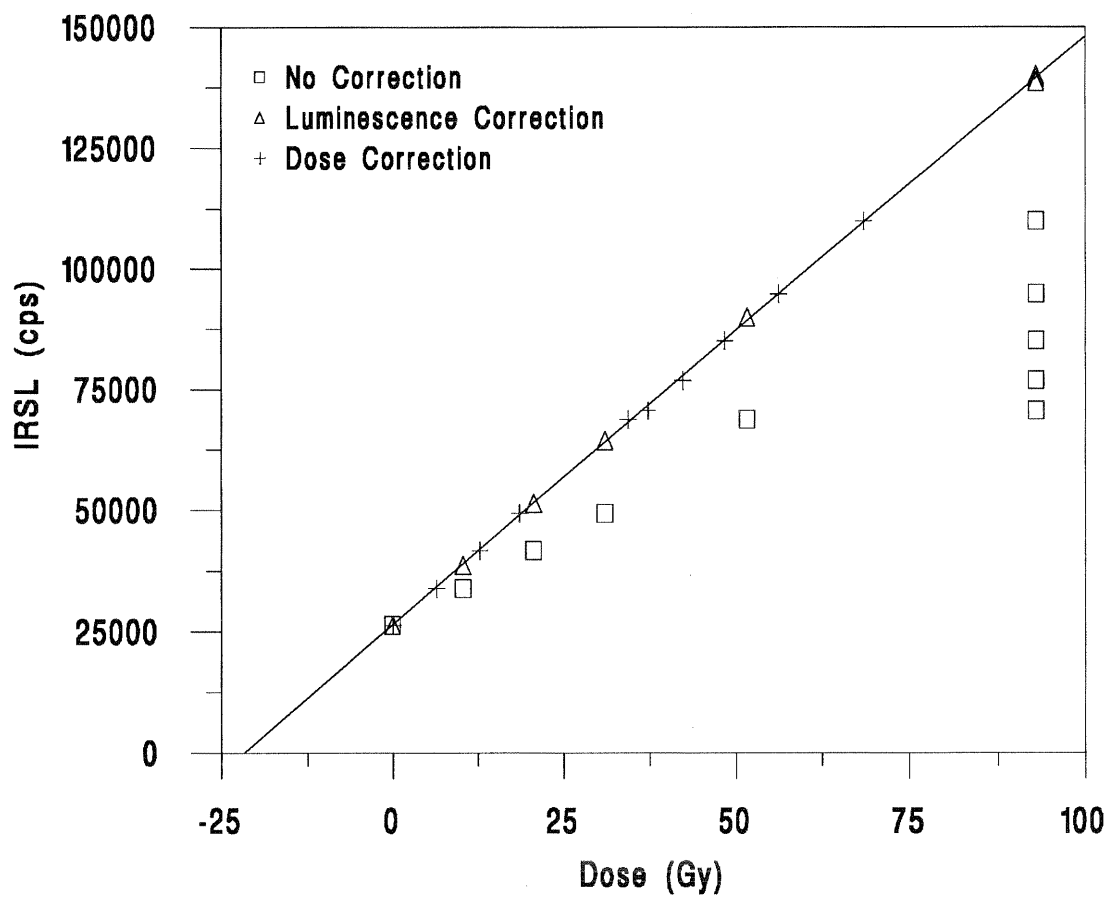


Figure 7.4.2: Comparison of the application of luminescence correction method B and the dose correction method to data derived from a single aliquot of GDNZ 17.

### 7.4.3 Testing the method on samples with non-linear growth

Samples which can best be fitted using a non-linear growth curve can also be corrected using a dose correction method. Figure 7.4.3(a) shows successive applications of the dose correction method to a single aliquot of GDNZ 7. During correction the ED was estimated without using the repeat measurements. Figure 7.4.3(b) shows how rapidly the ED estimate converges upon a stable value of approximately 107 Gy.

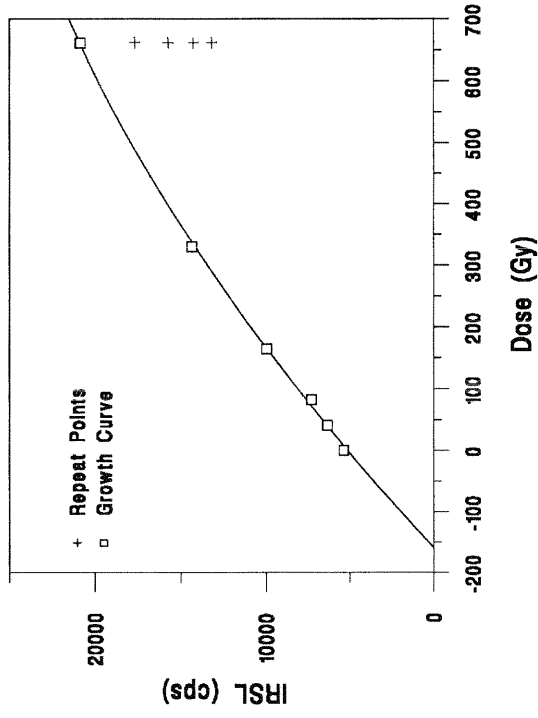
Figure 7.4.3(c) compares the growth curves for GDNZ 10 as measured using a single aliquot both with dose correction and luminescence correction method B. The dose correction method gives a very different growth curve, giving a far lower IRSL signal at any given dose. The ED calculated is significantly larger than that determined using the luminescence correction method (c.f. section 7.3.4).

Figure 7.4.3(a) clearly shows that in contrast with the linear samples in section 7.4.2, after dose correction repeat measurements after the largest irradiation do not fall on the growth curve. Instead they approximate to a straight line. Figures 7.4.3(d)-(k) show dose corrected results for a series of samples with progressively larger EDs (and consequently increased curvature in the form of their growth curve). The repeat measurements fall on, or very close to, the growth curve for samples (d) to (f) whose dose response is essentially linear. However, for samples (g) to (k) the repeat measurements fall progressively further away from the growth curve. Although some do appear to be linear (GDNZ 7), others are definitely not (GDNZ 14 and 10). The significance of this is unknown and is the subject of further study.

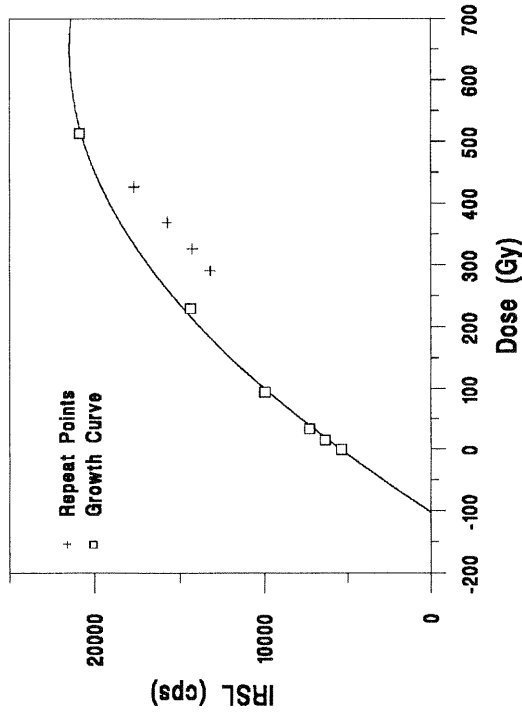
### 7.4.4 Comparison of equivalent doses determined using standard methods and single aliquot results corrected using the dose correction method

Table 7.4.4 compares single aliquot ED determinations, using the dose correction method, with results obtained using 'standard' multiple aliquot techniques. The results from table 7.4.4 are plotted in figure 7.4.4 and shows that using the dose correction method described in section 7.4.1, the single aliquot EDs determined for this suite of samples are similar to those determined by standard multiple aliquot techniques. Using dose correction on the single aliquot data, samples GDNZ 10 and 59 give EDs approximately 15% higher than when using luminescence correction method B.

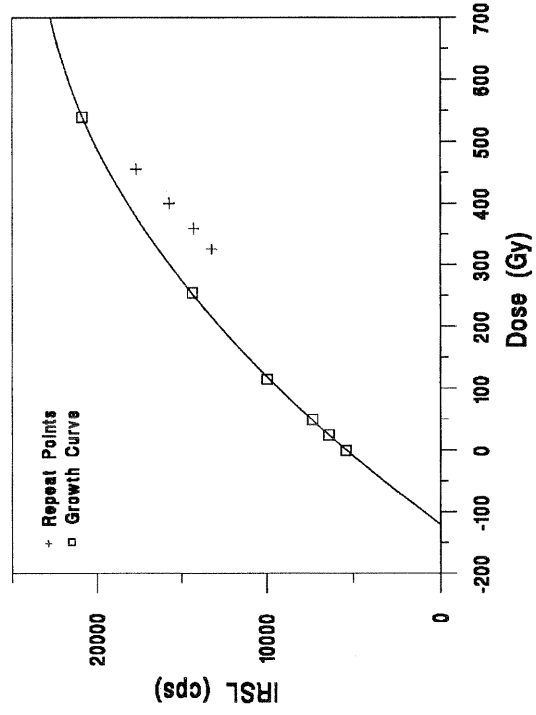
No Correction



First iteration



Second iteration



Third iteration

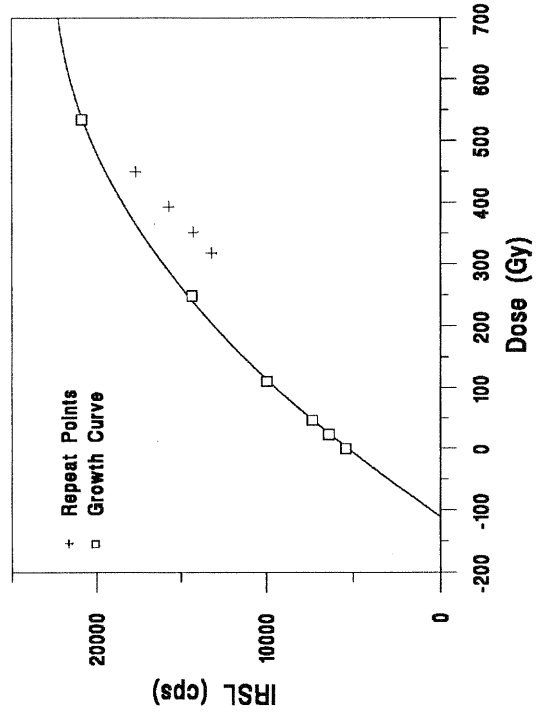


Figure 7.4.3(a): Successive growth curves generated for a single aliquot of GDNZ 7 applying the dose correction method. Each iteration uses the equivalent dose derived from the previous iteration as its starting point.

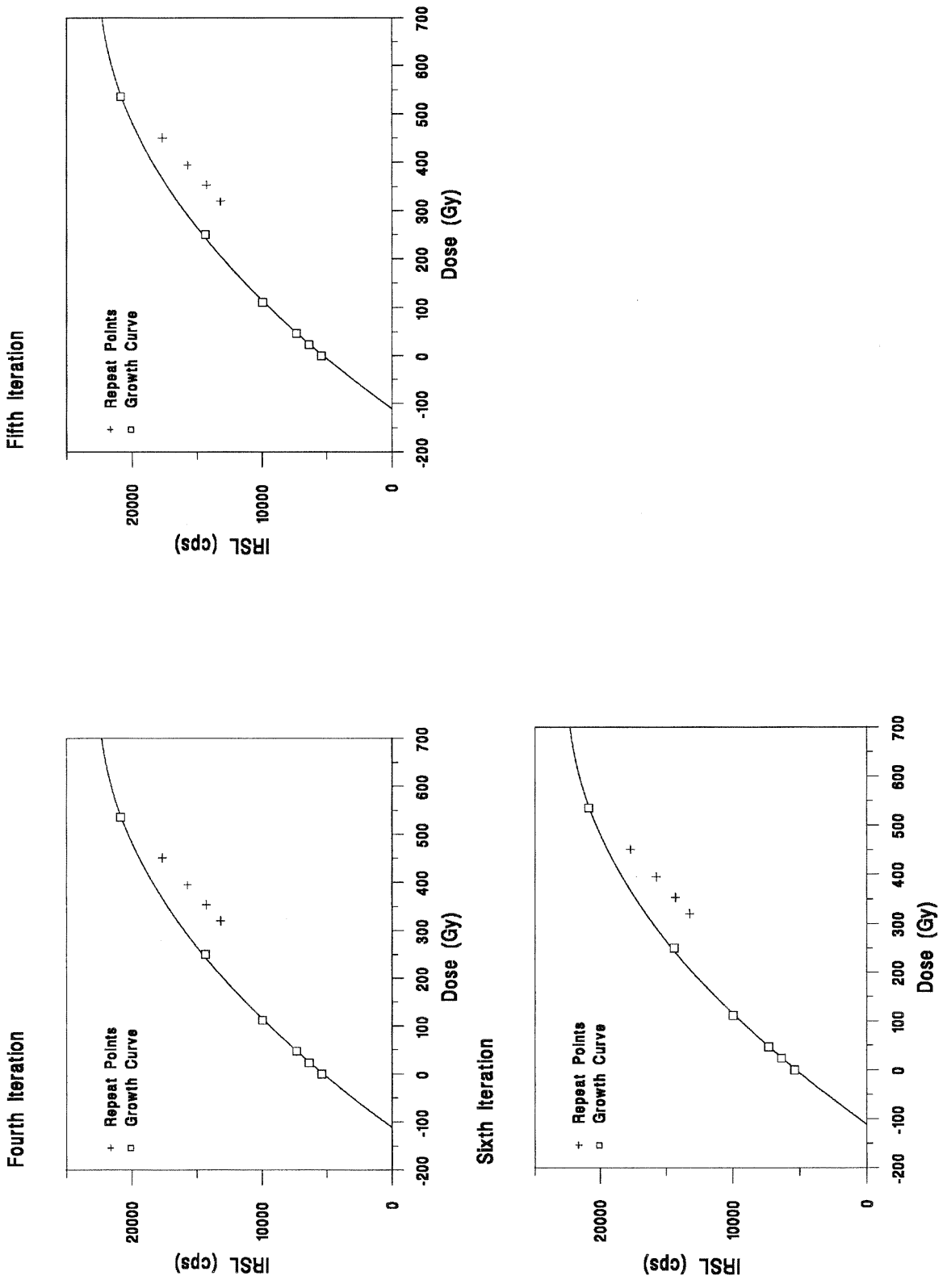


Figure 7.4.3(a) continued: Successive growth curves generated for a single aliquot of GDNZ 7 applying the dose correction method. Each iteration uses the equivalent dose derived from the previous iteration as its starting point.

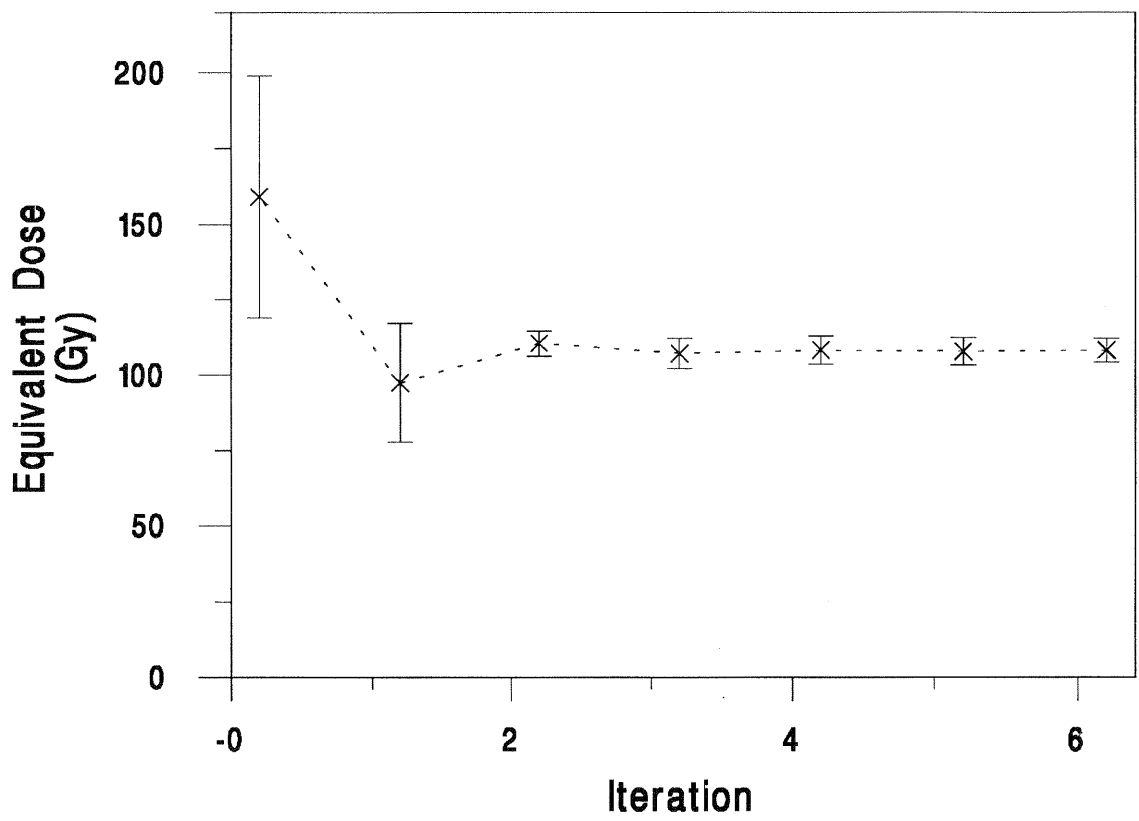


Figure 7.4.3(b): The variation of the equivalent dose during iteration, using the dose correction method, for the aliquot of GDNZ 7 shown in figure 7.4.3(a).

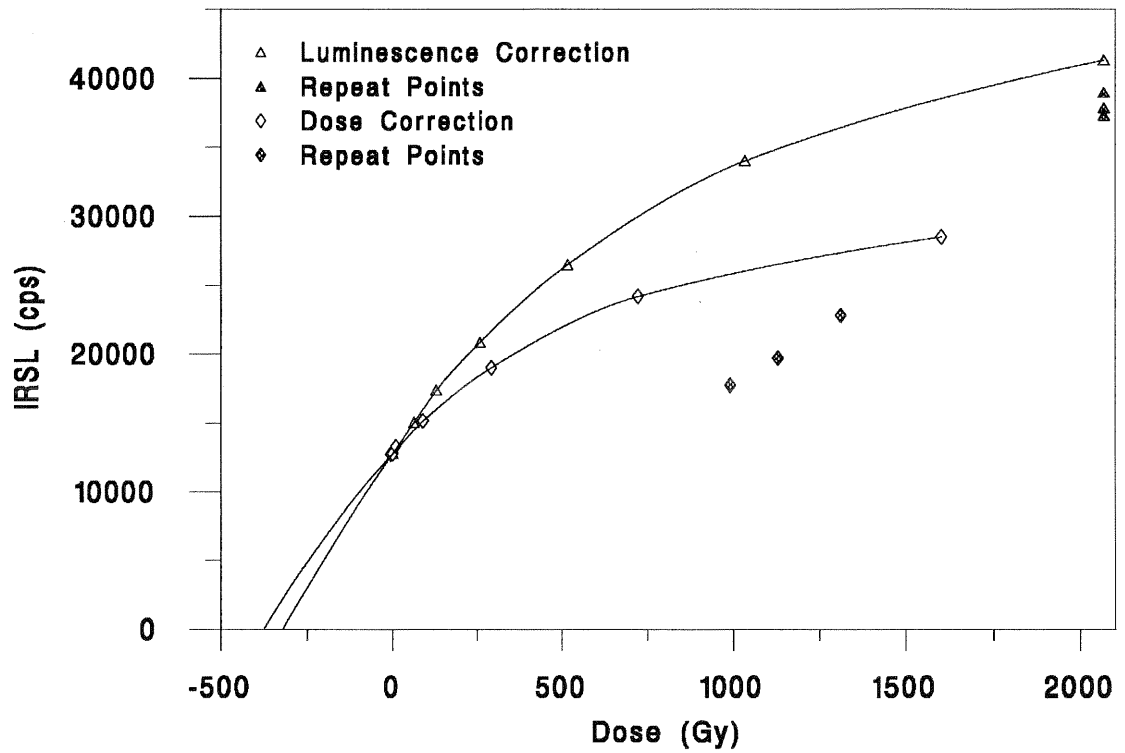


Figure 7.4.3(c): Comparison of the application of luminescence correction method B and the dose correction method to data derived from a single aliquot of GDNZ 10.

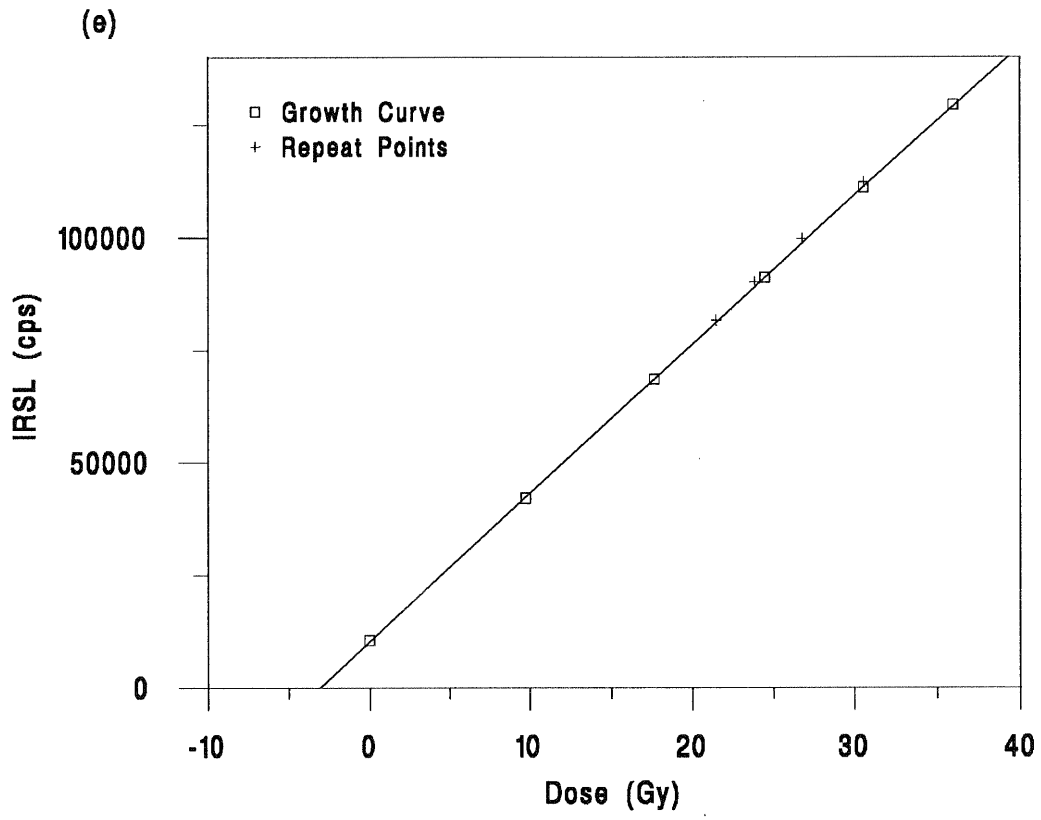
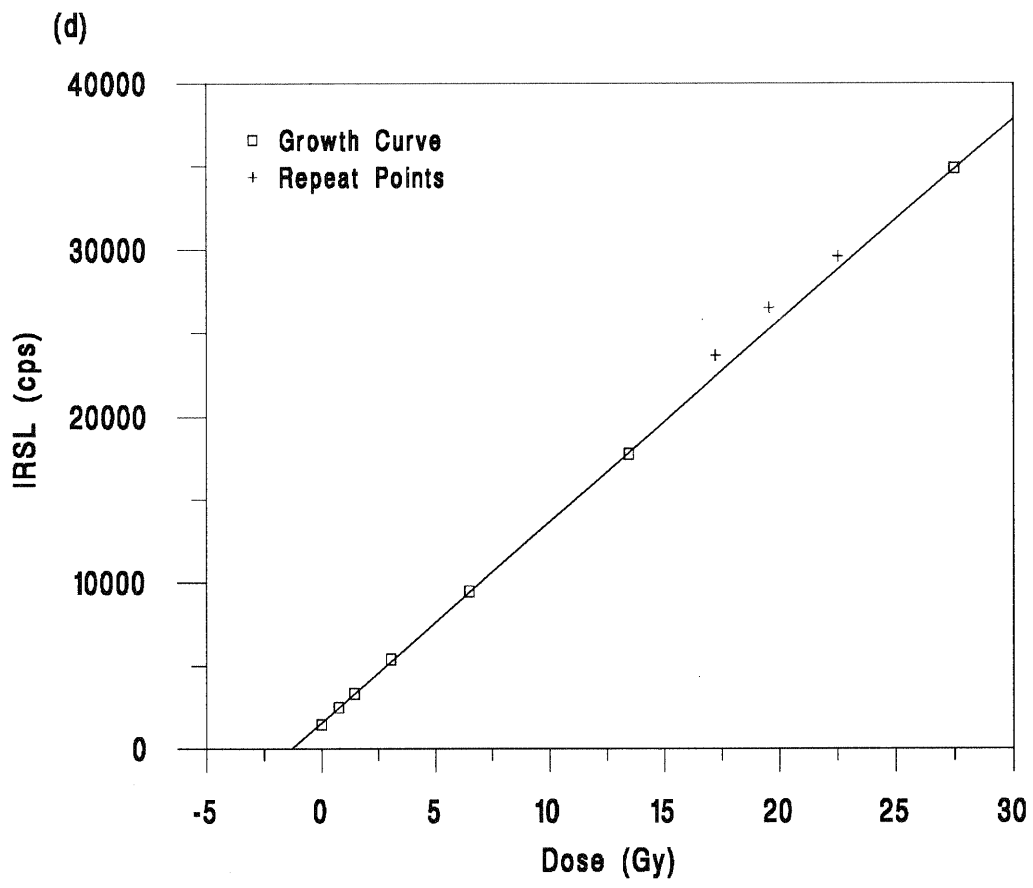


Figure 7.4.3: Single aliquot additive dose growth curve for samples (d) GDNZ 21 and (e) GDNZ 6 after 5 iterations of the dose correction method (the equivalent dose has reached a stable value).

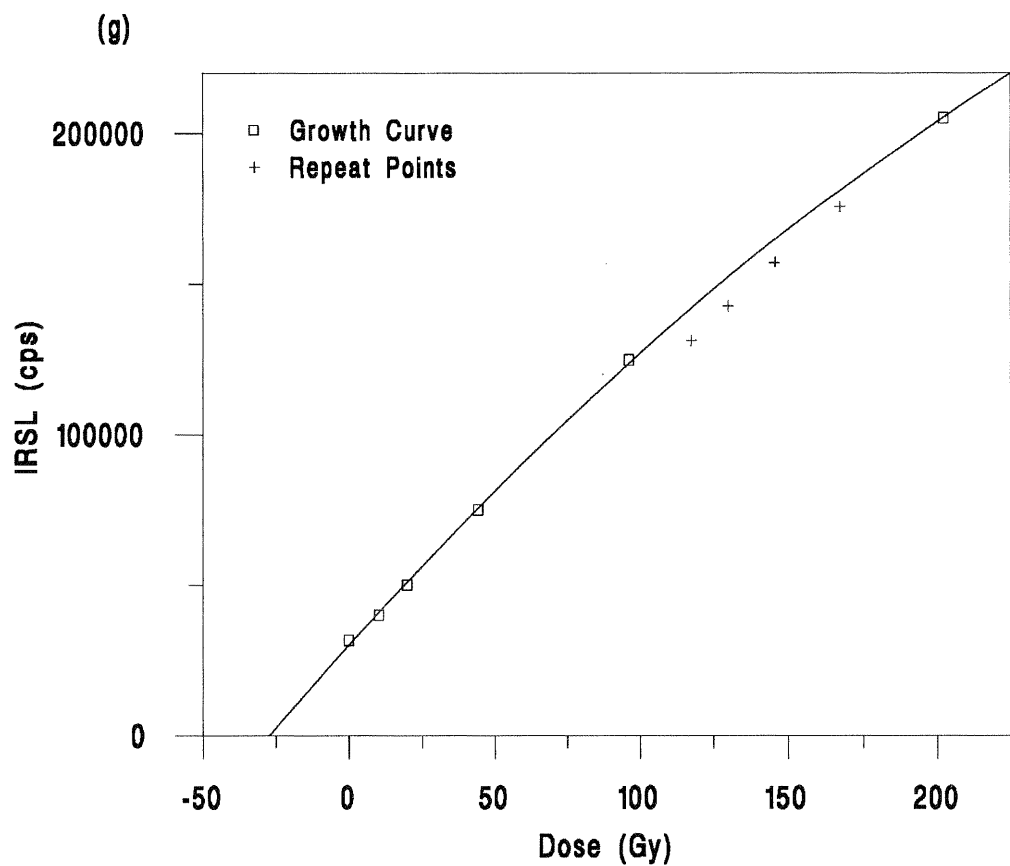
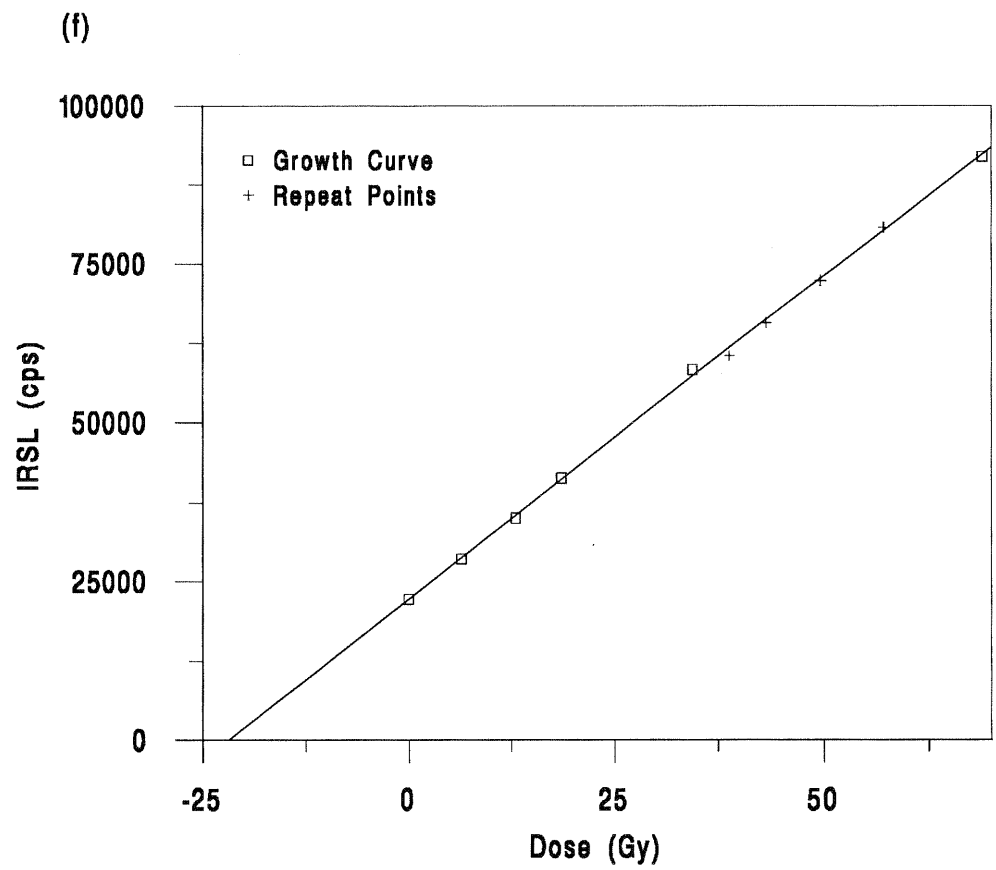


Figure 7.4.3: Single aliquot additive dose growth curves for samples (f) GDNZ 17 and (g) GDNZ 24 after 5 iterations of the dose correction method (the equivalent dose has reached a stable value).

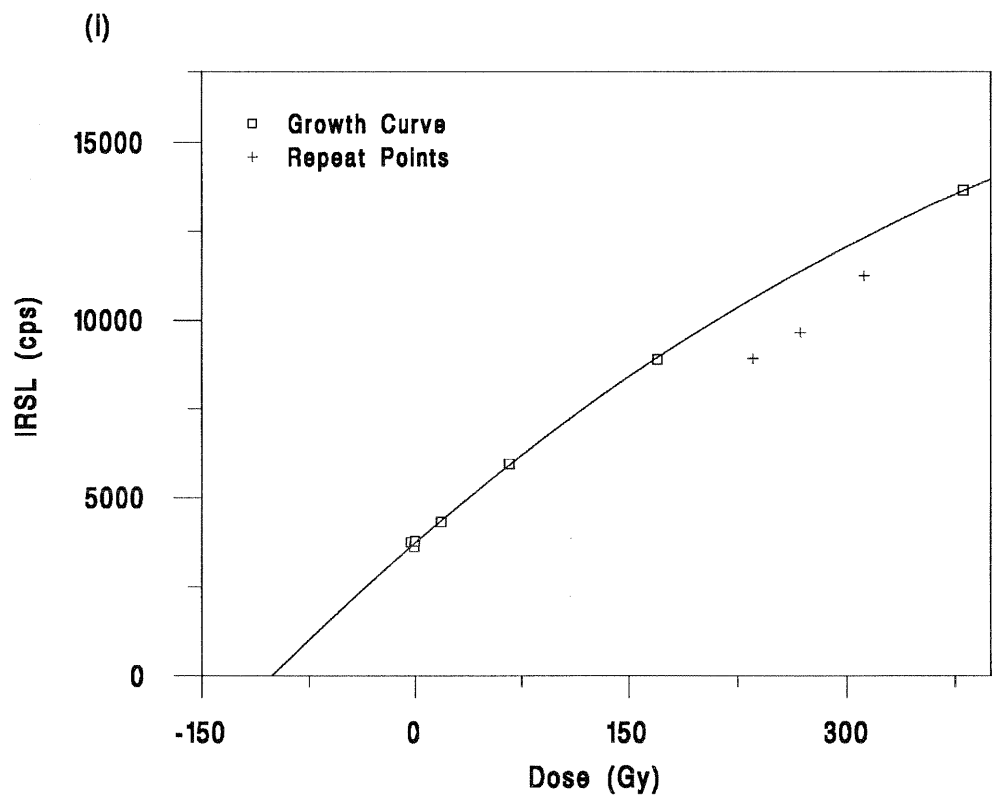
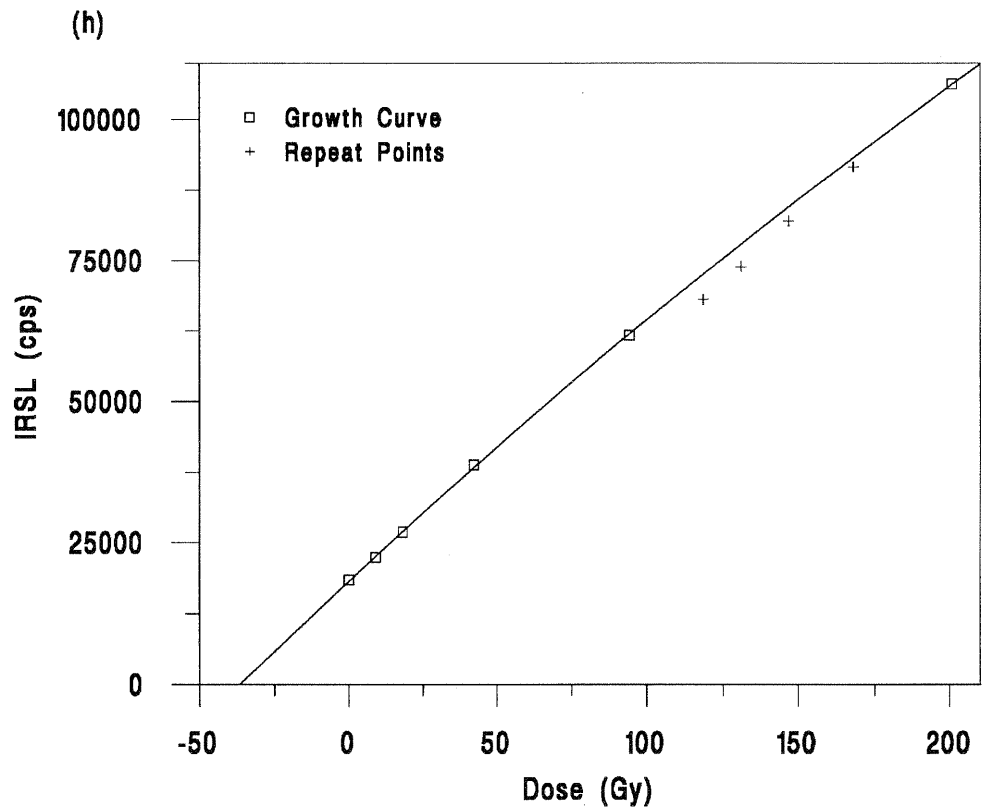


Figure 7.4.3: Single aliquot additive dose growth curves for samples (h) GDNZ 1 and (i) GDNZ 14 after 5 iterations of the dose correction method (the equivalent dose has reached a stable value).

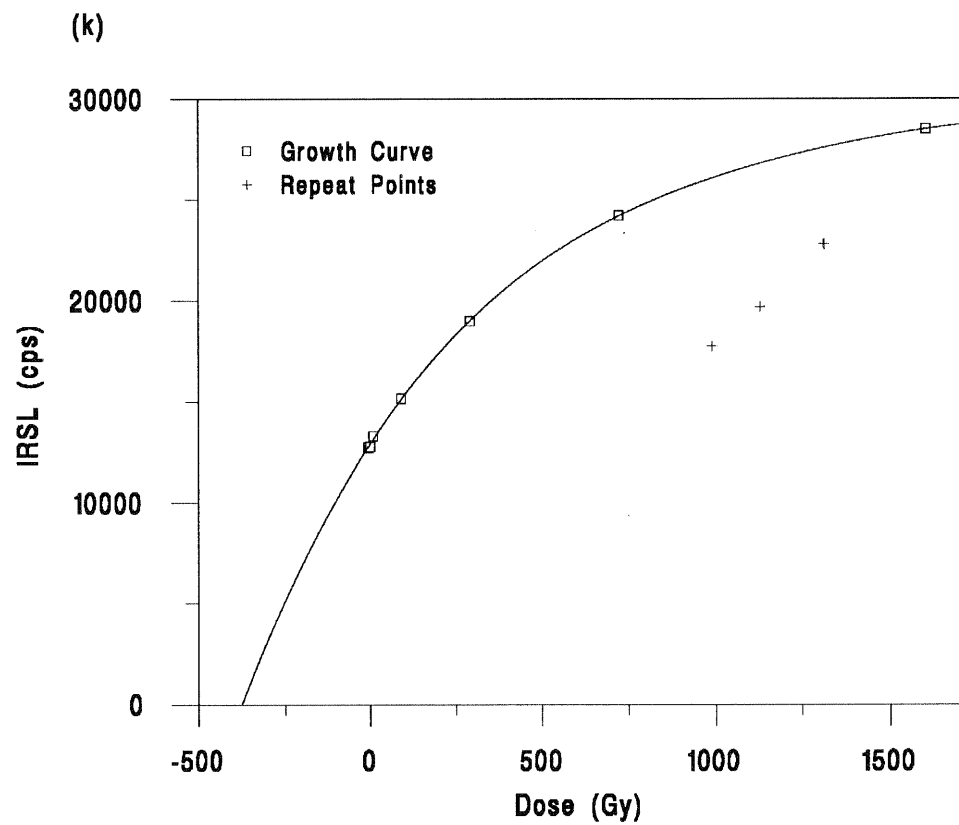
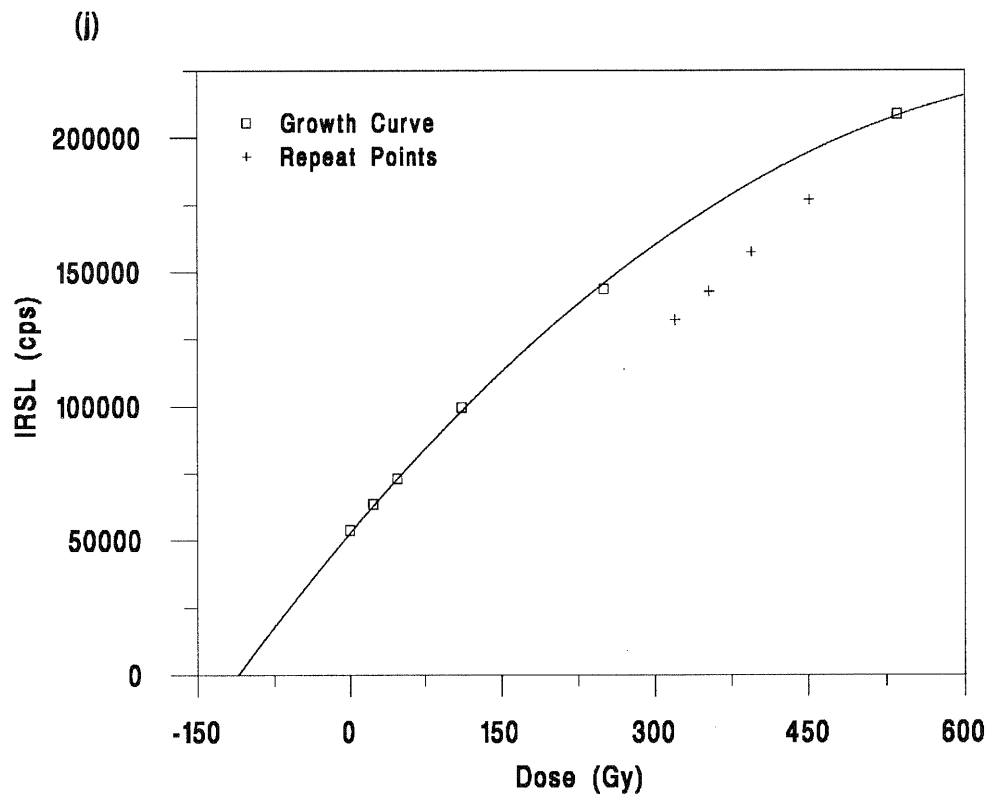


Figure 7.4.3: Single aliquot additive dose growth curves for samples (j) GDNZ 7 and (k) GDNZ 10 after 5 iterations of the dose correction method (the equivalent dose has reached a stable value).

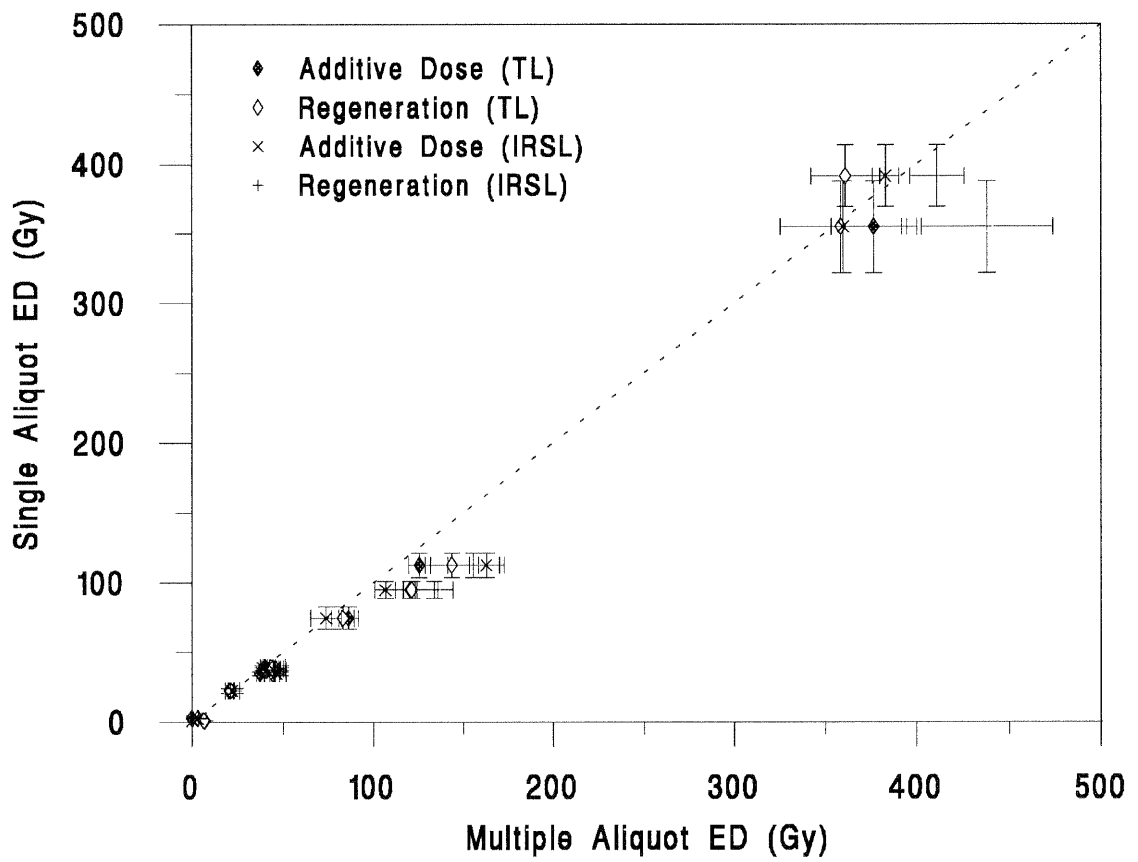


Figure 7.4.4: Comparison of equivalent doses determined using the single aliquot additive dose method, using dose correction, with those determined using standard multiple aliquot methods for samples collected from New Zealand.

Table 7.4.4

Comparison of equivalent doses determined using the single aliquot additive dose method with dose correction and standard multiple aliquot methods (TL and IRSL) for samples collected from New Zealand (table 5.4.5).

<u>Sample (GDNZ)</u> <sup>(a)</sup>	<u>Single Aliquot</u> <sup>(b)</sup>	<u>Multiple Disc Methods</u>			
		<u>Additive Dose (TL)</u> <sup>(b)</sup>	<u>Regeneration (TL)</u> <sup>(b)</sup>	<u>Additive Dose (IRSL)</u> <sup>(b)</sup>	<u>Regeneration (IRSL)</u> <sup>(b)</sup>
21	1.0± 0.1	7.1± 0.6	6.6± 1.0	0.1± 0.1	0.7± 0.1
6(NE)	2.8± 0.2	n.d.	3.3± 0.3	3.3± 0.0	3.6± 0.1
17	22.5± 1.8	20.5± 2.5	21.0± 1.3	21.8± 0.8	23.4± 2.5
5	34.8± 1.3	37.3± 2.2	44.3± 1.6	46.3± 1.6	48.5± 3.2
1	37.5± 1.6	38.4± 0.2	40.7± 2.3	44.7± 3.1	48.1± 3.7
13(NE)	38.4± 0.9	45.8± 1.7	44.3± 4.3	39.5± 1.4	47.5± 2.5
45	39.0± 1.8	40.0± 1.2	43.2± 1.1	38.5± 1.2	48.4± 2.5
52	74.7± 7.8	86.1± 5.4	83.0± 6.1	73.8± 8.5	n.d.
51	94.8± 6.1	120.4± 3.8	121.3±14.6	106.5± 5.9	133.7±10.6
7	112.6± 8.9	125.5± 6.2	143.6±14.9	163.0± 9.8	155.8±14.4
10	391.6±22.2	n.d.	361.3±19.0	383.2± 7.2	411.4±14.9
59	354.8±33.4	376.9±23.4	358.7±33.2	360.0±34.7	438.0±35.4

Note:

- (a) Samples that were not etched, using 10% HF acid for 40 minutes, are indicated with an (NE).
- (b) All equivalent doses are in grays. Multiple disc samples were irradiated using the Daybreak irradiator (3.81 Gy/min), single aliquot samples using the Risø irradiator (1.24 Gy/min).

### 7.4.5 Conclusions

On the basis of the results in table 7.3.4 (and figure 7.3.4) it is suggested that the single aliquot additive dose method, using luminescence correction (method B, see section 7.3.1), is able to give accurate and precise ED determinations for samples with EDs ranging from less than 10 to approximately 100 Gy. The value of 100 Gy is not significant in itself. The relevant fact is that for this particular suite of samples from New Zealand their response to irradiation becomes significantly non-linear, when attempting to date samples using an additive dose method, when they have EDs larger than approximately 100 Gy. For samples with EDs greater than 100 Gy, luminescence correction method B tends to underestimate the ED.

The dose correction method described in section 7.4.1, unlike luminescence correction method B, does not assume a constant luminescence efficiency per unit dose, and is thus able to accurately correct single aliquot additive dose data even for samples whose response to dose is highly non-linear. From table 7.4.4 (and figure 7.4.4) it can be seen that the dose correction method can be used to provide accurate and precise ED determinations for samples with EDs ranging from less than 10 Gy to at least 400 Gy. It is this method that is applied to a second suite of samples from New Zealand in chapter 8.

# **CHAPTER 8: Application of the additive dose single aliquot method to dating of Koputaroa phase dunes**

## 8.1 The Koputaroa dune phase

Cowie (1963) defined four recent dune phases in the Manawatu and Horowhenua regions of New Zealand. From youngest to oldest these were named Waiterere, Motuiti, Foxton and Koputaroa. The Koputaroa dunes were distinguished on the basis of the soil development on their surface (described in Cowie 1968), by the fact that most were located on the Tokomaru marine terrace, a raised marine terrace believed to date from the last interglacial (Hesp and Shepherd 1978), and the presence at some sites of Kawakawa tephra within the dune sand.

Although the presence of Kawakawa tephra in several sections fixes a single time when these dunes were active (24 ka), there is little evidence available to indicate the duration of dune activity before or after this time. The aim of the work presented in this chapter is to use the single aliquot additive dose method of luminescence dating to provide further evidence relating to the timing of dune activity as recorded in sections containing dunes that have previously been classified as belonging to the Koputaroa dune phase (Gibbs 1957, and Cowie 1963).

## 8.2 Description of samples analyzed

Samples were taken from every exposure of the Koputaroa dunes which has been discussed in the literature, except for one of the sites sampled by Shepherd (1985) which could not be relocated. As part of this analysis, samples GDNZ 1, 5, 13 and 45 were analysed by both multiple and single aliquot methods. These sites are described in section 5.2 and the multiple aliquot results discussed in section 5.5. Brief descriptions of the sites are given below (see figure 8.2 for their locations), and further information is given in appendix I.

### GDNZ 13, 14 and 15: Koputaroa road

Cowie (1963) described a section at this location with a basal purplish, black peaty silt, and two sand units separated by Kawakawa tephra and a clay loam (see appendix I.1 for discussion of the term). No work has been done on the site since that by Cowie (1963) and Fleming (1972) because the section had not been relocated. Fieldwork in 1988 enabled a

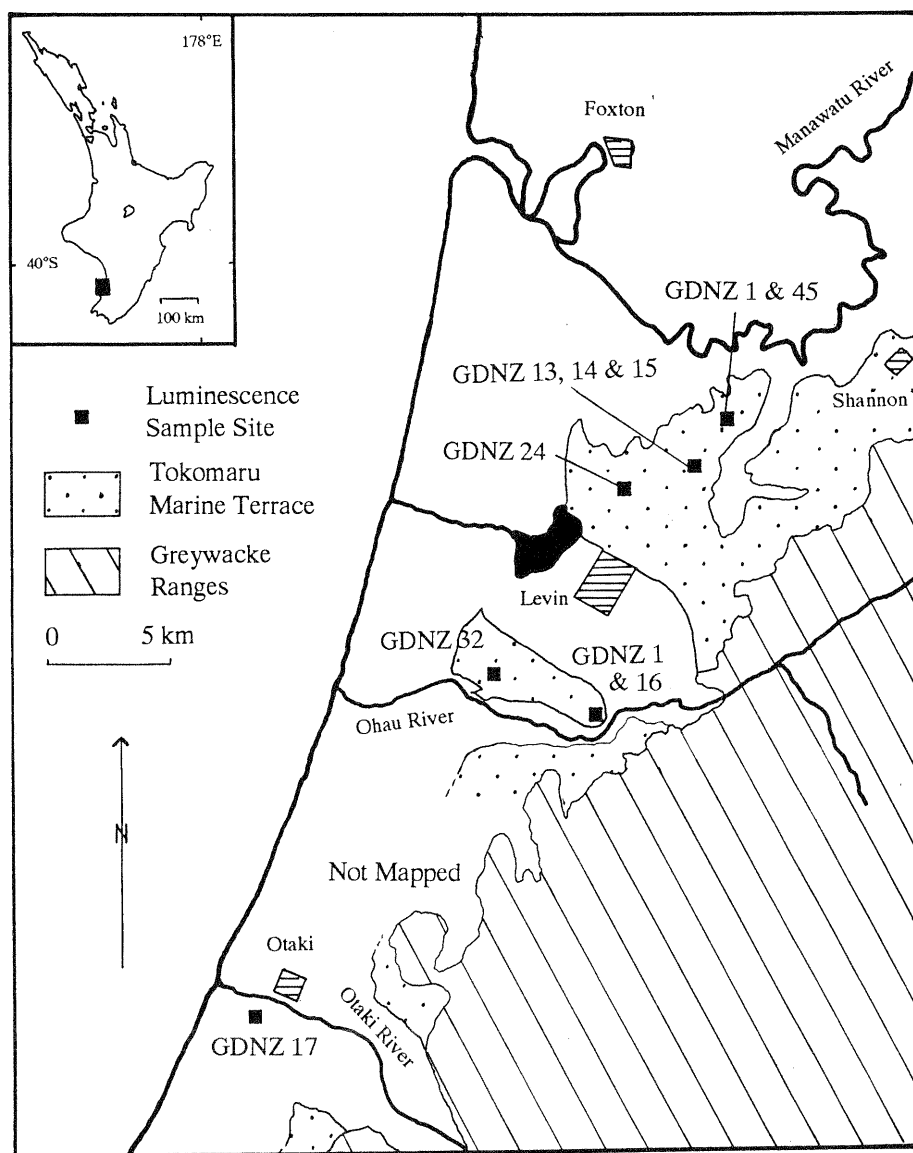


Figure 8.2: Map showing the location of samples collected for luminescence dating from Koputaroa phase dunes (and sample GDNZ 17). The extent of the Tokomaru marine terrace is also shown for the areas in which information is available (from Hesp and Shepherd 1978, Shepherd 1985 and Palmer *et al.* 1988).

very similar section to be uncovered within 100m of that described by Cowie (1963). The basal peaty silt was dated by Fleming (1972) at  $35,000 \pm 1,700$   $^{14}\text{C}$  yrs BP (N.Z.522). Overlying the basal silt is 1.6m of sand (GDNZ 14 was collected from 0.4m above the basal silt, and GDNZ 13 from 0.3m below the top of the unit), 0.15m of Kawakawa tephra, 0.4m of mottled clay loam, and finally 2m of sand (GDNZ 15 was taken from 0.3m above the clay loam).

#### GDNZ 16: McLeavy road

GDNZ 16 was taken from the same site as that from which GDNZ 1 was taken (see section 5.2 and appendix I). The section consists of dune sands resting immediately upon Kawakawa tephra, with a clay loam below it. GDNZ 1 was taken from about 0.3m above the tephra. Further dune sand occurs below the clay loam, and GDNZ 16 was taken 0.5m below the contact between the two units.

#### GDNZ 24: Heatherlea

Subdued dune forms occur over an area of several hundred square metres south of State Highway 1 (S.H.1) just north of Levin. The road has cut into one of these dunes giving a section approximately 2.5m in height. Sample GDNZ 24 was taken 1.3m below the dune surface.

#### GDNZ 32: Papaiatonga Lake road

Dune ridges, up to 4 metres in relief, occur in an area of complex topography near Lake Papaiatonga. Gibbs (1957) mapped part of this area as belonging to the Koputaroa soil association, but no subsequent work has been undertaken on this area. GDNZ 32 was taken from approximately 2.5m below the crest of the dune where it was cut by the road.

### 8.3 Results from single aliquot analysis

All samples listed above had their ED determined using the single aliquot, additive dose, method. Table 8.3(a) compares the EDs calculated using both luminescence correction method B, and the dose correction method outlined in section 7.4.1. Normally, six aliquots were used to determine the preheat response curve, and eighteen discs to determine the ED. The results from the two correction methods are very similar, though the dose correction method gives slightly larger EDs for the two samples with larger EDs (GDNZ 14 and 16).

On the basis of the comparison between the multiple aliquot and single aliquot methods described in section 7.3.4 and 7.4.4, the dose corrected results are preferred. Table 8.3(b) lists the dosimetry and ages for the nine samples from the Koputaroa dune phase and figure 8.3 shows the stratigraphic relationships between the samples.

Table 8.3(a)

Comparison of equivalent doses determined for samples from the Koputaroa dune phase using the single aliquot additive dose method using luminescence correction method B, and the dose correction method.

<u>Sample (GDNZ)<sup>(a)</sup></u>	<u>Single Aliquot (Luminescence Correction) ED (Gy)<sup>(b)</sup></u>	<u>Single Aliquot (Dose Correction) ED (Gy)<sup>(c)</sup></u>
1	37.9±1.7 (17)	37.5±1.6 (17)
5	34.5±1.2 (19)	34.8±1.3 (19)
13	37.7±0.9 (17)	38.4±0.9 (17)
14	87.8±5.8 (18)	92.5±6.1 (18)
15	35.4±0.7 (16)	35.7±0.8 (16)
16	83.2±3.1 (18)	87.0±3.7 (18)
24	27.2±0.9 (18)	27.2±0.9 (17)
32	32.4±1.2 (18)	32.8±1.2 (18)
45	38.5±1.9 (18)	39.0±1.8 (18)

Notes:

- (a) Samples 1, 5 and 45 had been etched using HF acid. The remaining samples were unetched and were 180-211µm in diameter.
- (b) Equivalent dose calculated using luminescence correction method B. Errors for the EDs are determined as one standard deviation of the mean of the individual determinations. The number of determinations used for the mean and standard deviation is given in brackets.
- (c) Equivalent dose calculated using the dose correction method. Errors for the EDs are determined as one standard deviation of the mean of the individual determinations. The number of determinations used is given in brackets.

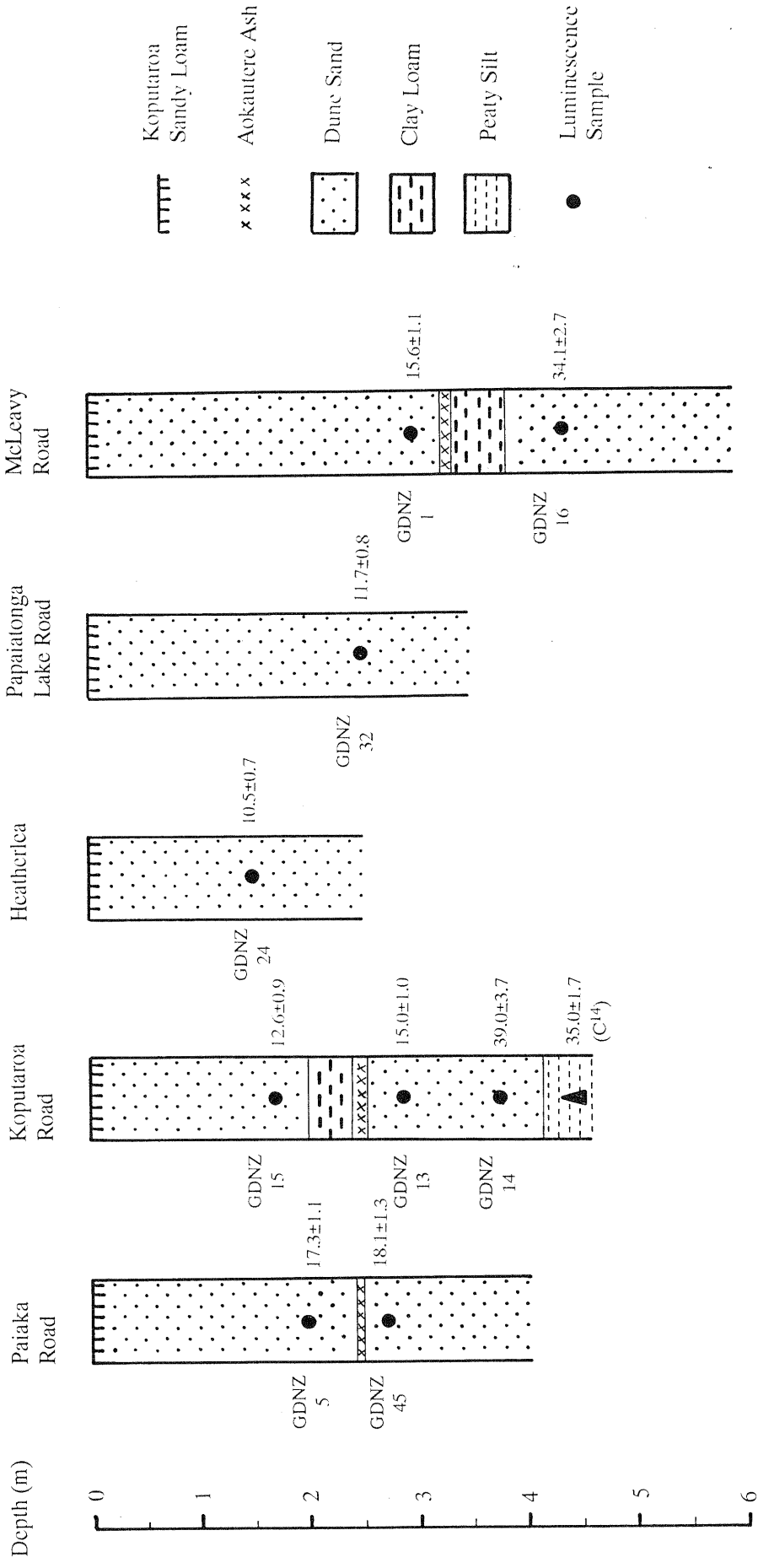


Figure 8.3: Luminescence ages for samples collected from dunes of the Koputaroa dune phase. All ages are given in ka.

Table 8.3(b)

Equivalent doses, dose rates, and ages for samples collected from the Koputaroa dune phase.

<u>Sample</u> (GDNZ) <sup>(a)</sup>	<u>Single Aliquot</u> <u>Additive Dose</u> ED (Gy) <sup>(b)</sup>	<u>External Dose</u> Rate (Gy/ka) <sup>(c)</sup>	<u>Internal Dose</u> Rate (Gy/ka) <sup>(d)</sup>	<u>Age</u> (ka)
1	37.5±1.6	1.929±0.110	0.475±0.070	15.6±1.1
5	34.8±1.3	1.710±0.098	0.296±0.044	17.3±1.1
13	38.4±0.9	2.069±0.138	0.487±0.061	15.0±1.0
14	92.5±6.1	1.884±0.150	0.490±0.061	39.0±3.7
15	35.7±0.8	2.487±0.183	0.336±0.042	12.6±0.9
16	87.0±3.7	2.031±0.157	0.522±0.065	34.1±2.7
24	27.2±0.9	2.017±0.134	0.573±0.071	10.5±0.7
32	32.8±1.2	2.410±0.162	0.400±0.050	11.7±0.8
45	39.0±1.8	1.750±0.111	0.408±0.051	18.1±1.3

Notes:

- (a) Samples 1, 5 and 45 had been etched using HF acid prior to ED determination. The remaining samples were unetched and were 180-211µm in diameter.
- (b) The single aliquot additive dose measurements have been derived using the dose correction method. Data are from table 8.3(a).
- (c) External dose rates are taken from table 5.3.3 and include the cosmic ray dose.
- (d) Internal dose rates are taken from table 5.3.4(a) and do not include any internal alpha dose.

The ages for the samples taken from immediately below the Kawakawa tephra (samples GDNZ 13 and 45), are younger than the 24 ka geological age estimate for the tephra (section 2.1.2). This may in part relate to underestimation of the water content at the two sites concerned (see discussion in section 5.5). Two other samples were taken from stratigraphically below the tephra. Sample GDNZ 16 was taken 0.5m below a clay loam, in the upper part of which the Kawakawa tephra can be seen. This gave an age of 34.1±2.7 ka and shows that this clay loam was deposited sometime between then and 24 ka. At Koputaroa road, sample GDNZ 14 was taken from 0.4m above a basal peaty silt that had previously yielded a radiocarbon age of 35±1.7 ka B.P (Fleming, 1972), and 1.2m below the Kawakawa tephra. The luminescence age for GDNZ 14 was 39.0±3.7 ka. Sample GDNZ 13, from the same section, underestimated the expected age, and it is thought that this was caused in part by uncertainties in the water content. Altering the water content used for calculation of the dosimetry from 10%, as used above, to 30% changes the calculated age from 15.0±1.0 ka to 18.6±0.9 ka. Similar problems may have affected GDNZ 14, and so the age of 39.0±3.7 ka should be viewed as a minimum age estimate. All the remaining samples gave luminescence ages in the range 10.5-17.3 ka, and this indicates that substantial dune mobilization occurred post-dating deposition of the Kawakawa tephra.

## 8.4 Implications for the age and duration of the Koputaroa dune phase

The Koputaroa dune phase has previously been defined primarily on the basis of the soil that has developed on the surface of the dunes (Koputaroa sandy loam described by Cowie 1963, 1968). Samples GDNZ 1, 5, 15, 24 and 32 were taken from sand units on top of which this type of soil had formed. At Koputaroa road and Paiaka road luminescence samples taken from below the Kawakawa tephra (GDNZ 45 and 13) underestimate the expected age of 24 ka, but the superposition of tephra upon sand indicates that at these sites the dunes were active when the Kawakawa tephra was deposited. At the McLeavy road and Paiaka road sites there is evidence that dune deposition was occurring immediately after deposition of the Kawakawa tephra (24 ka), and samples GDNZ 1 and 5 ( $15.6 \pm 1.1$  ka and  $17.3 \pm 1.1$  ka) were collected from directly above the tephra. At Koputaroa road the presence of the clay loam overlying the Kawakawa tephra indicates that there was a pause in dune activity at some time after 24 ka, but that it restarted at some time prior to  $12.6 \pm 0.9$  ka (GDNZ 15) before finally stabilising and allowing soil formation to occur. At Heatherlea and Papaiatonga Lake road the dunes were active at  $10.5 \pm 0.7$  ka and  $11.7 \pm 0.8$  ka respectively. These results show that dunes upon which the Koputaroa sandy loam has developed were active, possibly episodically, during the period immediately prior to 24 ka to about 10 ka. A luminescence age of 9.1 ka was obtained for sample GDNZ 17 from Te Waka road and suggests that the dunes preserved there should be considered as representative of the same extended dune phase as those strictly called Koputaroa dune phase.

At McLeavy road sample GDNZ 16 was taken from a sand unit below the Kawakawa tephra that is separated from it by 0.5m of clay loam. GDNZ 16 gives a luminescence age of  $34.1 \pm 2.7$  ka and indicates that there is no record of dune activity at this site for a period of 10 kyrs from 34 ka to 24 ka. At Koputaroa road GDNZ 14 was taken from the same unit as GDNZ 13 (immediately underlying the Kawakawa tephra), but only 0.4m above the basal peaty silt described by Cowie (1963). GDNZ 14 gives a luminescence age of  $39.0 \pm 3.7$  ka, almost 25,000 years older than GDNZ 13, 0.9m higher in the same unit. The sand grades in colour from grey near the base to a brownish-orange at the top, but there is no other basis on which to sub-divide this sand unit. A possible interpretation of the luminescence ages for GDNZ 13 and 14 is that the lower unit was deposited about 39 ka and that the upper part of the unit was mobilised at some time immediately prior to 24 ka prior to deposition of the Kawakawa tephra.

## 8.5 Conclusions

At the Koputaroa road and McLeavy road sites the luminescence ages indicate that dunes were active in the area between 39 and 34 ka. These were subsequently stabilised and no evidence of dune activity has been found until deposition of the Kawakawa tephra 24 ka. At all of the sites there is evidence of dune activity in the period following deposition of the tephra, with dates as young as 10.5 ka at Heatherlea and 9.1 ka at Te Waka road. Dune stabilisation occurred after this date and Koputaroa sandy loam developed on the surface of the dunes.

Age control for the Koputaroa dune phase has previously been limited to that provided by the occurrence of Kawakawa tephra interbedded with the dunes. The age of the tephra implies that the dunes were active at a time when eustatic sea level was at least one hundred metres below present (Chappell and Shackleton, 1986), and thus the coastline would have been at least 30km from the present location of the dunes (figure 2.1(b)). Cowie (1963) suggested that the sand for the dunes may have originated from "braided courses of rivers draining periglacial areas" rather than the coast which "would explain their limited extent" and their position relative to the coast at 24 ka. Shepherd (1985) showed that at least some of the sand in the dunes was of marine origin and suggested that the dunes may have resulted from the mobilisation of sands deposited during higher sea levels associated with interstadials. The luminescence ages presented here support this hypothesis, with initial deposition of sands prior to 35 ka, when eustatic sea levels frequently rose to less than 50m below the present level, and subsequent mobilisation in the period from 24 ka to 10 ka.

## CHAPTER 9: Conclusions

Three broad aims of this thesis were described in section 1.4. The conclusions reached as a result of study into each of these areas are discussed in sections 9.1 and 9.2 below. During the course of this work many results were obtained concerning the relationship between the IRSL and TL signals from potassium feldspars. These results are synthesised in section 9.3. Finally, some of the questions raised by the research in this thesis are highlighted in section 9.4 as topics that may be of interest for future study.

### 9.1 Luminescence dating using potassium feldspars

This part of the thesis was divided into two sections: the first used standard methods of ED determination to date a suite of samples which had independent age estimates, while the second applied a single aliquot method to dating samples from Koputaroa phase dunes, after establishing the validity of this new method.

#### 9.1.1 Comparison of luminescence age estimates with those derived from other methods

Chapter 5 was concerned with the application of standard multiple aliquot methods of equivalent dose determination to samples of dune sand that had some form of independent age control in an attempt to test the validity of luminescence dating methods based upon using potassium feldspar as the dosimeter. The independent age control was based upon other dating methods and hence was open to criticism in its own right (see sections 2.1.3, 5.2 and 5.5). Good agreement between the luminescence ages and the independent age estimates was found for the samples younger than 30 ka and one of the samples from the last interglacial (GDNZ 7). The luminescence ages for samples GDNZ 51 and 52 were younger than the age estimates proposed by Palmer (pers.comm.) but the basis of these independent age estimates was insufficient to state categorically that the luminescence ages were underestimated. However, the remaining two samples (GDNZ 10 and 59), which are thought to be aged 300-350 ka, seemed to significantly underestimate their expected ages. The most likely explanation lies in long-term fading of the luminescence signal as described by Mejdahl (1988, 1989), which would not be detected in samples younger than 130 ka. Overall the luminescence ages for the samples younger than 130 ka are in reasonable agreement with their expected ages, while those aged 300-350 ka are underestimated by about 30%.

Two forms of luminescence measurement, TL and IRSL, were made on all of the samples and no systematic differences were observed in the EDs produced. This implies that within the errors of the data presented in table 5.4.5, and over the age range represented by these samples, no systematic difference could be seen between the stability of the TL and IRSL signals measured. The rapid bleaching of the IRSL signal was seen to produce EDs that varied by less than 2% when using bleaching of 6, 60 and 600 minutes of exposure to the SOL2 solar simulator, while the TL EDs for the same aliquots varied typically by 20%. Additionally, the one modern sample studied gave ages of  $2.0 \pm 0.3$  ka and  $2.1 \pm 0.2$  ka using TL, but only  $27 \pm 19$  years and  $206 \pm 34$  years using IRSL. Thus it should be possible to reduce the uncertainty in the residual level by using IRSL measurements, and as a result obtain dates on younger material than would be possible using TL measurements. As well as using two forms of luminescence measurement, two different methods of ED determination were used; additive dose and regeneration. No systematic differences were observed between these two methods of ED measurement.

### 9.1.2 Dating Koputaroa phase dunes

Chapter 8 applied the single aliquot additive dose method, using dose correction, to a suite of samples from various sites that have previously been classified as belonging to the Koputaroa dune phase. The presence of the Kawakawa tephra (Aokautere ash) within several sections through Koputaroa dunes had previously been the primary age control on when these dunes were active. A maximum age limit for the dunes was set by their occurrence upon the Tokomaru marine terrace (believed to be last interglacial in age, Hesp and Shepherd (1978)). The luminescence ages showed that at two of the sites studied dunes had been active between 34 and 39 ka, but that there was no evidence for any dune activity between 34 ka and 24 ka when the Kawakawa tephra was deposited. Following deposition of this tephra, dune activity at the various sites studied seems to have occurred, perhaps episodically, until as recently as 10 ka. The results are interpreted as showing that the group of dunes in the Manawatu and Horowhenua regions classified as belonging to the Koputaroa dune phase were first active between 39 and 34 ka. There is no record of dune activity until 24 ka, when the Kawakawa tephra was deposited, and dune activity then continued until 10 ka before dune stabilisation occurred and formation of the Koputaroa sandy loam began.

## 9.2 The use of single aliquot methods for equivalent dose determination

Standard methods of equivalent dose determination are very labour intensive and time consuming. Chapters 6 and 7 described attempts to reduce the effort involved in ED determination by using a single aliquot for all the measurements (made possible because IRSL measurements are effectively non-destructive) and by using the computer controlled facilities of the Risø automated TL/OSL reader to reduce the amount of operator time required.

The regeneration method initially outlined in chapter 6, using the IR diodes within the reader to reduce the luminescence signal to a residual level between each luminescence measurement, suffered from changes in the luminescence sensitivity of the sample. This is thought to relate to the fact that although IR exposure is able to remove the majority of the IRSL signal, it leaves the majority of the TL signal intact. As successive irradiations are given to the aliquot the trapped charge (as probed by a TL measurement but not affected by exposure to IR) increases, and this leads to changes in the luminescence sensitivity (including the IRSL sensitivity) of the sample to subsequent irradiation.

Attempts to reduce the trapped charge population by bleaching using the SOL2 solar simulator led to a reduction in the degree to which the sensitivity of an aliquot changed, but was unable to eradicate the effect completely. Additionally, the need to transfer the samples from the Risø reader to the SOL2 solar simulator and back again increases the amount of operator time required and reduces the speed with which samples can be processed, negating the initial aim of this type of approach.

Heating the aliquots to 450°C removes the trapped charge within the crystal and it was found that after the first heating of the aliquot the sensitivity did not change after subsequent heating cycles (section 6.8.1). This type of approach is obviously not applicable to samples derived from unheated sediments, but is extremely useful as a method for inter-calibrating between radioactive sources.

In chapter 7 a single aliquot method based upon the additive dose approach was studied. Short IRSL measurements can be made after each irradiation that do not appreciably reduce the trapped charge population. However, it is essential to preheat the aliquot prior to each luminescence measurement, and any preheat used will inevitably remove part of the stable luminescence signal as well as all the unstable signal. The effect of the preheat can be characterised for each sample by repeated preheating and IRSL measurement of a group of

aliquots with no irradiation between each step. This characterisation of the reduction of IRSL signal due to each preheat can then be used to correct an additive dose data set in one of three ways. Two types of correction (designated luminescence correction A and B) view the preheat as removing part of the luminescence signal and calculate an increase in the luminescence signal measured at each point, while the third type of correction (dose correction) views each preheat as being equivalent to a 'negative dose', and reduces the value of the total dose against which the luminescence signal is plotted. The two luminescence correction methods were found to have problems. However, the dose correction method gave similar EDs to standard multiple aliquot methods for the suite of samples from New Zealand ranging in age from modern to 350 ka.

### 9.3 Characteristics of the infrared stimulated luminescence signal from potassium feldspars

The discovery that feldspars have a peak in their stimulation spectrum between 800 and 1000nm (Hütt *et al.* 1988, and Bailiff 1992) has enabled optically stimulated luminescence measurements to be made on feldspars using relatively simple equipment based on the use of IR emitting diodes (Bailiff and Poolton, 1989 and Spooner *et al.*, 1990). During the course of the work described in this thesis several experiments have been undertaken into the behaviour of the IRSL signal, and the relationship of this signal to that seen using TL measurements.

All the experiments have been undertaken on potassium rich feldspars separated from New Zealand dune sands, and the luminescence has been detected using a Corning 5-58 and Schott BG-39 filter in combination. The results of these experiments, together with their implications, can be summarised as follows:-

- a) The most fundamental difference between the TL and IRSL signals from potassium feldspars is in their response to exposure to light, be it IR (figure 6.6.2), green light (figure 6.6.3) or the broad wavelength emission from the SOL2 solar simulator (table 5.4).
- b) Raising the temperature of the sample enables a larger IRSL light sum to be released (figure 6.5.2(c)). This implies that at higher temperatures either a larger population of traps is being probed, or more of the trapped charge that is released results in luminescence. Figures 6.5.1(c) and (d) show that even after long exposure to IR at room temperature, and reduction of the IRSL signal as measured at 50°C to a negligible level, a substantial IRSL

signal can be obtained when the sample is held at 200°C. This suggests that a larger trapped charge population is probed when the sample is held at higher temperatures.

c) The TL signal is reduced by exposure of the sample to IR. However, the amount of the TL signal that is removed by exposure to IR does not vary with the temperature at which the sample was held during the exposure to IR (figure 6.5.3). Exposure of a sample to 10s of IR reduces the TL signal by 10%, and longer exposures (up to 6000s) do not reduce the TL signal any further. After 10s exposure to IR 32% of the IRSL signal has been removed but after 6000s exposure over 99% has been removed (figure 6.6.2).

These results can be interpreted in three ways. The first possibility is that the production of an IRSL signal, at room temperature, is very efficient compared with the generation of a TL signal at 250-400°C. Thus although there seems to be good evidence that in both the circumstances described above the production of an IRSL signal does not have an effect upon the TL signal, it may be that the magnitude of the effect is so small as to be unnoticeable given the errors in the TL measurements. The second possible interpretation is that only a small proportion of the TL traps are sensitive to IR. This seems very likely given the evidence described above, and does not preclude either of the other two possibilities. The third possible explanation is that exposure of the sample to IR, and the consequent generation of an IRSL signal, causes a reduction in the number of radiative recombination centres and that this is the cause of the reduction in the TL signal observed. A logical follow-on to this argument is that the trapped charge responsible for the TL signal is not directly affected by exposure to IR at all and that the IRSL and TL signals are probing totally separate populations of trapped charge.

d) The IRSL signal from an aliquot of potassium feldspar increases linearly with sample temperature from 50 to 200°C (figure 6.5.1(a)). If the sample is preheated prior to this analysis, the temperature range over which this increase occurs can be extended to 50 to 250°C (figure 6.5.1(b)). Irradiating the sample prior to analysis, producing a large TL peak at 180°C, does not affect this linear increase in IRSL signal with temperature. Pulse annealing of natural and irradiated aliquots shows that IRSL measurements on the two groups stimulate a similar distribution of traps, although the irradiated aliquots have a small shoulder in their trap depth distributions at 220°C (see figure 6.6.4(b)). These results imply that there is not an IRSL signal associated with the large, thermally unstable, TL peak at 180°C that is observed after irradiating a sample. However, there is a small IRSL signal seen at 220°C in the trap depth distribution of an aliquot that has been irradiated which is not seen in natural samples (figure 6.6.4(b)).

e) Previously published data for potassium feldspars show that the IRSL emission spectra, measured at room temperature, is very similar to the TL emission spectra integrated over the range 250-400°C (Huntley *et al.*, 1988, 1991). This implies that similar recombination centres are being used in the two processes. Figure 4.7.4 shows that for a set of aliquots receiving various preheat treatments there is a good relationship between the IRSL signal from an aliquot and its TL signal (0-450°C), provided that the sample does not have a significant TL signal below 250°C. This implies that the trapped charge populations giving rise to the two luminescence signals are responding to the preheating in similar ways, when allowance is made for the fact that there is no IRSL signal from trapped charge associated with the 180°C TL peak. This is also implied by the pulse annealing results (figure 6.6.4(b) and (c)) where the eviction of the TL and IRSL signals follow very similar patterns with the exception of the trapped charge associated with the 180°C TL peak. All of this evidence would suggest that the two luminescence signals use the same recombination centres and respond in a similar manner to preheating and pulse annealing.

Two fundamental questions arise from this work about the nature of the IRSL signal from potassium feldspars. The first is whether the trapped charge population that is responsible for the IRSL signal is different from that which gives the TL signal or whether it is just a sub-set of it. If it is considered that the IRSL signal arises from a trapped charge population that is a sub-set of that giving the TL signal, then the second question is why are some traps capable of yielding an IRSL signal and some not.

On the basis of the evidence in figure 6.6.2, as discussed in section (c) above, it is thought that the majority of the trapped charge responsible for the IRSL signal does not give rise to a TL signal, under the measurement conditions used here. However, the similarities in the response of the IRSL and TL signals to preheating, in their emission spectra and in their pulse annealing characteristics, suggests that some relationship may exist between the two trapped charge populations, though the nature of this is unclear at present.

## 9.4 Directions for further study

Many potential avenues of research are suggested by the results obtained in this thesis. Listed below are several topics that may be of interest for future study, with particular reference to dating applications.

a) This thesis has shown the feasibility of using a single aliquot for the determination of the ED of a sample. A logical extension of this technique would be to use the method to

determine EDs for aliquots that included only a single grain of the sample. This would permit the analysis of the relationship between ED and mineralogy, luminescence brightness and in particular internal alpha and beta dose rates.

b) Several 'rapid' methods of ED determination have been described in chapters 6 and 7. These allow EDs to be determined far more quickly than possible using standard multiple aliquot methods. However they still involve the separation of a potassium-rich feldspar fraction from a sample, which is a time consuming procedure in itself. It is thought that IR is incapable of stimulating a luminescence signal from quartz (Spooner and Questiaux 1989 and Short and Huntley 1992) and that the majority of the IRSL signal from a bulk sample originates from feldspathic minerals. Using IRSL measurements it may be possible to develop a rapid method of ED determination that does not require the separation of a specific mineral fraction. This would be a major advance in the application of luminescence dating to geological problems, allowing the processing of large numbers of samples in a relatively short time.

c) Determination of the internal alpha dose rate of potassium-rich feldspars is hindered at present by two problems. Firstly, relatively few measurements of the alpha efficiency have been made. Secondly, there is very little information about the uranium and thorium concentrations within potassium-rich feldspar grains (table 5.3.4(b)). This problem is compounded by the lack of information about the distribution of any uranium and thorium that may be detected within the separated potassium-rich feldspar fraction (see discussion in section 5.3.4). Any work that may be able to shed light on this problem would be extremely valuable.

d) Determination of luminescence ages for a larger number of samples from the Koputaroa dune phase may help further define the episodes of aeolian activity in the area, and enable these dunes to be used as a proxy palaeoclimatic record of enhanced wind strength.

e) Testing of the single aliquot additive dose method of luminescence dating has shown that it can give accurate dates in the age range from 0-130 ka when a dose correction procedure is used. This method could now be applied to dune sands, in this age range, found on fragments of raised marine terrace in the area west of Wanganui, the ages of which, as determined by amino-acid racemization and altitudinal correlations, are uncertain.

## **Appendix I: Sites from which samples were collected for luminescence dating**

Brief descriptions are given below for the various sites from which samples were taken for luminescence dating. The samples are arranged in order of sample number as listed below:-

<u>Section</u>	<u>Sample Numbers</u>
AI.1: McLeavy road	GDNZ 1 & 16
AI.2: Paiaka road	GDNZ 5 & 45
AI.3: Manawatu River section	GDNZ 6
AI.4: Penny road	GDNZ 7
AI.5: Mt.Curl Tephra type site	GDNZ 10
AI.6: Koputaroa road	GDNZ 13, 14 & 15
AI.7: Te Waka road	GDNZ 17
AI.8: Hokio Beach	GDNZ 21
AI.9: Heatherlea	GDNZ 24
AI.10: Papaiatonga Lake road	GDNZ 32
AI.11: Whenuakura River	GDNZ 51 & 52
AI.12: Rangitatau East road (Bushy Park Section)	GDNZ 59

### AI.1: McLeavy road (NZMS 1 N152 795974)

South of Levin a NE-SW trending dune ridge has been cut through by McLeavy road. To the south-east the dune has been eroded by lateral erosion of the Ohau river. The road lies approximately 4 metres below the dune crest. On the south-west side of the road a section has been exposed in which 3.25m of medium brown sand overlies 0.1m of Kawakawa tephra and 0.5m of grey clay loam. The clay loam lies upon at least 2.1m of medium light brown sand with iron mottling. Sample GDNZ 16 was taken from within this lower sand unit 0.5m below the clay loam, while sample GDNZ 1 was taken from 0.3m above the Kawakawa tephra in the upper sand unit. The term 'clay loam' has been used extensively by Cowie (1963) and describes a clay and silt-rich unit which also contains a small proportion of sand sized material. The term is normally used by soil scientists, but is used in this thesis for compatibility with the descriptions given by Cowie (1963).

### AI.2: Paiaka road (NZMS 260 S25 078683)

At this site, first described by Cowie (1963), a NE-SW trending dune ridge lies on the Tokomaru marine terrace, which is thought to be last interglacial in age (Hesp and Shepherd, 1978). Paiaka road cuts through the dune exposing up to 4m of dune sand. In one exposure Kawakawa tephra occurs within the dune as a 2cm thick band of fine grey ash. The tephra can be traced laterally over a distance of 5m and appears to have been deposited over a low ridge of sand (at least 1m in height). There is no indication of any weathering above or below the tephra to suggest that there was any hiatus before or after deposition of the tephra. Sample GDNZ 5 was taken 0.5m above the ash and GDNZ 45 from 0.3m below.

### AI.3: Manawatu River section (NZMS 260 S24 147814)

GDNZ 6 was taken from a mafic rich dune sand between two peat units in a section exposed by river erosion. Radiocarbon ages for the peats are 1860±65 years BP and 2380±110 years BP (NZ5221 and NZ5220 respectively, from Shepherd and Lees (1987) corrected for secular effects). GDNZ 6 was taken from the middle of the 0.5-0.6m gap between the two peats (figure AI.3).

### AI.4: Penny road (NZMS 1 N148 990 486)

Separating the flood plains of the Rangitikei and Manawatu rivers, Mt. Stewart has been uplifted by block displacement of the basement. Twenty metres south of the intersection of State Highway 3 and Penny road a road cutting, 2m in height, has exposed a dune sand underlying three loess units (Berryman and Hull, 1984). Half a metre of well cemented sand is exposed at the base of the section, below 1.5-2m of loess. The age is estimated only by counting loess units overlying the sand. Porewa, Rata and Ohakea loess overlie the dune sand, and Aokautere ash has been found within Ohakean loess at this site. Berryman and Hull (1984) concluded that the dune sand was deposited in the last interglacial.

### AI.5: Mt. Curl Tephra type Site (NZMS 260 S22 194344)

Milne (1973) defined the type section for the Mt. Curl Tephra. At the site a slightly mafic dune sand (Brunswick Dunesand) overlies Mt. Curl Tephra, though there is some evidence of weathering in the upper part of the tephra implying a hiatus in deposition. Recent evidence has shown this tephra to be correlative with the Rangitawa Pumice and to have a fission track age of 350±40 ka (Kohn *et al.* 1992, section 2.1.3). The site is a complex one

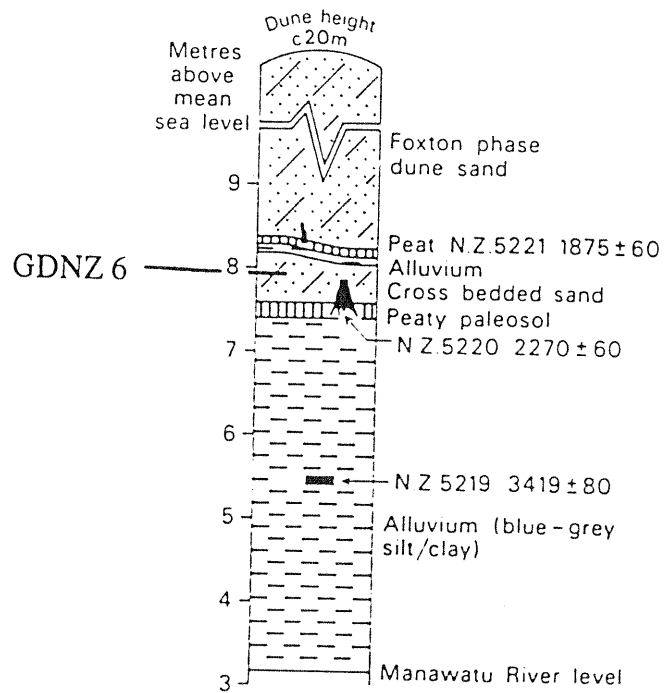


Figure A1.3: Stratigraphy at the Manawatu river section (from Shepherd and Lees, 1987) showing the location of sample GDNZ 6. Note that the  $^{14}\text{C}$  dates in the diagram are uncorrected (compare with text).

with intermittent exposure along a 150m length of road. The stratigraphy, and the nomenclature, as it was designated in 1988 are shown in figure AI.5. If the fission track age for the Mt. Curl Tephra produced by Kohn *et al.* (1992) is correct then the interpretation of this site may need to be altered. However, the relationship of the Brunswick Dunesand to the Mt. Curl Tephra is clear at the site. Sample GDNZ 10 was taken from the western end of the section, where a basal loess unit is overlain by 0.45m of Mt. Curl Tephra, 2m of Brunswick Dunesand and various loess units with tephra lenses amounting to a total sediment thickness of 5m. The sample was taken 1.5m above the Mt. Curl Tephra.

#### AI.6: Koputaroa road (NZMS 1 N152 833077)

This site, first described by Cowie (1963), lies approximately 2km south-west of the Paiaka road site. The site is exposed in a road cutting on the eastern side of Koputaroa road. It is impossible to determine whether the dune sand lies upon the Tokomaru marine terrace, as at the Paiaka road site, because the topography of the area has been altered by the cutting made for the Koputaroa road, construction of a group of houses on the western side of the road, and a cutting for the Wellington to Palmerston North railway which runs parallel to the Koputaroa road 15m to the east. A more complex sequence is exposed at this site, but once again Kawakawa tephra (Aokautere ash) occurs within a dune sand.

At the base of the section a purplish black peaty silt has been radiocarbon dated by Fleming (1972) at 35,000±1,700 yrs B.P. (NZ 522). This is overlain by 1.6m of medium sand passing from grey near the base to brownish-orange at the top. GDNZ 14 was taken 0.4m above the basal peaty silt and GDNZ 13 from 0.3m below the top of this sand unit. The unit is overlain by approximately 0.15m of Kawakawa tephra, which itself is overlain by 0.4m of mottled clay loam. Finally, the uppermost unit is a yellow and olive medium sand 2m in thickness. GDNZ 15 was taken from this sand unit 0.3m above the clay loam.

#### AI.7: Te Waka road (NZMS 260 R25 897457)

Dunes of shallow relief (2-3m) can be seen on an alluvial fan surface, south of Otaki, between State Highway One and Te Waka road. The alluvial fan, and the dunes, have been truncated at their seaward limit during the post-glacial sea level maximum (figure AI.7, Palmer *et al.*, 1988). Sample GDNZ 17 was taken from a 1.5m high exposure of dune sand on the easterly side of Te Waka road. Augering at this site showed that 3.1m of dune sand overlies fan gravels. The sample was taken 70cm from the crest of the dune where it is exposed in the road cutting.

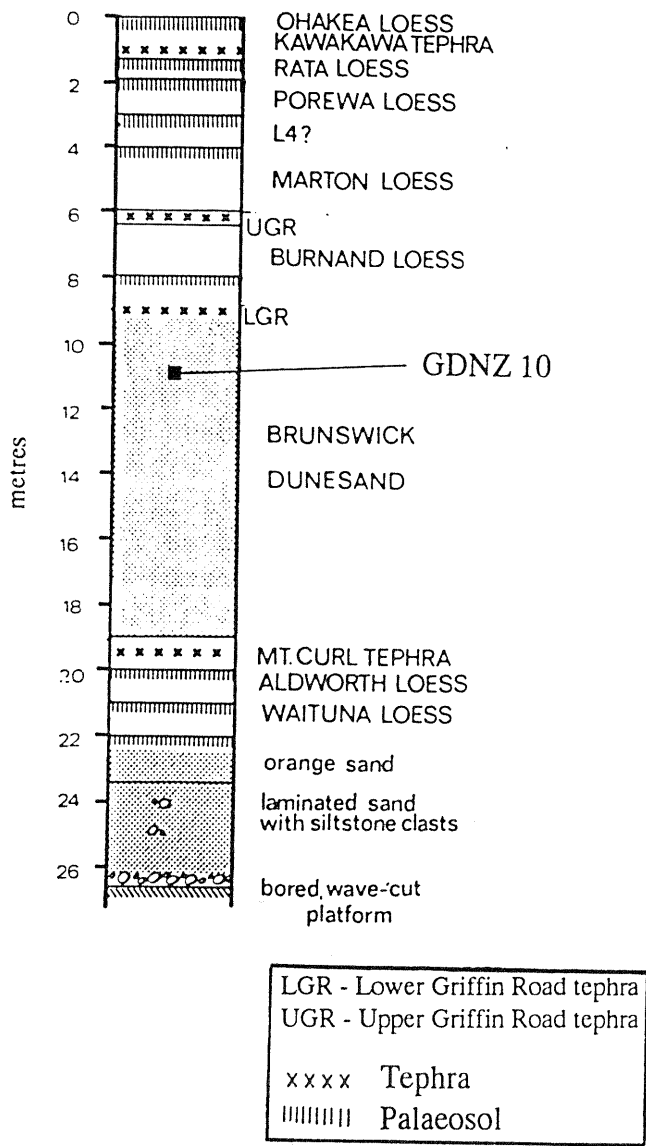


Figure A1.5: Stratigraphy at the Mt. Curl tephra type site (from Pillans 1988) showing the relative location of sample GDNZ 10.

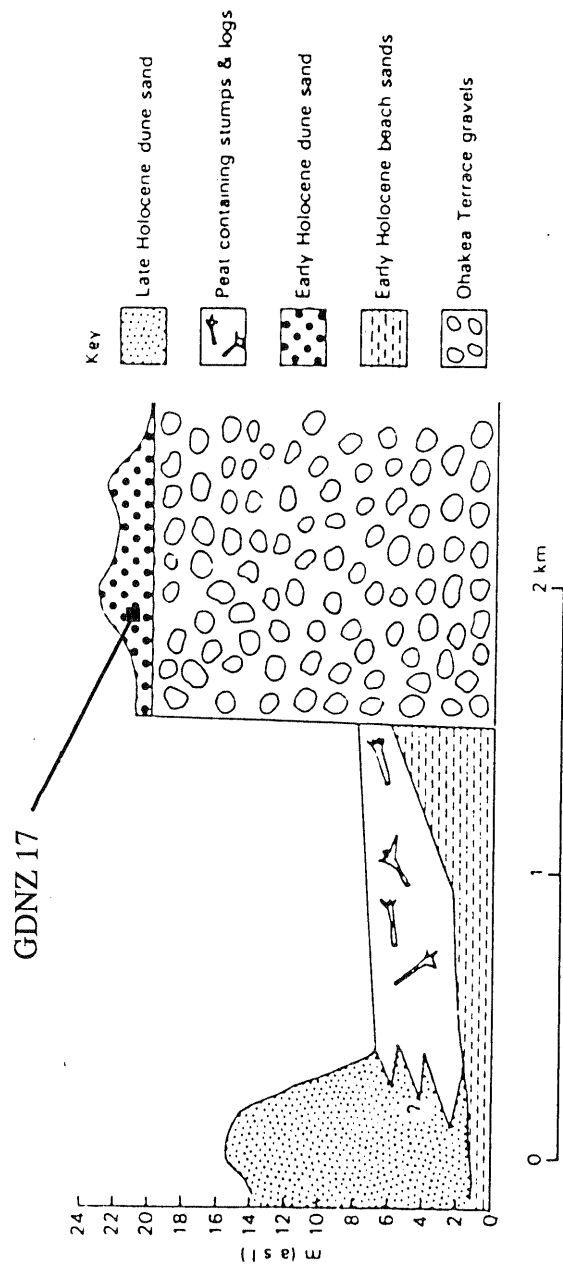


Figure AI.7: Schematic cross-section through the seaward end of the Ohakea surface showing the stratigraphic relationship of the dune sand sampled at Te Waka road (from Palmer *et al.*, 1988). The location of sample GDNZ 17 is shown.

### AI.8: Hokio Beach (NZMS 1 N152 706070)

GDNZ 21 was taken from a south facing active slip face of a modern dune ridge approximately 10m behind the high tide limit. As along all of the coastline of this part of New Zealand, the sand is grey to black in colour due to the high content of mafic minerals.

### AI.9: Heatherlea (NZMS 1 N152 810068)

Subdued dune forms (with less than 1m of relief normally) occur over an area of 1-2 square kilometres south of State Highway 1 just north of Levin. The road has cut into one of these dunes giving a section approximately 2.5m in height. Sample GDNZ 24 was taken 1.3m below the dune surface.

### AI.10: Papaiatonga Lake road (NZMS 1 N152 751992)

Dune ridges, up to 4 metres in relief, occur in an area of complex topography near Lake Papaiatonga. Gibbs (1957) mapped parts of this area as belonging to the Koputaroa soil association, but no further work has been undertaken on the area. Papaiatonga Lake road cuts through one of the dune ridges that trend NE-SW in this area. The sand is massively bedded with no indication of cross-bedding. Sample GDNZ 32 was taken from the section exposed to the north-east of the road, approximately 2.5m below the crest of the dune.

### AI.11: Whenuakura River (NZMS 260 Q22 423587)

Where the Whenuakura river has dissected the marine terrace a road cutting has been excavated to allow State Highway 3 to descend from the marine terrace to cross the river. The stratigraphy of the units covering the wave cut surface are exposed in the south side of the road cutting (figure AI.11). The wave cut surface is overlain by 1.5m of pebbly marine sand that grades up into a further 1-1.5m of mafic dune sand. GDNZ 51 was taken from 0.6m below the top of this sand unit. This is overlain by 0.5m of loess which is slightly weathered at its top. This is then covered by almost 3.5m of mafic dune sand, from which sample GDNZ 52 was collected (1.5-2m below the top of the unit), which is strongly weathered in its upper part. Over this lie three loess units with a total thickness of 3-3.5m.

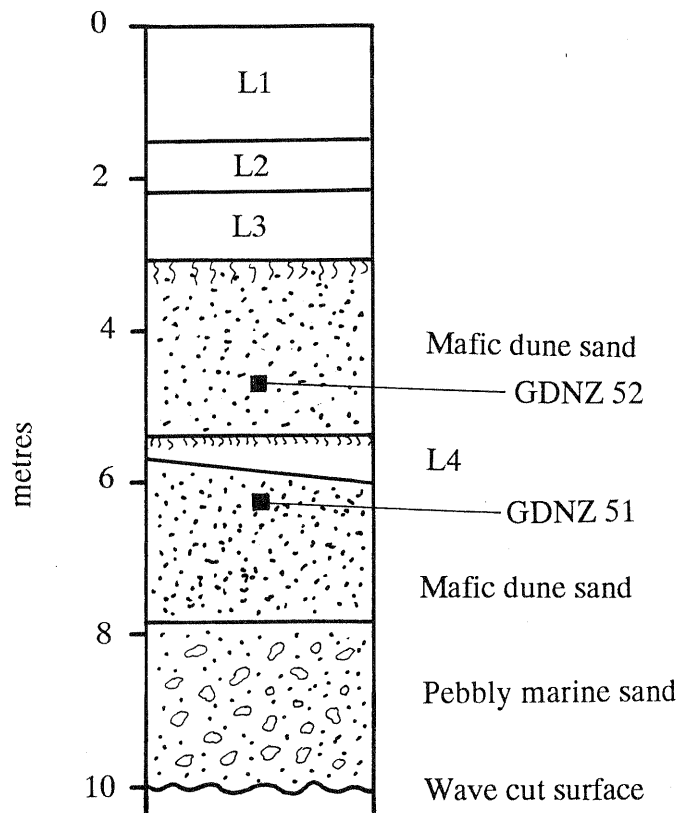


Figure AI.11: Simplified stratigraphy of the Whenuakura river section (Palmer pers. comm.) showing the locations from which samples GDNZ 51 and 52 were collected.

## AI.12: Rangitatau East road (NZMS 260 R22 754557) (Bushy Park Section)

A small road cutting on Rangitatau East road has exposed 4m of sand. Half a metre above road level a 5cm thick tephra unit occurs within a massively bedded mafic sand. A further 1-2m of sand overlies the tephra, and the top of the sand is marked by a chocolate coloured palaeosol. Sample GDNZ 59 was collected 0.6-0.7m above the tephra. The tephra is correlated with Rangitawa Pumice at the nearby site at Rangitatau East "by tephra mineralogy, loess stratigraphy and dune sand position in relation to tephra and loess" (Pillans, pers. comm.). No sign of weathering or any other indication of a hiatus was apparent above or below the tephra within the sand.

## Appendix II: Source Calibrations

Two  $^{90}\text{Sr}/^{90}\text{Y}$  beta sources were used for all the work in this study. One is mounted in a Daybreak automated irradiator unit, the other in the Risø automated TL reader. Samples were presented as monolayers of grains (normally 180-211 $\mu\text{m}$  in diameter) on aluminium discs approximately 0.5mm thick

### AII.1 Calibration against the Risø gamma source

Dr Vagn Mejdahl kindly provided three sub-samples of a Scandinavian feldspar (100-300 $\mu\text{m}$ ) irradiated in Risø using a  $^{60}\text{Co}$  gamma source. These had been annealed prior to irradiation to remove any TL signal. One batch had been given 20 Gy, another 40 Gy and the last batch was left unirradiated.

The unirradiated material was given a series of doses using the two beta sources in Aberystwyth. In this way, growth curves could be built up for each source, and the signal given by the gamma irradiated material compared with that from the beta sources. Table AII.1(a) lists the number of sample discs measured for each dose. The number was chosen so that all measurements could be made in two carousel loads on the Risø (discs for each dose were split evenly between the two runs to allow for any differences between runs).

The method used for sample measurement was as used by Dr Vagn Mejdahl. All samples were left at least 24 hours after irradiation, and were then preheated at 100°C for 1 week to remove any unstable TL components. They were then TL glowed on the Risø reader at 3°C/sec to 450°C with a preheat at 290°C for 10 seconds, using a Corning 5-60, Hoya HA3 and a neutral density 1.0 filter. Second glow normalisation was performed within the Risø reader, samples being irradiated for 5 minutes within the reader. They were then left for 12 hours before being TL glowed again.

Analysis of the data was performed in two ways. Firstly, the data from each of the beta sources was used to produce a growth curve. The 20 and 40 Gy  $\gamma$ -irradiated material was then compared with these growth curves to calculate a source calibration. The results are shown in table AII.1(b)

Table AII.1(a)

Numbers of discs used for the source intercalibration between Risø and Aberystwyth

<u>Source</u>	<u>Time (mins) or Dose (Gy)</u>	<u>Number of discs</u>	
		<u>Number run</u>	<u>Number used in analysis</u>
No Dose	0	10	9
$\gamma$ -source at Risø	20 Gy	9	8
$\gamma$ -source at Risø	40 Gy	5	5
Daybreak $\beta$ -source	4 mins	5	5
Daybreak $\beta$ -source	8 mins	5	5
Daybreak $\beta$ -source	12 mins	5	5
Risø reader $\beta$ -source	15 mins	5	5
Risø reader $\beta$ -source	30 mins	4	4
Total		48	46

Table AII.1(b)

Source strengths calculated using the 20 Gy and 40 Gy  $\gamma$ -irradiated samples.

<u><math>\beta</math>-Source</u>	<u><math>\gamma</math>-dose (Gy)</u>	<u><math>\beta</math>-source calibration (Gy/min)</u>
Daybreak $\beta$ -source	20	3.98±0.01
Daybreak $\beta$ -source	40	3.82±0.08
	<b>Average:</b>	<b>3.90±0.08</b>
Risø reader $\beta$ -source	20	1.29±0.02
Risø reader $\beta$ -source	40	1.23±0.03
	<b>Average:</b>	<b>1.26±0.04</b>

Clearly there is some systematic difference when using the 20 and the 40 Gy  $\gamma$ -irradiated material. An alternative method of analysis was to produce growth curves for all three sources. All are linear over the dose range used here, and so a calibration is possible by comparing slopes. For the three sources the slopes of the lines were calculated by a least squares fit:-

$$\text{Daybreak } \beta\text{-source} \quad 4553.97 \pm 24.40 \text{ TL(cps)/min} \beta r^2 = 0.9999$$

$$\text{Risø reader } \beta\text{-source} \quad 1477.80 \pm 7.67 \text{ TL(cps)/min} \beta r^2 = 1.0000$$

$$\text{Risø } \gamma\text{-source} \quad 1195.14 \pm 29.86 \text{ TL(cps)/Gy} \quad r^2 = 0.9994$$

Taking ratios of slopes gives calibration values for the two beta sources of:-

Daybreak  $\beta$ -source **3.81±0.12 Gy/min**

Risø reader  $\beta$ -source **1.24±0.04 Gy/min**

These were the preferred values adopted as a result of this calibration undertaken in December 1989. Table AII.1(c) shows the calculated drop in effective dose rate from the Daybreak and Risø reader  $\beta$ -sources due to the decay of the radioactive source. No allowance was made for this change in dose rate since its magnitude is small, over the time period during which measurements were made for this thesis, compared with other errors in luminescence dating.

Table AII.1(c)

Change in source strength due to radioactive decay (half-life of  $^{90}\text{Sr}$  is 28.0 years).

<u>Date</u>	<u>Daybreak <math>\beta</math>-source</u> (Gy/min)	<u>Risø <math>\beta</math>-source</u> (Gy/min)
December 1989	3.81	1.24
December 1990	3.72	1.21
December 1991	3.62	1.18

## AII.2 Intercalibration of Daybreak and Risø $\beta$ -sources

All irradiations for equivalent dose determination using standard 'multiple disc' methods (chapter 5) used the Daybreak  $\beta$ -source. Hence why this was the source that was calibrated using the most sample discs in the analysis described above. However, all the single aliquot analysis (chapters 6,7 and 8) uses only the Risø  $\beta$ -source, and so it became important to ensure that the calibration of this source was accurate. In particular it became important to ensure that the ratio of source strengths was correct so that comparisons of the EDs determined by the two methods could be made.

The procedure used was a modified version of the single aliquot regeneration method, each disc giving an estimate of the ratio of the two source strengths. Two batches of six aliquots of sample GDNZ 6 (180-211 $\mu\text{m}$ ) were used.

Each aliquot was TL glowed to 450°C at 3°C/sec to remove any luminescence signal and then given 3 minutes of irradiation on the Daybreak  $\beta$ -source. After preheating at 220°C

for 10 minutes the sample had its IRSL measured for 100 seconds at 50°C. It was then TL glowed to 450°C again before being irradiated by the Risø β-source, preheated and its IRSL remeasured. Any number of doses could be given, the signal being removed between each step by glowing to 450°C. Irradiations of 0, 180, 360, 540 and 720 seconds were given. All samples were linear over this range, no changes in sensitivity were apparent when doses were repeated and all samples gave a flat plot of 'ED' (see below) against IRSL exposure time for the 100 second period analysed. A growth curve was built up for the Risø β-source and the signal from the sample irradiated on the Daybreak β-source could be compared using the regeneration analysis program developed by R.Grün (figure AII.2). Results for the twelve discs analysed are listed in table AII.2.

Table AII.2

Results of the intercalibration between the Daybreak and Risø β-sources using twelve separate aliquots.

<u>Disc No.</u>	<u>ED (secs)(a)</u>	<u>Source ratio(b)</u>
1	552	3.07
2	557	3.09
5	541	3.01
6	564	3.13
9	623	3.46
10	582	3.23
13	584	3.24
14	565	3.14
17	614	3.41
18	605	3.36
21	617	3.43
22	555	3.08
		Average= <b>3.22±0.16</b>

Notes

- (a) 'ED' is the irradiation time using the Risø source necessary to match the signal produced by 3 minutes irradiation on the Daybreak source.
- (b) The source ratio is the ratio of Daybreak/Risø source strengths.

The calibration against the γ-source at Risø had given values of 3.81±0.12 Gy/min and 1.24±0.04 Gy/min. Assuming that the calibration for the Daybreak source was correct, the intercalibration here would give a source strength of 1.18±0.07 Gy/min. Thus the intercalibration lies within the error limits of each analysis and the original calibration of the source is used in all the single aliquot work presented here.

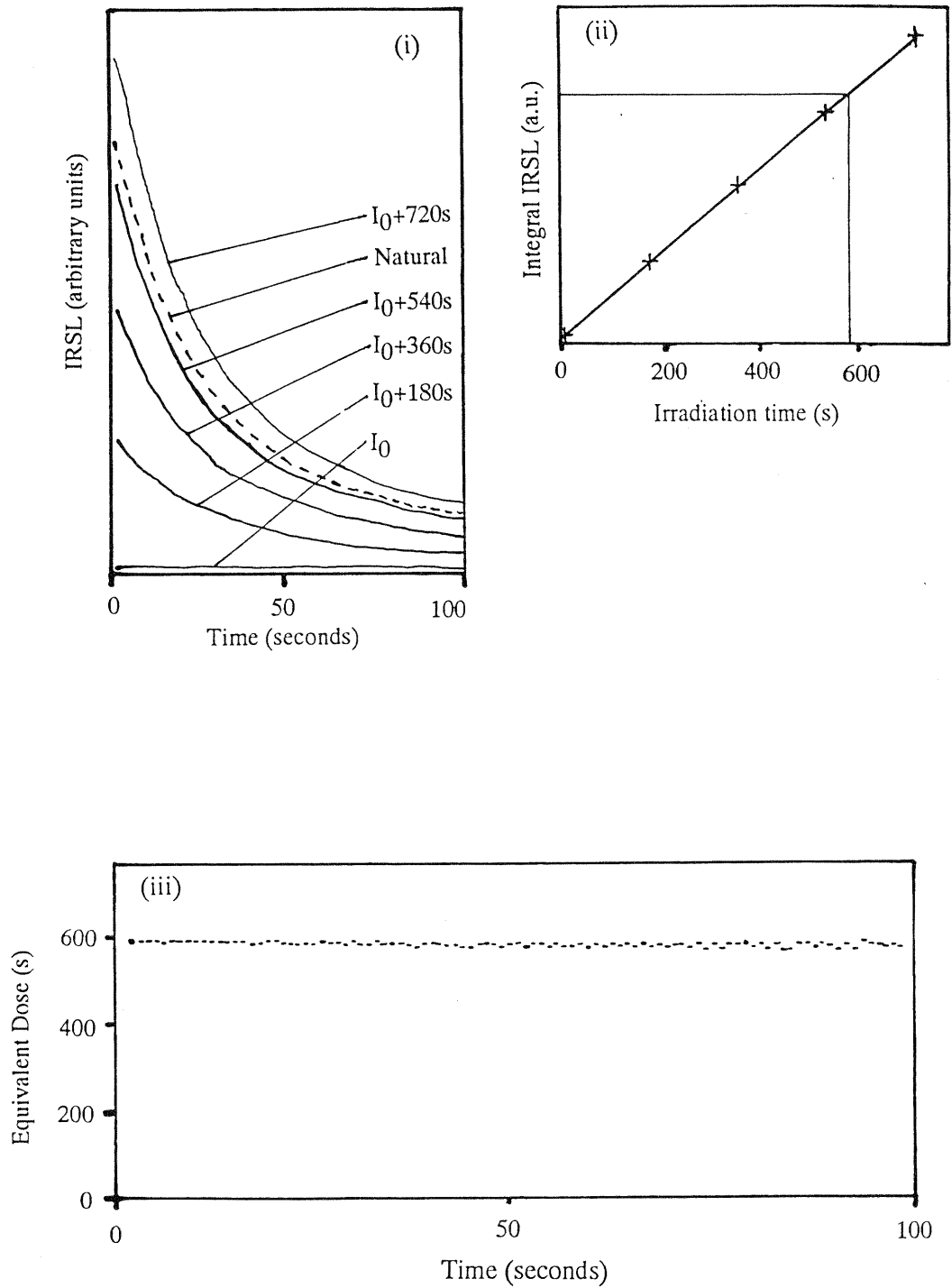


Figure AII.2: An example of the use of a single aliquot for intercalibration between the Daybreak  $\beta$ -source and that in the Risø reader. The IRSL decay curves (i), growth curve obtained by integrating the IRSL signal for all 100s of measurement (ii) and the variation in equivalent dose as a function of the period of measurement (iii), are shown for an aliquot of sample GDNZ 6.

## **Appendix III: Single aliquot results for samples from The Netherlands and the United States of America**

A number of samples from the Lutterzand area of The Netherlands and from the Mohave desert in the south-western USA were analyzed using the single aliquot additive dose method. Potassium feldspar was separated from the samples by Dr J.W.A. Dijkmans (Lutte samples) and by Dr H.M. Rendell (SW USA samples). In both cases it is difficult to compare the equivalent doses determined using the single aliquot method with those determined using standard multiple aliquot methods for a variety of reasons. Firstly, no direct intercalibration exists between the radioactive sources in Aberystwyth and Cambridge where Dr J.W.A. Dijkmans was working. Secondly, different emission filters were used by the various workers (Lutte; UG-11 and HA-3 used by Dr Dijkmans, 5-58 and BG-39 used for the single aliquot data shown here. SW USA; UG-11 and HA-3 or 5-58 and HA-3 used by Dr Rendell, 7-59 and BG-39 used for the single aliquot data shown here). Thirdly, many of the samples from SW USA show very high disc-to-disc scatter and ED determination using 'standard' multiple aliquot techniques has proved difficult (Rendell, pers.comm.). Finally, different methods of equivalent dose determination using multiple aliquots have been used for the two groups of samples together with different preheating procedures.

The single aliquot results for these two groups of samples, corrected using both luminescence correction method B (section AIII.1) and the dose correction method (section AIII.2), are shown below, together with the equivalent doses determined using multiple aliquot methods where they have been determined.

### AIII.1 Single aliquot EDs corrected using luminescence correction method B.

Table AIII.1(a) lists the equivalent doses determined for samples collected from south-western USA using the single aliquot additive dose method and luminescence correction B, along with equivalent doses determined by Dr H.M. Rendell using multiple aliquot methods.

Table AIII.1(a): Samples from SW USA

Comparison of equivalent doses determined using single aliquots with correction method B (section 7.3.2) with those determined using standard methods of ED determination for samples collected from the south-west United States of America.

<u>Sample</u>	<u>Single Aliquot(a)</u>	<u>Multiple Disc Regeneration (TL)(b)</u>		
		<u>Linear Fit</u>	<u>Exponential Fit</u>	
DL01	159.0 ± 11.6	154.7±10.9	233.2±39.0	(uv)
		220.2±22.0	310.1±50.4	(bl)
DL16	62.0 ± 10.8	78.3±10.5	151.8±33.9	(uv)
		101.3±12.2	124.5±19.7	(bl)
DL17	56.9 ± 6.1	77.8± 7.8	78.2±11.1	(uv)
DL18	73.8 ± 4.9	80.0± 5.8	-	(bl)
DL19	59.1 ± 2.8	71.6± 5.7	-	(bl)
DL22	37.9 ± 5.4	43.2± 4.6	56.1±15.1	(uv)
CD01	77.8 ± 12.5	145.8± 5.2	-	(bl)
CD03	42.8 ± 12.5	118.1± 4.9	-	(bl)
CD04	66.9 ± 4.3	91.5± 4.5	-	(bl)
CD07	33.4 ± 5.2	52.8± 1.2	-	(bl)
K30L	5.3 ± 0.6			
K31L	6.1 ± 0.5			

Notes:

- (a) Single aliquot analysis used a BG-39 and 7-59 filter, otherwise the analysis used the single aliquot additive dose method as described in sections 7.3 and 7.3.2.
- (b) Multiple disc EDs were determined by Dr H.Rendell at Sussex University. Samples marked (uv) used a UG-11 and HA-3 filter combination, while those samples marked (bl) used a 5-58 and HA-3.

Table AIII.1(b) lists the equivalent doses determined for samples from the Lutterzand area of The Netherlands using the additive dose single aliquot method with luminescence correction B, using multiple aliquot methods (Dijkmans and Wintle, 1991) and using the single aliquot regeneration method (bleaching using 10 hrs exposure to the SOL2 solar simulator).

Table AIII.1(b): Samples from Dutch Coversands

Comparison of equivalent doses determined using single aliquots with correction method B (section 7.3.2) with those determined using a standard multiple aliquot method and the single aliquot regeneration method, for samples collected from Dutch Coversands.

<u>Sample</u>	<u>Single Aliquot Additive Dose (IRSL)(a)</u>	<u>Multiple Disc Additive Dose (TL)(b)</u>	<u>Single Aliquot Regeneration (IRSL)(c)</u>
Lutte 1	14.9 ± 0.5 (6)	14.6 ± 0.4	18.1 ± 0.7 (4)
Lutte 2	12.0 ± 0.6 (6)	13.3 ± 0.3	13.7 ± 0.5 (8)
Lutte 3	12.1 ± 0.3 (6)	12.4 ± 0.3	14.1 ± 0.6 (4)
Lutte 8	22.4 ± 1.2 (4)	19.7 ± 0.2	28.5 ± 0.8 (6)
Lutte 9	14.2 ± 0.5 (6)	13.3 ± 0.4	17.3 ± 0.9 (4)
Lutte 12	15.8 ± 0.5 (6)	11.9 ± 0.6	19.7 ± 1.0 (8)

Notes:

- (a) Numbers in brackets show the number of aliquots determined for each sample.
- (b) From Dijkmans and Wintle (1991) using an approach adapted from method (a) of Wintle and Huntley (1980). The filters used were a UG-11 and HA-3.
- (c) See table 6.7(a). Numbers in brackets show the number of aliquots measured for each sample.

## AIII.2 Single aliquot EDs corrected using the dose correction method

Tables AIII.2(a) and (b) show the same data as tables AIII.1(a) and (b) but the single aliquot additive dose results have been corrected using the dose correction method. The majority of samples listed in tables AIII.2(a) and (b) have relatively small EDs, and their response to irradiation is not too curved. Hence the differences between the EDs determined using the two correction methods (luminescence correction B and dose correction) are quite small.

Table AIII.2(a): Samples from SW USA

Comparison of equivalent doses determined using the single aliquot (dose correction) method with those determined using standard multiple aliquot methods.

<u>Sample</u>	<u>Single Aliquot</u> (a)	<u>Multiple Disc Regeneration (TL)</u> (b)		
		<u>Linear Fit</u>	<u>Exponential Fit</u>	
DL01	n.d.(c)	154.7±10.9	233.2±39.0	(uv)
		220.2±22.0	310.1±50.4	(bl)
DL16	62.8 ± 11.1	78.3±10.5	151.8±33.9	(uv)
		101.3±12.2	124.5±19.7	(bl)
DL17	59.4 ± 6.8	77.8± 7.8	78.2±11.1	(uv)
DL18	75.4 ± 5.4	80.0± 5.8	-	(bl)
DL19	60.0 ± 3.1	71.6± 5.7	-	(bl)
DL22	37.4 ± 5.3	43.2± 4.6	56.1±15.1	(uv)
CD01	80.4 ± 13.2	145.8± 5.2	-	(bl)
CD03	42.8 ± 12.3	118.1± 4.9	-	(bl)
CD04	68.2 ± 4.5	91.5± 4.5	-	(bl)
CD07	33.2 ± 5.1	52.8± 1.2	-	(bl)
K30L	5.3 ± 0.6			
K31L	6.0 ± 0.5			

### Notes:

- (a) Single aliquot analysis used a BG-39 and 7-59 filter, otherwise the analysis used the standard single aliquot additive dose method as described in section 7.3 and 7.4.1.
- (b) Multiple disc EDs were determined by Dr H.Rendell at Sussex University. Samples marked (uv) used a UG-11 and HA-3 filter combination, while those samples marked (bl) used a 5-58 and HA-3.
- (c) The irradiations given to the sample were insufficient to give a reasonable growth in the luminescence signal. Using the dose correction method, all the data points lie very close together making extrapolation impossible.

Table AIII.2(b): Samples from Dutch Coversands

Comparison of equivalent doses determined using the single aliquot (dose correction) method with those determined using a multiple aliquot method and the single aliquot regeneration method.

<u>Sample</u>	<u>Single Aliquot Additive Dose (IRSL)(a)</u>	<u>Multiple Disc Additive Dose (TL)(b)</u>	<u>Single Aliquot Regeneration (IRSL)(c)</u>
Lutte 1	14.8 ± 0.5 (6)	14.6 ± 0.4	18.1 ± 0.7 (4)
Lutte 2	12.0 ± 0.6 (6)	13.3 ± 0.3	13.7 ± 0.5 (8)
Lutte 3	12.0 ± 0.3 (6)	12.4 ± 0.3	14.1 ± 0.6 (4)
Lutte 8	22.4 ± 1.2 (4)	19.7 ± 0.2	28.5 ± 0.8 (6)
Lutte 9	13.9 ± 0.5 (6)	13.3 ± 0.4	17.3 ± 0.9 (4)
Lutte 12	15.8 ± 0.5 (6)	11.9 ± 0.6	19.7 ± 1.0 (8)

Notes:

- (a) Numbers in brackets show the number of aliquots determined for each sample.
- (b) From Dijkmans and Wintle (1991) using an approach adapted from method (a) of Wintle and Huntley (1980). The filters used were a UG-11 and HA-3.
- (c) See table 6.7(a). Numbers in brackets show the number of aliquots determined for each sample.

## References

Aitken M.J., 1985, Thermoluminescence dating, Academic Press, London

Aitken M.J., 1990, Pairs precision required in alpha counting, Ancient TL, 8, 12-14

Andersson M., Jeannin M., Rendell H.M., Tardot A. and Townsend P.D., 1990, TL spectra of mineral mixtures: discrimination between different components, Nuclear Tracks and Radiation Measurements, 17, 569-577

Anderton P.W., 1981, Structure and evolution of the South Wanganui basin, New Zealand, New Zealand Journal of Geology and Geophysics, 24, 39-63

Bailiff I.K., 1992, Studies of the role of excited levels in optically stimulated luminescence in feldspar, Radiation Protection Dosimetry (in press)

Bailiff I.K. and Poolton N.R.J., 1989, The use of LEDs as an excitation source for photoluminescence dating of sediments, Ancient TL, 7, 18-20

Bailiff I.K. and Poolton N.R.J., 1991, Studies of charge transfer mechanisms in feldspars, Nuclear Tracks and Radiation Measurements, 18, 111-118

Balescu S., Packman S.C., Wintle A.G. and Grün R., 1989, TL dating of Pleistocene raised beaches from NW Europe using potassium feldspar coarse grains, Long and Short Range Limits in Luminescence Dating, Research Laboratory for Archaeology and the History of Art, Occasional Publication no. 9

Balescu S., Packman S.C. and Wintle A.G., 1991, Chronological separation of interglacial raised beaches from Northwestern Europe using thermoluminescence, Quaternary Research, 35, 91-102

Balescu S., Packman S.C., Wintle A.G. and Grün R., 1992, Thermoluminescence dating of the middle Pleistocene raised beach of Sangatte (northern France), Quaternary Research, 37, 390-396

Balescu S. and Lamothe M., 1992, The blue emission of K-feldspar coarse grains and its potential for overcoming TL age underestimation, Quaternary Science Reviews, 11, 45-51

Bard E., Hamelin B., Fairbanks R.G. and Zindler A., 1990, Calibration of the  $^{14}\text{C}$  timescale over the past 30,000 years using mass spectrometric U-Th ages from Barbados corals, Nature, 345, 405-409

Berger G.W. and Huntley D.J., 1989, Test data for exponential fits. Ancient TL, 7(3), 43-46

Berryman K.R. and Hull A.G., 1984, Guidebook to the North Island Scientific Excursions. Royal Society of New Zealand Misc. Series 8, 115

Berryman K.R., Ota Y. and Hull A.G., 1992, Holocene coastal evolution under the influence of episodic tectonic uplift: examples from New Zealand and Japan, Quaternary International, 15/16, 31-45

Boellstorff J.D. and Te Punga M.T., 1977, Fission track ages and correlation of middle Pleistocene sequences from Nebraska and New Zealand, New Zealand Journal of Geology and Geophysics, 20, 47-58

Bøtter-Jensen L., 1988, The automated Risø TL dating reader system, Nuclear Tracks and Radiation Measurements, 14, 177-180

Bøtter-Jensen L., Ditlefsen C. and Mejdahl V., 1991, Combined OSL(infrared) and TL studies of feldspars, Nuclear Tracks and Radiation Measurements, 18, 257-264

Bøtter-Jensen L. and Mejdahl V., 1988, Assessment of beta dose-rate using a GM multicounter system, Nuclear Tracks and Radiation Measurements, 14, 187-191

Bøtter-Jensen L. and Duller G.A.T., 1992, A new system for measuring OSL from quartz samples, Nuclear Tracks and Radiation Measurements, (in press)

Chappell J. and Shackleton N.J., 1986, Oxygen isotopes and sea level, Nature, 324, 137-140

Cowie J.D., 1963, Dune-building phases in the Manawatu district, New Zealand, New Zealand Journal of Geology and Geophysics, 6, 268-280

Cowie J.D., 1964a, Loess in the Manawatu district, New Zealand, New Zealand Journal of Geology and Geophysics, 7, 389-396

Cowie J.D., 1964b, Aokautere ash in the Manawatu district, New Zealand, New Zealand Journal of Geology and Geophysics, 7, 67-77

Cowie J.D., 1968, Pedology of soils from wind-blown sand in the Manawatu district, New Zealand Journal of Science, 11, 459-487

Dijkmans J.W.A., Wintle A.G. and Mejdahl V., 1988, Some thermoluminescence properties and dating of eolian sands from the Netherlands, Quaternary Science Reviews, 7, 349-355

Dijkmans J.W.A., van Mourik J.M. and Wintle A.G., 1992, Thermoluminescence dating of aeolian sands from polycyclic soil profiles in the southern Netherlands, Quaternary Science Reviews, 11, 85-92

Dijkmans J.W.A. and Wintle A.G., 1991, Methodological problems in thermoluminescence dating of Weichselian coversand and late Holocene drift sand from the Lutterzand area, E.Netherlands, Geologie en Mijnbouw, 70, 21-33

Duller G.A.T., 1992, Comparison of equivalent doses determined by thermoluminescence and infrared stimulated luminescence for dune sands in New Zealand, Quaternary Science Reviews, 11, 39-43

Duller G.A.T. and Bøtter-Jensen L., 1992, Luminescence from potassium feldspars stimulated by infrared and green light, Radiation Protection Dosimetry (accepted for publication)

Duller G.A.T. and Wintle A.G., 1991, On infrared stimulated luminescence at elevated temperatures. Nuclear Tracks and Radiation Measurements, 18, 379-384

Edwards S.R., 1991, Luminescence dating of sand from the Kelso dunes, California, Unpublished MSc. thesis, University of Wales, Aberystwyth

Edwards S.R., 1993, Luminescence dating of sand from the Kelso dunes, California, In: Pye K. (ed) The Dynamics and Environmental Context of Aeolian Sedimentary Systems. Geological Society, London, Special Publication (in press)

Ervanne H., Jungner H. and Rasanen M., 1992, Dating of fluvial sediments from the Amazon lowland in Peru, Quaternary Science Reviews, 11, 71-73

Fleming C.A., 1972, The contribution of C14 dates to the Quaternary geology of the 'Golden Coast' western Wellington, Tuatara, 19, 61-69

Frechen M., 1992, Systematic thermoluminescence dating of two loess profiles from the middle Rhine area (F.R.G.), Quaternary Science Reviews, 11, 93-101

Froggatt P.C., Nelson C.S., Carter L., Griggs G. and Black K.P., 1986, An exceptionally large late Quaternary eruption from New Zealand, Nature, 319, 578-582

Froggatt P.C. and Lowe D.J., 1990, A review of late Quaternary silicic and some other tephra formations from New Zealand: their stratigraphy, nomenclature, distribution, volume, and age, New Zealand Journal of Geology and Geophysics, 33, 89-109

Gibb J.G., 1986, A New Zealand eustatic sea level curve and its application to vertical tectonic movements, Royal Society of New Zealand Bulletin, 24, 377-395

Gibbs H.S., 1957, Provisional soil map of Horowhenua county, New Zealand Soils Bureau map 788L

Godfrey-Smith D.I., Huntley D.J. and Chen W.-H., 1988, Optical dating studies of quartz and feldspar sediment extracts, Quaternary Science Reviews, 7, 373-380

Grün R., Packman S.C. and Pye K., 1989, Problems involved in TL-dating of Danish cover sands using K-feldspar, Long and Short Range Limits in Luminescence Dating

Hesp P.A. and Shepherd M.J., 1978, Some aspects of the late Quaternary geomorphology of the lower Manawatu valley, New Zealand, New Zealand Journal of Geology and Geophysics, 21, 403-412

Hofmeister A.M. and Rossman G.R., 1983, Color in feldspars, Reviews in Mineralogy, 2, 271-280

Huntley D.J., Godfrey-Smith D.I. and Thewalt M.L.W., 1985, Optical dating of sediments, Nature, 313, 105-107

Huntley D.J., Godfrey-Smith D.I. and Haskell E.H., 1991, Light-induced emission spectra from some quartz and feldspars, Nuclear Tracks and Radiation Measurements, 18, 127-131

Huntley D.J., Godfrey-Smith D.I., Thewalt M.L.W. and Berger G.W., 1988, Thermoluminescence spectra of some mineral samples relevant to thermoluminescence dating, Journal of Luminescence, 39, 123-136

Huntley D.J. and Wintle A.G., 1981, The use of alpha scintillation counting for measuring Th-230 and Pa-231 contents of ocean sediments, Canadian Journal of Earth Sciences, 18, 419-432

Hütt G., Jaek I. and Tchonka J, 1988, Optical dating: K-feldspars optical response stimulation spectra, Quaternary Science Reviews, 7, 381-385

Hütt G. and Jaek I., 1989, Infrared stimulated photoluminescence dating of sediments, Ancient TL, 7(3), 48-51

Hütt G. and Jungner H., 1992, Optical and TL dating on glaciofluvial sediments, Quaternary Science Reviews, 11, 161-163

Jungner H., 1985, Some experiences from an attempt to date post-glacial dunes from Finland by thermoluminescence, Nuclear Tracks and Radiation Measurements, 10, 749-756

Jungner H., 1987, Thermoluminescence dating of sediments from Oulainen and Vimpeli, Ostrobothnia, Finland, Boreas, 16, 231-235

Jungner H., Landvik J.Y. and Mangerud J., 1989, Thermoluminescence dates of Weichselian sediments in Western Norway, Boreas, 18, 23-29

Kohn B.P., Pillans B., and McGlone M.S., 1992, Zircon fission track age for middle Pleistocene Rangitawa Tephra, New Zealand: stratigraphic and palaeoclimatic significance, Palaeogeography, Palaeoclimatology, and Palaeoecology, 95, 73-94

Kolstrup E., 1980, Climate and stratigraphy in northwestern Europe between 30,000 B.P. and 13,000 B.P., with special reference to The Netherlands, Mededelingen Rijks Geologische Dienst, 32-15: 181-253

Kolstrup E., Grün R., Mejdahl V., Packman S.C. and Wintle A.G., 1990, Stratigraphy and thermoluminescence dating of Late Glacial cover sand in Denmark. Journal of Quaternary Science, 5, 207-224

- Kolstrup E. and Mejdahl V., 1986, Three frost wedge casts from Jutland (Denmark) and TL dating of their infill, Boreas, 15, 311-321
- Koster E.A., 1988, Ancient and modern cold-climate aeolian sand deposition: a review, Journal of Quaternary Science, 3, 69-83
- Kronborg C. and Mejdahl V., 1989, Thermoluminescence dating of Eemian and early Weichselian deposits in Denmark, Quaternary International, 3/4, 93-99
- Kyle P.R. and Seward D., 1984, Dispersed rhyolitic tephra from New Zealand in deep-sea sediments of the Southern Ocean, Geology, 12, 487-490
- Lewis K.B., 1979, A storm-dominated inner shelf, Western Cook strait, New Zealand, Marine Geology, 31, 31-43
- Li S-H., 1991a, Removal of the thermally unstable signal in optical dating of K-feldspar. Ancient TL, 9, 26-29
- Li S-H., 1991b, A cautionary note: apparent sensitivity change resulting from curve fitting, Ancient TL, 9, 12-13
- Li S-H. and Aitken M.J., 1989, How far back can we go with the optical dating of K-feldspar, Long and short range limits in luminescence dating, Research Laboratory for Archaeology and the History of Art, Occasional Publication no. 9
- Li S-H. and Wintle A.G., 1991, Sensitivity changes of luminescence signals from colluvial sediments after different bleaching procedures, Ancient TL, 9, 50-53
- Li S-H. and Wintle A.G., 1992, Luminescence sensitivity change due to bleaching of sediments, Nuclear Tracks and Radiation Measurements, (in press)
- Lundqvist J. and Mejdahl V., 1987, Thermoluminescence dating of eolian sediments in central Sweden, Geologiska Foreningens i Stockholm Forhandlingar, 109, 147-158
- Martinson D.G., Pisias N.G., Hays J.D., Imbrie J., Moore Jr. T.C. and Shackleton N.J., 1987, Age dating and the orbital theory of the Ice Ages: Development of a high resolution 0 to 300,000 year chronostratigraphy. Quaternary Research 27, 1-29

- McKeever S.W.S., 1985, Thermoluminescence of solids, Cambridge University Press
- Mejdahl V., 1983, Feldspar inclusion dating of ceramics and burnt stones, PACT, 9, 351-364
- Mejdahl V., 1985, Thermoluminescence dating of partially bleached sediments, Nuclear Tracks and Radiation Measurements, 10, 711-715
- Mejdahl V., 1987, Internal radioactivity in quartz and feldspar grains, Ancient TL, 5(2), 10-17
- Mejdahl V., 1988, The plateau method for dating partially bleached sediments by thermoluminescence, Quaternary Science Reviews, 7, 347-348
- Mejdahl V., 1989, How far back: Life times estimated from studies of feldspars of infinite ages, Long and short range limits in luminescence dating, Research Laboratory for Archaeology and the History of Art, Occasional Publication no. 9
- Mejdahl V., 1992, Thermoluminescence dating of late-glacial sand sediments, Nuclear Tracks and Radiation Measurements, 18, 71-75
- Mejdahl V. and Winther-Nielsen M., 1982, TL dating based on feldspar inclusions, PACT, 6, 426-437
- Milne J.D.G., 1973, Mount Curl Tephra, a 230,000 year old marker bed in New Zealand and its implications for Quaternary chronology, New Zealand Journal of Geology and Geophysics, 16(3), 519-532
- Milne J.D.G. and Smalley I.J., 1979, Loess deposits in the southern part of the North Island of New Zealand: an outline stratigraphy, Acta Geologica Academiae Scientiarum Hungaricae, 22, 197-204
- Nelson C.S., 1988, Revised age of a late Quaternary tephra at DSDP site 594 off eastern South Island and some implications for correlation, Geological Society of New Zealand Newsletter, 82, 35-40

Ota Y., Berryman K.R., Hull A.G., Miyauchi T. and Iso N., 1988, Age and height distribution of Holocene transgressive deposits in eastern North Island, New Zealand. Palaeogeography, Palaeoclimatology and Palaeoecology, 68, 135-151

Palmer A.S., Barnett R., Pillans B.J., and Wilde R.H., 1988, Loess, river aggradation terraces and marine benches at Otaki, southern North Island, New Zealand, In: Loess: Its distribution, geology and soils, (eds) Eden D.N. and Furkert R.J., 163-174, Balkema

Pearce N.J.G., Perkins W.T., Abell I., Duller G.A.T. and Fuge R., 1992, Mineral microanalysis by laser ablation inductively coupled plasma mass spectrometry, Journal of Analytical Atomic Spectrometry, 7, 53-57

Pillans B., 1983, Upper Quaternary marine terrace chronology and deformation, South Taranaki, New Zealand. Geology 11, 292-297

Pillans B.J., 1988, Loess chronology in Wanganui basin, New Zealand. In: Loess: Its distribution, geology and soils. (eds) Eden D.N. and Furkert R.J., 175-192, Balkema

Pillans B.J. and Kohn B.P., 1981, Rangitawa Pumice: A widespread (?) Quaternary marker bed in Taranaki-Wanganui, Victoria University of Wellington Geology Department publication, 20, 94-104

Prescott J.R., Akber R.A. and Gartia R.K., 1990, Three-dimensional thermoluminescence spectroscopy of minerals. In: Coyne L.M., McKeever S.W.S. and Blake D.F., Spectroscopic Characterization of Minerals and their Surfaces, pp. 180-189, American Chemical Society, Washington, DC.

Prescott J.R. and Hutton J.T., 1988, Cosmic ray and gamma ray dosimetry for TL and ESR, Nuclear Tracks and Radiation Measurements, 14, 223-227

Rendell H.M., 1992, A comparison of TL age estimates from different mineral fractions of sands, Quaternary Science Reviews, 11, 79-83

Rendell H.M. and Townsend P.D., 1988, Thermoluminescence dating of a 10m loess profile in Pakistan, Quaternary Science Reviews, 7, 251-255

Rendell H., Worsley P., Green F. and Parks D., 1991, Thermoluminescence dating of the Chelford Interstadial, Earth and Planetary Science Letters, 103, 182-189

- Rhodes E.J., 1990, Optical dating of quartz from sediments. Unpublished DPhil. thesis, University of Oxford
- Sanderson D.C.W., 1988, Thick source beta counting (TSBC): A rapid method for measuring beta dose-rates Nuclear Tracks and Radiation Measurements, 14, 203-207
- Sarnthein M., Stremme H.E. and Mangini A., 1986, The Holsteinian interglaciation: Time-stratigraphic position and correlation to stable-isotope stratigraphy of deep-sea sediments, Quaternary Research, 26, 283-298
- Schwarcz H.P. and Grün R., 1988, Comment on M.Sarnthein, H.E.Stremme, and A.Mangini, "The Holsteinian interglaciation: Time-stratigraphic position and correlation to stable-isotope stratigraphy of deep-sea sediments", Quaternary Research, 29, 75-79
- Seward D., 1974, Age of New Zealand Pleistocene substages by fission-track dating of glass shards from tephra horizons. Earth and Planetary Science Letters 24, 242-248
- Seward D., 1976, Tephrostratigraphy of the marine sediments in the Wanganui basin, New Zealand, New Zealand Journal of Geology and Geophysics, 19, 9-20
- Seward D., 1979, Comparison of zircon and glass fission-track ages from tephra horizons, Geology, 7, 479-482
- Shepherd M.J., 1985, The origin of the Koputaroa dunes, Horowhenua, New Zealand, New Zealand Journal of Geology and Geophysics, 28, 323-327
- Shepherd M.J. and Lees C.M., 1987, Holocene alluviation and transgressive dune activity in the lower Manawatu valley, New Zealand, New Zealand Journal of Geology and Geophysics, 30, 175-187
- Shepherd M.J. and Price D.M., 1990, Thermoluminescence dating of late Quaternary dune sand, Manawatu/Horowhenua area, New Zealand: a comparison with  $^{14}\text{C}$  age determinations, New Zealand Journal of Geology and Geophysics, 33, 535-539
- Short M.A. and Huntley D.J., 1992, Infrared stimulation of quartz, Ancient TL, 10, 19-21

Singhvi A.K., Sharma Y.P. and Agrawal D.P., 1982, Thermoluminescence dating of sand dunes in Rajasthan, India. Nature, 295, 313-315

Smith B.W., Aitken M.J., Rhodes E.J., Robinson P.D., and Geldard D.M., 1986, Optical dating: Methodological aspects. Radiation Protection Dosimetry, 17, 229-233

Smith B.W. and Prescott J.R., 1984, A cautionary note on the measurement of quartz TL immediately after irradiation, Ancient TL, 2(2), 14-18

Southgate G.A., 1985, Thermoluminescence dating of beach and dune sands: Potential of single-grain measurements. Nuclear Tracks and Radiation Measurements, 10, 743-747

Spooner N.A., 1987, The effect of light on the thermoluminescence of quartz, Unpublished MSc. thesis, University of Adelaide

Spooner N.A., 1992, Optical dating: Preliminary results on the anomalous fading of luminescence from feldspars, Quaternary Science Reviews, 11, 139-145

Spooner N.A., Aitken M.J., Smith B.W., Franks M. and McElroy C., 1990, Archaeological dating by infrared stimulated luminescence using a diode array, Radiation Protection Dosimetry, 34(2), 83-86

Spooner N.A. and Franks M., 1990, Some characteristics of infrared emitting diodes relevant to luminescence dating, Ancient TL, 8, 16-19

Spooner N.A. and Questiaux D.G., 1989, Optical dating - Achenheim beyond the Eemian using green and infra-red stimulation, Long and short range limits in luminescence dating, Research Laboratory for Archaeology and the History of Art, Occasional Publication no. 9

Strickertsson K., 1985, The thermoluminescence of potassium feldspars - glow curve characteristics and initial rise measurements, Nuclear Tracks and Radiation Measurements, 10, 613-617

Te Punga M.T., 1952, The geology of Rangitikei valley, New Zealand Geological Survey Memoir, 8, 44p

Van der Hammen T. and Wijmstra T.A., (eds), 1971, The upper Quaternary of the Dinkel valley, Mededelingen Rijks Geologische Dienst, 22, 55-214

Wheeler G.C.W.S., 1988, Optically stimulated phosphorescence and optically transferred TL as a tool for dating, Quaternary Science Reviews, 3, 407-410

Wilson C.J.N., Switsur V.R. and Ward A.P., 1988, A new  $^{14}\text{C}$  age for the Oruanui (Wairakei) eruption, New Zealand, Geological Magazine, 125, 297-300

Wintle A.G., 1973, Anomalous fading of thermoluminescence in mineral samples, Nature, 245, 143-144

Wintle A.G., 1975, Thermal quenching of thermoluminescence in quartz, Geophysical Journal of the Royal Astronomical Society, 41, 107-113

Wintle A.G. and Duller G.A.T., 1991, The effect of optical absorption on luminescence dating, Ancient TL, 9, 37-39

Wintle A.G. and Huntley D.J., 1980, Thermoluminescence dating of ocean sediments, Canadian Journal of Earth Sciences, 17, 348-360

Wintle A.G. and Huntley D.J., 1982, Thermoluminescence dating of sediments. Quaternary Science Reviews, 1, 31-53

Wintle A.G. and Proszynska H., 1983, TL dating of loess in Germany and Poland. PACT, 9, 547-554